Osr1 controls the pro-regenerative response of fibroadipogenic progenitors

Inaugural Dissertation
to obtain the academic degree
Doctor of Philosophy (Ph.D.)

to the Department of Biology, Chemistry, Pharmacy
of the Freie Universität Berlin
by

GEORGIOS KOTSARIS

Berlin, May 2022

This thesis was carried out during the period of March 2017 and May of 2022 at the **Freie Universität Berlin, Max-Planck-Institute for Molecular Genetics** and **BIH Center for Regenerative Therapies** under the supervision of Prof. Dr. Sigmar Stricker and Dr. Ing. Sven Geißler.

1st Reviewer: Prof. Dr. Sigmar Stricker

Institute for Chemistry and Biochemistry

Freie Universität Berlin

Thielallee 63, 14195 Berlin

Tel.: +49 30 838 75799

E-Mail: sigmar.stricker@fu-berlin.de

2nd Reviewer: Dr. Ing. Sven Geißler

BIH Center for Regenerative Therapies (BCRT)

Berlin Institute of Health at Charité – Universitätsmedizin Berlin

Föhrer Straße 15, 13353 Berlin

Tel.: +49 30 450 659539

E-Mail: sven.geissler@bih-charite.de

Date of defense: 01.07.2022

Statutory Declaration

I declare that this thesis entitled "Osr1 controls the pro-regenerative response of fibroadipogenic progenitors" has been composed solely by myself and that it has not been submitted, in whole or in part, in any previous application for a degree. Except where stated otherwise by reference or acknowledgment, the work presented is entirely my own.

Berlin, May 2022

_____

Georgios Kotsaris

Table of Contents

Graphical Summary

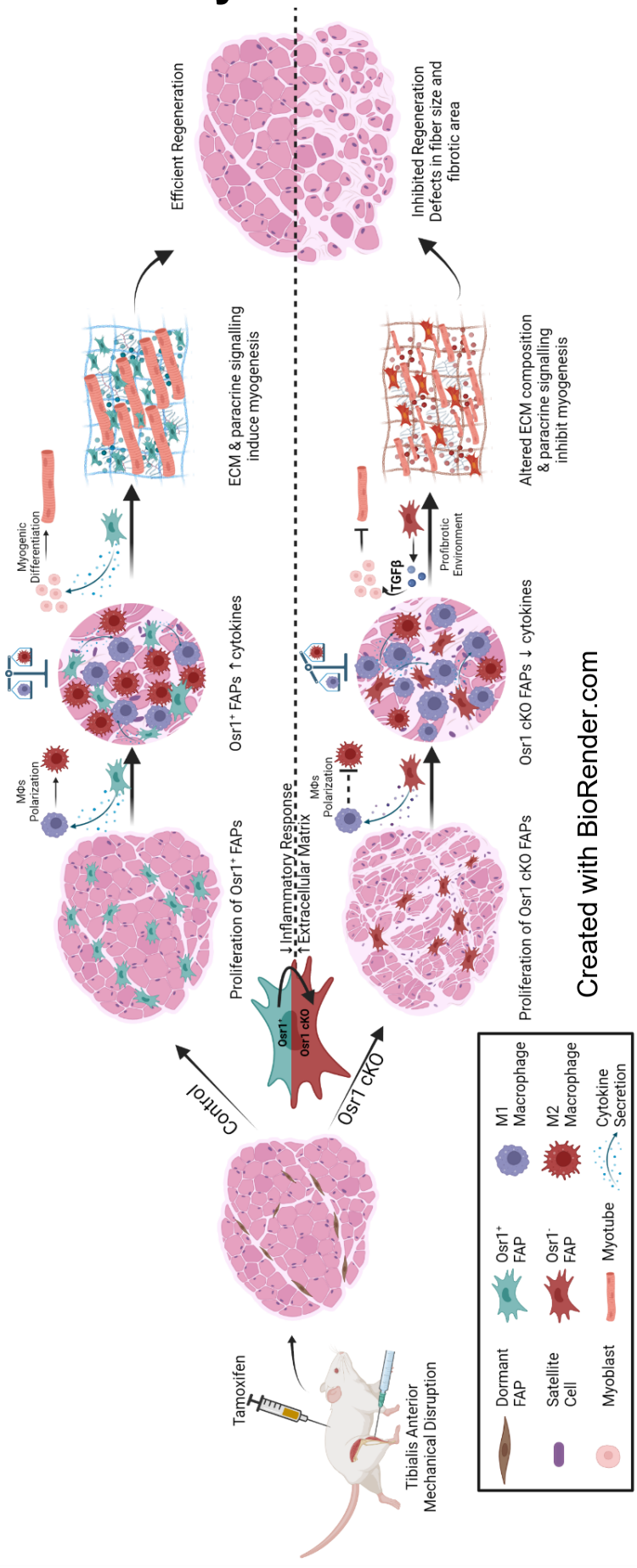

Key findings:

- Conditional inactivation of *Osr1* in adult mice impairs muscle regeneration.
- Loss of *Osr1* prior to injury results in smaller size of regenerating fibers and increased fibrotic tissue accumulation with lower stiffness values.
- Deletion of *Osr1* affects MuSCs proliferation and differentiation in a non-cell autonomous manner.
- Expression of *Osr1* regulates FAPs pool expansion *in vivo* and *in vitro*.
- *Osr1* deficient FAPs dysregulate genes related to ECM formation and inflammatory response.
- *Osr1* is mediating FAPs-immune cells crosstalk and induces regenerative macrophage polarization.
- *Osr1* is a key regulator of a group of genes defining FAPs subtypes and prevents them from acquiring a dystrophic FAP phenotype.
- The composition of the ECM deposited by Osr1 cKO FAPs inhibits myogenic fusion.

Abstract

Skeletal muscle injuries alongside with degenerative diseases represent a great part of medical focus globally since in mammals 30-40% of the total body mass is comprised of skeletal muscle. The regenerative capacity of the muscle tissue depends on the interplay of local cells comprising of the muscle stem cells called also satellite cells (SCs), the fibroadipogenic progenitors (FAPs) as well as the infiltration of immune cells from the circulatory system. Despite the high regenerative potential of muscle, chronic pathologies might lead to connective tissue and fat accumulation, especially in pathologies with degenerative loops of inflammation. Although FAPs are essential for efficient muscle regeneration, they are the source of fibrofatty infiltrations. The mechanisms that regulate FAPs plasticity and behavior are not yet fully understood.

In skeletal muscle development FAP like cells reside in close proximity to newly developed myofibers. They orchestrate muscle development through signaling molecules secretion and shaping the extracellular matrix. Upon acute muscle injury, FAPs re-express *Osr1* but whether adult Osr1^{+} FAPs retain their beneficial developmental role during regeneration had been an unresolved question. This study shed light on the pro-regenerative role of *Osr1* expression in FAPs by following the course of muscle trauma healing in a conditional Osr1 knock-out mouse model. Histological analysis at several timepoints revealed an impaired/delayed regeneration upon *Osr1* deletion, characterized by smaller size of myofibers and persistence of immature myofibers at later points of regeneration. Moreover, mutant injured animals showed higher deposition of fibrotic extracellular matrix which resulted in accumulation of scar tissue with softer stiffness values. Furthermore, *in vivo* experiments demonstrated a non-cell autonomous defect of *Osr1* deficient FAPs. The population of MuSCs was reduced in the mutants at the onset of regeneration while at later timepoints a skew in their activated population was detected. In this study, a conditional recombination of the *Osr1* locus was established in *in vitro* assays with FAPs, which resulted in reduced cell numbers and increased apoptotic rates. Interestingly, in vivo Osr1 cKO FAPs exhibited the same defects. To elucidate the defects in FAPs functions upon loss of *Osr1*, transcriptome analysis was performed at two timepoints. Similar to their developmental transcriptome analysis, *Osr1* regulated genes in the mutants were found to be related to cytokine secretion and extracellular matrix formation. *In vivo* experiments at 3 dpi did not show a difference in the number of immune cells infiltrating

in the trauma region. However, a defect in the macrophage inflammation status was observed. Moreover, Osr1 cKO FAPs regulate similar genes with dystrophic FAPs, leading to a higher secretion of a collagenous matrix. *In vitro* experiments revealed that Osr1 cKO FAPs inhibit myogenic fusion through first the production of an anti-myogenic ECM and second through the activation of the TGFβ pathway, which is known for its antimyogenic role.

This study reveals a previous unknown intrinsic factor of FAPs differentiation and function during the regeneration process. It was demonstrated that Osr1$^+$ FAPs are essential for efficient muscle regeneration since they influence MuSCs proliferation and differentiation. This work highlights the novel role of FAPs in regulating macrophage polarization and attributes a bidirectionality to the FAPs-immune system crosstalk. These data highlight *Osr1* as a key regulator of coordinating crucial regenerative processes and demonstrate that its deficiency ascribes a dystrophic phenotype to FAPs. This knowledge can foster the generation of a novel perspective on the cellular network in the regenerative niche, especially on skeletal myopathies or aging, as well as on the development of new tools for therapies.

Zusammenfassung

Verletzungen der Skelettmuskulatur sowie degenerative Erkrankungen nehmen weltweit einen großen Teil des medizinischen Interesses ein, da 30-40% der gesamten Körpermaße bei Säugetieren aus Skelettmuskeln besteht. Die Regenerationsfähigkeit des Muskelgewebes hängt vom Zusammenspiel lokaler Zellen ab, zu denen die Muskelstammzellen, auch Satellitenzellen (SCs) genannt, die fibroadipogenen Progenitoren (FAPs) sowie die Infiltration von Immunzellen aus dem Kreislaufsystem gehören. Trotz des hohen Regenerationspotenzials des Muskels können chronische Pathologien zu Bindegewebes- und Fettansammlungen führen, insbesondere bei Pathologien mit degenerativen Entzündungsschleifen. Obwohl FAPs für eine effiziente Muskelregeneration unerlässlich sind, sind sie die Quelle von Fibrofettinfiltrationen. Die Mechanismen, die die Plastizität und das Verhalten der FAPs regulieren, sind noch nicht vollständig geklärt.

Bei der Entwicklung der Skelettmuskulatur befinden sich FAP-ähnliche Zellen in unmittelbarer Nähe der neu entstehenden Muskelfasern. Sie steuern die Muskelentwicklung durch die Sekretion von Signalmolekülen und die Bildung der extrazellulären Matrix. Nach einer akuten Muskelverletzung exprimieren FAPs erneut *Osr1*, aber die Frage, ob Osr1$^+$ FAPs ihre positive Entwicklungsrolle während der Regeneration beibehalten, war bisher ungelöst. Diese Studie betrachtet die pro-regenerative Rolle der *Osr1*-Expression in FAPs, indem sie den Verlauf der Heilung von Muskelverletzungen in einem konditionalen Osr1-Knock-out-Mausmodell verfolgt. Die zu verschiedenen Zeitpunkten durchgeführte histologische Analyse zeigte eine beeinträchtigte/verzögerte Regeneration bei *Osr1*-Deletion, die durch eine geringere Größe der Myofasern und die Persistenz unreifer Myofasern in den späteren Stadien der Regeneration gekennzeichnet war. Darüber hinaus wiesen verletzte Osr1-cKO Tiere eine stärkere Ablagerung von fibrotischer extrazellulärer Matrix auf, was zu einer Ausbildung von weichem Narbengewebe mit geringer Steifigkeit führte. Darüber hinaus zeigten *In vivo*-Experimente einen nicht zellautonomen Defekt von *Osr1*-defizienten FAPs. Die Population der MuSCs war in den Osr1 cKO Mutanten zu Beginn der Regeneration reduziert, während zu späteren Zeitpunkten ein Defekt in ihrer aktivierten Population festgestellt wurde. In dieser Studie wurde eine konditionale Rekombination des *Osr1*-Locus in *In vitro*-Tests mit FAPs nachgewiesen, was zu einer geringen Zellteilung und einer erhöhten Apoptoserate führte. Interessanterweise

wiesen in vivo Osr1 cKO FAPs die gleichen Defekte auf. Um die Defekte in den Funktionen der FAPs nach dem Verlust von *Osr1* aufzuklären, wurde zu zwei Zeitpunkten eine Transkriptomanalyse durchgeführt. Ähnlich wie bei der Transkriptomanalyse in der Embryogenese wurde festgestellt, dass die von *Osr1* regulierten Gene in den Mutanten mit der Zytokinsekretion und der Bildung der extrazellulären Matrix in Zusammenhang stehen. *In vivo* Experimente nach 3 dpi zeigten keinen Unterschied in der Menge der Immunzellen, die in die Traumaregion eindringen. Es wurde jedoch ein Defekt im Makrophagen-Entzündungsstatus beobachtet. Darüber hinaus regulieren Osr1 cKO FAPs ähnliche Gene wie dystrophe FAPs, was zu einer höheren Sekretion einer kollagen angereicherten Matrix führt. *In vitro*-Experimente zeigten, dass Osr1 cKO FAPs die myogene Fusion erstens durch die Produktion einer anti-myogenen ECM und zweitens durch die Aktivierung des TGFβ-Signalwegs hemmen, der für seine anti-myogene Rolle bekannt ist.

Diese Studie enthüllt einen bisher unbekannten intrinsischen Faktor der FAPs-Differenzierung und -Funktion während des Regenerationsprozesses. Es wurde gezeigt, dass Osr1 FAPs für eine effiziente Muskelregeneration wesentlich sind, da sie die Proliferation und Differenzierung von MuSCs beeinflussen. Diese Arbeit unterstreicht die neuartige Rolle der FAPs bei der Regulierung der Makrophagenpolarisierung und schreibt dem FAP-Immunsystem-Crosstalk eine Bidirektionalität zu. Diese Daten heben *Osr1* als Schlüsselregulator für die Koordinierung wichtiger Regenerationsprozesse hervor und zeigen, dass ohne *Osr1*, FAPs einen dystrophen Phänotyp entwickeln. Dieses Wissen kann eine neue Perspektive auf das zelluläre Netzwerk in der regenerativen Nische eröffnen, insbesondere bei Skelettmyopathien oder beim Altern, sowie bei der Entwicklung neuer Therapien.

Acknowledgements

„Οὐδὲν γὰρ ἄλλο ἔχουσα εἰς Ἅιδου ἡ ψυχὴ ἔρχεται πλὴν τῆς παιδείας τε καὶ τροφῆς“ – Πλάτων 427-347 π.Χ.

„The soul arrives in Hades carrying nothing except its education and nurture” – Plato 427-347 B.C.

It is difficult to realize that five years have passed since I started this journey. There have been up and downs during this trip, I had to learn from the beginning who I am and to love me for whom I have become. I consider myself to be lucky for all the things I learned by accomplishing my PhD. It is impossible to perceive the amount of knowledge that has been offered to me in these past years. I wouldn`t be here if it were not for all the amazing people that have been on my side these years. It is time to thank everyone who encouraged and believed in me when I was daily tortured by the dipole of excitement and frustration. It was because of them that I learned that if one makes a mistake and does not correct it, then one has made a greater mistake.

First of all, I would like to express my gratitude to my PhD supervisor, Prof. Dr. Sigmar Stricker, for trusting and supporting me in this journey. Your ambition and passion for science have been always acting as my driving force. You saw more ability within me, than I saw in myself and you helped me to bring it out. I believe that your charisma is that you always see a possible future and help one to believe it can be obtained. Thank you for the patience you have showed when I had been asking why we needed to do this and that, the countless times that you welcomed me in your office to discuss about my project and your enthusiasm to join me in the microscope room when I needed to show you an exciting finding. One of the moments I will never forget was during the BSRT assessment center where I had decided to apply for cancer-related projects. The security and the ambitious environment that I encountered, though, during my Erasmus internship with you, made me have a change of heart, as I remember telling you when I met you in the foyer. I must of course acknowledge the fact that apart of science, I enjoyed sharing with you a mutual appreciation for good whiskey and wine. I would like to sincerely thank you for igniting the scientific fire in me by challenging our inspiration through endless brainstorming sessions.

Secondly, I want to thank Dr. Ing. Sven Geißler, who co-supervised my thesis. Thank you for the trust you have showed to me from the first time we met and for always

being there for me. I am truly amazed by your ambition every time we were discussing my project. After every meeting with you, I came out with self-confidence and new ideas to take our research to a new level. You have always been walking next to me and showing me what I can do, nourishing this way my creative abilities. I am grateful for adopting me as a member of your group and thus making me feel comfortable when I was around the BCRT. Because of you, I had the chance to collaborate with numerous scientists from other institutes and thus to develop my project in ways that I would never have imagined. Sven, I would like to thank you for always having my back and for your constant need to be sure that I have everything needed.

I would also like to give a special thanks to Prof. Dr. Petra Knaus, who apart from a scientific adviser, has also been a pillar of support throughout the last years. Your kind personality in combination with your scientific passion were enough to make me decide from the first time we met that I would like to join your research group. I still believe that this happened in some way since you always were there to guide me, offering me scientific advice and providing me with your support. I will never forget the talk we had in your office when you listened to my problems, and you genuinely consoled me. Thank you for being an inspiring supervisor and a person to look up to.

I would like to offer a special thank you to my PhD mentor and friend, Dr. Taimoor H. Qazi. They say that a truly great mentor is hard to find, difficult to part with and impossible to forget. I couldn't find better words to describe the way I feel about you Taimoor. I consider myself lucky to have you assigned as my BSRT mentor. You have transmitted valuable skills to me that have helped me evolve not only as a young scientist but also as a person. Thank you for making 6.5k kilometers feel like 10.

I would like to thank the Berlin Brandenburg School of Regenerative Therapies for selecting me for a doctoral scholarship and for providing me with soft skills and network opportunities that made the quality of my work even better. Dr. Sabine Bartosch you have helped me numerous times, I will never forget our collaboration while organizing the BSRT symposium in 2018.

My access to the Max Planck institute of molecular genetics has been crucial to the completion of my PhD project. Therefore, I would like to thank everyone there who supported me. Firstly, Prof. Stefan Mundlos for providing me with access to his laboratory resources. Moreover, Ludgar Hartman and Katja Zill from the animal facility and Uta Marchfelder from the FACS facility.

None of this would have been possible without the everyday support, emotionally and practically, from my teammates, the Stricktastics. Sophie, you were the reason that I was looking forward coming to the lab every day. We have experienced and learnt so many things together. Despite the difficult moments we might had, we always found a way to end up crying and laughing with each another. Thank you for being a big sister for me, I owe you big time. Pedro thank you for all the support and the guidance you have offered me all these years. For all the hours spent troubleshooting and trying to come up with alternative solutions in the lab. I will never forget your face every time you were shocked from what I might came up saying during lunch. Aru, I still remember the first time I met you in the cryostat room. You made me feel like I met an old friend again. Thank you for all the knowledge you passed to me, scientifically or not, and for trusting me with your deepest secrets. Xiao, I miss scaring you and receiving as a payback a big hug. Thank you for bringing joy to the lab every day and for calming me down every time I was frustrated by a failure. Angelos, I did not expect that I would make a new friend before I left the lab. You made the lab feel even more a bit like home for me, thank you for all your willingness to learn and for kindly offering me help whenever needed. Zarah, thank you for the emotional support and the relaxed conversations we always had during the breaks. You guys have a group name to live up to.

In these years I met people that introduced themselves as colleagues but became close friends and part of my everyday life. Vladimir, I did not believe that one can make beasties once he is 25 years old. Thank you for all the special moments we have experienced together, the awkward jokes and the two souls that live in one body thing. A special thanks to Dr. Christian Bucher for all the hours we spent together prepping animals, labelling tubes, and isolating immune cells. A special thanks to my BSRT family, Matthias, Aline, Ana, Melanie and Lorenz, people with whom I could always discuss about science but at the same time I could talk to them about all my concerns.

The biggest source of my strength is my friends. I am blessed to be born with a lifelong partner, a sister that walks by my side all these years, supporting me and loving me genuinely. Ναταάσα, you will always be my other half. Κωνσταντίνε, I wish everyone would experience how having a true friend feels like. You have been motivating and advising me for years, you are my harshest judge but at the same time my most loyal supporter. Ευγενία, I feel like a child every time we pick up the phone and we start talking about everything that comes in our mind. Thank you for making me always

believe to myself and for being available whenever I needed something. There is a Greek saying that says “We do not choose our family members, but we do choose our friends”. A special thanks to my friends in Thessaloniki, the family that keeps on reminding me how much they love me for who I really am and not for whom they would like me to be. Αντώνη, Δήμητρα, Σοφία, Βαλεντίνα, Χριστιάννα, Τατιάνα, Σάκη and Χριστίνα, I cannot imagine my life without you guys.

A special thanks to the people that supported me throughout all these years and always believed in me. Mom thank you for always making the distance Berlin-Athens feel like zero with the long conversations we had on the phone. Thank you for teaching me the importance of investing on one’s education and for always caring for me. Dad thank you for providing me with the means to reach this point right now and for always sharing your enthusiasm with my smallest achievements. I owe a lot to my grandparents since these are the people whose eyes and voice are always filled with pure innocent love. In their eyes I have achieved even more than one would possibly have done by winning a Nobel prize. Detlef and Doris thank you for welcoming me in your family and for making Berlin feel like a second home for me. Dirk, you are the first person that made me feel good with myself, who took me by the hand and walked next to me. Thank you for making me feel safe. For putting up with all my mood swings, my absence from our home, my homesickness, and my loudness. I will never forget all the things you have done for me.

Last but not least, a special mention to my sister Σταυρούλα. My most hardcore fan, the person who is always rooting for me, the one that is there cheering for me no matter what I have done. Thank you for your trust and your sincere love. Living away from you, I learned that caring for your siblings is as if one is caring for himself. This one is for you. Αφιερωμένο.

1 Introduction

1.1 Skeletal muscle in homeostasis: from whole muscle to single fibers

1.1.1 Main architecture of skeletal muscle

Striated skeletal muscle is one of the most plastic and abundant tissues of the human body. With more than 600 muscles in our body, it comprises almost 40% of our total body weight and it accounts for almost half of whole-body protein turnover. Muscle mass depends on several factors, some of them being nutrition, secretion of hormones, exercise, injuries or diseases (Qazi et al., 2019). Reduction in body`s muscle mass leads to partial impairment in stress response and chronic diseases. The main function of skeletal muscle is to use mechanical energy in order to generate force and motion, maintain our posture and produce movement. Apart from its mechanical functions, it possesses an important metabolic role as it produces heat for our core and consumes the majority of oxygen during exercise (Frontera and Ochala, 2015).

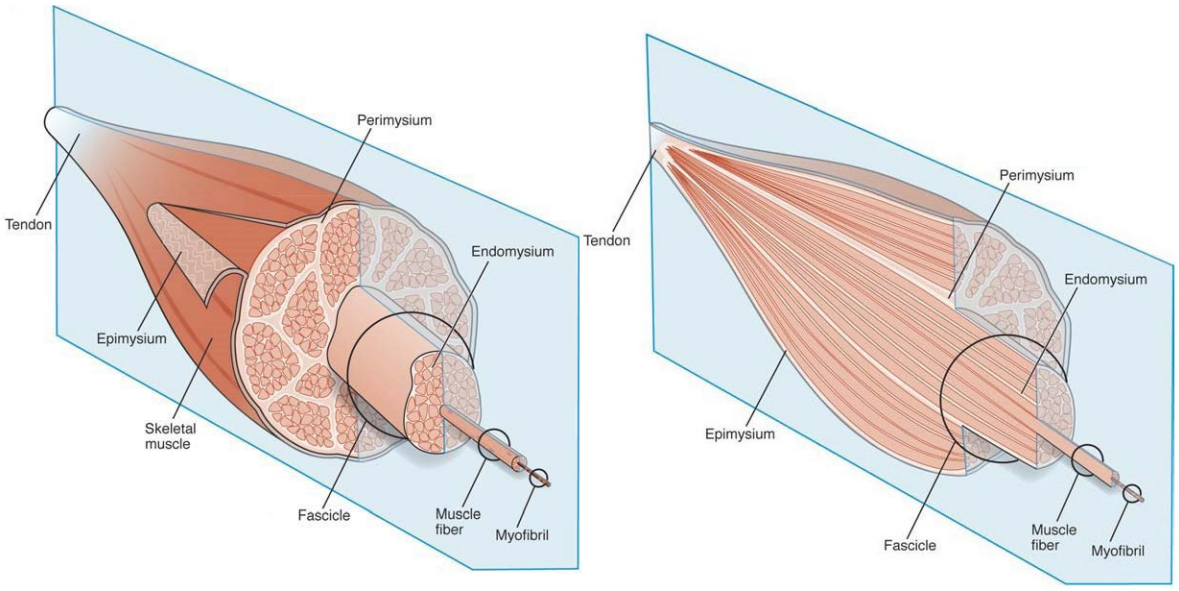

Figure 1: Skeletal muscle organization
Adult skeletal muscle generates movement transmitting contractile forces to bones through the tendons. The epimysium is a connective tissue sheath around a strand of muscle containing many fascicles. Each fascicle is wrapped in the perimysium, a process which is repeated within the fascicle with the endomysium surrounding the single muscle fibers. The cross-section on the right indicates that the perimysium can be connected with the tendon whereas the endomysium is restrained in the muscle fascicles. Figure adapted from (Gillies and Lieber, 2011).

Skeletal muscle connects bones through tendon linkages and comprises of unidirectional arranged muscle fibers (also called myofibers) and connective tissue. Each muscle is wrapped inside a layer of connective tissue called the epimysium. Fibers inside the muscle are grouped and arranged in bundles surrounded by the perimysium. In mature fibers, the myonuclei are positioned in the periphery of the fiber, underneath the sarcolemma and the adjacent layer of basal lamina, an extracellular matrix (ECM) structure made out of collagen IV and laminin (Sanes, 2003). Finally, individual fibers in a fascicle are surrounded by the endomysium, a region rich in extracellular matrix components as collagen VI and fibronectin (figure 1).

MuSCs were first described in 1961, when upon examination of frog muscle tissue with an electron microscope, these cells were observed to reside underneath the basal lamina of the muscle fiber (Mauro, 1961). For this reason, they were first called satellite cells (SCs) and this term is still used broadly in research articles. Being the stem cells of the muscle, MuSCs have been the main focus of muscle research for decades studying their regenerative potential. Adult MuSCs stay in a quiescent state during homeostasis with low turnover rates during our lifetime (Chakkalakal et al., 2012a). However, upon muscle injury MuSCs become activated and enter the cell cycle. Following the most basic adult stem cell prerequisite, MuSCs proliferate to give rise to daughter cells that either replenish and maintain the stem cell pool or differentiate into myoblasts for muscle repair (Le Grand and Rudnicki, 2007). Quiescence of MuSCs is regulated mainly by the intrinsic key transcription factors Pax7 and MyoD (Yin et al., 2013). The last years, research has also shed light on extrinsic cues that can activate MuSCs such as the composition of the ECM and the stiffness of the environment (Cosgrove et al., 2009, Trensz et al., 2016).

1.1.2 Muscle interstitium resident cells

Apart from the MuSCs, several other non-myogenic cell populations reside in the interstitial space, around the muscle fibers. These cells orchestrate various events of the muscle homeostasis and contribute to wound healing upon injury (figure 2).

Fibro-adipogenic progenitors (FAPs) have emerged as master regulators of efficient skeletal muscle stem cell function and key-players of muscle regeneration. FAPs reside in the muscle interstitium, in the space outside of the myofiber lamina. This population of muscle resident mesenchymal stromal cells were initially described to

represent the majority of PDGFRa^{+} interstitial cells and hold a bipotent differentiation ability, either to fibroblasts or adipocytes (Joe et al., 2010, Uezumi et al., 2010). Recent advanced studies have expanded the known spectrum of FAPs differentiation potential and attempt to decipher their regulatory network in muscle homeostasis but most importantly in regeneration.

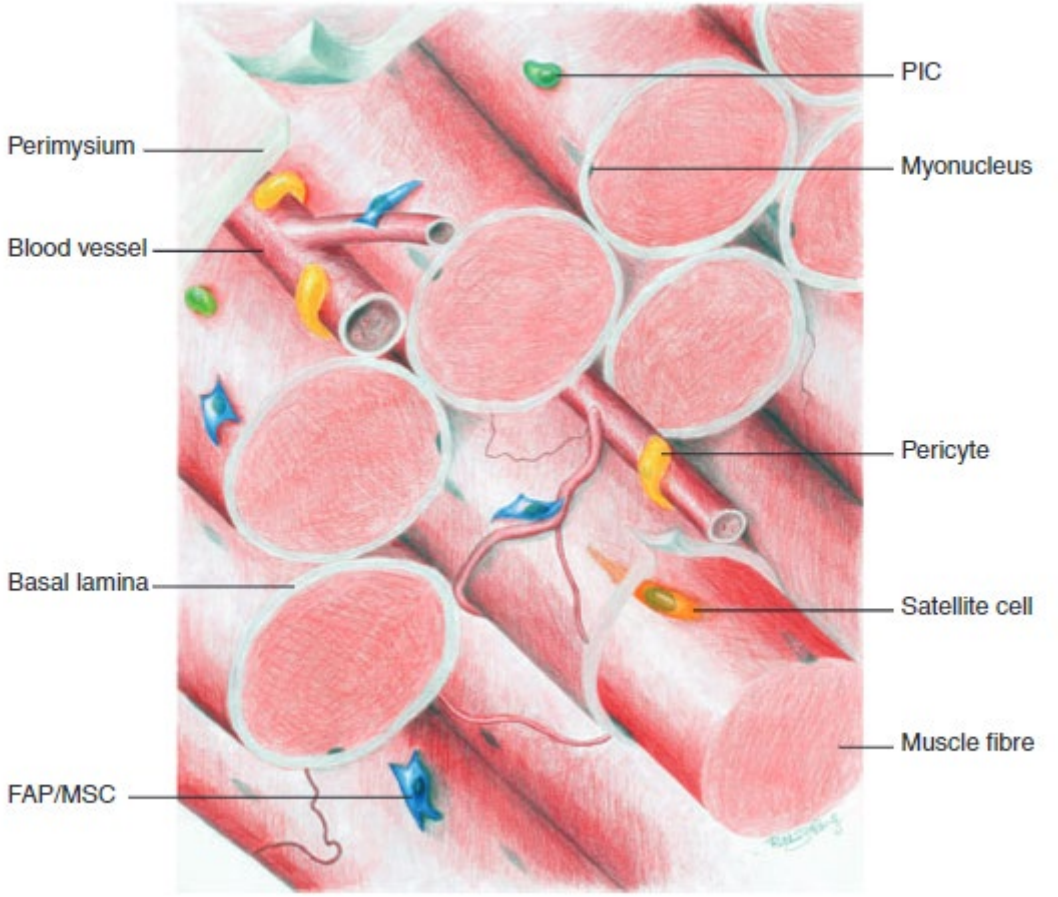

Figure 2: Diverse cell populations reside in the interstitium of the skeletal muscle
The perimysium and the endomysium consist of extracellular matrix, rich in collagens and other proteins facilitating interaction of the different cell types. Blood vessels and nerve fibers use the connective tissue network to enter the muscle. MuSCs or satellite cells are found underneath the basal lamina, pericytes are in close proximity to blood vessels whereas PICs and FAPs are located arbitrarily in the interstitial area. Figure adapted from (Judson et al., 2013).

A non-MuSC myogenic progenitor population named PICs has been identified through the expression of the stress mediator PW1 (PW1^{+} / Pax7^{-} interstitial cells) in the neonate. These cells hold an enhanced myogenic potential *in vitro*, but also *in vivo* were shown to be able to generate new myofibers when transplanted into a regenerative environment (Mitchell et al., 2010). However, PICs and MuSCs do not share a common progenitor and it is still unclear whether in adult muscle a phenotypically similar population is present (Pannérec et al., 2012).

Another population that possess myogenic potential is the pericytes which are phenotypically linked to mesoangioblasts. Isolation of pericytes showed that are negative for myogenic markers but express reliably high levels of AP (alkaline phosphatase) (Dellavalle et al., 2007). Under appropriate stimulation these cells enter myogenic differentiation *in vitro* as well as *in vivo* but only during development or in the early post-natal period. Evidence shows that a small percentage of MuSCs derive from an AP^+ progeny. Nevertheless, AP^+ cells do not have a high myogenic contribution in the adult regenerative environment (Dellavalle et al., 2011).

1.2 Introduction to Fibro-adipogenic Progenitors (FAPs)

1.2.1 Developmental origin of FAPs

The main components of adult muscle connective tissue (MCT) are collagens I and III, elastin, fibronectin and proteoglycans possibly produced by mesenchyme resident cells, the mesenchymal progenitors (lately referred as muscle fibroblasts) (Chapman et al., 2016, Chapman et al., 2017). Although, many studies try the last years to elucidate the structure and role of adult MCT, there is a lack of information about the origin and function of the developmental interstitial muscle cells (Helmbacher and Stricker, 2020, Sefton and Kardon, 2019a).

The developmental origin of muscle connective tissue cells was first described in 2000 by the pioneering work of Kardon and colleagues. They identified a mesodermal population characterized by the expression of *Tcf7l2* (then known as T cell factor 4 [TCF4]) that guides the patterning of chick muscle limbs by regulating the differentiation and localization of myogenic progenitor cells (Kardon et al., 2003). The *Tcf7l2*$^+$ cells derive from the lateral plate mesoderm but they lack myogenic potential since they do not form myotubes and are negative for classical myogenic markers (e.g. *Pax7*). However, *Tcf7l2*$^+$ cells in the MCT are critical for proper patterning of the muscle system since they create a niche that is important for determining myogenic cell differentiation in the developing limb. Moreover, these MCT progenitors secrete factors that regulate the type of limb myofibers and diaphragm muscles (Kardon et al., 2002, Kardon et al., 2003, Mathew et al., 2011).

Later studies from the Logan group helped further our understanding of the MCT progenitors contribution into muscle morphogenesis. Conditional deletion of the T-box transcriptions, Tbx4 and Tbx5, demonstrated their importance in muscle and tendon formation during development. Intriguingly, genetic deletion of *Tbx5* in the myogenic lineage did not affect the correct position of myoblasts but deletion of *Tbx4* and *Tbx5* in the MCT cells resulted in perturbation of MCT organization and thus to defects in limb muscle patterning. Moreover, although absence of *Tbx4/5* expression did not affect expression of *Tcf7l2*$^{+}$ but a defect in the spatiotemporal distribution of *Tcf7l2*$^{+}$ cells (Hasson et al., 2010). Another set of genes that code transcriptions factors responsible for positional information in development, are the Hox genes. Hox11 genes determine the proximal distal axis of the limb musculoskeletal system. *Hoxa11* is amongst other cells also expressed exclusively by the *Tcf7l2*$^{+}$ cells at E14.5 (E = embryonic day) but it is not expressed in bone or myogenic cells. However, deletion of *Hoxa11/Hoxd11* resulted in, apart from severe bone defects, interruption of correct muscle and tendon regionalization (Swinehart et al., 2013).

Recently another marker expressed by MCT cells was identified, the Odd skipped related 1, a transcription factor that its expression is also crucial for generating a beneficial microenvironment for limb muscle patterning (Vallecillo-Garcia et al., 2017). Vallecillo-Garcia and colleagues showed that these cells are the main source of developmental ECM in limb muscles and are in a great extent PDGFRa^{+} progenitors, thus embryonic-like FAPs. The significance of *Osr1* expression in MCT cells in development and in adults FAPs will be further discussed in following sections.

1.2.2 Differentiation potential of FAPs

Adult FAP were initially thought to have a bipotent ability to differentiate into fibroblasts or adipocytes, which explains the name fibro-adipogenic progenitor cells (figure 3) (Joe et al., 2010, Uezumi et al., 2010). *In vitro* FAPs can spontaneously give rise to these two types of cells. Induction of their fibrogenic potential can be achieved with TGFβ stimulation whereas promotion of their adipogenic differentiation has been described in a medium containing insulin and dexamethasone (Marinkovic et al., 2019, Uezumi et al., 2011). Perilipin^{+} adipocytes that originate from *PDGFRa*$^{+}$ FAPs have been observed upon glycerol or cardiotoxin induced injuries of PDGFRa-creERT Rosa26^{EYFP} reporter mice (Kopinke et al., 2017). Furthermore, lineage tracing studies

with the Tcf7l2$^{CreERT2/+}$ R26R$^{mTmG/+}$ reporter line provided a confirmation that *Tfc7l2*$^{+}$ FAPs differentiate into fibroblasts expressing the marker a-smooth muscle actin (aSMA) (Murphy et al., 2011).

However, the knowledge about the differentiational capacity of FAPs has been expanded the last years revealing an advance multipotency. Under treatment with the bone morphogenic proteins BMP-2/7/9, FAPs can differentiate into osteocytes or chondrocytes. *In vivo* intramuscular injection with BMP2/matrigel mix together with FAPs demonstrated that FAPs contribute to bone and cartilage formation. Moreover, lineage tracing experiments in BMP2 induced heterotopic ossification *in vivo* showed that the majority of osteogenic cells in the lesions are of FAPs progeny (Eisner et al., 2020, Lees-Shepard et al., 2018, Wosczyna et al., 2019). In the last five years, it has been proven that FAPs are the main muscle resident cell population that contributes to the formation of heterotopic lesions in FOP patients (fibrodysplasia ossificans progressive). The role of FAPs in rare connective tissue diseases will be further discussed later.

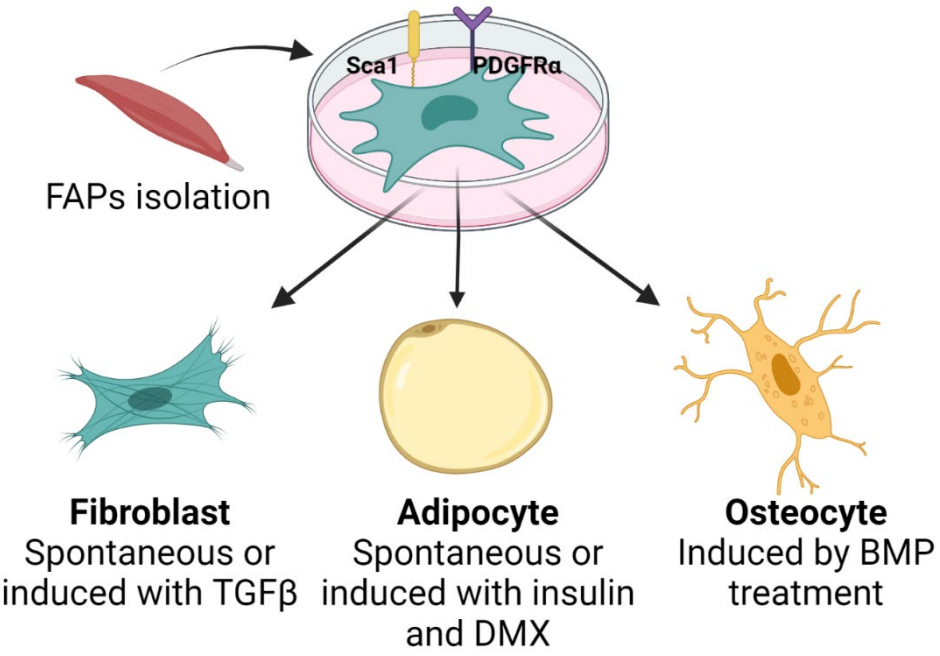

Figure 3: Differentiation potential of FAPs *in vitro*
FAPs are multipotent mesenchymal stem cells expressing the stem cell antigen-1 (Sca1) and the platelet derived growth factor α (PDGFRα). FAPs can differentiate spontaneously into fibroblasts or adipocytes but they can also differentiate into osteocytes under specific conditions. Image created with BioRender.com.

1.2.3 Heterogeneity and role of FAPs in muscle homeostasis

The evolution of scRNA seq technique in the last years shed light in the cellular heterogeneity of the FAP population in the homeostatic muscle. First, the study of Scott and colleagues in 2019 showed that there are two sub/populations of FAPs in the uninjured muscle, one that expresses mainly genes associated to the ECM (e.g. *Col4a1, Col6a1, Podn* etc.) and one rich in genes related to cell signaling pathways (e.g. Sfrp4, Dpp4, Tgfbr2 etc.) (Scott et al., 2019) . One year later the study of Oprescu and colleagues verified also the subdivision of quiescent FAPs in two groups, the *Cxcl14*$^{+}$ FAPs responsible for ECM gene expression (*Col4a1, Col6a1, Smoc2*) and the *Dpp4*$^{+}$ FAPs expressing signaling genes involved in several biological processes (*Igfbp5, Wnt2, Sema3c* etc.) (Oprescu et al., 2020). A third study identified also two different FAP groups, the *Tek*$^{+}$ (encoding for Tie2), rich in the uninjured muscle and expressing genes involved in Wnt and BMP signaling, and the smaller in size *Vcam+* FAPs. The *Vcam*$^{+}$ population exhibits a strong pro-fibrogenic profile as it mainly expresses fibrotic genes (e.g. *Acta2, Lox, Timp1* etc.) and is highly enriched upon muscle injury (Malecova et al., 2018). The aforementioned subdivision of resting FAPs was also validated in a more recent study using the same markers, where the *Vcam*$^{+}$ population was further subdivided into a third cluster marked by the expression of *Thbs4* (thrombospondin-4) and *Fbln7* (fibulin-7). These cells show an increased expression of genes related to the ECM formation or metallopeptidases activity (Camps et al., 2020). The authors attributed possible differences in the number of FAPs populations or the density of their clusters to the different purification techniques and the performed bioinformatic analysis. Nevertheless, these studies managed to highlight the heterogeneity of FAPs prior to injury and identify common gene signatures.

Following these observations, a question that arises is what is the role of FAPs in muscle homeostasis by the time that these cells proliferate mainly upon injury? FAPs though are the largest mononuclear cell population in the uninjured muscle and *Hic1* (hypermethylated in cancer-1) regulates their quiescence (Scott et al., 2019). *Hic1* deficiency resulted in FAPs spontaneous cell cycle entry and in their expansion. The importance of FAPs presence in homeostatic muscle has been reported in different animal models where the FAP population had been depleted. These animals exhibit reduction of muscle mass, reduced myofiber size, defected muscle force and muscle atrophy even in the absence of injury. Long term effects of reduction in the population

of MuSCs was also observed (Uezumi et al., 2010, Wosczyna et al., 2019, Roberts et al., 2013b, Uezumi et al., 2021). In sum, FAPs are essential also in adult homeostasis for the MuSCs population and healthy myofiber growth. Similar to the defects of the FAP-like cells absence during embryonic development discussed in the previous subsection, FAPs themselves might not be participating in myogenesis but they secrete essential factors inducing this procedure.

1.3 From muscle injury to regeneration

1.3.1 Macrophages and the inflammatory phase initiation

Acute sterile muscle injuries result in an orchestrated inflammatory response progressing towards the removal of dead cells, coordination of the regeneration and finally reestablishment of tissue homeostasis. The first phase of inflammation is the vascular one, where vasodilatation takes place, followed by increased blood flow and vascular permeability, leading at its end to edema formation. The cellular phase follows next, where leukocytes extravasate from blood and traffic towards the inflamed area (Sugimoto et al., 2019). Neutrophils are the first immune cells that arrive to the trauma region, which have very short life and whose function is to mount the proinflammatory response so that monocytes are recruited (Chazaud, 2020) (figure 4). While tissue resident macrophages (TRM) are described in many studies, in muscle research literature there is an ongoing debate. Some support the presence of TRM (Theret et al., 2022) while others report that there is no evidence up to now that they exist in skeletal muscle (Chazaud, 2020). Thus, the indispensable Ccl2/Ccr2 interaction axis is one of the first described not only in muscle but also in liver and heart, to induce monocyte infiltration (Lu et al., 2011a, Kaikita et al., 2004). Once extravasated, blood monocytes will differentiate into macrophages and lose *Ccr2* expression (monocyte-derived macrophages). These cells are considered to be key regulators of the early mononuclear cell infiltration and act to orchestrate the breakdown of the destroyed tissue and to clear cellular debris via phagocytosis (Tidball, 2011, Sass et al., 2018). The last years, the crosstalk and interaction between macrophages and MuSCs/ FAPs has been extensively studied and is known now to be an essential mediator of the cellular response. Although the phenotypical transition between macrophages cannot

be represented by distinct phenotypes but more by continuum, the terminology M1 and M2 will be used from this point on, for the sake of simplicity (Novak and Koh, 2013).

The proinflammatory M1 macrophages are amongst the first cells to appear in the regenerative milieu. These cells are the main producers of proinflammatory cytokines such as ADAMTS1 (A disintegrin and metalloproteinase with thrombospondin motifs 1), IFNγ (interferon gamma), IGF1 (insulin growth factor 1), IL6 (interleukin 6), IL1β (interleukin 1β) and TNFα (tumor necrosis factor α) (Theret et al., 2021). Thereby, proliferation of MuSCs is induced in this environment while at the same time their differentiation and fusion are inhibited (Saclier et al., 2013a, Tidball and Villalta, 2010). Moreover, the study of Lemos and colleagues in 2015 showed that during regeneration an early TNFα-rich environment, secreted by the M1 macrophages, is essential to restrain FAPs expansion and their later transition into fibrocytes (Lemos et al., 2015). In sum, the main events of this early proinflammatory phase is the scavenger activity of immune cells leading to the phagocytosis of debris and MuSCs proliferation.

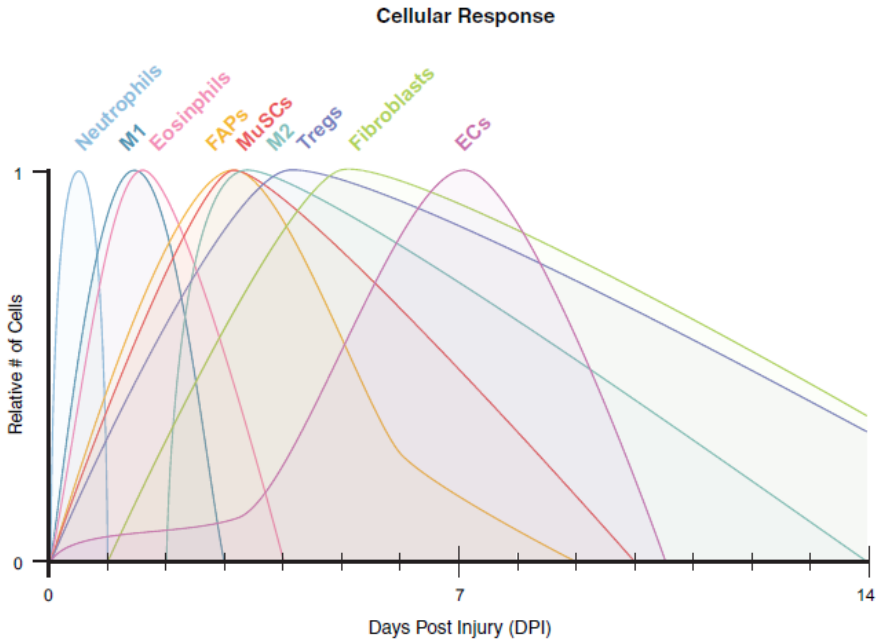

Figure 4: Expansion of cellular populations to skeletal muscle injury
Upon acute muscle injury there is an initial expansion of several cell populations in the first two weeks of the regenerative process. The expansion of each cell population might be depended on the injury technique that was used and on the assay that calculated the cell numbers. Tregs: regulatory T cells, ECs: endothelial cells. Figure adapted from (Wosczyna and Rando, 2018).

1.3.2 Activation of MuSCs

Adult MuSCs reside in a quiescent state in the homeostatic skeletal muscle. However, upon muscle injury they get rapidly activated, aiding the recovery process through proliferation and differentiation (figure 4). Several MuSCs depletion studies have demonstrated the pivotal role of these cells in muscle regeneration. Acute muscle injury on MuSCs depleted mice revealed their reduced myogenic potential, resulting in enhanced damage and muscle tissue loss (Sambasivan et al., 2011, Fry et al., 2015, Lepper et al., 2011).

Although MuSCs are a heterogeneous population in terms of function diversity and differentiation status, they can be identified through the expression of a genetic marker set (Biressi and Rando, 2010). The expression of *Pax7* (paired box protein 7) has been used for many years as the definite marker for MuSCs in a quiescent state as well as the MRFs (muscle regulatory factors) *MyoD*, *Myf5* and *Myogenin* for the identification of their further states (figure 5) (Seale et al., 2000, Gros et al., 2005). *Pax7* is essential for MuSCs survival and is expressed by all states of MuSCs. Therefore, MuSCs in quiescence express *Pax7* but lack the expression of the key transcription factor *MyoD*. Upon muscle injury, proliferative MuSCs express both *Pax7* and *MyoD* and are now primed to further differentiate into myogenic progenitors that begin to express *Myf5* (also called myoblasts) or they will return to quiescence by downregulating the expression of *MyoD*. In sum, expression of *Pax7* gradually decreases in the myogenic progenitors as they differentiate into myocytes and begin to fuse in order to generate multi-nucleated myofibers (Relaix and Zammit, 2012).

The balance of MuSCs population after skeletal muscle injury is maintained with the partial reversion of activated MuSCs to the quiescent state. This maintenance is governed by several mechanisms (Kuang et al., 2007). One of them is the upregulation of *Spry1*, a receptor tyrosine kinase (RKT) signaling inhibitor, in reverted quiescent MuSCs. RKT signaling is crucial to MuSCs for their proliferation and differentiation, therefore disruption of *Spry1* prevents them from returning to quiescence and results in a MuSC pool reduction in homeostasis (Shea et al., 2010). One more critical regulator of MuSCs quiescence suppressing their proliferation is the Notch signaling pathway. It has been shown that disruptions in Notch signaling result in MuSCs escaping quiescence and beginning to express proliferation and differentiation markers even in the absence of injury or stimulus (Mourikis and Tajbakhsh, 2014, Mourikis et

al., 2012). However, apart from the cell autonomous mechanisms in MuSCs that regulate their function, exit of quiescence and MuSCs differentiation is regulated through cellular interactions in the injured milieu and the structure of the regenerative niche (Yamakawa et al., 2020). Direct effects on myogenesis have been also reported by M1 macrophages (described before), FAPs, M2 macrophages, the extracellular matrix components and the stiffness of the microenvironment that will be further discussed in following sections.

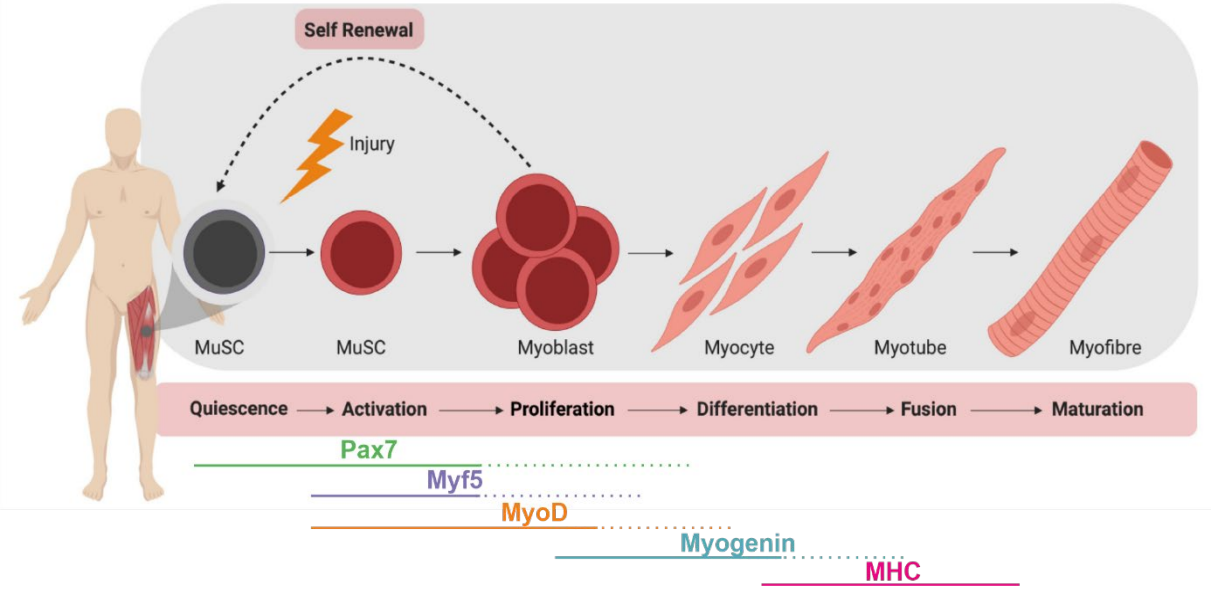

Figure 5: Progression of myogenic lineage and expression profile of muscle regulatory factors
MuSCs become activated upon injury, start to proliferate and generate myoblasts which will differentiate into myocytes. Finally, these will fuse into myotubes and maturate into myofibers, the skeletal muscle contractive unit. The dynamic expression of the myogenic regulatory factors is depicted in the lower part. Figure modified from (Nguyen et al., 2019). Image created with BioRender.com.

1.3.3 Dynamic expansion of FAPs

Immediately upon skeletal muscle injury, FAPs enter the cell cycle, proliferate and expand rapidly even faster than the MuSC population leading to an elevated ratio of FAPs/ MuSCs in the first few days (figure 4). In 2015 the study of Lemos and colleagues showed that FAPs numbers reach their peak at 3-4 days post myotoxin induced damage and from then on excess FAPs undergo apoptosis (figure 6) (Lemos et al., 2015). This increase has been reported that is strongly dependent on the type and the severity of the injury method (Lemos et al., 2015, Uezumi et al., 2011). FAPs are essential for the process of regeneration and that has been verified by studies that used conditional ablation experiments. Targeted depletion of FAPs induced by tamoxifen injection on PDGFRa CreER-DTX mice did not alter myofiber density in uninjured muscles. However, it resulted in significantly reduced myofiber cross-

sectional area. Moreover, a significant deficit in regeneration was observed upon intramuscular $BaCl_2$ injection with the injured muscled manifesting prolonged necrosis. This defect was rescued when healthy FAPs from wild type mice were transplanted into the injured muscles of the ablated mice, underlining the pivotal role of FAPs in skeletal muscle regeneration (Uezumi et al., 2021, Wosczyna et al., 2019).

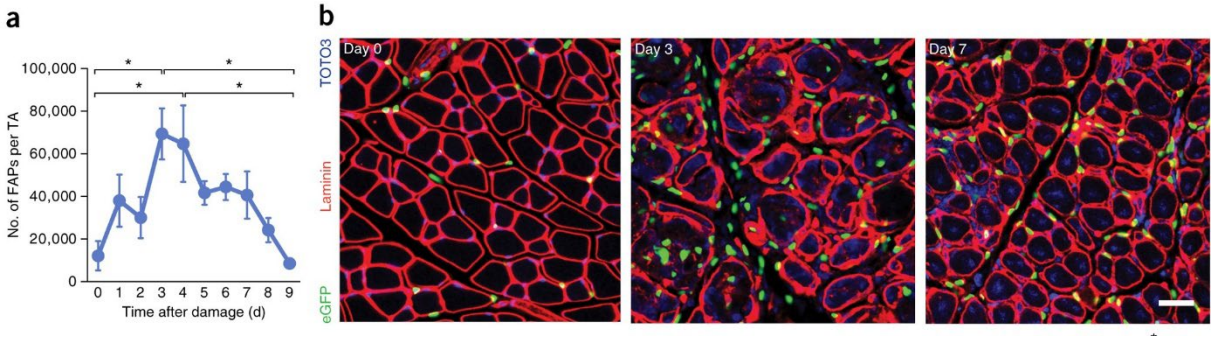

Figure 6: Dynamic expansion of the FAPs population after acute muscle injury
(a) FAPs numbers quantifications in the injured Tibialis anterior (T.A.) muscle of WT mice. (b) Immunofluorescence images of $PDGFRa^{GFP}$ reporter mice showing increase number of FAPs (GFP cells) upon injury in the interstitial space. Figure adapted from (Lemos et al., 2015).

In the last years advanced single cell RNA seq studies have revealed the heterogeneity of FAPs populations not only in homeostasis (described before) but also during regeneration. At 2 days post injury, FAP clusters are shown to be rich in cytokine secretion (such as Ccl7, CxCl5 and Ccl2) which as referred before are essential for the infiltration of neutrophils and monocytes to the site of injury (De Micheli et al., 2020a, Oprescu et al., 2020). At the same timepoint, another study showed that there is an expansion of the $Tie2^{low}$ $Vcam1^{high}$ FAPs subpopulation which mainly express fibrogenic genes (Malecova et al., 2018). At 5 days post injury genes related to the ECM secretion (*Col3a1*, *Col11a1*, *Tnc* and *Fn2*) are upregulated in a $Wisp1^{+}$ FAP population while at around day 10 post injury the expression profile of FAPs assimilates the one described in the uninjured muscles, expressing again markers like *CD34* and *Spry1*. Finally, at 21 days post injury almost all FAPs express the transcription factor of Osr1, which has been shown to be upregulated in FAPs upon injury (Stumm et al., 2018), indicating that these cells did not enter back to quiescence up to that timepoint (Oprescu et al., 2020).

The dynamic changes in FAPs population in muscle regeneration must be a procedure regulated by both intrinsic and extrinsic mechanisms. One intrinsic mechanism was described in the study of Mueller and colleagues in 2016, where they show that different transcriptional variants of *PDGFRa* are expressed by FAPs. One of these includes an intronic variant coding for a truncated kinase domain, which is being

upregulated during regeneration and therefore, acts as a decoy receptor to inhibit PDGF signaling and prevents FAPs expansion (Mueller et al., 2016). Another intrinsic mechanism of FAPs function is the generation of cilia by pre-adipogenic FAPs. Genetic removal of FAP ciliation, over-activated the Hedgehog signaling and inhibited adipogenesis upon glycerol induced muscle injury (Kopinke et al., 2017). Moreover, the beneficial regulation of FAPs cell fate decision and numbers by the retinoic acid signaling has been recently described. Retinoic acid FAPs treatment was shown to induce cells proliferation and to maintain them in an undifferentiated state. On the other hand, loss of signaling led to increased adipogenic differentiation, expansion of the population due to decreased apoptosis and delayed their clearance upon injury (Zhao et al., 2020).

Not much is known regarding intrinsic mechanisms that regulate FAPs activity; however, extrinsic cues have also a definite impact on FAPs function. It is reported that different injury models for instance can modulate FAPs differentiation. Cardiotoxin injured muscles do not exhibit normally any fat infiltration whereas induced adipogenesis is observed in glycerol injured muscles. Transplantation of FAPs derived from muscle injured with cardiotoxin to one injured with glycerol showed that FAPs favor adipogenic differentiation, while fat infiltration did not occur when the transplantation approach was reversed (Uezumi et al., 2010). That was the first indication that cell fate in FAPs might not be a cell autonomous regulated procedure but may also be regulated by the extrinsic environment, including cell-cell interactions. Therefore, the cellular crosstalk of FAPs in the regenerative milieu with MuSCs and macrophages will be further discussed in the following section.

1.3.4 Resolution of inflammation by anti-inflammatory macrophages

Efferocytosis is an essential procedure in the resolution of inflammation. This is a phagocytocic process of apoptotic and necrotic cells, comprising of two important steps: rewiring of macrophages inflammatory status and cleansing of the injured tissue area to permit efficient healing (Doran et al., 2020). Following the initial phase of M1 macrophage infiltration and the subsequent proliferation of MuSCs and FAPs (figure 4), the anti-inflammatory M2 macrophages are now the most prominent macrophage phenotype in the injured tissue (figure 7). In 2012 the study of Deng and colleagues showed that the phenotypical switch of macrophages in skeletal muscle regeneration

is regulated by the IL-10 (interleukin 10) and this transition is essential to efficient healing of the trauma (Deng et al., 2012). In case this procedure becomes delayed and the M1 pro-inflammatory phase is prolonged, then myogenesis is impaired due to the rich inflammatory environment. This event underlines the importance of the on-time phenotypical switch of macrophages. Therefore, the presence of M2 macrophages

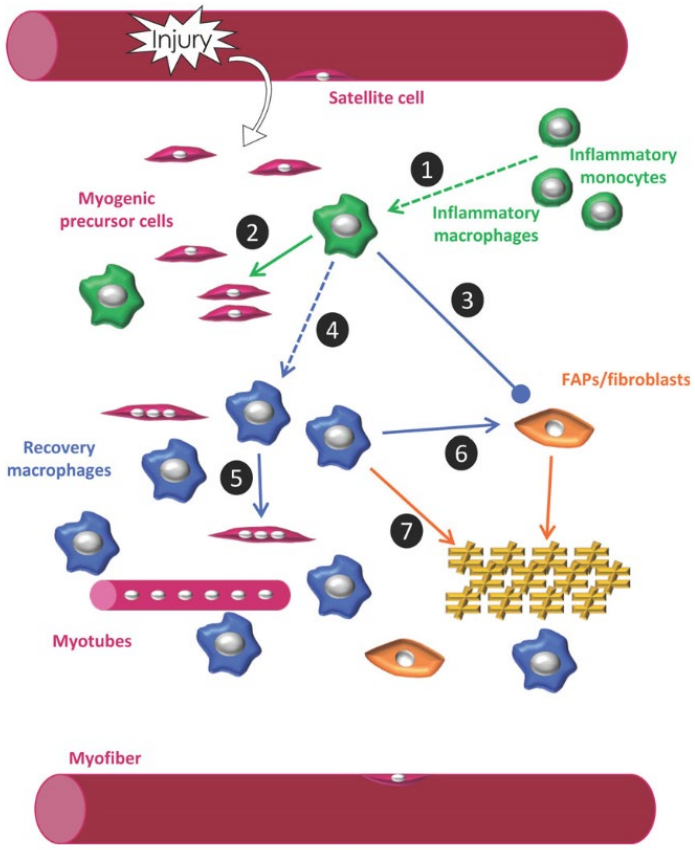

Figure 7: Roles of macrophages in skeletal muscle regeneration
First circulating monocytes enter the injured tissue and concert into M1 pro-inflammatory macrophages (1). These promote proliferation of MuSCs (2) while limiting FAPs expansion (3). The phenotypic transition from a pro- to an M2 anti-inflammatory macrophage follows after (4). Anti-inflammatory macrophages secrete cytokines that induce MuSCs differentiation while stimulating the fibrogenic differentiation of FAPs (6) which together with the M2 macrophages secrete components that build the ECM (7). Figure adapted from (Juban and Chazaud, 2017).

mark the initiation of the restorative phase and they induce myogenesis through the secretion of high IGF-1 (insulin like growth factor 1) levels, a factor shown to be beneficial for MuSCs proliferation (Tonkin et al., 2015). Moreover, there is an immediate transition from a TNFα to a TGFβ rich environment, since M2 macrophages secrete lower levels of TNFα and higher levels of TGFβ. This way fibrotic tissue formation is promoted (Saclier et al., 2013b, Lemos et al., 2015). M2 macrophages are also the predominant source of GDF3 (growth differentiation factor 3) in the regenerating muscle, a factor who has a specific action on the last step of myogenesis,

inducing multinucleated structure fusion and thus, fostering myogenesis (Juban and Chazaud, 2017, Varga et al., 2016). Although M2 macrophages are often referred to as the recovery macrophages, a prolonged anti-inflammatory phase is not beneficial and has been reported to have the opposite effects by inducing fibrosis. The accumulation of M2 macrophages in the muscle is also believed to be the reason for abnormal fibrosis in the aged muscles. Many studies have assessed the regenerative capacity of injured muscle in macrophage depleted lines. Increased accumulation of inflammatory cytokines and absence of myogenic beneficial factors have been reported, that lead to decreased myogenesis and accumulation of fibrotic tissue (Xiao et al., 2016, Liu et al., 2017). However, up to now targeted depletion of the M1 or M2 population has not been achieved and therefore the aforementioned defects result from the total ablation of macrophages in the whole organism. That adds up the necessity of a system where the effect would be localized only in the tissue of interest in order to exclude the possibility of a systemic defect.

1.3.5 Additional inflammatory cells with potential contribution

Macrophages have been the main immune population in the skeletal muscle regeneration research, but attention has also been paid to other cells in the recent years. More specifically, eosinophils and a subtype of Tcell called regulatory Tcells (Treg) have been studied for their pro-regenerative potential. Eosinophils expand at the same time with the M1 macrophages (figure 4) and are the main producers of IL-4 (interleukin 4) which was shown to promote FAPs proliferation while at the same time inhibiting their adipogenic potential. Intriguingly, this eosinophil dependent fate transition of FAPs does not only support myogenesis through shaping a beneficial niche for MuSCs but also through a phagocytic ability that FAPs gain in order to clear necrotic debris (Heredia et al., 2013). Tregs population reaches a peak at 4 days post injury (figure 4) and they co-exist in the regenerative milieu simultaneously with proliferative FAPs and MuSCs (Schiaffino et al., 2017). It has been shown that IL-33 (interleukin 33) regulates Treg homeostasis in young mice and has been linked with their recruitment in the injured area. Interestingly, FAPs are the main producers of IL-33 in the regenerative muscle and therefore act as key regulator to Tregs recruitment which ameliorate muscle healing (Cayrol and Girard, 2014, Kuswanto et al., 2016). At last, neutrophils are the first immune cell population to infiltrate muscle upon injury.

They generate reactive oxygen species in order to form the early necrotic environment and the following clearance of necrotic tissue (Tidball and Villalta, 2010, Butterfield et al., 2006). As it was also described in the beginning of this section, the initial wave of infiltrated neutrophils secretes pro-inflammatory cytokines with the purpose of recruiting monocytes and thereby macrophages. Although it is known that the specific pro-inflammatory cytokines induce MuSCs proliferation, their function was studied at a later point when they are produced by monocytes and M1 macrophages (Yang and Hu, 2018, Tidball and Villalta, 2010). Thereby, the impact of neutrophils in MuSCs regenerative dynamics is not yet described.

1.4 Cellular crosstalk of FAPs in regenerating muscle

1.4.1 FAPs and immune cells

The rapid inflammatory response that follows acute muscle injury mainly consists of polymorphonuclear leucocytes, monocytes and lymphocytes, the population density of which reaches the maximum together with FAPs (figure 4). Therefore, FAPs reside in an environment rich in immune cells and regulate the function and accumulation of monocytes and neutrophils by secreting chemokines like *Ccl2* and *Ccl7* (figure 8) (De Micheli et al., 2020a). Development of the interactome network using single cell RNA seq data verified that FAPs exhibit strong ligand-receptors interactions with immune cells (Oprescu et al., 2020). Until today there are only a couple of studies that show a FAP sourced defect on immune cells populations. As previously mentioned, one study showed that depletion of FAPs by tamoxifen injection resulted in reduced infiltration of $CD45^{+}$ cells upon injury and another one showed that IL33 derived from FAPs is essential for Treg recruitment and thus for efficient myogenesis (Uezumi et al., 2021, Wosczyna et al., 2019, Kuswanto et al., 2016, Cayrol and Girard, 2014). Furthermore, the transcriptional profile of one FAP subpopulation was shown to regulate canonical pathways related to dendritic cell maturation, which was suggested to play a role in the phenotypical switch of macrophages (Malecova et al., 2018). Finally, proliferating FAPs express IL-10 (interleukin 10), a factor which is known to promote the anti-inflammatory M2 phenotype (Lemos et al., 2012).

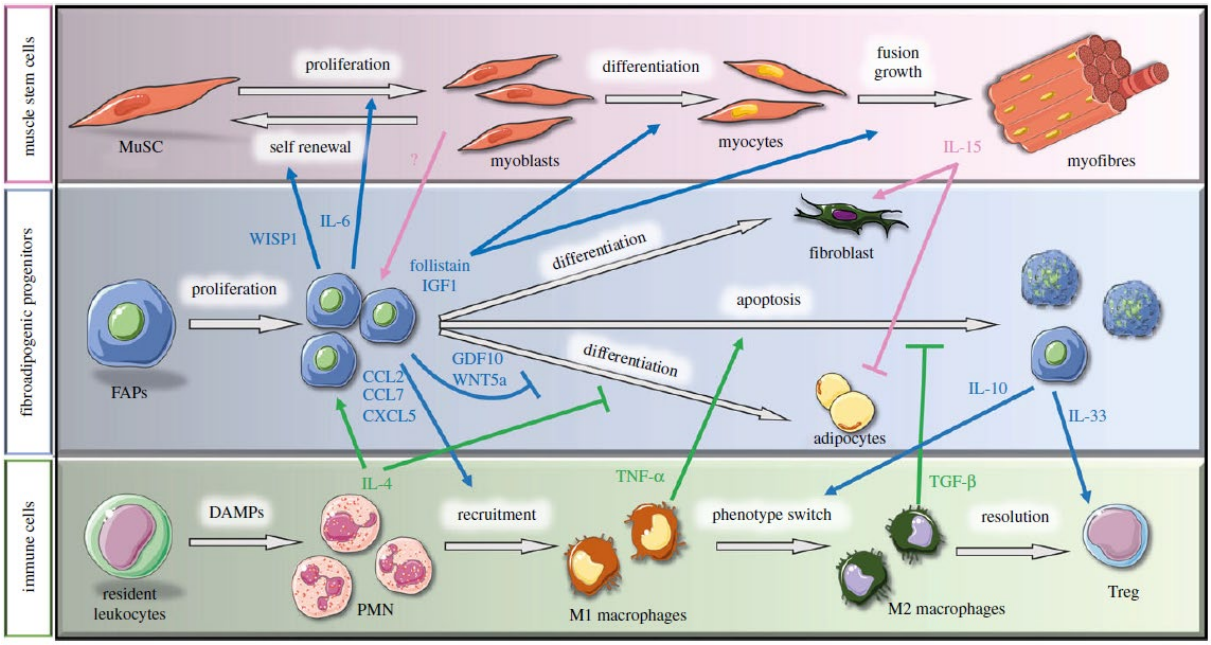

Figure 8: Cellular crosstalks in the regenerative milieu
Schematic representation of the known interactions between MuSCs (pink), FAPs (blue) and immune cells (green). Arrows represent molecules secreted by one cell population and inducing/ inhibiting functions of another one. (DAMPs, damage-associated molecular pattern; PMN, polymorphonuclear cells). Figure adapted from (Molina et al., 2021).

Several inflammatory cell populations regulate also the function of FAPs, attributing a bilateral character to this interaction. Amongst the polymorphonuclear cells that infiltrate the injured regions are the eosinophils. These cells are known to secrete IL-4 regulating FAPs proliferation, differentiation and phagocytosis (Heredia et al., 2013). The effect of macrophages on FAPs regulation has been studied extensively the last years. Depletion of macrophages, in one study using clodronate (bisphosphonate that induces macrophage apoptosis) prior to muscle injury and in a second one using a Ccr2 mutant mouse line (inhibition of monocyte infiltration), resulted in persistence of the FAPs pool and increased fibro-fatty infiltrations (Marinkovic et al., 2019, Lemos et al., 2015). These effects derive from deregulated apoptosis and not from FAPs proliferation, since TNFα secreted by M1 macrophages has been shown to be the mediator in FAPs apoptosis (Lemos et al., 2015). In addition, M1 macrophages secrete IL-1α/β that inhibits adipogenic differentiation of FAPs (Vumbaca et al., 2021). During the progress of regeneration, TGFβ competes with TNFα inducing FAPs survival and fibrogenic differentiation. The factor TGFβ has been also recently shown to downregulate the expression of *PDGFRa* and *Tcf47l2* in FAPs as well as their downstream signaling pathways (Contreras et al., 2019a, Contreras et al., 2019b). Lastly, *in vitro* experiments revealed that FAPs adipogenic differentiation was inhibited when FAPs were cultured in conditioned medium (CM) from IL-1β induced M1

macrophages while this effect was reversed when they were cultured in CM from IL-4 stimulated M2 macrophages (Moratal et al., 2018). In sum, the phenotypic switch of macrophages should be tightly regulated in order to restrain FAPs excessive accumulation and fibrogenic differentiation, and to aid the return into homeostasis.

1.4.2 Interaction of FAPs with MuSCs

Since the first description of FAPs in 2010 it was noticed that the ratio of FAPs/ MuSCs increases in the first days of regeneration, indicating a potential important role of FAPs to myogenesis (Joe et al., 2010, Petrilli et al., 2020). Indeed, a reduction both in the myofiber size and in the myogenic pool have been observed not only in the FAPs depleted muscles of the PDGFRα Cre ER-DTX mouse line but also in Nilotinib treated mice. Nilotinib is a kinase inhibitor that promotes FAPs apoptosis and reduces FAPs numbers in the injured muscle (Lemos et al., 2015, Wosczyna et al., 2019). The beneficial effect of FAPs to myogenesis has been also proved *in vitro* where direct but also indirect (*Tcf7l2*$^{+}$ cells) co-culture experiments with myoblasts showed induced differentiation and increased size of fused myofibers (Mathew et al., 2011, Uezumi et al., 2010). Moreover, *in vivo* deletion of *Tcf7l2*$^{+}$ fibroblasts in neonatal mice resulted in an elevated expression of developmental myosin heavy chain, indicating a delay in the switch between fetal and adult muscle (Mathew et al., 2011).

One way that FAPs regulate myogenesis is through the secretion of a cytokine cocktail, being a predominant source of paracrine signaling (figure 8). The myokine IL-6 (interleukin 6) is under homeostatic condition secreted in the myofibers during exercise. During regeneration FAPs are the main IL-6 composers, secreting ten times higher concentrations of it, promoting thus MuSCs proliferation and differentiation (Serrano and Muñoz-Cánoves, 2017, Tierney et al., 2014). Another factor that aids myogenesis and is secreted by FAPs is WISP1 (WNT1-inducible-signaling pathway protein), which induces MuSCs asymmetric divisions, fostering their expansion and myogenic commitment (Lukjanenko et al., 2019). Moreover, FAPs secrete IGF-1 that promotes advanced skeletal muscle growth due to the activation of the Akt signaling pathway (Schiaffino and Mammucari, 2011). Finally, follistatin is an activin-binding protein acting as an antagonist of myostatin, a muscle growth inhibitor. In the regenerative milieu FAPs are the main source of follistatin and therefore myoblastic

fusion into large multinucleated tubes is enhanced (Reggio et al., 2020, Mozzetta et al., 2013).

Multiple studies have though studied FAPs/MuSCs interaction from the opposite side, revealing that MuSCs regulate as well FAPs function. Depletion of the MuSCs pool using a Pax7 CreERT2-DTX mouse model, led to delayed expansion of *Tcf7l2*$^{+}$ FAPs during muscle regeneration. Moreover it resulted in FAPs prolonged accumulation and increased fibrotic deposition at later timepoints (Murphy et al., 2011). MuSCs can also regulate the extracellular matrix production by FAPs. Collagen secretion by *Tcf7l2*$^{+}$ FAPs was inhibited via the miR206, found in the exosomes secreted by MuSCs (Fry et al., 2017). CM derived from MuSCs was also shown to have a beneficial effect on FAPs proliferation, since it had been found to be rich in betabellulin and epidermal growth factor (EGFR), two ligands of the EGFR receptor (Vumbaca et al., 2021). Interestingly, another study showed that CM derived from differentiated myotubes inhibits FAPs adipogenesis while it favors their fibrogenic differentiation (Moratal et al., 2019). Another myokine secreted this time by MuSCs upon injury and not by FAPs, is IL-15 (interleukin 15) which regulates FAPs main functions. Administration of IL-15 was shown to have a pro-proliferative effect on FAPs proliferation both *in vivo* and *in vitro* through the regulation of the Jak-Stat pathway. Inhibition of this pathway resulted in defected FAPs proliferation and inhibited fibrotic tissue formation after injury. Moreover, IL-15 regulates FAPs fate decision by blocking their adipogenic differentiation. In sum, the myokine IL-15 affects FAPs proliferation inducing their fibrogenic while preventing their adipogenic potential (Kang et al., 2018, Li et al., 2014, Quinn et al., 2005).

1.4.3 Crosstalk of FAPs and other cells in the interstitium

The recent study of Camps and colleagues in 2020 validated the presence of different progenitor populations in muscle by performing single cell RNAseq analysis. They checked the clusters for key markers expression: *Sca1* for FAPs, *Pdgfra* for mesenchymal progenitors, *Alpl* for mesoangioblasts/ pericytes and *Peg3* or *Pw1* for PICs. These cells were separated in three clusters, two of them expressing high levels of adipogenic related genes and one cluster expressing *CD142*. The *CD142*$^{+}$ cells possess a strong fibrogenic profile and when co-cultured together with the *CD142*$^{-}$ cells inhibited their adipogenic differentiation (Camps et al., 2020). Moreover, in skeletal

muscles the main producers of Wnt protein signaling are FAPs. Secretion of Wnt5 in FAPs can regulate their autocrine response, switching on β-catenin signaling and thus, blocking adipogenesis. Remarkably, Schwann cells might as well regulate FAPs differentiation. Schwann cells overexpress *Dhh* (desert hedgehog signaling pathway) upon injury, upregulating its downstream target *Timp3* (tissue inhibitor of metalloproteinase 3), a repressor of adipogenesis (De Micheli et al., 2020a). Therefore, Dhh increased signaling mediated by Schwann cells has been observed in cardiotoxin injured muscles but not in glycerol injuries studies (high deposition of adipose tissue), indicating a correlation between Dhh signaling and FAPs derived fatty infiltration (Kopinke et al., 2017). The exact crosstalk of FAPs and endothelial cells is not well defined. However, taking into consideration the perivascular localization of FAPs and the fact that are the main source of VEGF (vascular endothelial growth factor promoting angiogenesis) (Verma et al., 2018a), it is not surprising to see that FAPs and endothelial cells have strong ligand-receptors interactions (Oprescu et al., 2020). In the FAPs depleted mouse model, no vasculature interruptions were reported in the uninjured mice. Nevertheless, vessel impairments, disorganization and increased permeability were observed upon hindlimb ischemia (Santini et al., 2020).

1.5 Role of FAPs in the pathogenesis of muscular diseases

1.5.1 Defects in FAPs induce pathological processes

Myopathies are neuromuscular disorders in which the primary symptom is muscle weakness due to muscle fiber dysfunction. Amongst the first symptoms that a patient manifests are loss of muscle mass and increased fibro-fatty tissue formation. FAPs hold an intrinsic ability to differentiate to adipocytes or fibroblasts. Due to this potency, more and more studies in the recent years have focused on the contribution of these cells in myopathies and have put dystrophic FAPs under the microscope.

Duchenne muscular dystrophy (DMD), the most studied myopathy, is caused by a mutation in the gene coding for dystrophin, the protein responsible for connecting the actin cytoskeleton of the myofibers to the ECM, through the dystrophin-dystroglycan complex (Constantin, 2014). Loss of dystrophin function leads to muscle wasting, chronic inflammation and increased fibrosis (Klingler et al., 2012). Fibrofatty infiltration

has been the only symptom connected with poor motor performance and therefore, needs to be therapeutically targeted. In dystrophic muscles, the population of FAPs remains constantly elevated (figure 9) (Contreras et al., 2016). The main source of fibrosis in mdx mice (muscle cells from these mice produce a small, nonfunctional dystrophin protein) has been shown to be the PDGFRa^{+} and Sca1^{+} cells, since they were secreting high amounts of collagenous matrix (Col.1a1 GFP reported mice) (Ieronimakis et al., 2016).

Changes in the distribution of FAPs populations have been observed in mdx mice. In non-injured mice Sca1^{low}/CD34^{low} FAPs are predominant while in injured muscles Sca1^{high}/CD34^{high} FAPs are enriched. Interestingly, both of these populations were present in the mdx uninjured mice (Marinkovic et al., 2019). Moreover, the Sca1^{high} population was recently showed to proliferate faster and to hold a stronger adipogenic potential than the Sca1^{low} population in the mdx line (Giuliani et al., 2021a). Another study identified an accumulation of the PDFGRa^{low} FAPs population in dystrophic muscles that mainly expresses fibrogenic genes like *Tgfβ1* and *Col.1a1* (figure 9) (Contreras et al., 2019a). As it was described in a previous section, the *Vcam1*$^{+}$ FAPs population is mainly present in wild type muscles only during regeneration.

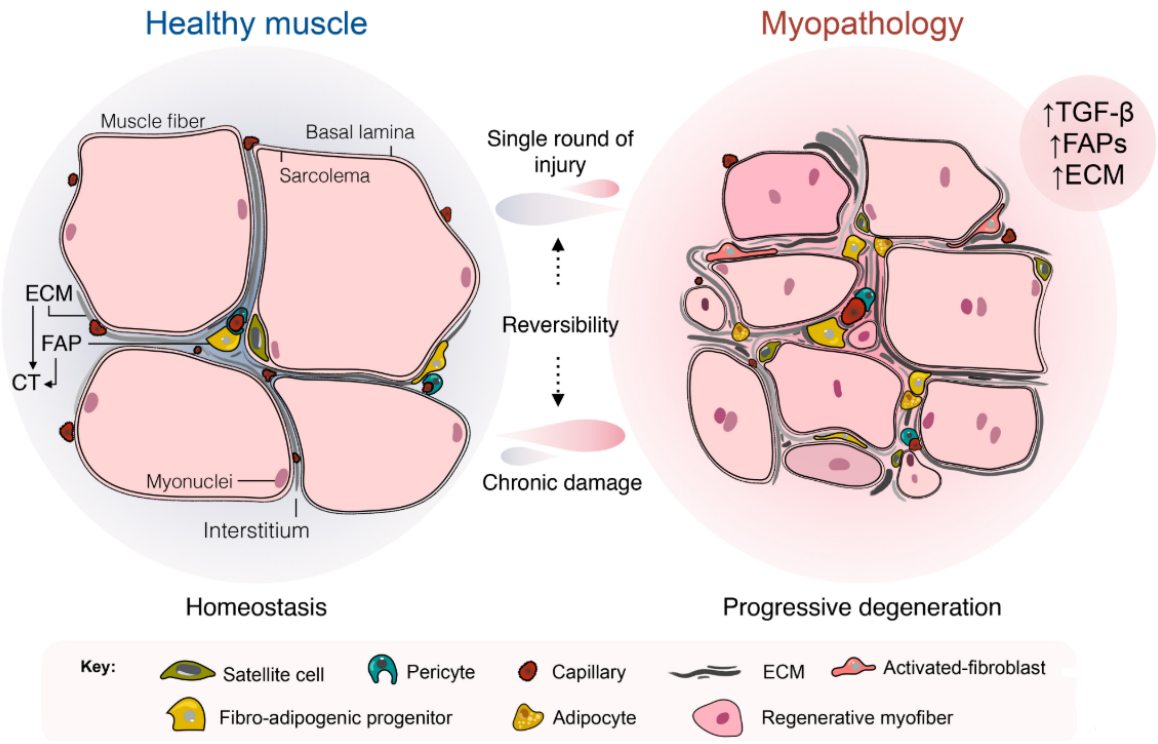

Figure 9: FAPs contribute to development of myopathologies via fibro-fatty infiltrations
Chronic injury requires constant regeneration which translates to induced waves of activated FAPs that produce extensive amounts of ECM, leading to hyperplasia. In several cases adipogenic differentiation of FAPs is also detrimental. Increased number of FAPs, rich TGFβ environment and enhanced fibrosis result in muscle degeneration. Figure adapted from (Theret et al., 2021).

Remarkably, in mdx uninjured muscle both the *Vcam1*$^{-}$ and *Vcam1*$^{+}$ subsets can be identified, with the *Vcam1*$^{+}$ upregulating pro-fibrotic genes and proliferating highly. Finally, the *Tie2*$^{+}$ FAPs in wild type injured muscles expresses genes related to muscle growth and dendritic cell maturation, which was not observed in the *Tie2*$^{+}$ population of the DMD muscle (Malecova et al., 2018).

Considering all the cellular crosstalks described before with FAPs, the defected dystrophic FAPs behavior might be linked to the degenerative environment. Cardiotoxin induced injury of mdx mice does not induce a transient expansion of FAPs population, an essential event for myogenic differentiation and macrophage phenotypical switch (Petrilli et al., 2020). The molecular signals from DMD myogenic cells to FAPs are also perturbed as shown by using CM by DMD patients' myogenic cells on FAPs. Under these conditions FAPs proliferation was induced as well as their fibrogenic fate (Moratal et al., 2019). Furthermore, although in healthy muscle Notch signaling from differentiating myoblast is proved to inhibit FAPs adipogenic differentiation in direct cell contact, this was not observed in FAPs from dystrophic mice (Marinkovic et al., 2019). Defects in the autocrine signaling of dystrophic FAPs have also been reported, which might influence their differentiation. Genes coding for WNT ligand and receptors are downregulated in mdx derived FAPs which might contribute to increased adipogenesis, considering the role of Wnt5/Gsk3/β-catenin pathway in the downregulation of FAPs adipogenic fate (Reggio et al., 2020).

Apart from DMD, FAPs are also involved in the development of several muscular diseases. In LGMD2B (limb girdle muscular dystrophy type 2) a disease caused by mutations in dysferlin, fatty infiltration is correlated with the severity of the disease. Muscle damage (induced even in exercise) in these cases lead to increased deposition of annexin-a2 in the ECM, mediating FAPs proliferation and adipogenic differentiation (Hogarth et al., 2019). Congenital laminin-α2 deficient muscular dystrophy is connected with TGFβ secretion that is regulating the severity of the disease (Kölbel et al., 2019, Taniguchi et al., 2006, Accorsi et al., 2020). Inhibition of fibrotic deposition in these patients has been achieved via losartan treatment, an angiotensin II blocker that reduces TGFβ secretion (Elbaz et al., 2012). Likewise, in Ullrich congenital muscular dystrophy (mutations in COL6a1, 2, or 3) an excessive accumulation of PDGFRa^{+} cells and abnormal fibrosis have been reported (Noguchi et al., 2017).

1.5.2 TGFβ a key regulator of FAPs fibrogenesis

During inflammation M1 macrophages secrete TNFα to control FAPs expansion while M2 pro-regenerative macrophages produce TGFβ affecting FAPs survival and the generation of the regenerative ECM. Balanced coordination of TGFβ secretion is important for the reestablishment of the ECM (Juban et al., 2018, Muñoz-Cánoves and Serrano, 2015).

Elevated levels of TGFβ1 have been found in muscle and blood plasma of DMD patients (Ishitobi et al., 2000, Song et al., 2017, Bernasconi et al., 1999). Independently from DMD, treatment of mice with TGFβ1 induces *Col.1a1* expression and fibrotic tissue formation (Mendias et al., 2012). The asynchronous wave of myofiber damage and chronic need of regeneration in DMD acts as an inducer for TGFβ1 mediated fibrosis (Dadgar et al., 2014). Nevertheless, increased formation of fibrotic tissue derived from FAPs is not the only way that TGFβ1 acts in myopathies. Binding of TGFβ1 or myostatin to their TGFβ receptors has been shown to decrease the secretion of the muscle fiber hypertrophic factor IGF-1 (Liang et al., 2017, Girardi et al., 2021).

Apart from FAPs, TGFβ1 is also expressed by endothelial cells but mainly by macrophages (over 75% measured in mdx diaphragm) (Ismaeel et al., 2019, Gosselin et al., 2004). Treatment with Nilotinib (blocking the TGFβ1 effect produced by macrophages) rescued the mdx dystrophic phenotype, decreasing FAPs numbers and fibrosis (Lemos et al., 2015). Interestingly, proinflammatory macrophages derived from a dystrophic environment lose their potential to promote FAPs apoptosis but induce instead secretion of Col.1a1. This effect was rescued when an anti-TGFβ1 antibody was used. Furthermore, fibrotic levels are not always directly correlated with TGFβ expression levels since secreted TGFβ1 might also be inactive in its latent form (LTBP). Proinflammatory mdx macrophages secrete more LTBP4, while at the same time mdx FAPs produce the proteases MMP14 (matrix metalloprotease 14) and BMP1 (bone morphogenic protein 1) which release TGFβ1 from LTBP4 and then becomes stabilized in the ECM (Juban et al., 2018). Several studies have shown that the asynchronous waves of inflammation in dystrophies lead to a vicious cycle of proinflammatory macrophage infiltration and LTBP4 secretion, resulting in a chronic TGFβ rich environment. That results in an atypical function of proinflammatory macrophages, where they don’t anymore function to repair myofiber damage but to induce fibrosis (Nitahara-Kasahara et al., 2014, Vidal et al., 2008b, Juban et al., 2018).

At this point it is worth referring to the fact that FAPs are not the only cell population targeted by TGFβ signaling in muscle. MuSCs and endothelial cells express also TGFβ receptors and respond to TGFβ signaling with decreased myotube and angiotube formation while at the same time upregulate fibrotic genes like *Col.1a1* and *Eda-Fn1* (fibronectin extra domain A) (Pessina et al., 2015, Massague et al., 1986, Olson et al., 1986). Infiltrating macrophages in dystrophic muscles are also affected by TGFβ signaling, expressing as well more *Col.1a1* and less *CD45*. However, the total percentage of profibrotic MuSCs, endothelial cells and macrophages are estimated to be around 1-2% of the total fibrogenic population. Therefore, while they don't have a major contribution to fibrotic tissue formation, TGFβ derived effects do not permit these cells to support anymore myogenesis or angiogenesis (Latroche et al., 2017, Verma et al., 2018b, Hogarth et al., 2021).

1.5.3 Origin of heterotopic ossification in myopathologies

Under normal conditions, deposition of intramuscular calcium is not observed in homeostasis. However, this phenomenon has been identified in muscles from DMD patients or the mdx mice. Upon proper stimulation FAPs can enter the osteogenic lineage *in vitro* while it has been reported that stromal cells prone to osteogenesis accumulate in events of injury, intramuscular BMP2 injection and transplantation (Oishi et al., 2013, Leblanc et al., 2011, Uezumi et al., 2010). Interestingly, these cells were shown to aid the bone fracture healing process in mice (Glass et al., 2011). Accumulating evidence the last years has highlighted these cells as the source of ectopic bone formation in muscles. Indeed, this hypothesis was recently verified when FAPs were identified as the responsible cell population for HO lesion formation in fibrodysplasia ossificans progressive (FOP), a genetic disease caused by mutation in the activin receptor (ACVR1) (Dey et al., 2016, Upadhyay et al., 2017, Lees-Shepard et al., 2018, Stanley et al., 2022, Shore et al., 2006). In the study of Eisner and colleagues, lineage tracing experiments in BMP2 induced HO showed that $PDGFRa^{+}$ FAPs are the main source of ectopic ossification and that these are muscle resident FAPs and not bone derived $PDGFRa^{+}$ cells (Eisner et al., 2020). Interestingly, FAPs in DMD environment hold a pro-osteogenic signature and their osteogenic potential is directly connected to the severity of the dystrophy (higher in D2-mdx mice), type of muscle injury and TGFβ signaling. Inhibition of the TGFβ pathway *in vivo*

(intramuscular injection of the inhibitor ITD-1) was reported to reduce fibro-calcification and tissue degeneration (Mázala et al., 2020).

1.6 ECM remodeling during muscle regeneration

1.6.1 ECM and myogenesis

The interstitial muscle connective tissue (ICMT) network mechanically supports the muscle fibers as well as the nerves and the blood vessels. In addition to this primary role, the interaction between myoblasts and the ECM is of crucial importance for several procedures. These include embryogenic development, normal growth and muscle regeneration (Csapo et al., 2020). Although, MuSCs and macrophages secrete some collagens, FAPs are the main producers of ECM components (Song et al., 2000, Pessina et al., 2015). The IMCT and the connective tissues produced by FAPs dictate and promote both myogenesis and muscle morphogenesis (Sefton and Kardon, 2019b). Fibrosis has a central role in congenital muscular dystrophies and FAPs are in charge of a pathological ECM development in most of them, as it was described in previous section.

The ECM in regeneration acts as a dynamic environment, transmitting mechanical and chemical signals that influence MuSCs proliferation and differentiation. *In vitro* studies have demonstrated that a higher amount of mouse or porcine myoblasts expressed *Pax7* when were cultured on Matrigel (mixture of ECM proteins and growth factors). Moreover, myogenic fusion was induced by Matrigel but not by substrates made from single ECM components (Grefte et al., 2012, Wilschut et al., 2010). The ECM importance for the maintenance of MuSCs quiescence has also been verified in a study where removal of MuSCs from their niche forced them to enter cell cycle and to lose their myogenic differentiation capacity. This effect was rescued when MuSCs were cultured directly on laminin tethered hydrogels (Gilbert et al., 2010). In addition, ECM has been shown to affect MuSCs division. Several components of the regenerative niche have been identified as essential for regulating the balance between MuSCs differentiation and self-renewal (e.g. Fibronectin, collagen VI, syndecan 4, perlecan, decorin) and, thus, the preservation of muscle's regenerative potential (Brack et al., 2008, Bentzinger et al., 2013b, Urciuolo et al., 2013, Cornelison et al., 2001). The

secretion of many from these components are regulated by FAPs and more specifically by FAPs-derived fibroblasts. These cells deposit extensively a fibrillar ECM, consisting mainly from collagens and fibronectin, as well as basement membrane constituents. Fibrosis can be a result not only of increased deposition of matrix but also of lower level of ECM degradation. Primary enzymes for this process, like matrix metalloproteinases (MMPs) and tissue inhibitors of MMPs (TIMPs), are also secreted by FAPs (Bentzinger et al., 2013a).

1.6.2 Mechanical properties of ECM and effects on myogenesis

Skeletal muscle force is highly non-linear to stretch and it increases rapidly in order to prevent damage caused by overstretching a muscle (Calvo et al., 2010). An important consideration is also that muscle is viscoelastic, meaning that the stiffness depends on the velocity of the stretch (Meyer et al., 2011). In cases of excessive muscle passive stiffness, the function range of muscle`s motion is reduced which results in muscle contracture, a prevalent feature of cerebral palsy and muscular dystrophies, being a disability cause in these patients (Pingel et al., 2017, Skalsky and McDonald, 2012, Lieber and Fridén, 2019).

Fibrosis is commonly assessed by quantifying collagen, either biochemically or histologically. Fibrotic diseases are usually connected with increased tissue stiffness, such as in liver fibrosis where it serves as a marker for the disease progression (Carrión et al., 2010, Georges et al., 2007). Fibrillar collagens are the main mechanical load bearing structures in ECM and the levels of the most abundant collagen I increase together with elastic stiffness (Swift et al., 2013). Intriguingly, collagen amount in mice fibrotic muscles is a poor predictor of stiffness, implicating that there must be also other factors other than ECM abundance that contribute to increased muscle stiffness (Smith and Barton, 2018). One of the post translational modifications that collagens undergo in order to facilitate their incorporation into the ECM is collagen crosslinking. It has been demonstrated that this modification can increase the stiffness of the collagen fibers and has been connected with tissue stiffness in several conditions (Jones et al., 2018, Georges et al., 2007). Extensive collagen crosslinking has been reported in many dystrophic patients and animal models (Smith et al., 2016); however, its degree could not be correlated with the observed passive muscle stiffness in injured muscle (Chapman et al., 2015). In cerebral palsy muscles, the ration of collagen I to collagen

II was found to account for muscle contractures stiffness, demonstrating that ECM reorganization rather than a single component can have a direct effect (Smith et al., 2021). Many of the ECM constituents can alter ECM stiffness through modifying the fibrillar collagen network architecture (Taufalele et al., 2019); decreased collagen alignment in tendons is connected to decreased stiffness (Riggin et al., 2014). The recent study of Brashear and colleagues used the mdx mice to show that the assumption of decreased muscular function due to increased collagen deposition is not valid. Using polarized light microscopy, tissue stiffness was shown to be highly dependent on collagen fiber alignment in control mice but not in the mdx mice (Brashear et al., 2021).

Microenvironment`s stiffness/ elasticity modulates MuSCs functions and regenerative potential (Gilbert et al., 2010, Trensz et al., 2015); more specifically it has been demonstrated *in vitro* that their proliferation is depended on substrate`s elasticity while the coating protein affected their differentiation (Boonen et al., 2009). On traditional plastic culture dishes MuSCs exit quiescence and begin to rapidly proliferate (Shefer et al., 2006). Interestingly, MuSCs lost their regenerative potential when cultured first *in vitro* and then get transplanted in an injured muscle (DiMario and Stockdale, 1995). However, they exhibited greater functional capacity when they were transplanted directly upon isolation or when they were first cultured on soft hydrogel (Sacco et al., 2008, Cosgrove et al., 2014). Remarkably, substrate stiffness was also shown to affect myoblasts self-renewal potential as well as their ability to become tissue integrated and to replenish the stem cell pool upon transplantation (Gilbert et al., 2010). Several studies have demonstrated that changes in the ECM composition can lead to biomechanical defects (e.g. Collagen VI deficiency lead to increased fibrosis with lower tissue stiffness and poor regenerative potential), which can in turn alter the proliferation and differentiation of MuSCs (Gattazzo et al., 2014, Boonen et al., 2009, Urciuolo et al., 2013). Conclusively, changes in the function of MuSCs in aging have now been attributed to microenvironment changes and not to intrinsic modifications (Brack et al., 2007, Chakkalakal et al., 2012b, Scimè et al., 2010).

1.7 *Osr1* in skeletal muscle development and regeneration

1.7.1 Role of *Osr1* during embryogenesis

The zinc finger transcription factors Odd skipped (Odd) in Drosophila and Odd skipped related (Osr1 and Osr2) in vertebrates are encoded by genes of the pair rule class. In drosophila Odd skipped is essential for initial developmental processes since it regulates zygotic segmentation during embryogenesis, during which is expressed in stripes (Nüsslein-Volhard and Wieschaus, 1980, Coulter et al., 1990, Coulter and Wieschaus, 1988). In later stages of Drosophila embryogenesis, it exhibits a dynamic expression and functionally can act both as a repressor and as an activator (Goldstein et al., 2005, Saulier-Le Dréan et al., 1998).

In vertebrates two homologous gene to Odd skipped have been identified, Odd skipped related 1 (*Osr1*) and 2 (*Osr2*). Both of these genes are highly conserved amongst vertebrates including human (Stricker et al., 2006, Lan et al., 2001, Debeer et al., 2002, Katoh, 2002, So and Danielian, 1999). *Osr1* consists of three exons and the starting codon ATG is located in exon 2. The protein OSR1 consists of 266 amino acids, and three zinc fingers domains are located in the C-terminal half of the protein. It is involved in the activation or repression of downstream targets that induce a mesenchymal progenitor state (Goldstein et al., 2005, Saulier-Le Dréan et al., 1998, James et al., 2006, Tena et al., 2007, James and Schultheiss, 2005).

Both of *Osr1* and *Osr2* are expressed in distinct regions during chicken development with partial overlaps, where initially *Osr1* expression is located in the intermediate mesoderm and in the lateral plate mesoderm while *Osr2* is located in the endoderm (Stricker et al., 2006). On later stages *Osr1* expression is strong in the limbs, in the heart and other mesenchymal derived tissues. In mouse embryos, *Osr1* has been identified as one of the earliest markers of irregular connective tissue. Its expression is located in the limb mesenchyme and is connected to early pre-muscle masses at developmental stages E11.5 and E12.5 (Stricker et al., 2012).

In vitro and *in vivo* studies have demonstrated that *Osr1* regulates mesenchymal cells differentiation and progression of cell cycle. More specifically, *Osr1* expression is essential for repressing chondrogenesis/osteogenesis since its *in vitro* knock-out in connective tissue cells resulted in their differentiation from a fibroblastic like cells to

chondrocytes (Stricker et al., 2012). Additionally, loss of *Osr1 in vivo* was shown to decrease numbers of G2/M cells, highlighting it potential role in controlling cellular proliferation as well (Zhou et al., 2015). Gene targeting experiments in mice manifested the lethality of *Osr1* deficient embryos between the embryogenic stage E14-E15 due to severe heart and intermediate mesoderm (giving rise to the urogenital system) development defects. Lastly, *Osr1* holds a crucial role in the intermediate mesenchyme since it is involved in kidney development (James et al., 2006, Mugford et al., 2008, Xu et al., 2014).

1.7.2 Osr1$^+$ FAPs in regeneration reactivate a developmental program

In 2017 the study of Vallecillo García and colleagues showed that Osr1$^+$ connective tissue cells dictate efficient muscle patterning and formation in development (figure 10a). These cells were shown *in vivo* to be located in close proximity to developing myofibers, co-expressing partially *Tcf4* while *in vitro* were positive also for Pdgfra and other connective tissue markers (figure 10b). *Osr1* deficient embryos exhibited reduced number of myogenic cells, defected myogenesis and reduced myoblast fusion to myofibers. Transcriptome analysis of the mutants revealed defects in gene expression related to the ECM formation and organization, including collagen VI, the anchor of the basement membrane to the underlying connective tissue. Immunostainings with collagen VI delineated myofibers showed disruptions in the morphology of the developing myofibers. Furthermore, the expression of several signaling factors were also affected in the mutants. For instance, CXCL12 was found to be downregulated, whose signaling has been shown to be involved in myogenic progenitors' migration and maintenance. Interestingly, lineage tracing experiments in order to study the fate of *Osr1* expressing cells verified that at E11.5 Osr1$^+$ cells are non-myogenic but contribute to the interstitial cells pool at the late stage E18.5. Lastly, *In vitro* these cells exhibited a fibrogenic but also an adipogenic potential. In sum, *Osr1*$^+$ interstitial cells in development were shown to share similar characteristics and role with the adult FAPs and *Osr1* was therefore termed as a marker for the embryonic FAP like population (Vallecillo-Garcia et al., 2017).

A year later, the study of Stumm and colleagues claimed that *Osr1* is also expressed by adult FAPs in homeostatic conditions but only in a few cells. Interestingly, *Osr1*

expression was shown to be upregulated upon acute skeletal muscle injury in cells found in the interstitial area (figure 10c). The authors demonstrated that these cells are *Osr1*⁺ FAPs and that contribute further to adipogenic infiltration and generation of post-injury resident FAPs. Therefore, *Osr1* expression was proposed to mark expanding FAPs during active periods of myogenesis, for instance during muscle regeneration, and *Osr1*⁺ FAPs were thus, termed as active FAPs. In previous sections the induction of myogenesis by FAPs as well as the crucial role of MuSCs-*Tcf4*⁺ cells interaction in muscle regeneration were discussed. Moreover, *Osr1*⁺ FAP like cells hold a pivotal role in embryonic development since they generate a pro-myogenic niche that promotes myogenic precursors survival and proliferation. Considering thus all these facts, the authors suggested that adult FAPs reactivate upon muscle injury a developmental program to enhance efficient muscle healing (Stumm et al., 2018).

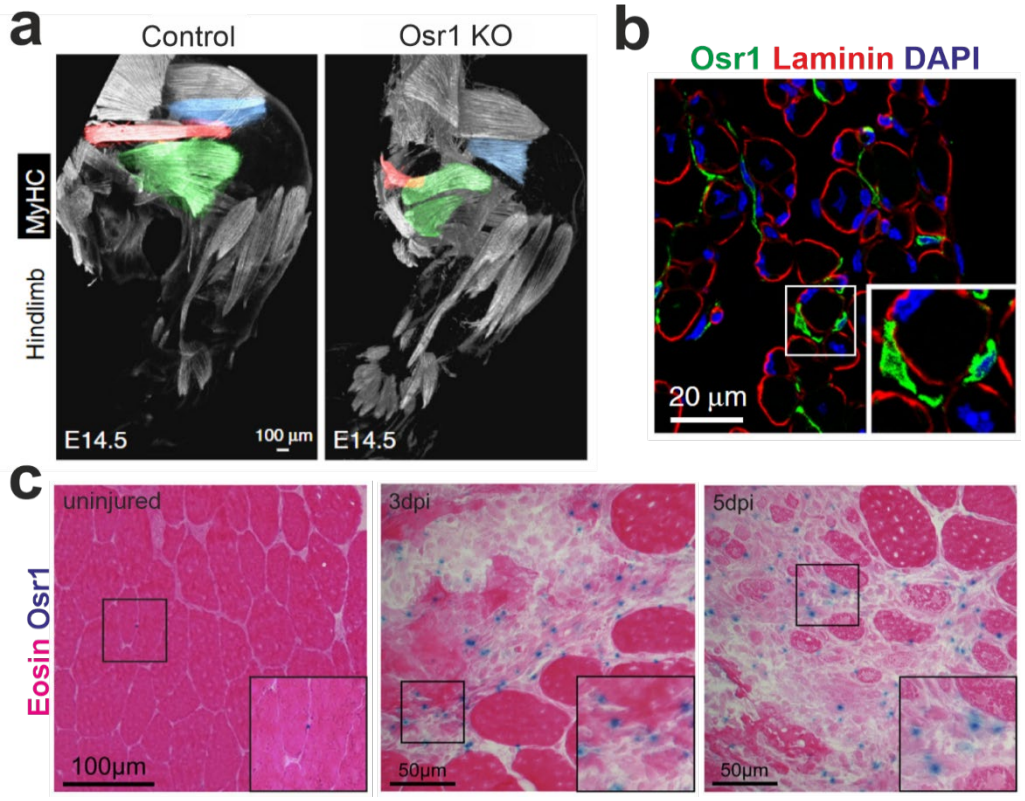

Figure 10: Osr1 is expressed in FAPs during embryogenesis and re-expressed in adult FAPs in muscle regeneration
(a) Immunofluorescence staining for myosin heavy chain revealed muscle patterning defects in E14.5 control and Osr1 KO embryos. (b) Osr1+ cells detected in close proximity to developing laminin stained myofibers in Osr1 cell lineage tracing of E18.5 embryos. (c) Osr1 staining in adult tibialis anterior uninjured and injured muscles identified accumulation of Osr1⁺ cells in the injured region. Figure adapted from (Stumm et al., 2018, Vallecillo-Garcia et al., 2017)

1.8 Aims of the study

Muscle regeneration is a dynamic process involving the intricate interplay of many different cell types in a rapidly changing microenvironment. For many years in the focus of muscle research was the regenerative capacity of MuSCs since they have been shown to be essential for muscle regeneration. However, in the last decade FAPs and their crosstalk with MuSCs have gained more attention due to FAPs ability of assuming many different roles over time, guiding and orchestrating the regeneration process. The recent advancement of single cell RNA techniques started to resolve the dynamic nature of FAPs by demonstrating the existence of distinct FAPs subpopulations with distinct functions. The involvement of the immune response is a key procedure in efficient muscle healing. Therefore, the infiltration of macrophages had also been studied extensively both in regeneration and in several myopathies. Researchers have been trying to elucidate the mechanisms under which the different immune populations limit FAPs function and regulate their differentiation. However, a gap of knowledge exists in the FAPs feedback mechanisms that attribute a unidirectional crosstalk between themselves and the macrophages. Despite the increasing knowledge on the function of FAPs during the regenerative process, no intrinsic regulator guiding key aspects of all these functions is known.

The zinc finger transcription factor Osr1 was described as a key regulator for the pro-myogenic function of an embryonic FAP-like cell population, that also gives rise to a part of adult FAPs (Vallecillo-Garcia et al., 2017). While *Osr1* reporter gene and protein expression was undetectable in homeostatic muscle, it became re-activated during muscle regeneration (Stumm et al., 2018). This study, therefore, specifically aims to understand:

What is the role of Osr1$^+$ FAPs in adult muscle regeneration?

In order to answer this question, the necessity of *Osr1* expression in FAPs will be challenged using a systemic combination of both *in vivo* and *in vitro* systems to answer the following questions:

1. What is the effect of loss of *Osr1* expression by FAPs during skeletal muscle regeneration? For this purpose, an *Osr1* conditional knock-out mouse model will be used and a longitudinal histological analysis will be performed.
2. How does *Osr1* deletion affect the regenerative populations of FAPs and does that affect the myogenic potential and expansion of MuSCs? That will be

addressed with immunostainings of primary sorted cells but also of muscle injured tissue sections.

3. What are the changes inflicted in the transcriptome of *Osr1* deficient FAPs? For this purpose, RNA sequencing will be performed on FAPs at two different timepoints after injury and a comparative analysis will reveal the dynamics changes of the gene expression in time and in absence of *Osr1* expression.
4. Can the crosstalk between FAPs and the immune response get defected upon deletion of *Osr1* concomitant to injury? This will be answered deploying an extensive FACS gating analysis that allows for thorough screening of the immune cells' distributions in the Osr1 knockout (KO) animals.
5. Why is *Osr1* expression in FAPs essential for MuSCs myogenesis? To approach this, *in vitro* assays of co-culture systems and decellularized scaffold experiments will be used to assess the mechanisms under which *Osr1*$^{+}$ FAPs induce the myogenic potential of cultured myoblasts.

In summary, this research will provide new insights into the role of FAPs in skeletal muscle regeneration. This project will contribute into understanding FAPs crosstalk with MuSCs/ macrophages in the regenerative niche and will identify the importance of *Osr1* expression as an intrinsic regulator of FAPs main functions. In the long run, the knowledge gained from this study could be used to gain new insights into muscle regenerative efficiency and FAPs related contribution into inflammatory diseases.

2 Materials

2.1.1 Mouse lines

The mice used in this study were breed and maintained in an enclosed SPF animal facility. The mouse lines were maintained on a C57BL/6 background. All experiments were performed in accordance with the European Union legislation for the protection of animals used for scientific purposes, and approved by the Landesamt für Gesundheit und Soziales Berlin under license numbers ZH120, G0114/14 and G0198/19.

Osr1$^{flox/+}$ line: The line was generated using the Osr1LacZ/+ reporter line used in the study of Stumm and colleagues (Stumm et al., 2018). This line carried on a multifunctional allele, a LacZ-reporter cassette which after mating with the FLP recombinase mouse (Rodríguez et al., 2000) resulted in a Osr1 exon 2 floxed mouse. In this transgene line the Osr1 exon 2 is flanked by the loxP sequences (flox) which upon mating with a Cre-recombinase mouse line results in the excision of exon 2. At the same time, the GFP cassette is inverted and its expression is depended on the activation of the Osr1 promoter.

CAGG$^{CreERt2/+}$ line: A transgene expressing a Cre-recombinase gene under the CAGG promoter. In this construct, the cytomegalovirus enhancer is fused to the chicken beta-actin promoter (Hayashi and McMahon, 2002). This line was provided by Dr. Heiner Schrewe.

CAGG$^{CreERt2/+}$ Osr1$^{flox/+}$ line: The inducible CAGG$^{CreERt2/+}$ line was breed with the Osr1$^{flox/+}$ line. In this study, the conditional Osr1 knock-out mice carried the genotype CAGG$^{CreERt2/+}$ Osr1$^{flox/flox}$ and will be further termed as Osr1 cKO. As control animals in the transcriptome analysis, primary FAPs extraction and FACS analysis, CAGG$^{CreERt2/+}$ Osr1$^{flox/+}$ animals were used and will be further termed as control.

Cell lines

In this study the murine myoblast C2C12 cell line was used. The cells were kindly provided by the cell bank of Stefan Mundlos.

2.1.2 Instruments

Table 1: Instruments

NAME	TYPE	SUPPLIER
Thermal PCR Cycler	ProFlex PCR System	Thermo Scientific
Real time PCR Cycler	ABI Prism HT 7900	Applied Biosystems
Microwave	DO2329	DOMO
Thermomixer	compact 5350	Eppendorf
Water bath	MD	Julabo
Microscope	IX50	Olympus
Fluorescence microscope	DMi8	Leica
Confocal laser scanning microscope	SP8	Leica
FACS	Aria II SORP	BD Pharmingen™
Protein electrophoresis equipment	Mini	Bio-Rad
Protein transfer system	Mini Trans-Blot	Bio-Rad
Power supply	EPS301	Amersham Bioscience
Nanodrop	2000	Thermo Scientific
Tissue Lyser	LT	Qiagen
Cryotome	H560	Microm
pH meter	HI2211	HANNA Instruments
Automated cell counter		Luna™
Piuma		Optics 11 Life
GentleMACS Dissociator		Miltenyi Biotec

2.1.3 Chemicals

Chemicals were purchased from Roth, Merck, Roche and Thermo Fisher unless otherwise specified.

Table 2: Buffers and solutions

BUFFER	FORMULA
Tamoxifen solution	Dissolve 30 mg/ml tamoxifen in 95% Corn Oil / 5% ethanol solution and incubate at 37°C until completely dissolved, protect from light. Aliquot and store in -20°C.
10x PBS	80g NaCl; 2g KCl; 14.4g Na_2PO_4; 2.4g KH_2PO_4; add 800ml bidest H20 and set pH to 7.4; Final volume: 1L
PBX	100 ml of 10x PBS solution. 1 ml of TritonX-100. Add bidest to 1L
10x TBS	24g Tris- HCl; 5.6g Tris base; 88g NaCl, dissolved in 900 ml bidest H20; adjust pH to 7.6; bring volume up to 1L with H_2O
TBST	Mix 100 ml of 10x TBS solution with 1 ml Tween-20. Bring volume up to 1L with H_2O
RIPA Buffer	10mM Tris-HCl, pH 7.5; 150mM NaCl; 0.5mM EDTA; 1% Triton-X100; 1% NA-Deoxycholate; 0.1% SDS
Protein lysis buffer	200µl RIPA buffer; 1mg/ml DNase1; 2.5mM MgCl2; 1mM PMSF
10x Transfer buffer	30.2g Tris; 144g Glycine; dissolve in bidest H_2O to 1L
10x Running buffer	30g Tris base; 144g Glycine; 10g SDS; dissolve in bidest H_2O to 1L
1x Transfer buffer	Mix 100 ml of 10x transfer buffer with 200 ml methanol and 700 ml bidest H_2O
1x Running buffer	Dissolve 100ml 10x running buffer in 900 ml bidest H_2O
4% Stacking gel (2 gels)	Mix 990µl 30% Acrylamid; 1.89ml 0.5M Tris-HCl pH 6.8; 75µl 10% SDS; 6.03ml bidest H_20; 7.5µl TEMED; 75µl 10% APS (total volume: 15ml)
10% Separation gel (2 gels)	Mix 5ml 30% Acrylamid; 3.75ml 0.5M Tris-HCl pH 8.8; 150µl 10% SDS; 4.5ml bidest H20; 7.5µl TEMED; 37.5µl 10% APS (total volume: 7.5ml)

6x Protein loading buffer	Mix 3.75 ml 1M Tris pH 6.8; 1.2 g SDS; 6 ml Glycerol; 0.006g bromophenol blue; 0.462g DTT; Total volume: 10 ml
50x TAE buffer	242g Tris; 18.61g EDTA; 57.1g Glacial acetic acid; add bidest H_2O to 1L
6x Orange G DNA loading dye	Mix 2ml of 50x TAE buffer; 0.15 g Orange G, 60 ml Glycerol and add bidest H_2O to 100 ml
5% IF blocking solution	Dissolve 5g BSA powder in 100ml 1x PBS
0.5% Oil Red O solution	Dissolve 0.5g ORO powder in 100ml pure isopropanol (store stock solution in the dark)
0.1% Sirius Red	Dissolve 0.1g SR powder in 100ml 1.3 % citric acid in H_2O
Genomic DNA extraction buffer	10mM TrisHCl; 10mM EDTA; 0.2% SDS; 100mM NaCl; freshly added 0.2 mg/ml Proteinase K
4% Gelatin solution	Mix 4 g of porcine gelatin in 100 ml H_2O; warm solution at 37°C for it to get dissolved
Decellularization buffer	Mix 0.5% Triton-X and 20mM of 15% aqueous solution NH_4OH in 10ml 1x PBS
Collagenase A digestion buffer	Dissolve 500 mg of Collagenase in 5 ml of 1x PBS

2.1.4 Materials used in cell culture

Table 3: Cell culture products

PRODUCT	SUPPLIER
DPBS	PAN BIOTECH
FBS	PAN BIOTECH
HS	PAN BIOTECH
100 U Penicillin/ 10mg/ml Streptomycin	PAN BIOTECH
Poly-lysine	Millipore/ Merck
1% Gelatine	Carl Roth
Trypsin	PAN BIOTECH

DMEM 4.5 g/l glucose	PAN BIOTECH
SB431542	Selleckchem # S1067-10MG
IL4	Thermo Fisher Scientific # PMC0046
IFNγ	Thermo Fisher Scientific # PMC4031
L-Ascorbic acid 2-phosphate	Thermo Fisher Scientific A8960
4-Hydroxitamoxifen	Merck 68392-35-8
M-CSF	Thermo Fisher Scientific # RP-8615

Table 4: Cell culture medium

MEDIUM	**COMPOSITION**
Growth medium	500ml DMEM; 50ml FCS; 5ml 100x Penicillin/Streptomycin
Monocyte isolation	500ml M199; 50ml FCS; 5ml 100x Penicillin/Streptomycin
Myogenic differentiation medium	100ml DMEM; 2ml HS; 1ml 100x Penicillin/ Streptomycin
Matrix deposition medium	500ml DMEM; 50ml FCS; 5ml 100x Penicillin/Streptomycin; 50µM L-Ascorbic acid 2-phosphate

Table 5: Enzymes

NAME	**SUPPLIER**
Collagenase A	Roche
TrypLE Express Enzyme	Thermo Fisher Scientific
Dispase II	Merck
Taq-Polymerase	Mundlos Lab
Trypsin-EDTA	PAN BIOTECH
M-MuLV reverse transcriptase	Enzymatics
RNAse inhibitor	Enzymatics
Proteinase K	Carl Roth
DNAse	Qiagen

Table 6: Reagent Kits

KIT	SUPPLIER
Direct-zol RNA Microprep	Zymo Research
Direct-zol RNA Miniprep	Zymo Research
Biozym Blue S`Green qPCR Kit Separate ROX	Biozym
M-MuLV Reverse transcriptase	Enzymatics
DeadEnd™ Fluorometric TUNEL System	Promega

2.1.5 Antibodies

Table 7: Primary antibodies

NAME	HOST	DILUTION	SUPPLIER
MHC3 (eMHC)	Mouse	1:50	DSHB
MF20 (MYH1)	Mouse	1:100	DSHB
Pax7 (supernatant)	Mouse	1:20	DSHB
Pax7	Guinea pig	1:100	Kindly provided by Prof. C. Birchmeier
Ki67	Mouse	1:100	BD Biosciences
Ki67	Rabbit	1:1000	Abcam
Laminin (Lam)	Rabbit	1:1000	Sigma-Aldrich
Collagen VI	Goat	1:200	Southern Biotechnology Associates
MyoD	Mouse	1:100	BD Biosciences
Fibronectin (Fn1)	Mouse	1:500	Merck
Smad2/3	Rabbit	1:1000	Cell Signaling
pSmad2	Rabbit	1:1000	Cell Signaling
pSmad3	Rabbit	1:1000	Cell Signaling
GAPDH	Rabbit	1:2000	Cell Signaling
Myogenin (Myog)	Mouse	1:100	Santa Cruz
Vinculin (Vinc)	Mouse	1:4000	Merck
CD80	Rabbit	1:150	Invitrogen
CD206	Rat	1:150	Bio-Rad
Perilipin (Plin)	Rabbit	1:300	Sigma-Aldrich

Table 8: Conjugated antibodies

NAME	CONJUGATE	DILUTION/ CONCENTRATION	SUPPLIER
CD31	APC	3 µg ml^{-1}	Invitrogen
CD45	APC	6 µg ml^{-1}	Invitrogen
TER119	APC	6 µg ml^{-1}	Invitrogen
a7-integrin	PE	1.5 µg ml^{-1}	Ablab
Ly-6A/E (Sca1)	APC-Cy7	1.5 µg ml^{-1}	Biolegend
CD45	AF488	0.25 µg ml^{-1}	BioLegend
CD3e	PE-Cy7	0.4 µg ml^{-1}	BioLegend
CD19	PE-Cy7	0.2 µg ml^{-1}	BioLegend
CD335	PE-Cy7	0.6 µg ml^{-1}	BioLegend
CD11c	PerCP-Cy5.5	0.4 µg ml^{-1}	BioLegend
CD11b/Mac-1	BV510	0.4 µg ml^{-1}	BioLegend
Ly6-G	APC-Fire750	0.6 µg ml^{-1}	BioLegend
MHC class II	BV785	0.05 µg ml^{-1}	BioLegend
CD80	BV650	0.2 µg ml^{-1}	BioLegend
CD86	BV421	0.2 µg ml^{-1}	BioLegend
CD163	PE	0.1 µg ml^{-1}	Thermo Fisher
VEGF	AF647	0.225 µg ml^{-1}	Novus Biologicals
CD206	PE-Dazzle594	0.2 µg ml^{-1}	BioLegend
Phalloidin	Texas Red®-X	1:250	Thermo Fischer

Table 9: Secondary antibodies

NAME	REACTIVITY	DILUTION	SUPPLIER
Alexa Fluor ® 488, 568, 680	Anti-rabbit		
Alexa Fluor ® 488, 568, 680	Anti-mouse		
Alexa Fluor ® 488, 568, 680	Anti-goat	1:500	Invitrogen
Alexa Fluor ® 488, 568	Anti-guinea pig		
Alexa Fluor ® 488, 568	Anti-rat		
IgG-HRP	Anti-mouse	1:1000	Kindly provided by
IgG-HRP	Anti-rabbit	1:1000	Prof. S. Mundlos

2.1.6 Ladders

Table 10: DNA and protein ladders

LADDER	SUPPLIER
100bp DNA ladder	Fermentas
1kb DNA ladder	
Protein ladder	Thermo Scientific
Page Ruler^{TM} Plus Prestained 10-250 kDa	

2.1.7 Primers

Table 11: Genotyping primer list

PRIMER NAME	PRIMER SEQUENCE (5´→ 3´)
Cre F	GAGTGATGAGGTTCGCAAGA
Cre R	CTACACCAGAGACGGAAATC
COIN F	GCTTAGAATTCAGGAACTGGG
COIN R	CTGGCAGAGACATACATGTTG
GAGG Cre mut F	GCTAACCATGTTCATGCCTTC
GAGG Cre mut R	AGGCAAATTTTGGTGTACGG
GAGG Cre wt F	CAAATGTTGCTTGTCTGGTG
GAGG Cre wt R	GTCAGTCGAGTGCACAGTTT

Table 12: qRT-PCR primer list

PRIMER NAME	PRIMER SEQUENCE (5´→ 3´)
Pax7 F	CGATTAGCCGAGTGCTCAGAA
Pax7 R	CCAGACGGTTCCCTTTGTCG
Myod1 F	CGCCACTCCGGGACATAG
Myod1 R	GAAGTCGTCTGCTGTCTCAAAGG
Myf5 F	CAGCCCCACCTCCAACTG
Myf5 R	GGGACCAGACAGGGCTGTTA
Osr1 F	CCTGTATGGTTTCAGCGCTC

Osr1 R	TGGCTTAGGGTGAATGACGT
Gapdh F	CTGCACCACCAACTGCTTAG
Gapdh R	GGATGCAGGGATGATGTTCT
Tgfβ1 F	GACCCCCACTGATACGCCTG
Tgfβ1 R	GCGCTGAATCGAAAGCCCTG
Tgfβ2 F	CCGGAGGTGATTTCCATCTA
Tgfβ2 R	GCGGACGATTCTGAAGTAGG
Tgfβ3 F	GATGAGCACATAGCCAAGCA
Tgfβ3 R	ATTGGGCTGAAAGGTGTGAC
Cd68 F	GGCGGTGGAATACAATGTGTCC
Cd68 R	AGCAGGTCAAGGTGAACAGCTG
Cd86 F	ACGTATTGGAAGGAGATTACAGCT
Cd86 R	TCTGTCAGCGTTACTATCCCGC
Cd163 F	GGCTAGACGAAGTCATCTGCAC
Cd163 R	CTTCGTTGGTCAGCCTCAGAGA
Cd206 F	GTTCACCTGGAGTGATGGTTCTC
Cd206 R	AGGACATGCCAGGGTCACCTTT
Arg1 F	AACACGGCAGTGGCTTTAACC
Arg1 R	GGTTTTCATGTGGCGCATTC
Albumin F	CTGCAATCCTGAACCGTGT
Albumin R	TTCCACCAGGGATCCACTAC
Ccl2 F	TGGCTCAGCCAGATGCAGT
Ccl2 R	TTGGGATCATCTTGCTGGTG
Ccl3 F	ACTGCCTGCTGCTTCTCCTACA
Ccl3 R	ATGACACCTGGCTGGGAGCAAA
iNOS F	CGAAACGCTTCACTTCCAA
iNOS R	TGAGCCTATATTGCTGTGGCT
IL1b	TGGACCTTCCAGGATGAGGACA
IL1b	GTTCATCTCGGAGCCTGTAGTG
IL6 F	TACCACTTCACAAGTCGGAGGC
IL6 R	CTGCAAGTGCATCATCGTTGTTC
RetnLa F	CAAGGAACTTCTTGCCAATCCAG
RetnLa R	CCAAGATCCACAGGCAAAGCCA
Chi3l1 F	GCTTTGCCAACATCAGCAGCGA

Chi3l1 R	AGGAGGGTCTTCAGGTTGGTGT
IL4 F	ATCATCGGCATTTTGAACGAGGTC
IL4 R	ACCTTGGAAGCCCTACAGACGA
IL10 F	CGGGAAGACAATAACTGCACCC
IL10 R	ACCTTGGAAGCCCTACAGACGA

2.1.8 Tools and software

Table 13: Software

PURPOSE	NAME	SUPPLIER
Microscopy/ imaging	ZEN 2010	Zeiss
Microscopy/ imaging	LAS-X 3.7	Leica
Image processing	Fiji	Wayne Rasband
Vector graphics editor	CorelDraw 2021	Corel Corporation
Documentation and data analysis	Excel, Word, Powerpoint	Microsoft Office
Scientific 2D graphing and statistics	Prism 8	GraphPad
Scientific 2D graphing and statistics	RStudio	RStudio Inc.
RTqPCR analysis	SDS 2.4	Applied Biosystem
FACS analysis	FlowJo	BD Bioscience
Transcriptome analysis	Galaxy 21	Galaxy Europe
Reference management	EndNote 20	Clarivate Analytics

Table 14: Online tools for bioinformatic analysis and data graphing

NAME	WEBSITE
NCBI Primer Blast	https://www.ncbi.nlm.nih.gov
NCBI GEO	https://www.ncbi.nlm.nih.gov/
DAVID Bioinformatics	https://david.ncifcrf.gov/
Enrichr	https://maayanlab.cloud/Enrichr/
ShinyGO	http://bioinformatics.sdstate.edu/go/

g:Profiler	https://biit.cs.ut.ee/gprofiler/gost
Integrative Genomics Viewer	https://igv.org/
InteractiVenn	http://www.interactivenn.net/

Table 15: GCE accession numbers for transcriptome and single cell analysis

GSE NUMBER	GEO TITLE	PUBLICATION
GSE100474	RNA-seq of muscle Fibro-Adipogenic Progenitor subpopulations and bulk from different injury contexts	(Malecova et al., 2018)
GSE110038	Hic1 defines quiescent mesenchymal progenitor subpopulations with distinct functions and fates in skeletal muscle regeneration	(Scott et al., 2019)
GSE138826	10X skeletal muscle regeneration scRNA-seq	(Oprescu et al., 2020)

3 Methods

3.1 Animal related methods

3.1.1 Tamoxifen administration for Osr1 locus recombination

The Cre enzyme from the inducible CreERT2 is fused to the estrogen receptor type 2 and thus, it remains in the cytoplasm upon expression. Upon tamoxifen injection, it binds to the estrogen receptor of the fusion protein and it is translocated in the nucleus, where Cre mediated DNA recombination takes place. Therefore, all adult mice (including controls) were injected intraperitoneally with 3mg tamoxifen using a 0.6mm syringe needle. As control $CAGG^{+/+}$ $Osr1^{flox/flox}$ or $CAGG^{+/+}$ $Osr1^{flox/+}$ animals were used for histological analysis and stiffness measurements, while $CAGG^{CreERt2/+}$ $Osr1^{flox/+}$ animals were used as control for experiments involving FACS of Osr1-mGFP+ FAPs (transcriptome analysis and *in vitro* assays).

3.1.2 Freeze and pierce injury

The freeze/pierce technique was used to generate a mechanical injury on the tibialis anterior (T.A.) muscle of the hindlimbs. Mice were anaesthetized by intraperitoneal injection of 10% (v/v) ketamine / 2% (v/v) xylazine (Rompun® 2%) in sterile PBS (5 µl / g body weight), while animals were on a 37°C heating plate. After that, the skin above the T.A. was opened and the T.A. was pierced longitudinally five times using a syringe needle pre-cooled in liquid nitrogen. The wound was then surgically sutured and until recovery mice were kept in cages on heating plates warmed to 37°C. The injured T.A. was collected at 3, 5, 7, 10, 17- and 28-days post injury (dpi).

3.1.3 Tissue Preparation

Directly upon dissection, muscle was embedded in 6% (w/v) gum tragacanth (Sigma-Aldrich) dissolved in H_2O and snap frozen in ice-cold isopentane (precooled in liquid nitrogen, -160°C). Muscle tissue was sectioned at 10 µm thickness onto Superfrost Plus slides (Thermo Scientific) using a cryostat set to -20°C chamber temperature and -22°C blade temperature. Slides were stored in -80°C until use.

3.2 Genotyping

3.2.1 DNA extraction for genotyping

Biopsies derived from embryonic tail tissue or adult ear tissue were used for DNA extraction. Biopsies were treated with 50µl QuickExtract™ solution and incubated in a thermomixer for 6 mins at 65°C. The reaction was stopped by deactivating the enzymes with a 2 min heat shock at 98°C. Samples were then placed on ice for 10 mins and the obtained DNA extracts were ready to be used for genotyping.

3.2.2 DNA extraction for genomic RT-qPCR

Biopsies from muscle tissue were incubated overnight at 55°C in the genomic DNA extraction buffer (table 2). The following day 200µl 8M LiCl and 2ml isopropanol was added and the DNA was pelleted through centrifugation at 10.000 rpm for 20min at 4°C. Solution was removed and the pellet was washed with 70% ethanol until evaporated. DNA was then dissolved in 100µl of clean water.

3.2.3 Genotyping to identify Cre recombinase sequence

The Cre sequence of the GACC-CreERt2 was identified with the PCR introduced in table 15. The amplified PCR-products were loaded and quantified through agarose gel electrophoresis. The size of the amplified band is 650bp.

Table 16: Cre reaction master mix and PCR program

VOLUME	REAGENT
16 µl	bidest H_2O
2.5 µl	10x PCR buffer (15 mM)
2 µl	dNTP (1.25 mM)
1 µl	Reverse Cre (10 mM)
1 µl	Forward Cre (10 mM)
0.5 µl	Taq polymerase 10 U / µl
1.5 µl	Template
24.5 µl	Total

TEMP.	TIME (min)	CYCLE
95°C	5	
95°C	0.5	35x
66°C	0.5	
72°C	1	
72°C	10	
4°C	∞	

3.2.4 Genotyping to identify the Osr1^{floxed} allele

To identify the insertion of the loxP sites in the exon 2 of Osr1, the PCR described in table 16 was followed. The amplified PCR-products were loaded and quantified through agarose gel electrophoresis. The size of the amplified band is 356bp for the wild type and 295bp for the heterozygous band.

Table 17: Osr1^{flox} reaction master mix and PCR program

VOLUME	REAGENT
17 µl	bidest H_2O
2.5 µl	10x PCR buffer (15 mM)
2 µl	dNTP (1.25 mM)
1 µl	Rev./ For. Osr1 mut (10 mM)
1 µl	Rev./ For. Osr1 wt (10 mM)
0.5 µl	Taq polymerase 10 U / µl
2 µl	Template
26 µl	Total

TEMP.	TIME (min)	CYCLE
95°C	2	
95°C	0.5	10x (-0.5°C /cycle)
57°C ↓	0.5	
72°C	0.5	
95°C	0.5	25x
52°C	0.5	
72°C	0.5	
72°C	5	
4°C	∞	

3.2.5 Genotyping to identify CAGG Cre recombinase sequence

For validation of the general Cre PCR, the specific CAGG-CreERT2 PCR can also be performed following the protocol described in table 17. The amplified PCR-products were loaded and quantified through agarose gel electrophoresis. The size of the amplified band is 200bp for the wild type and 180bp for the heterozygous band.

Table 18: CAGG Cre reaction master mix and PCR program

VOLUME	REAGENT
15 µl	bidest H_2O
2.5 µl	10x PCR buffer (15 mM)
2 µl	dNTP (1.25 mM)
1 µl	Rev./ For. CAGG Cre mut (10 mM)
1 µl	Rev./ For. CAGG Cre wt (10 mM)
0.5 µl	Taq polymerase 10 U / µl
2 µl	Template
26 µl	Total

TEMP.	TIME (min)	CYCLE
95°C	2	
95°C	0.5	10x (-0.5°C /cycle)
65°C ↓	0.5	
72°C	0.5	
95°C	0.5	25x
60°C	0.5	
72°C	0.5	
72°C	5	
4°C	∞	

3.3 Agarose gel electrophoresis

Agarose gels were prepared by dissolving 1-4g agarose in 100ml 1x TAE buffer, depending on the product size. The mixture was warmed up in the microwave and upon cool down, EtBR was added under the hood in a 1:15.000 dilution. Loading dye was added in the PCR products (5µl from the 6x dye) and then were loaded in the gel together with the appropriate DNA ladder. As running buffer 1x TAE buffer was used. The voltmeter was set to 120-130V and electrophoresis was stopped when the desired bands were visible. The amplified PCR products were visualized in a gel documentation system.

3.4 Staining procedures

3.4.1 Immunolabeling on muscle tissue sections

Prior to antibody labelling, sections were slowly brought to room temperature (RT). Slides were immersed in PBS for 5 min and fixed in 4% PFA for 10 min at RT. Slides were briefly washed in PBS and then permeabilized with 0.4% (v/v) Triton X-100 (Sigma Aldrich) in phosphate buffer (PBS) for 10 minutes. Sections were blocked with 5% bovine serum albumin (Sigma Aldrich) in 0,1% Triton X-100 in PBS for 1 hour at RT. Primary antibodies were diluted in 5% BSA in 0,1% Triton X-100 in PBS and incubated overnight at 4°C, the following day slides were washed three times in PBS for 5 min. Secondary antibodies were diluted in 5% BSA in PBS and incubated for 1 hour at room temperature, followed by three short washes in PBS for 5 min. Nuclei were stained with 5 µg / µl 4′,6-diamidino-2-phenylindole (DAPI; Invitrogen) and slides were mounted with FluoromountG (SouthernBiotech).

For MHC3 immunostaining, antigen retrieval was performed upon fixation. Sections were treated in chilled methanol, kept in -20°C for 6 min, and subsequently washed in PBS. Then, slides were immersed in 1 mM Ethylendiaminetetraacetic acid (Roth) at 95°C for 10 min. The slides were left at RT for 30 min and washed in PBS. Blocking and antibody staining was performed as described above.

For Pax7 immunostaining, upon fixation with 4% PFA, slides were permeabilized in chilled methanol for 6 min at RT. Epitope retrieval was performed in boiling 1mM citric acid pH 6 for 2 min and 30 sec in a microwave. Slides cooled to RT, washed in PBS and blocked in 5% BSA IgG-free (Jackson Immuno Research) in PBS. To decrease

background, sections were incubated with anti-mouse IgG Fab fragments (Jackson Immuno Research) diluted in PBS 1:100 for 30 min at RT. Primary and secondary antibody were diluted in 5% BSA IgG free and staining was performed as described above.

3.4.2 Immunolabelling on cells

For cell immunostaining, FACS sorted cells were added on the poly-L-lysine coated coverslips. A 1:1000 dilution of poly-L-Lysine in water was used to coat the coverslips for 1 hour at RT. Coverslips were washed three times with bidest water and coverslips were allowed to dry under the hood. Coated coveslips were stored at 4°C until further use. Primary cells were allowed to adhere for 1 hour at 4°C and the plate was spun at 50rcf for 10min. In case cultured cells were used, medium was aspirated and cells were washed gently with PBS. Then, cells were fixed in 4% PFA for 15 min at RT and washed shortly in PBS. Samples were permeabilized in 0,4% (v/v) Triton X-100 (Sigma Aldrich) in phosphate buffer (PBS) for 10 min. Primary and secondary antibody labelling followed as described in section 3.5.1. Cytospun collected cells were stained following the same procedure. TUNEL staining on cytospun and cultured cells was performed using the DeadEnd™ kit (Promega) according to the manufacturer`s instructions.

3.4.3 Hematoxylin and eosin staining

Cryosections were hydrated in PBS and then fixed in 4% PFA in PBS for 10min at RT followed by two short washing steps with PBS. The sections were shortly rinsed in bidest water and the slides were transferred in Mayer`s Hematoxylin for 3min at RT and then rinsed in running tap water for 10min. Sections were then rinsed again shortly in bidest water H2O and placed in eosin staining solution for 1-3min activated by 0.5% glacial acetic acid. Slides were rinsed twice in bidest water and dehydrated in an ethanol series, starting with a short washing step in 70% for 1min at RT. The slides were subsequently washed in 90% and in 100% ethanol for 2min each and finally were immersed in Ultraclear for 10min at RT. Slides were mounted using Entellan®.

3.4.4 Picrus Sirius red staining

Slides were left at RT for 30min to reach RT temperature. Without hydrating or fixing the sections, the slides were directly put in 0.1% SR in picric acid solution and incubated for 1h at RT. Slides were carefully washed in 0.5% acetified water (adding pure acetic acid) until most of the staining was washed (around 10sec). The slide was immersed in a new cuvette with acetified water and no visible red staining should be visible being washed out at this point. Dip the slides shortly in 70% ethanol and the staining quality is shortly checked under the microscope. In case the red staining is too intense, the acetified water washing step needs to be repeated. If the staining is efficient, dip the slides in a series of ethanol by swirling them inside using forceps, starting from 70% to 80% and finally to 96% ethanol. Slides were left for 2min in 100% ethanol and then this step was repeated in a clean cuvette with 100% ethanol. At the end, slides were immersed in xylol for 2min or until the mounting with Entellan® was completed. Stained samples from n=3 mice per genotype per timepoint (3, 5, 10,17 and 28 dpi) were imaged in total using a Leica brightfield microscope equipped with an automated XY scanning stage. The area size of the collagenous matrix deposition was quantified in Image J from the picrosirius red staining and was further normalized to the size of the total area size of the whole regenerative region.

3.5 RNA extraction and qPCR

3.5.1 RNA extraction from whole tissue lysate

Injured muscle tissue samples were dissected and placed in 600µl TRI Reagent® on ice. A grinding metallic bullet ball was added in each tube. The Tissue Lyser was set to 30Hz and the tissue was homogenized after three rounds of 1min each. The tissue lysate was then centrifuged at 20.000rcf for 20min at 4°C and the supernatant was transferred in a clean tube. Equal volume of clean pure ethanol was added and mixed thoroughly. The Zymo Research mini RNA isolation kit was used for the extraction of the RNA.

3.5.2 RNA extraction from cell samples

Medium was aspirated from the plate and the cells were washed once in PBS. TRI Reagent® was added directly in the well and collected in a clean tube. The well was washed with an equal amount of 100% ethanol and then mixed thoroughly. For FACS sorted cells, isolated cells were pelleted first through 15min centrifugation at 500rcf and supernatant was discarded. TRI Reagent® was added to lyse the cells and then mixed with equal amount of pure ethanol. The Zymo Research RNA isolation micro kit was used for the extraction of the RNA.

3.5.3 Reverse transcription and RT-qPCR

Reverse transcription for cDNA synthesis was performed using M-MuLV Reverse Transcriptase (Enzymatics, Qiagen) and RNAse Inhibitor (Biotechrabbit). Upon adding the master mix in the RNA, 1µl of RNase inhibitor was added in every sample. The components of the master mix and the PCR program for reverse transcription are listed in table 18. The volume of RNA and master mix were diluted up to 100µl with water. Complementary DNA (cDNA) was stored in -20°C.

Table 19: Reverse transcription master mix and PCR program

VOLUME	REAGENT
10 µl	10x M-MuLV Buffer
22 µl	MgCl2 (25 mM)
20 µl	dNTP (2.5 mM)
5 µl	Random Hexamer (50 µM)
2.5 µl	M-MuLV Reverse Transcriptase (200.000 U/ µl)
59.5 µl	Total

TEMP.	TIME (min)
25°C	10
48°C	30
95°C	5
4°C	∞

RT-qPCR was performed in a 384-well plate, in a 12 µl mixture consisting of 6 µl Blue SYBR Green mix (Biozym) or GOTaq qPCR Master Mix (Promega), 2 µl primer pairs (2.5 µM each) and 5 µl template of cDNA. RT qPCR was performed in three technical replicates from each of at least three biological replicates (representing individual animals or cells derived from one animal). Analysis was performed using the ABI Prism

HT 7900 real time PCR detection system (Applied Biosystems) equipped with SDS software version 2.4 (ThermoFisher Scientific) or the QuantStudio 7 (Applied Biosystems) with the software version 1.3 (ThermoFischer Scientific). The mean relative values of the three technical replicates were normalized to the values of GAPDH or albumin, which were used as a housekeeping gene. To calculate the relative expression level of the respective gene, the double delta Ct (ΔΔCt) method was used. All primers used were purchase from Eurofins Scientific and are listed in table 12.

3.6 Protein extraction and western blot

3.6.1 Protein isolation from cells

Cultured cells were trypsinized and pelleted via 10min centrifugation at 500rcf. The cell pellet was dissolved in RIPA buffer and vortexed for 5min in highest speed. Cells were then placed on ice for 10min and this procedure was repeated another two times. Protein lysate was centrifuged at highest speed at 4°C for 10min and the supernatant was transferred in a clean tube. For protein concentration measurement 2µl were used in the Pierce BCA protein assay kit and protein light absorption at 562nm was measured with an ELISA reader. The BCA standard curve was used to calculate the protein concentration in the sample. The sample was further diluted to a final concentration of 1.5 µg/µl by adding the necessary amount of 6x SDS loading buffer. The samples were incubated at 95°C for 5min to completely denaturate the protein and were then stored in -20°C until further use.

3.6.2 SDS-PAGE

SDS-PAGE (sodium dodecyl sulfate-polyacrylamide gel electrophoresis) was used to separate charged proteins based on their molecular mass. The concentration of the separating gel is determined based on the target protein mass. Gels were prepared according to the following protocols shown in table 19. First the separating gel was prepared and covered with 100% ethanol until gel was polymerized. Ethanol was removed carefully and the stacking gel was added on top. A comb was inserted to create space for the protein loading slots and the gel was allowed to polymerize.

Gels were transferred in a gel chamber and immersed in 1x running buffer. Protein ladder and pre-heated at 95°C protein samples were loaded in the gel. The voltage was set to 80V for as long proteins were in the stacking gel and upon their entry in the separating gel, voltage was increased to 120V.

Table 20: Protocols for four stacking / separating gels

Stacking Gels	4%	Separating Gels	10%	12%
Bidest H_2O	9 ml	Bidest H_2O	10 ml	8.38 ml
30% Acrylamide	1.98 ml	30% Acrylamide	8.3 ml	10 ml
0.5M Tris (pH 6.8)	3.78 ml	1.5M Tris (pH 8.8)	6.25 ml	6.25 ml
10% SDS	150 µl	10% SDS	250 µl	250 µl
10% APS	75 µl	10% APS	125 µl	125 µl
TEMED	15 µl	TEMED	12.5 µl	12.5 µl

3.6.3 Western blot

Transfer buffer is prepared and stored in -20°C supplemented with fresh 20% methanol every time. Running of the proteins in the gel is completed when the dye has reached the bottom of the gel. Stacking gel was removed and the size of the separation gel was measured. Same size filter sheets and PVDF (polyvinylidene fluoride) membrane were cut. The membrane was activated by immersion in pure methanol for 30sec and then washed in 1x transfer buffer for 3min. Sponges and filter sheets were placed inside the chamber with 1x transfer buffer. For the transfer of the protein from the gel to the membrane the following order was followed in the stack: sponge, three filter sheets, gel, PVDF membrane, three filter sheets, sponge. Excessive bubbles were removed with rolling gently a glass pipette on top. The stacked gel-membrane complex was transferred in the chamber with the gel facing the side of the cathode. Ice packs were placed around and inside the chamber in order to ensure low temperatures. The transfer was performed in 100V for 1.5h. Upon its completion, the membrane was stained with ponceau to validate protein transfer and then the dye was washed away with PBST. The membrane was blocked with 5% milk powder in TBST for 1h at RT on a shaker. Primary antibodies were diluted in 5% milk powder in TBST and the membrane was incubated at 4°C overnight. The following day the membrane was washed three times in TBST. Secondary antibodies were diluted in TBST and added on the membrane for 1h at RT. A three times washing step with TBST followed after.

An ECL mixture was prepared fresh before membrane documentation, in which the membrane was incubated for 1min at RT. Excessive ECL solution was removed and the membrane was images in the gel documentation system.

3.7 Fluorescence-activated cell sorting

3.7.1 FAPs and MuSCs isolation

FAP and MuSC isolation from muscle was performed as was performed as described in (Vallecillo-Garcia et al., 2017). The TA muscle was isolated and roughly minced with a small scissor in high-glucose DMEM medium (PAN Biotech) containing 10% fetal bovine serum (PAN biotech), 1% Penicillin Steptomycin (P/S) solution (PAN Biotech, 10.000 U/ml) and 2,5 mg/ml Collagenase A (Roche) for 45 min at 37% with gentle shaking. Muscle lysates were further digested with 2 IU/ml of Dispase II (Sigma Aldrich) diluted in minimum amount of PBS for 30 min. To stop the enzymatic digestion, 10% FCS DMEM was added in the sample and subsequently the sample was passed ten times through a 20G syringe needle. Cells were filtered first through a 70μm and then through a 40 μm strainer (Fischer Scientific) and collected by centrifugation at 400G for 10 min. Cells were resuspended in filtered FACS buffer containing 1% BSA and 2 mM EDTA, labeled with FACS antibodies (Table S4) for 30 min on ice and washed three times with FACS buffer prior to sorting. Propidium iodide was used as a viability dye. Cell sorting and analysis was performed on FACS Aria II (BD Biosciences). Unstained controls were used for setting the sorting gates. Data were collected using the FACSDIVA software. Bioexponential analyses were performed using the FlowJo 10 (FlowJo LLC) software.

3.7.2 Immune cell flow cytometry analysis

Muscles were cut into small pieces and transferred to a gentleMACS C tube (Miltenyi Biotec, Bergisch Gladbach, Germany) containing TrypLE Express Enzyme (ThermoFisher, Waltham, MA, USA) in a 37°C water bath for 5 min. The sample was run on a gentleMACS Dissociator (Miltenyi Biotec, Bergisch Gladbach, Germany) using the predefined program for murine muscle dissociation. The tube was transferred back to the 37°C water bath for another 5 min and the dissociation program was repeated. The dissociated tissue was then filtered through a 40μm nylon mesh

(ThermoFisher, Waltham, MA, USA) and thoroughly washed with PBS. Cells were counted and incubated with live-dead stain (LIVE/DEAD Fixable Blue for UV excitation, ThermoFisher, Waltham, MA, USA) at 4°C. Washing steps were performed using PBS supplemented with 0,5 % w/v bovine serum albumin and 0,1 % sodium acid (both Sigma-Aldrich, St. Louis, MO, USA). Surface marker incubation was performed before intracellular staining at 4°C. Intracellular staining for epitopes was achieved using the fixation buffer and intracellular permeabilization buffer kit (BioLegend, San Diego, CA, USA). Antibodies are listed in Table S4. Flow analysis was run on a CytoFlex LX system (BeckmanCoulter, Brea, CA, USA) and population gating and tSNE analysis were performed with FlowJo (BD Biosciences, Franklin Lakes, NJ, USA). The gating strategy was adapted as previously published (Bucher et al., 2019).

3.8 Nanoindentation

The surface elasticity of 15 µm sections from injured TA muscles was measured using the Piuma nanoindenter. The system was calibrated for Young`s modulus measurement, approaching the slide surface and performing an initial wavelength scan. The cantilevers used had a tip radius in the range of 9.5 µm and stiffness of 0.52 N/m. Tissues were immersed in deionized water for 10 min prior to the measurements. Matrix scans of 10X10 were performed setting the step size of the cantilever to 15µm. The data were acquired using the Piuma software.

3.9 RNA sequencing

GFP+ FAPs were isolated via FACS from injured muscles from 4 Controls and 4 Osr1 cKO animals at 3 dpi and from 8 Controls and 8 Osr1 cKO animals at 7 dpi. 2 samples each at 3 dpi, and 4 samples each at 7 dpi were pooled and served as a biological replicate. RNA was isolated using the Micro RNA Kit (Zymo Research), the RNA concentration was measured using a QubitFluorometer (Invitrogen), and the quality of the RNA yield was measured with the Bioanalyzer 2100 (Agilent). After quality control using Agilent's Bioanalyzer sequencing libraries were prepared from 100ng of total RNA per sample following Roche's stranded "KAPA RNA HyperPrep" library preparation protocol for dual indexed Illumina libraries: First the polyA-RNA fraction was enriched using oligo-dT-probed paramagnetic beads. Enriched RNA was heat-fragmented and subjected to first strand synthesis using random priming. The second

strand was synthesized incorporating dUTP instead of dTTP to preserve strand information. After A-tailing Illumina sequencing compatible unique dual index adapters were ligated. Following bead-based clean-up steps the libraries were amplified using 11-12 cycles of PCR. Library quality and size was checked with qBit, Agilent Bioanalyzer and qPCR. Sequencing was carried out on an Illumina HiSeq 4000 system in PE75bp mode and on NovaSeq4000 in PE100bp mode, respectively. Read mapping to the mouse genome (mm10) was performed using STAR in the Galaxy Europe platform, and differential gene expression analysis was performed using DESeq2. Genes were considered as being differentially expressed if the fold-change of KO vs Control was greater than 1.2, if the p-value was below 0.05 for the 3 dpi samples and if the Benjamini-Hochberg adjusted p-value (padj) was below 0.1 for the 7 dpi samples. Transcripts per million (TPM) abundances were calculated from the mean normalized fragment counts given by DESeq2 for all samples. Gene ontology and pathway analysis was performed using the functional annotation tools Enrichr (Kuleshov et al., 2016) and g:Profiler (Reimand et al., 2019).

3.10 *In vitro* assays

3.11 Adherent fibroblast isolation for in vitro culture

Adherent connective tissue fibroblasts that are phenotypically identical to FAPs were isolated from skeletal muscle in essence as described before (Contreras et al., 2019b), thus we refer to these cells as FAPs. For analyzing differentiation, proliferation and apoptosis upon Osr1 deletion, cells from wild type animals were used. For generation of CM, co-culture assays and for the decellularization assays, cells were isolated from contralateral hindlimbs of injured 7 dpi animals. This was done to reduce animal usage and to achieve a pre-activated state of FAPs (Rodgers et al., 2014, Stumm et al., 2018). For cell isolation, briefly, the TA, gastrocnemius and the quadriceps muscles were carefully isolated and cut with a scissor. Tissue digestion was performed as for flow cytometry. After centrifugation, cells were resuspended in DMEM with 10% FCS, placed in a 10 cm dish and allowed to attach for 90 min at 37°C. Supernatant was removed, containing non- attaching cells, adherent cells were washed once with PBS and fresh DMEM with 10% FCS was added (Passage 0). After 3-4 days of growth, cells were trypsinized, counted using the automated LUNA^{TM} cell counter (Logos

Biosystem), and immediately used for the respective assay (Passage 1). For every experiment, freshly isolated FAPs (Passage 1) were used.

3.12 *In vitro* recombination of the *Osr1* locus

0.5 µM of 4-hydroxytamoxifen (4-OHT) was added to the medium of freshly isolated passage 0 control or Osr1cKO FAPs. 4-OHT treatment was repeated on day 1 and day 2 of culture, without discarding the old medium. The efficiency of the recombination was measured via genomic qPCR for the exon 2 of Osr1 and by RT-qPCR. For differentiation assays, cells were trypsinized upon 50-60% confluency to avoid spontaneous differentiation. Approximately 25.000 FAPs were seeded on coverslips in 24 well plates and cultured in DMEM 10% FCS for 6 days. Fresh medium was added every 2 days. Cells were fixed with 4% PFA and immunolabeled as described above.

3.13 Isolation of bone derived monocytes

Femur and tibia bone were isolated upon complete removal of attached muscles and tendons. The bones were shortly washed with 96% ethanol and then placed in 1x PBS. Proximal and distal end of each bone was cut with a fine scissors that granted access to femoral and tibial shafts. The bones were flashed with warm medium (M199 supplemented with 10% FCS and 1% P/S). A 1ml syringe with a 28G needle was used for the rinsing. The bone was rinsed until it turned semi-translucent and the bone marrow was filtered through a 70µm strainer. The cell suspension was centrifuged at 250rcf for 10min at RT. The supernatant was discarded and the cells were resuspended in medium. The centrifugation step was repeated again. The cells were seeded in low attachment surface plates to prevent permanent adhesion to the bottom of the plate. In order to promote monocyte to macrophage differentiation, cell suspension was supplemented with 20 ng/ml M-CSF.

3.14 Indirect co-culture of macrophages with FAPs

200.000 primary isolated monocytes ready to differentiate were seeded in a 24-well plate suitable for trans-well assays. Cells were allowed to attach for 6h and then a transwell insert was placed carefully on top with the help of a forceps. Approximately 80.000-100.000 FAPs were placed in the insert in monocyte proliferation medium.

Monocytes without FAPs on top were treated either with 50 ng/ml IFNγ or with 10 ng/ml IL4 to stimulate M1 and M2 polarization respectively. Co-culture was stopped two days later and RNA was isolated from the cultured macrophages attached on the bottom of the plates.

3.15 Indirect co-culture of FAPs and C2C12

For transwell assays, 10.000 *in vitro* recombined control or Osr1cKO FAPs were seeded in the insert and cultured in transwell plates for 14 days in proliferation medium (high glucose DMEM, 10% FBS, 1% P/S). Upon confluency, 100.000 C2C12 cells per well were seeded in the chamber wells and allowed to attach for 4 hours. Proliferation medium was then removed and replaced with differentiation medium (high glucose DMEM, 2% horse serum (PAN biotech), 1% P/S). After 4 days of differentiation, cells were fixed for immunolabeling. To analyze C2C12 fusion, four different areas per sample were analyzed and the number of nuclei in $MyHC^+$ fibers was normalized to the total number of nuclei.

3.16 Generation of conditioned medium (CM)

30.000 *in vivo* recombined control or Osr1 cKO FAPs were seeded on 24-well plates and expanded in DMEM 10% FCS and 1% P/S until they reached confluency. Cell expansion was monitored daily through an optical microscope and when they reached 100% confluency the generation of CM started. Cells were shortly washed with PBS, then 300µl of DMEM 1% P/S without FCS was added. After 24h CM was collected, spun for 15min in 4°C at 3.000 rcf and supernatant was isolated. CM was stored in -80°C and thawed on ice before use. If necessary CM was also passed through a 0.22 µm filter in order to ensure removal of cellular debris although this procedure lead also to loss of material.

3.17 Differentiation assays using FAPs conditioned medium

For CM treatment, 50.000 C2C12 cells were seeded on coverslips in 24-well plates and kept in proliferation medium (high glucose DMEM, 10% FCS, 1% P/S) for 3 days. Conditioned medium (500 µl) was thawed slowly on ice, supplemented with 2% HS and used as differentiation medium for the C2C12 cells. As positive control, fresh

differentiation medium (high glucose DMEM, 2% horse serum, 1% P/S) was used. New CM was added on cells on day 2, and on day 4 cells were fixed with 4% PFA and immunolabeled as described above. Fusion index was calculated as the ratio of nuclei in MHC positive fibers versus the total number of nuclei. Four different areas per sample were imaged and quantified.

3.18 Differentiation assays upon inhibition of the TGFβ pathway

20.000 C2C12 were seeded on an 18-well IBIDI µ slide in proliferation medium. On the following day, cells were starved for 5h in high glucose DMEM with 0% FCS and then cells were pre-treated for 1h with 0.5 µM SB431542 (Selleck chemicals), for the inhibition of TGFβ pathway. Pre-treatment medium with SB431542 was aspirated, and the chamber well was shortly washed with PBS. Following that, CM from Control and Osr1 cKO aFbs was supplemented with 2% HS and 0.5 µM SB431542 and added to the cells. As positive control, fresh differentiation medium with SB431542 was used. On day 3 of differentiation, cells were fixed in the chamber slide and immunostained for myosin heavy chain. Each chamber of the slide was imaged, and the fusion index was quantified as described above.

3.19 Decellularization and dECM assays

Coverslips in 24-well plates were coated with 0.1% gelatin (Roth) for 1h in the cell incubator at 37°C. Gelatin was aspirated and the plate was allowed to dry inside the cell culture hood. If not used the same day, coated plates were stored at 4°C for maximum two weeks. To generate the dECM scaffolds, 30.000 *in vivo* recombined control or Osr1cKO FAPs were seeded on 0.1% gelatin coated coverslips in 24-well plates. Cells were cultured in matrix medium consisting of high glucose DMEM, 10% FCS, 1% P/S and 50 µM of ascorbic acid. Matrix medium was changed every 2-3 days. Cells were cultured for approximately two weeks until a visible thin layer of matrix formed, after which cells were removed using the prewarmed at 37°C 0,5% Triton-X-100 and 20 mM NH_4OH in PBS. Afterwards the three-dimensional matrices were gently washed with PBS and either used directly or stored in PBS at 4°C for maximum two weeks.

100.000 C2C12 were suspended in 500µl proliferation medium and added on the dECM scaffolds. Proliferation medium was carefully changed upon attachment (1-2h

later) after removing approx. 80% of the volume in the well. Differentiation medium (high glucose DMEM, 2% horse serum, 1% P/S) was added in the same way 6h later. Cells were allowed to differentiate for 2 or for 5 days. Half of the medium was then aspirated and 4% PFA was added for 15min at RT. Attached cells and ECM scaffolds were immunolabeled as described above. It is important to note that the washing steps and the staining procedure took place inside the wells without removing the entire volume of the liquid in order to avoid disruption of the matrix.

3.20 CSA calculation

The regenerative injured region in the muscle scan was selected by identifying nuclei accumulation and centrally nucleated fibers. Laminin immunofluorescence stainings were transformed into binary images. Using the free hand selection tool in ImageJ, the lamina around the fibers in the injured region was encircled. Every region was saved in the ROI manager and the area of each saved fiber was quantified in μm^2 via the measure function of ImageJ. The fibers were grouped based on their size and ranked from smallest to largest. The amount of fibers belonging to each size group was divided by the total amount of measured fibers. The average percentage of each fiber size group was plotted for every timepoint and group of animals (CSA distribution).

3.21 Statistical analysis

All the experiments were performed with at least 3 mice for each group. Two tailed student`s t-test was used for p-value calculation. In the quantification of the immune cells via FACS, the Mann-Whitney test was performed. Outliers were identified with the ROUT method and excluded from the analysis. For depiction of the mechanical stiffness, violin plots depicting the mean value and the first/third quartile were used. Significance in each graph is shown in the diagrams with stars. The standard error of the mean was calculated and plotted together with the mean values. The number of replicates used is indicated in the respective figure legend. For heatmap visualization of the transcriptome data, the Z-score of the transcript reads was used.

4 Results

Skeletal muscle regeneration has been intensively in the focus of research the last decade. Since the discovery and definition of the FAPs population, the function of these cells and their role in regeneration has been continuously described. Despite this increasing knowledge, no intrinsic regulator capable of guiding key aspects of these functions is known. This project focuses on the regenerative potential of FAPs, designating the transcription factor Osr1 as an essential part of positive FAPs function for beneficial wound healing in muscle injury and thus myogenesis.

4.1 Conditional inactivation of *Osr1* impairs muscle regeneration

We previously identified the zinc finger transcription factor Osr1 as a key regulator for the pro-myogenic function of an embryonic FAP-like cell population, that also gives rise to a part of adult FAPs (Vallecillo-Garcia et al., 2017). While Osr1 reporter gene and protein expression was undetectable in homeostatic muscle, it was re-activated during muscle regeneration (Stumm et al., 2018). To identify the importance of Osr1 expression in FAPs upon injury, the regenerative capacity of Osr1 conditional knock-out animals was monitored on multiple timepoints after injury.

4.1.1 Generation of the Osr1 cKO line

Deficiency of *Osr1* during embryonic development leads to lethality at E14.5 - E15.5. to circumvent the prenatal lethality of constitutive *Osr1* inactivation we generated a conditional *Osr1* allele based on our previous *Osr1* multifunctional allele (Stumm et al., 2018). In order to study the effect of *Osr1* deletion in the regeneration process Osr1-flox mice were mated to CAGG-CreER animals to allow timed inactivation of Osr1 based on tamoxifen delivery concomitant with injury (figure 11a). The animals were injected three times with tamoxifen, on the same day of the injury and the two following days, leading to recombination of exon 2 of *Osr1*. In this line, Cre-mediated recombination also inverts a GFP cassette to be expressed by the endogenous *Osr1* promoter. The advantage of this mouse line is that it allows generation of a knock-out allele but at the same time it enables us to separate cells that would express *Osr1* by

isolating GFP$^+$ cells (figure 11a). Osr1-deficient Osr1$^{flox/flox}$;CAGG-CreER animals are further termed Osr1 cKO. In this study we used as controls i) Osr1$^{flox/+}$;CAGG-CreER animals where GFP$^+$ cells were needed (active promoter of *Osr1*) (e.g. RT-qPCR, RNAseq) and ii) Osr1$^{flox/+}$ or Osr1$^{flox/flox}$ for histological analysis. Of note, all animals were injected with tamoxifen, including also the Osr1$^{flox/+}$ / Osr1$^{flox/flox}$ animals (figure 11b).

In order to evaluate the efficiency of this mouse line, the relative expression of *Osr1* was measured on RNA isolated from cells of whole injured muscle tissue on 3 days post injury (dpi). *Osr1* mRNA expression was decreased by 90% in the Osr1 cKO samples, validating the successful recombination of the *Osr1* locus (figure 11c). In addition, qPCR for the exon 2 of *Osr1* performed on the genomic DNA of muscle tissue from injured animals at 3, 5 and 17 dpi showed an approximately 50 - 60% recombination of the Osr1 genomic locus (figure 11d). We additionally verified the expression of the GFP cassette upon inversion via flow cytometry at 3 dpi, where GFP was successfully detected in FAPs (lin$^-$;a7-integrin$^-$; Sca1$^+$) (figure 11e).

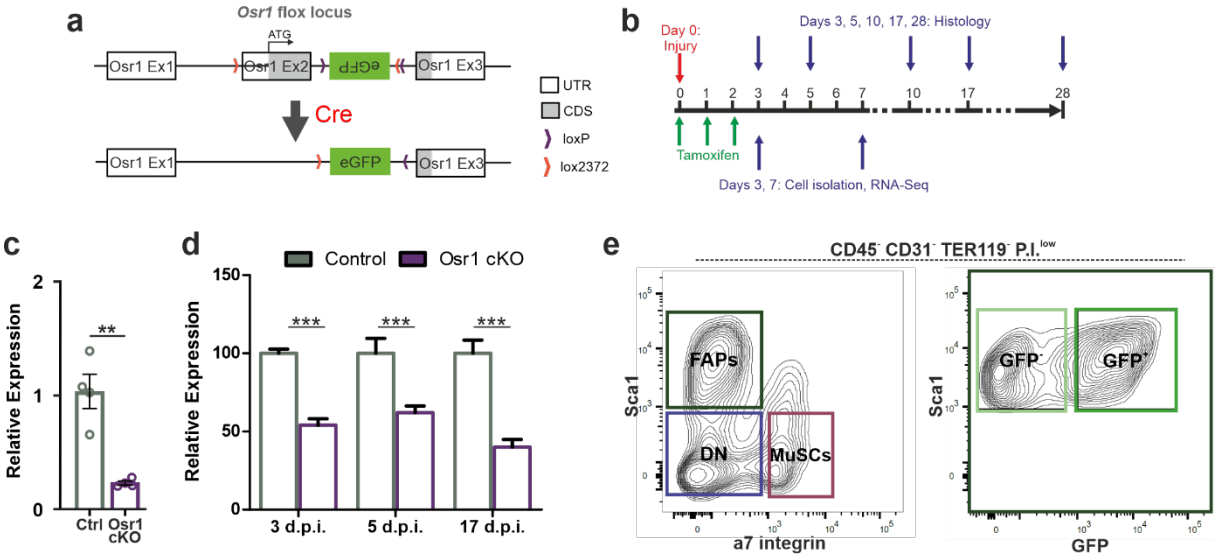

Figure 11: *Osr1* locus recombination in the Osr1 cKO mouse line
(a) Schematic representation of the *Osr1 cKO* locus representation. (b) Schematic representation of the tamoxifen administration and injury time plan. (c) *Osr1* expression on 3 dpi whole muscle tissue sample measured via RT-qPCR showed a decrease in the Osr1 cKO sample. (d) *Osr1* exon 2 genomic locus recombination efficiency at 3, 5 and 17 dpi measured with qPCR in genomic DNA from muscle tissue. A 2-fold decrease was observed in all timepoints. (e) FACS gating strategy for FAPs isolation (left) and green fluorescence detected from GFP expression in FAPs (right). Data are presented as mean ± SEM (n = 4); statistical analysis was done using two-tailed Student's t tests: ** p<0.01, ***p<0.001.

In conclusion, the generated mouse line can be efficiently used for the study of the conditional knock-out effect of *Osr1*, with high efficiency of recombination and detectable GFP expression by flow cytometry in recombined cells.

4.1.2 *Osr1* expression in adult muscle tissue

The expression of Cre recombinase in the aforementioned mouse line is regulated by the CAGG promoter. This construct carries a cytomegalovirus (CMV) major immediate-early enhancer, which results in high expression of the Cre recombinase in all the cells of the animal (Qin et al., 2010). Therefore, *Osr1* locus is recombined in all the cells of the CAGG ^{Cre} Osr1 ^{flox} animals and thus, the question how specific is *Osr1* expression in FAPs arose.

In order to specify which muscle resident cell population expresses *Osr1*, several approaches were followed. To begin with, we tracked GFP expression (*Osr1* expression) via flow cytometry in the CAGG ^{cre} Osr1 ^{flox} animals at 3 dpi (figure 12a). Single cells were isolated from the injured T.A., stained and analyzed. The first gating separated live from dead cells, where ~80% of the cells were viable. Following that, we separated immune, endothelial and hematopoietic cells (termed as Lin^+, 74% of the total live cells, red box in figure12a) from the muscle resident cells (termed as Lin-, 23,8% of the total live cells, dark blue box). We then analyzed each of these two populations for GFP expression. In the Lin^+ population, almost the entire population was found to be GFP^- (99,5% of the cells, light blue box) whereas an inconsiderable amount of Lin^+ cells expressed GFP (0,25% of the cells, light green box). Therefore, we excluded the possibility that *Osr1* might be expressed in the Lin^+ cell population. On the other hand, a significant amount of Lin^- cells were found to be GFP positive (11,9% of the cells, deep green box) while the majority of the cells still were GFP negative (87% of the cells, deep red box). This fact indicates that transcription of *Osr1* is a trait of only muscle tissue resident cells in injured muscle.

Since the term muscle resident cells includes several cell populations like FAPs, MuSCs, myoblasts etc., we confirmed that *Osr1* is specifically expressed only by FAPs. For this purpose, single cell datasets from the study by Oprescu et al. were used, which included a profiling of the FAP subpopulations identity at different timepoints during regeneration (Oprescu et al., 2020). Meta-analysis of their data performed by William Jarassier from the research group of Fabien Le Grand, showed that *Osr1* together with

PDGFRa are explicitly expressed by FAPs not only at all the timepoints of regeneration but also in uninjured muscle (figure 12b). Expression of *Sca1* (*Ly6a*) was proved to be more specific in FAPs in uninjured conditions, at 0.5, 2 and 21 dpi, while at 3.5, 5 and 10 dpi *Sca1* was also expressed by macrophages, endothelial cells and lymphocytes, as expected. These data, provided further proof that *Osr1* is expressed in muscle tissue specifically by FAPs and most importantly that its expression is identical to the cell population expressing *PDGFRa*, the most accepted identity marker of FAPs cells (Wosczyna et al., 2019).

To further strengthen our finding that Osr1 can be used as a solid FAPs marker in adult muscle tissue, we used the bulk RNA sequencing data acquired from the study of Scot et al. 2019. In this study they performed RNA sequencing on several muscle cell populations under homeostasis (Scott et al., 2019). There, the same FACS strategy as ours was used that first separated Lin^+ from Lin^- cells and then used Sca1 as a marker to identify FAPs in the Lin^- subpopulation. We used these data and mined for *Osr1* expression in the different cell populations (figure 12c). The mapped reads per kilobase of *Osr1* exons were found to be significantly low in the RNA isolated from total muscle cells as well as in the Lin^+ population, whereas its expression was a lot higher in the Lin^- population, where also FAPs belong to. More precisely, *Osr1* expression was insignificant in the Lin^- $Sca1^{low}$ population but reached its highest amount of reads in the FAPs population which is termed as Lin^- $Sca1^{high}$ population, verifying once again our previous findings.

Overall, the GFP analysis of the CAGG ^{cre} Osr1 ^{flox} line together with latest single cell RNA and bulk RNA sequencing data, show that Osr1 expression is limited in FAPs population in muscle homeostasis as well as in injured conditions. This allowed us to further proceed with injury experiments using the CAGG ^{cre} Osr1 ^{flox} line, eliminating the possibility of attributing any phenotypical defect following loss of Osr1 to any other cell population but to FAPs.

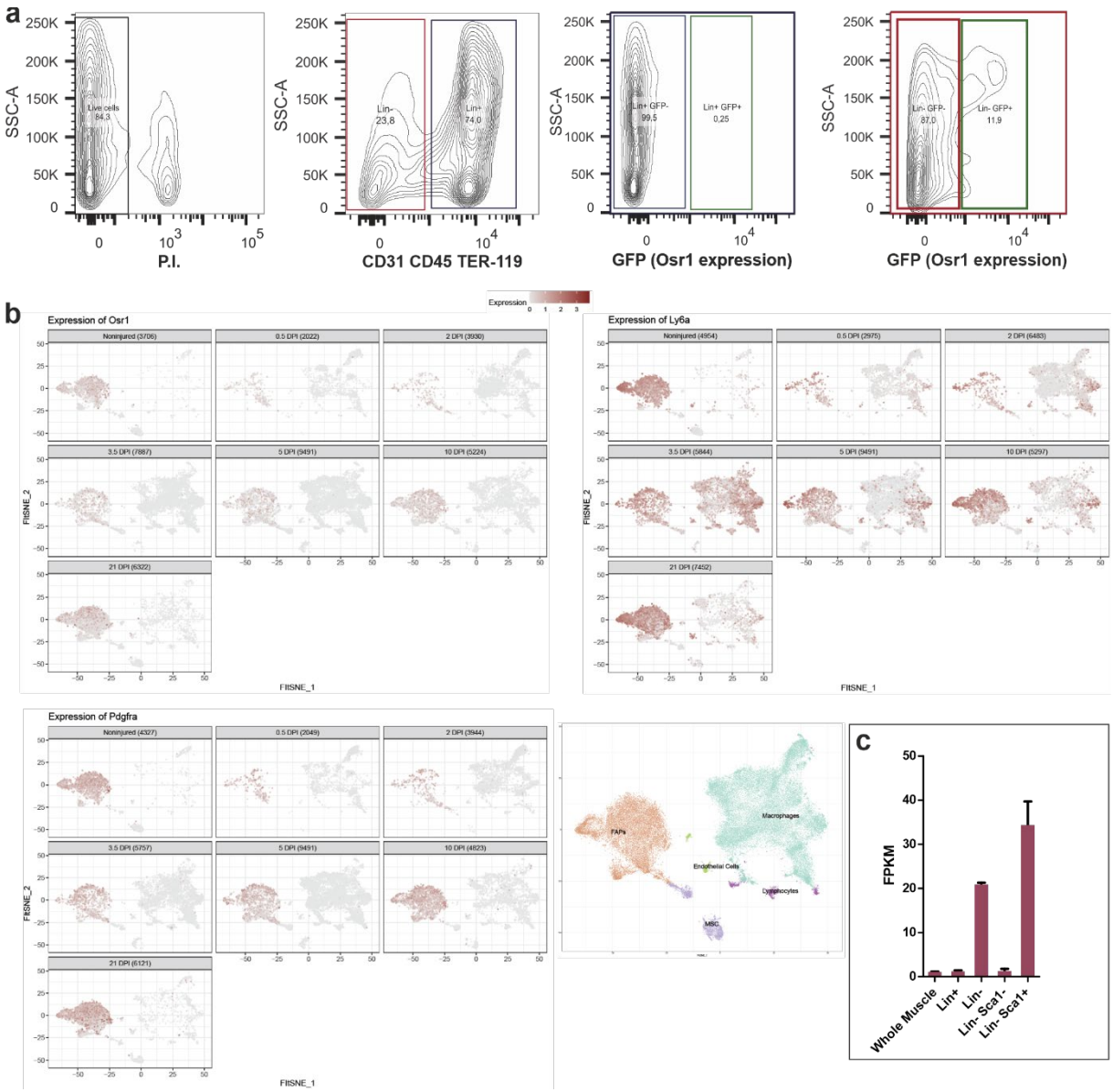

Figure 12: *Osr1* is expressed explicitly in FAPs
(a) FACS gating of cells derived from 3 dpi CAGG ^{cre} Osr1 ^{flox} animals showing GFP expression detected only in Lin^{-} Sca1^{high} population. Almost the whole Lin^{+} Sca1high population is negative for GFP expression. (b) tSNE plots of Osr1, Sca1 (Ly6a) and PDGFRa expression on muscle tissue cell clusters upon different points of regeneration (data from Oprescu et al., 2020). Osr1 and PDGFra expression are detected only in the FAPs cluster throughout regeneration. (c) Average depiction of the FPKM reads for *Osr1* gene expression in different cell populations of the uninjured muscle (data from Scott et al., 2019). The Lin- population and more specifically the Lin^{-} Sca1^{+} subpopulation express *Osr1*.

4.1.3 Defects of *Osr1* deletion at early stages of regeneration

In order to study the importance of *Osr1* expression in FAPs upon injury, we performed a longitudinal histological analysis of regeneration. We first analyzed the regenerative ability of the injured tissue at different timepoints starting from 3 dpi and 5 dpi, since FAPs population has been described to reach its peak in numbers at around day 3-4 of regeneration (Joe et al., 2010).

Developmental/ embryonic myosin heavy chain (Myh3 – termed here as eMHC) is used as a common marker for regeneration in the field of muscle regeneration (Yoshimoto et al., 2020). Newly formed fibers express eMHC on the first days of regeneration, its expression is later lost upon fiber maturation. To investigate the regenerative potential of the injured T.A.s at 3 dpi we sectioned and stained the injured muscle tissue of control and Osr1 cKO animals with eMHC and laminin. Laminin is a protein marker of the extracellular matrix, a major constituent of the muscle basal lamina, used extensively after staining in accessing fiber morphology and size. Figure 13a depicts the combination of eMHC and laminin staining at 3 dpi animals, where we noticed small eMHC positive fibers emerging in the regenerative region of the control animals whereas zero eMHC positive fibers were found in the injured area of the Osr1 cKO tissue. We proceeded with the common histological staining of hematoxylin and eosin (H&E), the most widely used stain in medical diagnosis of muscle pathology. Regarding the morphology of the fibers and the infiltration of cells in the injured area, no differences were observed between the two groups on this timepoint (figure 13b). Calculating the area of a muscle fiber (CSA cross sectional area) by measuring first the diameter of the fiber is used as a direct indication of the fiber maturation and state of health (Gilda et al., 2021). When the fiber size of every fiber of the tissue is plotted as a distribution curve, it can provide important information about the regeneration speed. Higher percentage of smaller in size fibers is usually attributed to more new regenerative fibers, whereas bigger fibers indicate advanced regeneration. In figure 13c the CSA distribution curve of the two groups did not show any significant difference in any of the size groups of the fibers. This result was expected by the time there was not an obvious difference of the fiber size in the histological staining discussed before, although the average distribution of the Osr1 cKO is higher in the area with the smaller fibers (than the control) and lower in the range of medium – large fibers.

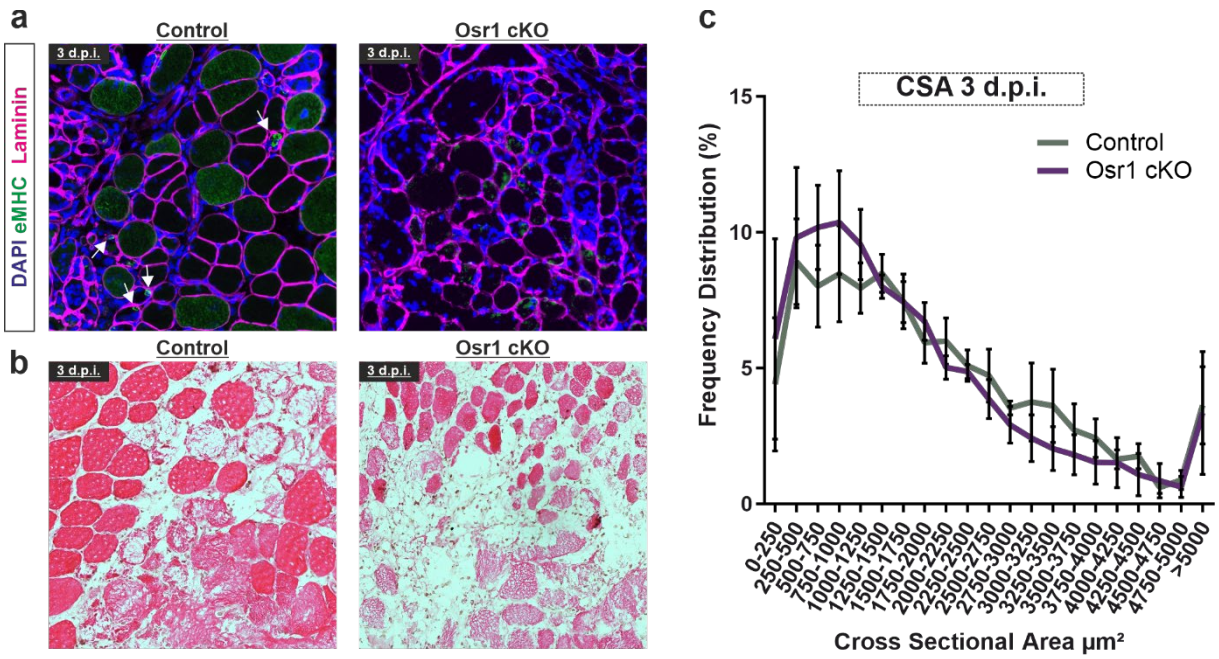

Figure 13: Histological analysis and impact of *Osr1* deficiency at 3 dpi
(a) eMHC / Laminin co-staining of injured T.A. sections at 3 dpi. White arrows point to eMHC⁺ fibers. eMHC+ fibers were found only in the control. (b) Hematoxylin and eosin staining of injured T.A. sections, no significant differences observed at this timepoint. (c) CSA distribution derived from diameter quantification of laminin staining at 3 dpi. Data are presented as mean ± SEM (n = 3); statistical analysis was done using two-tailed Student's t tests, all the differences shown are not significant.

Having found the existence of eMHC positive fibers at 3 dpi only in the injured muscle of the control group, we proceeded in assessing regenerative capacity at a slightly later timepoint, at 5 dpi. At 5 dpi no difference was detected in the number of eMHC positive fibers between the control and the Osr1 cKO groups (figure 14a). One can appreciate though that in the control animals, there is not a high accumulation of cells between the regenerated fibers. On the other hand, in the Osr1 cKO there is an augmentation of infiltrating cells in the injury region. Further histological H&E stainings did not reveal differences between the two groups (figure 14b). We then were prompted to verify whether the tendency of the CSA distribution, as described at 3 dpi, becomes more apparent at 5 dpi Interestingly, higher percentage of the smallest group of fibers was quantified for the Osr1 cKO animals, while at the same time a gain in the range of the medium-large fibers was quantified in the control animals. Consequently, this result indicates a defect in the regeneration ability of the Osr1 cKO animals at 5 dpi.

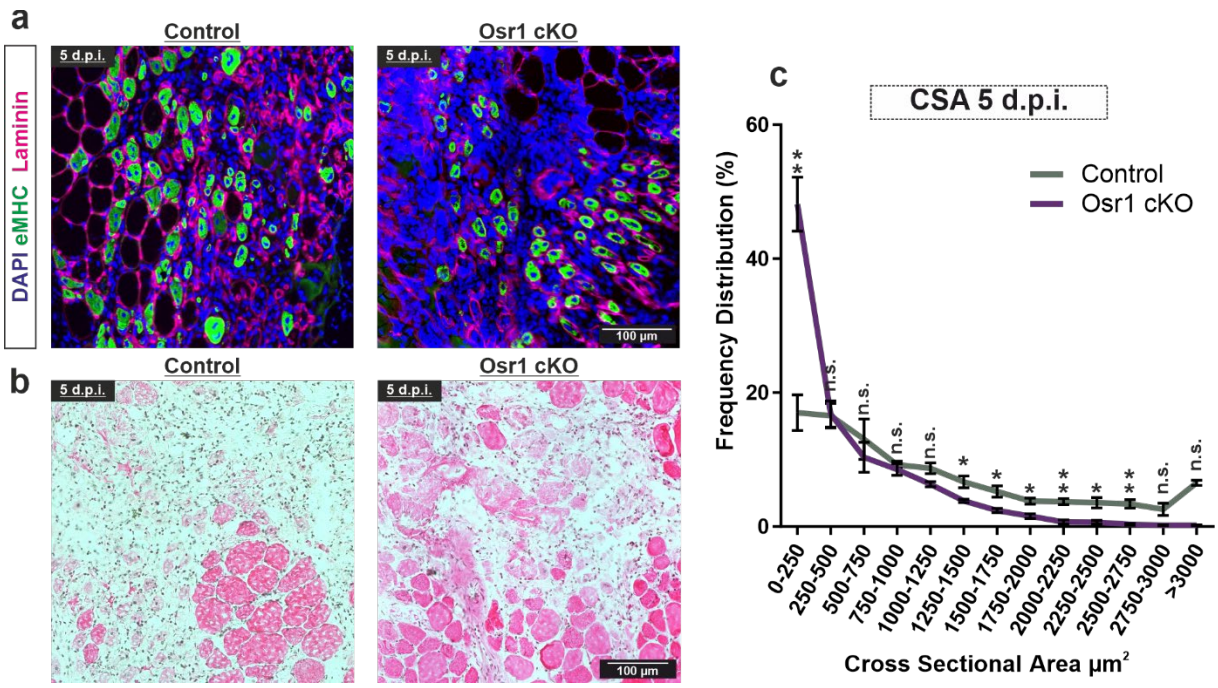

Figure 14: Histological analysis and impact of *Osr1* deficiency at 5 dpi
(a) eMHC / Laminin co-staining of injured T.A. sections at 5 dpi. Same amount of eMHC⁺ fibers in the regenerative region is observed in both groups. (b) Hematoxylin and eosin staining of injured T.A. sections. Infiltration of cells and resolution of fibers indicate the start of the regenerative process. (c) CSA distribution derived from diameter quantification of laminin staining at 5 dpi. Higher percentage of smallest fiber is observed in the Osr1 cKO while the control is richer in middle-large size fibers. Data are presented as mean ± SEM (n = 3); statistical analysis was done using two-tailed Student's t tests: n.s. not significant, * p<0.05, **p<0.01.

Taken together, the earlier appearance of eMHC positive fibers at 3 dpi in the control group along with the CSA distribution differences between control and Osr1 cKO at 5 dpi, show that Osr1 expression by FAPs in early regeneration might be crucial for the healing efficiency of the muscle injury.

4.1.4 High impact of Osr1 deficiency at later stages of regeneration

Having found the defects of loss of Osr1 expression at the early timepoints 3 and 5 dpi, we were prompted to perform similar histological analysis and quantifications at later stages of regeneration. In this subchapter, the results of the analysis at 10, 17 and 28 dpi will be discussed.

Figure 15a depicts the eMHC stainings at 10 dpi, where medium size of fibers (1000-2500 µm) was found in the injured region of the control muscles, surrounded by centrally nucleated fibers. Centrally located fibers are used as a marker of newly regenerated muscle fibers while those of mature muscle fibers are peripherally located

(Rodrigues et al., 2016). The organized structure of the injured area of the control tissue (distinct healthy mature fibers of different sizes, infiltration of cells around fibers which are being resolved) was also verified by H&E stainings, as it can be seen in figure 15b. On the contrary, small eMHC fibers were stained and imaged throughout the injured region of the Osr1 cKO muscles. We noticed the persistence of non-resolved big fibers, probably also necrotic, on whose perimeter eMHC positive fibers were emerging (figure 15a). Intriguingly, formation of fibrotic tissue and extensive deposition of matrix was also observed in these animals (figure 15a, 15b). Additionally, at this timepoint the differences in the fiber size were calculated to be significantly different in the majority of the size groups (figure 15c). Note again the difference in the smallest fiber size range (0-250 µm) between the control and the Osr1 cKO, with the later exhibiting almost 30% more fibers of this size. On the other hand, the control showed a faster regenerative ability. Its distribution curve moved more towards the medium range of fiber size, exhibiting significantly higher amounts of regenerated mature fibers, starting with 750 µm up to 3000 µm. These results demonstrate that *Osr1* deficiency has a strong impact through regeneration, with the implications being the most prominent at the 10 dpi injured animals.

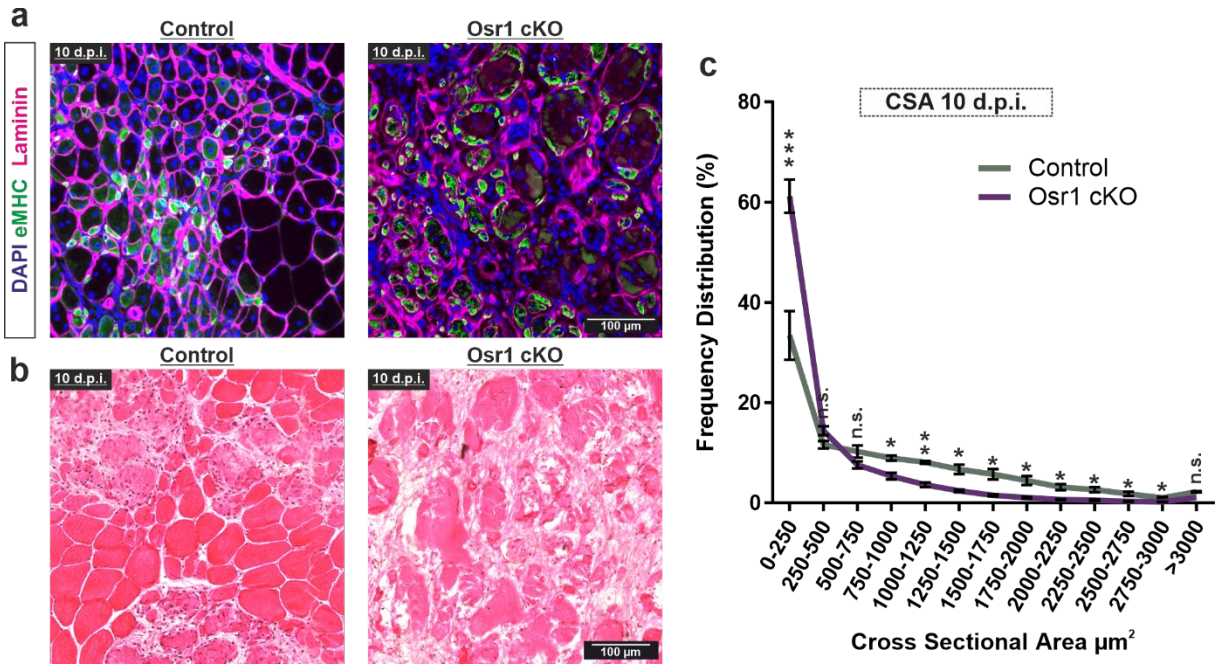

Figure 15: Loss of *Osr1* has a strong regeneration defect at 10 dpi
(a) eMHC / Laminin co-staining of injured T.A. sections at 10 dpi. Higher number of eMHC+ fibers were detected in the Osr1 cKO. (b) Hematoxylin and eosin staining of injured T.A. sections showed first indications for a defect in the resolution of necrotic fibers and fibrotic tissue formation in the mutant. (c) CSA distribution derived from diameter quantification of laminin staining at 10 dpi. Once again, the Osr1 cKO is richer in the smallest size of fibers while the control shows advance regeneration with enrichment in the middle-large range of fibers. Data are presented as mean ± SEM (n = 3); statistical analysis was done using two-tailed Student's t tests: n.s. not significant, * p<0.05, **p<0.01, ***p<0.001.

At 17 dpi no eMHC positive fibers were detected in the control group whereas very small fibers in the Osr1 cKO were stained eMHC positive (figure 16a). These fibers were always found in a region with dense matrix deposition and were always encircled by other small fibers. In figure 16b the differences in the fiber size between the two groups are obvious. Mature centrally mono- or bi-nucleated fibers are distributed all across the regenerated area in the control tissue, indicating an advanced regenerative state. However, the Osr1 cKO exhibited an accumulation of small size of fibers, with some of them being centrally mono-nucleated, as well as a smaller number of mature nucleated fibers, in comparison to the control. The fiber size distribution curve in figure 16c, shows a further reduction in the amount of small regenerating fibers in the control (in contrast to the previous timepoint), while it became higher in the range between 1000-2000 µm.

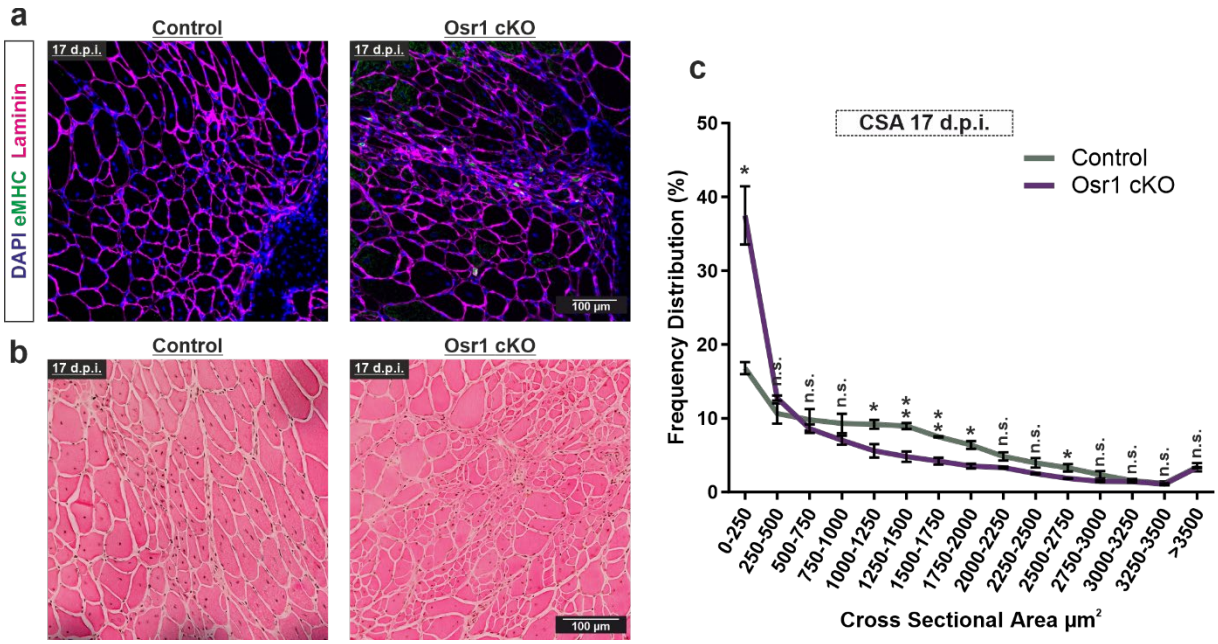

Figure 16: Osr1 cKO exhibit persistent small size of regenerating fibers
(a) eMHC / Laminin co-staining of injured T.A. sections at 17 dpi. In the Osr1 cKO eMHC⁺ small fibers were detected around the injured region. (b) Hematoxylin and eosin staining of injured T.A. sections. Centrally nucleated fibers are visible in both groups; however, they are smaller in size in the mutant muscle. (c) CSA distribution derived from diameter quantification of laminin staining at 17 dpi. Highest percentage of the smallest fibers still persists in the Osr1 cKO while middle size fibers are richer in the control tissue. Data are presented as mean ± SEM (n = 3); statistical analysis was done using two-tailed Student's t tests: n.s. not significant, * p<0.05, **p<0.01.

Conversely, CSA distribution for the Osr1 cKO at 17 dpi did not exhibit significant changes in comparison with the one at 10 dpi, indicating a noteworthy inhibition in efficient regeneration.

Results

The differences observed between the two groups at 17 dpi were persistent also until the last examined timepoint, at 28 dpi. As expected, fibers of the control injured muscles did not express eMHC. In the injured region of the Osr1 cKO animals, we found few eMHC small fibers but not as many in numbers as at the previous timepoint (figure 17a). Around the fibrotic scar tissue of the control animals (figure 17b) centrally nucleated big fibers can be seen, representing the end of regeneration process. However, in the Osr1 cKO smaller fibers were observed, with an ongoing resolution of dead fibers taking place in the proximity of the scar tissue. The percentage of the smallest fibers in the control animals dropped and the next two groups of fibers became more enriched (250-500 μm and 500-750 μm). Finally, the fiber distribution of the mutants in the three smallest size groups was significantly higher also at this timepoint than the in the control muscles (figure 17c).

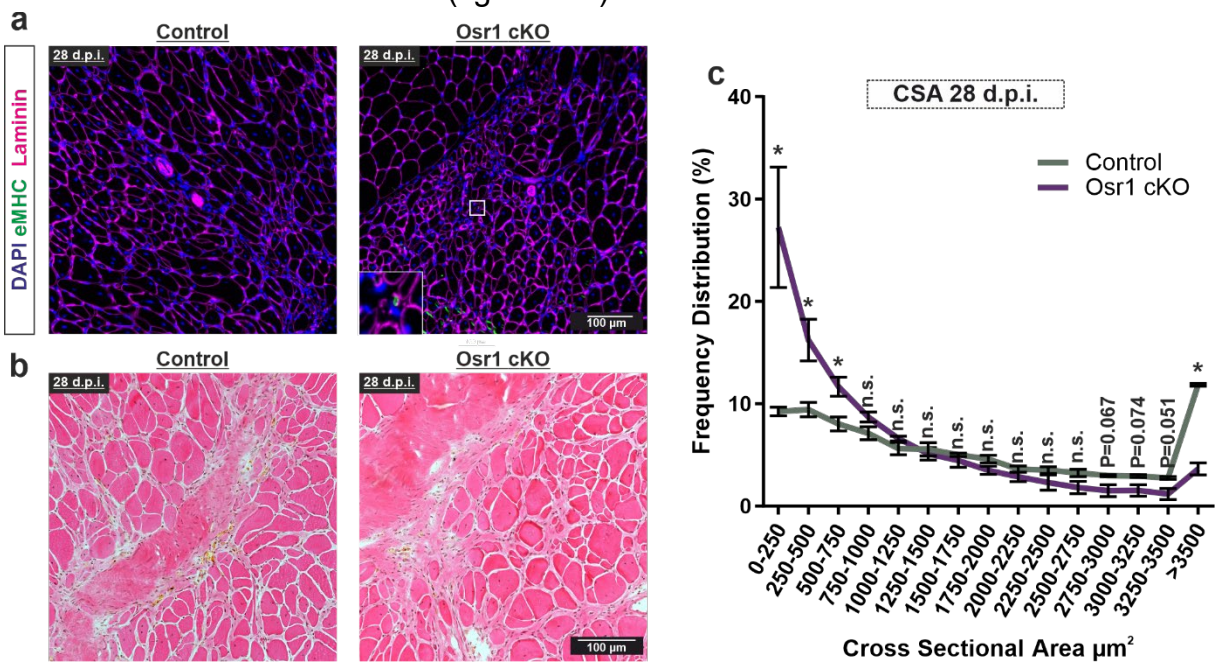

Figure 17: Small fiber size and eMHC⁺ fibers persist until 28 dpi upon deletion of *Osr1*
(a) eMHC / Laminin co-staining of injured T.A. sections at 17 dpi. Some eMHC⁺ fibers were detected in the Osr1 cKO. (b) Hematoxylin and eosin staining of injured T.A. sections. Fibrotic tissue formation was observed in both groups however thicker deposition was observed between the fibers of the Osr1 cKO. (c) CSA distribution derived from diameter quantification of laminin staining at 17 dpi Osr1 cKO tissue is richer in all the groups of the small range of fibers. Data are presented as mean ± SEM (n = 3); statistical analysis was done using two-tailed Student's t tests: n.s. not significant, * p<0.05, **p<0.01.

In sum, the data acquired from these timepoints point towards a severe phenotype of delayed or impaired regeneration of the Osr1 cKO, especially at 10 dpi. The defects of Osr1 deletion persist from 10 dpi to 17 dpi. Moreover, at 28 dpi indications of higher fibrosis are present, as well as accumulation of granulous tissue and delayed appearance of mature fiber size in the regenerative region.

4.1.5 Defected fiber maturation and increased accumulation of necrotic tissue lead to impaired regeneration

Calculating and plotting the CSA distribution at all the collected timepoints, provided us with information regarding maturation of newly formed fibers after injury in the Osr1 cKO. Although the CSA distribution can be used as a direct read-out for the speed of new fiber formation as well as of fiber maturation, the average values of the CSA can further indicate the overall regenerative status of the injured muscle. Figure 18a depicts the average fiber area (in the injured region) of every timepoint analyzed before. As expected, the size of the injured fibers declines from 3 dpi to 5 and to 10 dpi (many fibers are destroyed and new ones are emerging), while it increases from 10 dpi to 17 and 28 dpi. At 3 dpi there was no difference in the size of the fibers, indicating that there is not an initial privilege in fiber size of the control animals in comparison to the Osr1 cKO. At 5 dpi we noticed the first difference in the fiber size, when the Osr1 cKO exhibited almost 50% smaller fibers than the control. The average size was significantly smaller at 10, 17 and 28 dpi in Osr1cKO mice with a consistent overall approx. 30-40% decrease. While in controls, a steep increase in fiber size was observed especially between 17 and 28 dpi, fiber size remained constant in the mutant during this phase.

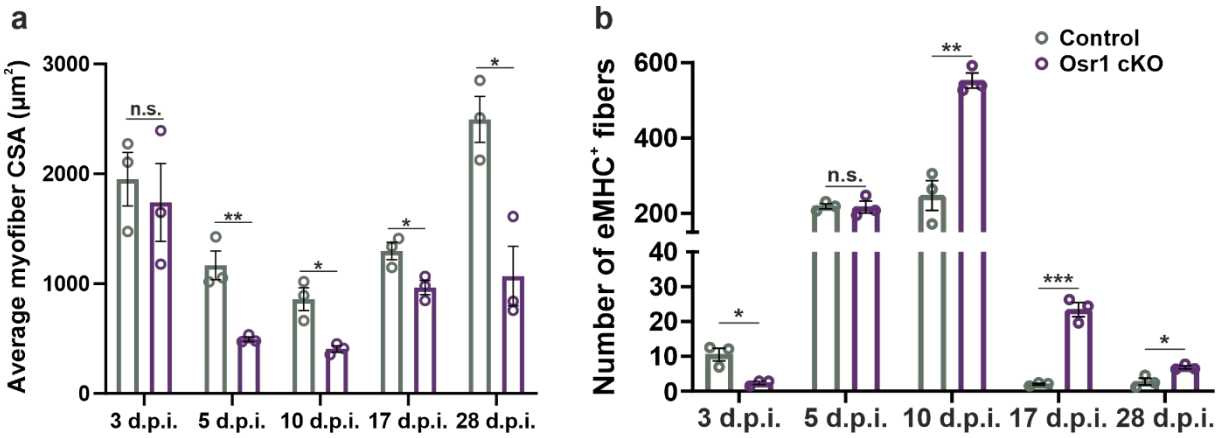

Figure 18: Myogenesis is defected *in vivo* upon deletion of *Osr1*
(a) Average CSA depiction of fibers only in the injured region. No differences were detected at 3 dpi. However, size of Osr1 cKO was found to be always lower at all following timepoints. (b) Quantification of the number of the eMHC$^+$ fibers plotted against the size of the respective injured area in µm^2. At 3 dpi lower number of eMHC$^+$ fibers were counted in the mutant tissue, at 5 dpi this difference was no longer detectable and at 10,17 and 28 dpi the mutants exhibited higher number of eMHC$^+$ fibers. Data are presented as mean ± SEM (n = 3); statistical analysis was done using two-tailed Student's t tests: n.s. not significant, * p<0.05, **p<0.01, ***p<0.001.

The amount of eMHC positive fibers was then quantified and normalized to the area of the injury (figure 18b). That showed a delay in the formation of new fibers at 3 dpi (as also reported in figure 13a), which was however, equalized at 5 dpi. Conversely, at 10 dpi, an increased number of eMHC positive fibers were seen in the Osr1 cKO animals. Interestingly, this defect was persistent in the mutants beyond 17 dpi, when in controls they were not apparent any more. Overall, these results suggest a defect in initial formation but also in further maturation of regenerating myofibers.

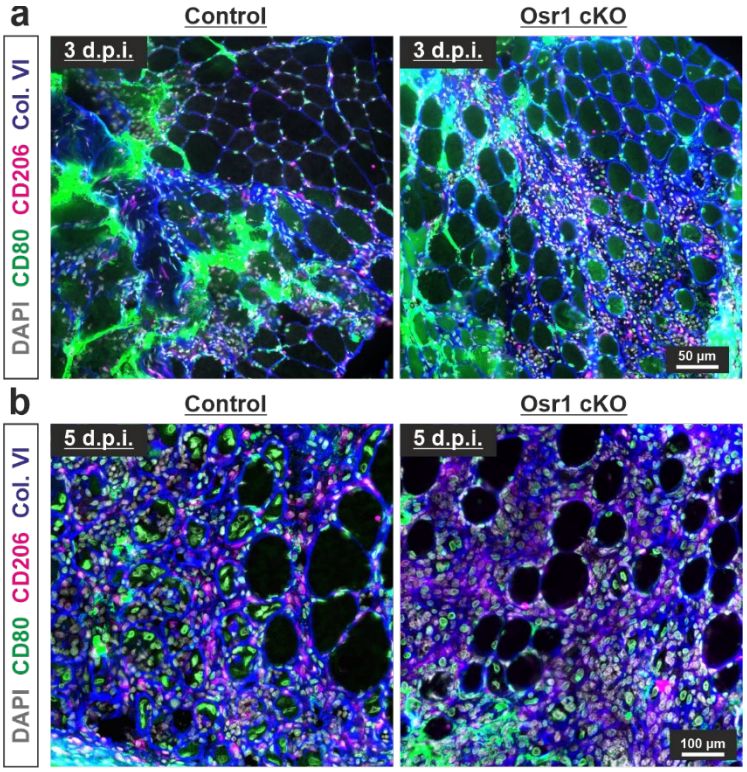

Figure 19: Immune cells located centrally in the fibers on the onset of regeneration
(a) Immunostaining for CD80 (M1 macrophages) and CD206 (M2 macrophages) at 3 dpi show increased infiltration of these cells in the region between the damaged fibers (b) Cells located inside the damaged or new developing fibers are not myonuclei at 5 dpi but M1 ($CD80^{+}$) macrophages.

In the field of myopathies and muscle regeneration, for many years now, centrally nucleated fibers (CNF) are generally recognized as regenerated fibers (Narita and Yorifuji, 1999). Over the last decade many automated tools have been generated to measure not only the amount of CNF but also the number of nuclei in a CNF. These measurements serve as a regeneration speed index (Kastenschmidt et al., 2019). Remarkably, staining for CD80 (mainly a marker for M1 macrophages) and for CD206 (M2 macrophage marker) at 3 and at 5 dpi showed that almost all the cells located in a myofiber during regeneration are M1 macrophages and not myonuclei (figure 19a, 19b). Therefore, counting CNF fibers in the onset of regeneration as an indication of regenerative fibers is not a reliable approach.

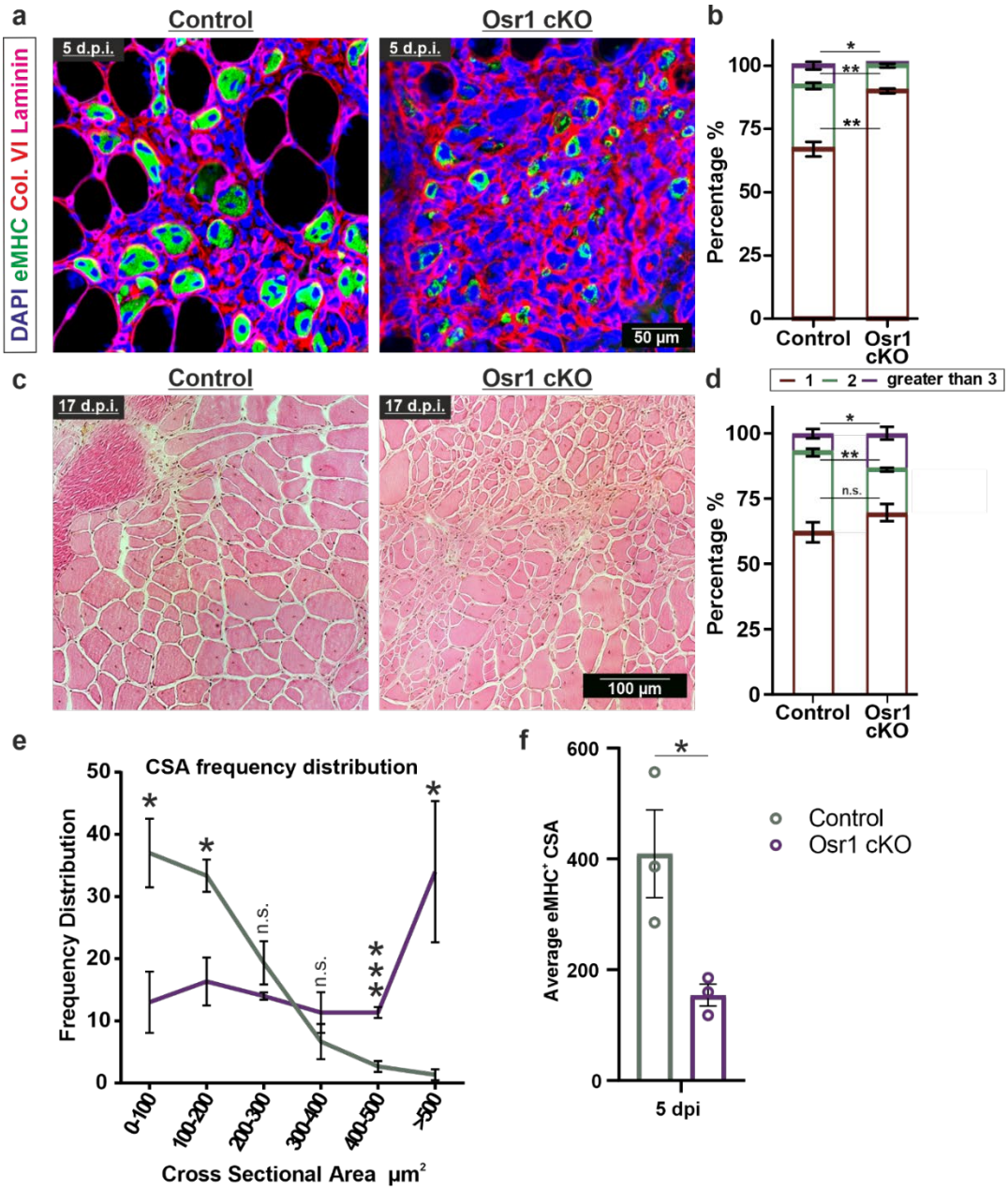

Figure 20: Delayed maturation of regenerating myofibers in the Osr1 cKO
(a) Immunostaining of tissue section at 5 dpi with eMHC, laminin and Collagen VI. At 5 dpi eMHC$^+$ fibers in the control are usually bi-nucleated whereas in the Osr1 cKO mostly eMHC$^+$ mononucleated fibers are observed. (b) Quantification of the number of myonuclei located in eMHC$^+$ fibers at 5 dpi show increased number of mononucleated fibers in the Osr1 cKO. (c) Hematoxylin and eosin staining of injured tissue at 17 dpi. Regenerating fibers with three or more nuclei inside can be spotted in the mutants at 17 dpi (d) Quantification of the centrally myonuclei at 17 dpi highlighted the higher number of tri-nucleated fibers in the mutant. (e) Frequency distribution chart of eMHC$^+$ fibers 'area at 5 dpi show accumulation of smaller size of regenerating fibers in the mutant. (f) Average size of regenerating fibers at 5 dpi indicate an advantage in regeneration of the control in contrast to the mutant. Data are presented as mean ± SEM (n = 3); statistical analysis was done using two-tailed Student's t tests: n.s. not significant, * $p<0.05$, ** $p<0.01$.

Having found that, co-staining with eMHC and laminin was used, in order to measure the number of nuclei specifically in newly regenerated fibers of the injured tissue at 5 d.p.i (eMHC$^+$) (figure 20a). Interestingly, almost 90% of the eMHC$^+$ fibers in the Osr1 cKO were found to be mononucleated whereas these fibers in the control were approximately 65% (figure 20b). The formation of bi- and tri-nucleated CNF was higher in the control group than in the Osr1 cKO, indicating a defect in the maturation process of a newly formed fiber at 5 dpi. Histological analysis via H&E staining at 17 dpi showed the existence of many CNF in the Osr1 cKO which had three or more nuclei inside (figure 20c). At this timepoint cells in the fibers can be safely measured as myonuclei. Quantification of tri- or higher nucleate CNF, showed an increase of these fibers in the mutants when compared to the control (figure 20d). No difference was observed in the mononucleated CNF between the groups but a higher amount of binucleated CNF was present in the control animals. This finding, which is in part inverted in the Osr1 cKO muscle from the 5 dpi to the 17 dpi, proves that Osr1 deficiency in FAPs delays myogenesis during regeneration.

In order to further support the finding of delayed formation of new fibers in the mutant, the size specifically of the eMHC positive fibers was quantified at 5 dpi, the fibers were categorized in group sizes and finally the percentage of its group was normalized to the size of the total injury. At this point we need to state that the exact mechanism under which eMHC is expressed is not well described, it is known though that the switch to adult MHCs expression is taking place upon fiber`s maturation (Schiaffino et al., 2015). The eMHC stainings and the plot in figure 20e depict the higher accumulation of small eMHC positive fibers in the mutants, while the regenerative fibers in the control group were already more mature. Furthermore, the average size of the eMHC$^+$ fibers at this timepoint is approximately 2.5-fold lower in the mutant (figure 20f). This serves as an additional proof that regeneration is impaired upon Osr1 deletion. Apart from the higher amount of new small fibers, one can appreciate with a closer look at the 10 dpi mutants, the large empty spaces encircled with laminin that lack centrally located nuclei. In contrast, the controls display a well-organized fiber structure and fibrotic tissue resolution, which was confirmed by Phalloidin staining. Phalloidin detects filamentous actin, which is not present in necrotic fibers (figure 21a). This showed a clear persistence of necrotic fibers in the Osr1 cKO animals at 10 dpi (approx. 60 necrotic fibers per mm^2 of injured area), a time point when in control animals tissue necrosis was already fully resolved (figure 21b).

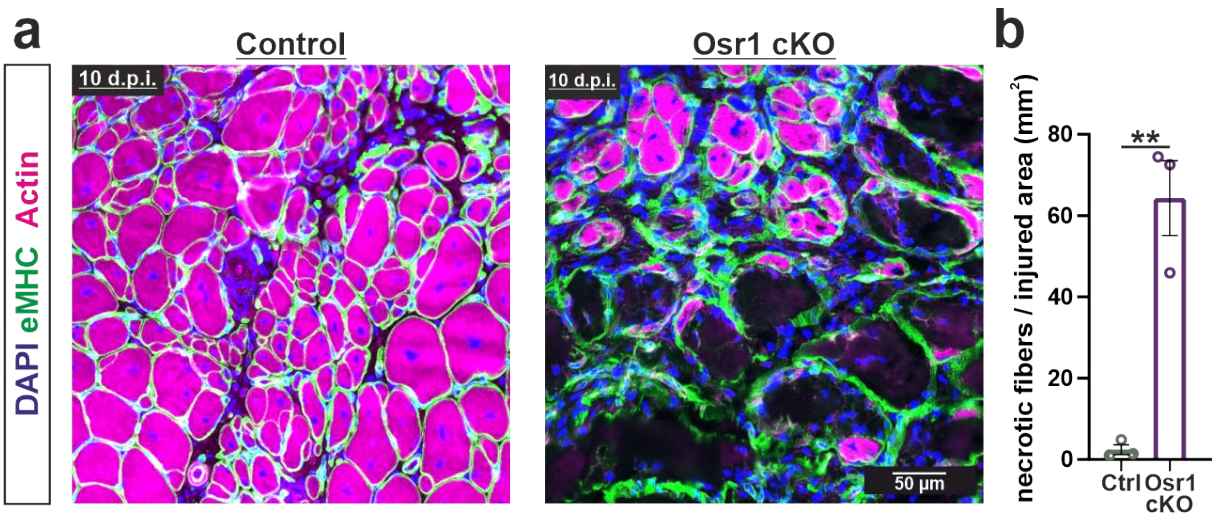

Figure 21: Delayed fiber formation and accumulation of necrotic tissue in the Osr1 cKO
(a) eMHC / Actin co-staining of injured muscle tissue at 10 dpi and (b) quantification of necrotic fibers per size of injured area. 60-fold increase in the amount of necrotic fibers was quantified for the mutant injured tissue. Data are presented as mean ± SEM (n = 3); statistical analysis was done using two-tailed Student's t tests: n.s. not significant, * p<0.05, **p<0.01.

Even though the mutants i) exhibit a defect in regeneration because of delayed myofiber formation and also ii) manifest a fiber size reduction upon injury, the Osr1 cKO animals do not suffer from muscle atrophy. No differences between the groups were observed on the ratio of the injured T.A. weight versus total body weight, both in early (at 3 dpi) (figure 22a) and late (28 dpi) regeneration (figure 22b). Note that the injury method used in this study generates small lesions in the muscle and thus, smaller regenerating fibers are only met in these regions. This underlines the fact that loss of *Osr1* leads to all the defects that are described in this chapter for the mutant`s phenotype and does not cause atrophy of the adjacent uninjured muscle tissue.

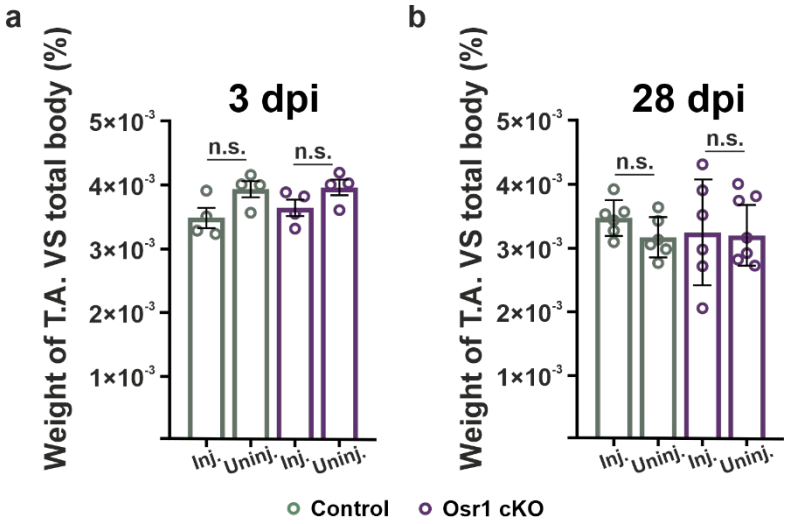

Figure 22: Deficiency of Osr1 does not result in muscle atrophy
Ratio of weight of injured / uninjured T.A. (g) versus total mouse weight (g) plotted as percentage in two different timepoints (a) at 3 dpi and (b) at 28 dpi. No differences can be observed neither between injured and uninjured limbs nor between the two groups. Data are presented as mean ± SEM (n = 4-7); statistical analysis was done using two-tailed Student's t tests: n.s. not significant.

Taken together, this section provided proofs that *Osr1* is explicitly expressed in FAPs before and after muscle injury and revealed the necessity of *Osr1* expression in FAPs for efficient muscle regeneration. *In vivo* data demonstrated that conditional inactivation of *Osr1* led to delayed eMHC^{+} fibers appearance at early stages which resulted in smaller fiber size at later timepoints along with increased necrotic fiber accumulation.

4.2 Increased fibrotic tissue formation with altered mechanics in the injured Osr1 cKO

4.2.1 Defects in scar tissue development of the injured region

Increased tissue necrosis upon injury and defective resolution of the dead fibers are events that typically appear in patients with muscular dystrophies, like in Duchenne muscular dystrophy (dmd) (loss of dystrophin expression). The muscle fibers of dmd patients become vulnerable to contractions and thus, the constant necrotic events eventually lead to abnormal formation of fat and fibrous tissue (Serrano and Muñoz-Cánoves, 2017). Based on the defected myofiber formation observed in the histological stainings shown in the previous section (figures 13-17), how is the fibrotic tissue formation affected during these processes in the Osr1 cKO animals was then addressed. To answer this question, stainings for the collagenous matrix were performed at several timepoints of regeneration.

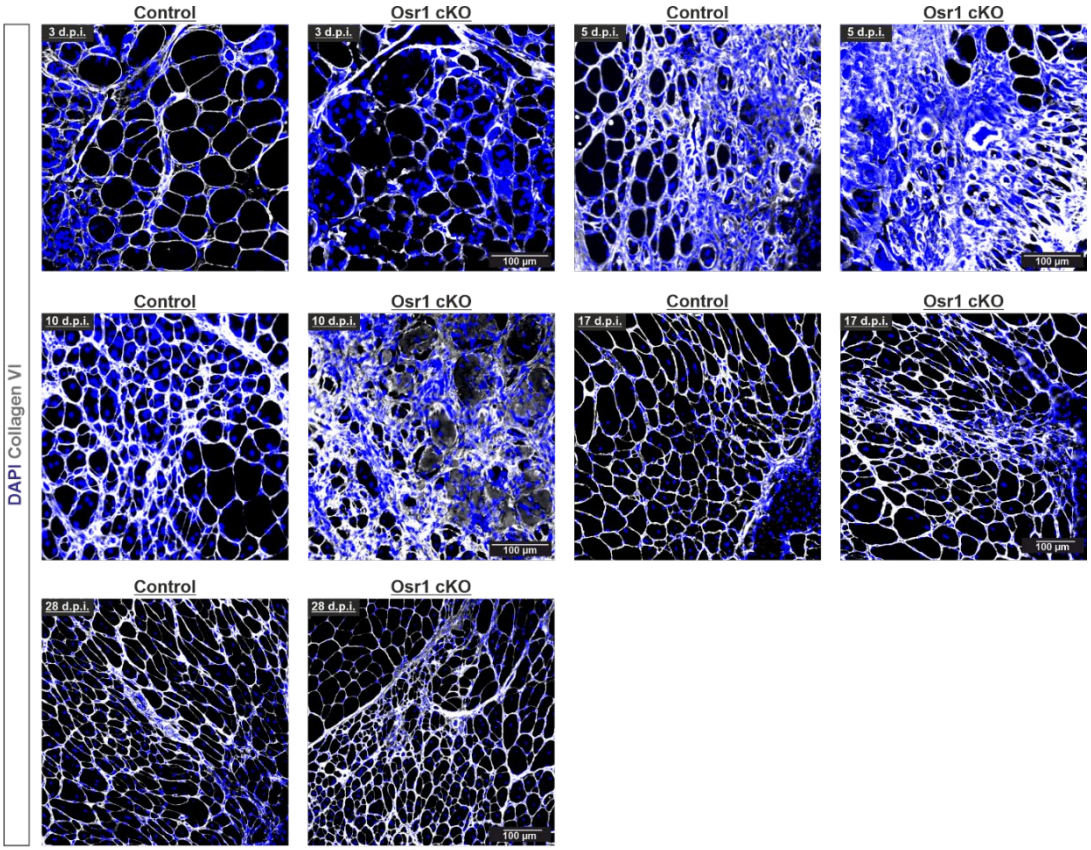

Figure 23: Osr1 mutants exhibit persistent fibrotic tissue formation
Collagen VI immunofluorescence staining at different timepoints of the control and the Osr1 cKO groups. At 3 dpi infiltration of cells can be observed in the injured region of both groups. At 5 and 10 dpi collagenous matrix is more visible in the Osr1 cKO, being persistent throughout regeneration. Notice the structural organization of the injured control at 17 and 28 dpi while in the mutant, small fibers with thick deposition of collagen VI are more prominent.

Tissue stainings of the different timepoints for Collagen VI verified indeed elevated deposition of collagenous matrix in the mutants (figure 23). A constant increase in secretion of collagen VI was exhibited in the Osr1 cKO, which expanded over the area of necrotic fibers at 10 dpi and decreased throughout 17 and 28 dpi. Finally, that resulted in thicker collagenous deposition in between the smaller fibers of the mutants. Despite the initial production of collagen VI in the control animals at 3 and at 5 dpi, they displayed a well-organized fiber structure at 10 dpi, which was resolved in the following time-points.

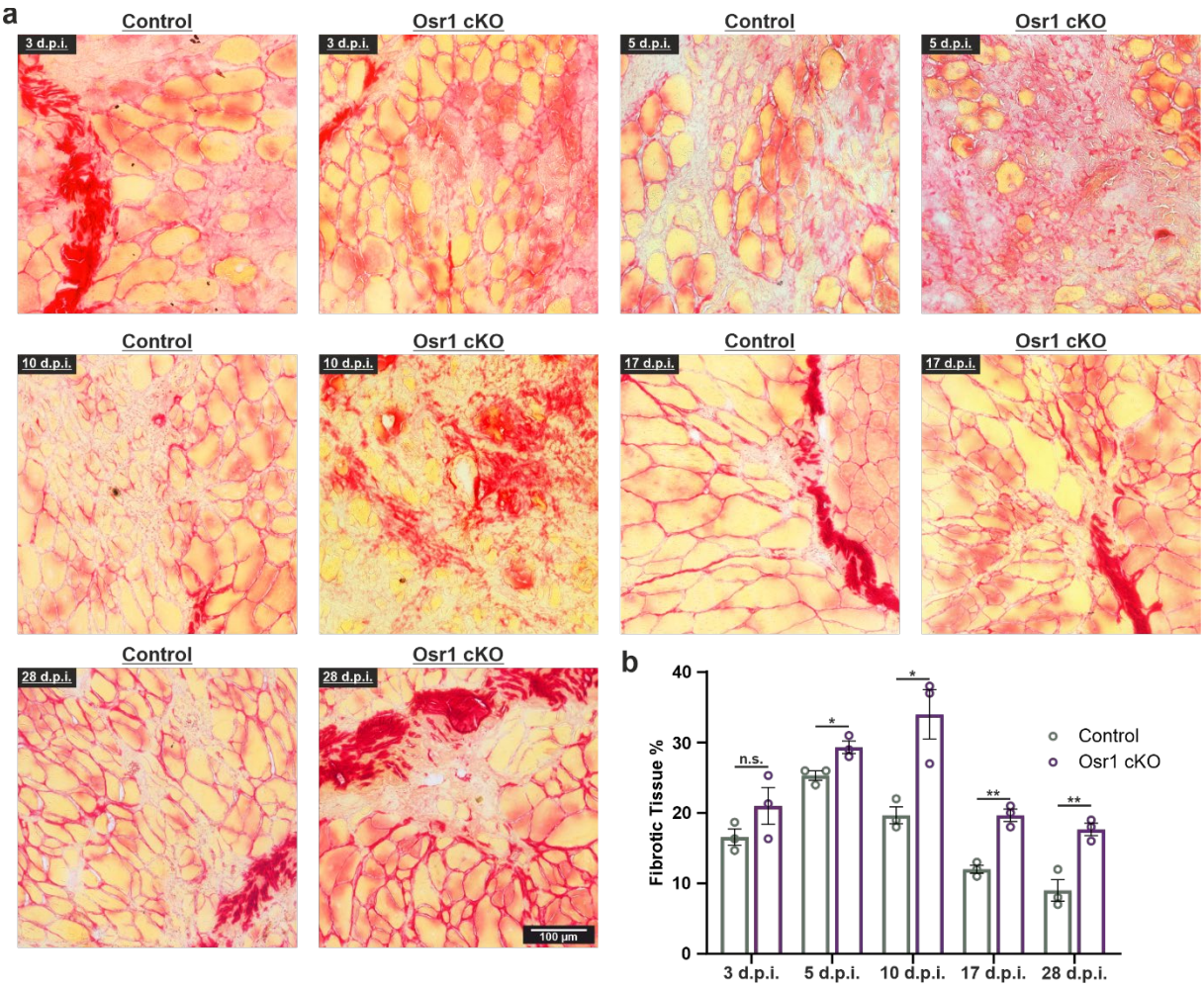

Figure 24: Increased collagenous fibrotic tissue formation in Osr1 cKO
(a) Sirius Red staining throughout regeneration revealed accumulation and thicker deposition of collagenous matrix between the fibers of the Osr1 cKO injured muscle. (b) Quantification of the area of the red staining (collagen fibers) normalized to the total area of the injured tissue showed persistent increased values at all timepoints upon loss of Osr1 expression. Data are presented as mean ± SEM (n = 3); statistical analysis was done using two-tailed Student's t tests: n.s. not significant, * $p<0.05$, ** $p<0.01$.

Having observed the defects in Collagen VI deposition in the injured region, Sirius red staining was performed on the muscle sections. Sirius red is one of the most common diagnostic approaches used in order to observe fibrosis levels in cases of regeneration or inflammation, staining specifically Collagen I and III in the scar tissue. The area of positive tissue stained with Sirius red was also quantified and normalized to the size of the regenerative region for every individual animal. No significant difference was observed at 3 dpi (figure 24a,24b) indicating a normal initial transient fibrotic response, which is a normal feature of the regeneration process. However, from 5 dpi on an increased accumulation of fibrotic ECM was observed in Osr1cKO animals relative to controls (figure 24a, 24b). This was in line with the collagen VI staining shown above. While in controls ECM remodeling led to a marked decrease in picrosirius red staining starting between 5 and 10 dpi, picrosirius red staining in Osr1cKO animals peaked at 10 dpi, and only showed a decrease between 10 and 17 dpi (figure 24a, 24b). At 17 and 28 dpi, Osr1cKO animals still showed approx. twofold picrosirius red staining levels than controls (figure 24a, 24b). In sum, these results corroborate the increased Collagen VI staining observed in the later timepoints of the injured Osr1 cKO animals and indicate that apart from delayed regeneration these animals exhibit increased fibrosis as well.

4.2.2 Decreased injured tissue stiffness in the Osr1 cKO

Fibrotic scar formation is typically associated with increased tissue stiffness (Yang and Plotnikov, 2021), as also observed in mdx animals (Brashear et al., 2021). However, these observations regularly are made in “endpoint” studies that assess passive tissue stiffness at a late time point of disease (Kiriaev et al., 2021, Smith and Barton, 2018). To assess the impact of altered tissue remodeling capacities and accumulation of picrosirius red-positive ECM in Osr1cKO animals during the dynamic regeneration process, nanoindentation was performed (figure 25a). This is a modern technological approach to probe the mechanical properties of the regenerating muscle. The method was first established on muscle sections of wild type uninjured and injured mice at 3, 4 and 5 dpi. Topography scan was performed to distinguish myofiber and extracellular matrix area from the glass slide. The stiffness of the injured area was then measured. A transient increase in Young`s modulus was observed at 3 dpi in comparison to the uninjured individuals, which then remained at similar levels at 4 dpi and decreased

back to the uninjured range already at 5 dpi (figure 25b). Following that, the mechanical properties of the injured tissue from the injured Osr1 cKO were then measured and compared to the injured control. In the regenerating muscle of Osr1cKO animals no transient increase in stiffness was observed at 3 dpi (figure 25c). Moreover, Osr1cKO stiffness stayed consistently softer compared to control tissue at 5 dpi and even at 10 dpi (figure 25c).

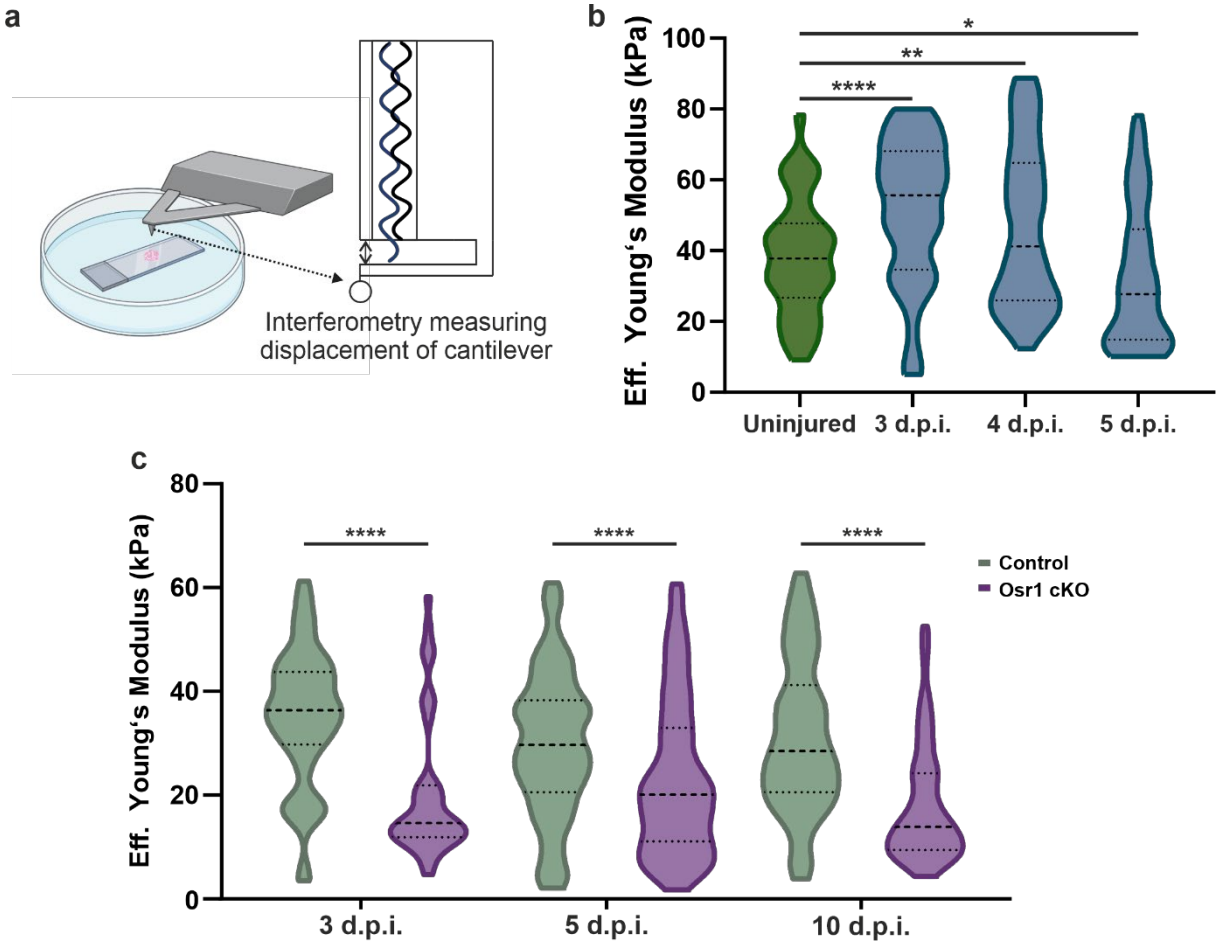

Figure 25: Defects in tissue stiffness of the regenerative area of the Osr1 cKO
(a) Schematic representation of a nanoindenter. Muscle sections were placed underneath the cantilever and topographic analysis was performed collecting load-displacement curves. (b) Stiffness of the injured area was increased at 3 d.p.i and at 4 dpi, but returned to approx. uninjured levels at 5 dpi. (c) Decreased stiffness of the Osr1 cKO at all timepoints indicating a defect in the bio-mechanical properties of the regenerative microenvironment. Data are presented as mean ± SEM (n = 3); statistical analysis was done using two-tailed Student's t tests: * p<0.05, **p<0.01, ***p<0.001, ****p<0.0001. Image created with BioRender.com.

Taken together, these findings suggest that *Osr1* expression in FAPs during regeneration is essential not only for restricting excessive scar tissue formation but also for governing the composition of the regenerative ECM and thus its stiffness. These altered bio-mechanical properties of the Osr1 cKO tissue microenvironment might also negatively affect the healing process. Expansion and activation of MuSCs

is essential to efficient myogenesis. The mechanical forces exerted from the fibrotic ECM and the MuSCs microenvironment can alter their function and thus, their regenerative ability (Trensz et al., 2016). Therefore, in the next session the effect of Osr1 deletion on the population of MuSCs was investigated.

4.3 Loss of *Osr1* in FAPs affects MuSCs during regeneration

Skeletal muscle possesses the ability to regenerate, even after repeated injury, requiring the contribution of MuSCs to the generation of thousands of myoblasts on each occasion. It is known that lack of MuSCs or even interventions that affect their function can be correlated with insufficient or failed regeneration (Relaix and Zammit, 2012). We described in the previous section that *Osr1* deletion has a major impact on muscle trauma healing. Thus, I asked whether this muscle regeneration defect was preceded by a defect in MuSCs.

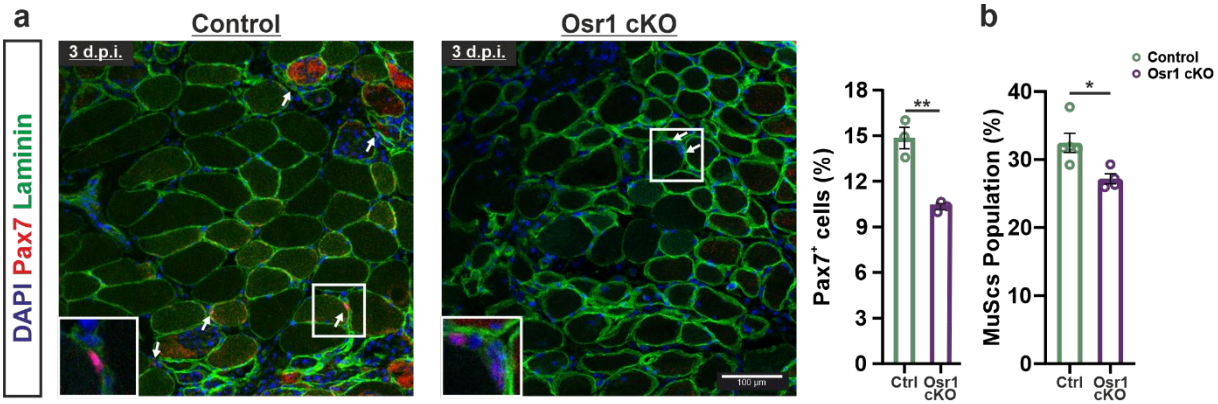

Figure 26: Lower number of MuSCs in the Osr1 cKO at 3 dpi
(a) Co-Immunostaining of Pax7 and laminin in injured muscle at 3 dpi, white arrows point at positions where Pax7$^+$ cells were located, lower number of Pax7$^+$ found in the Osr1 cKO. (b) MuSCs population normalized to muscle resident tissue cells numbers. Data are presented as mean ± SEM (n = 3-5); statistical analysis was done using two-tailed Student's t tests: * p<0.05, **p<0.01.

Consequently, MuSCs' state and function were analyzed at two different timepoints. Directly upon injury, MuSCs start proliferating in order to support the pool expansion, then they become activated and reach their highest number on day 3-4 post injury (Wosczyna and Rando, 2018). For this reason, the first timepoint that I investigated MuSCs numbers was at 3 dpi. Immunostainings for Pax7 on injured tissue sections at this timepoint revealed a decrease in Pax7$^+$ cell numbers in the Osr1 cKO versus the control animals (figure 26a). Quantification of the Pax7 cell numbers only in the injured area of the tissues showed that this difference was approximately 30% (figure 26a). Post analysis of the flow cytometry data at the same timepoint for CD31$^-$ CD45$^-$ TER119$^-$ a7 integrin$^+$ cells revealed also a reduction in the MuSCs population of the mutants, although this was only 5% (figure 26b). Considering the small lesion size in our model, the discrepancy between the two results of MuSCs counting may be explained by the fact that in figure 26a Pax7 cells were counted in the injured region only, whereas for FACs analysis the whole injured muscle was used (mixture of injured and uninjured sites).

Since MuSCs population appeared to be smaller in the mutants, I further analyzed whether this decrease in number could be due to a decreased MuSCs proliferation rate. Freshly isolated MuSCs were cytospun and stained for Ki67, a common used marker of proliferation present in all the active phases of the cell cycle (figure 27a).

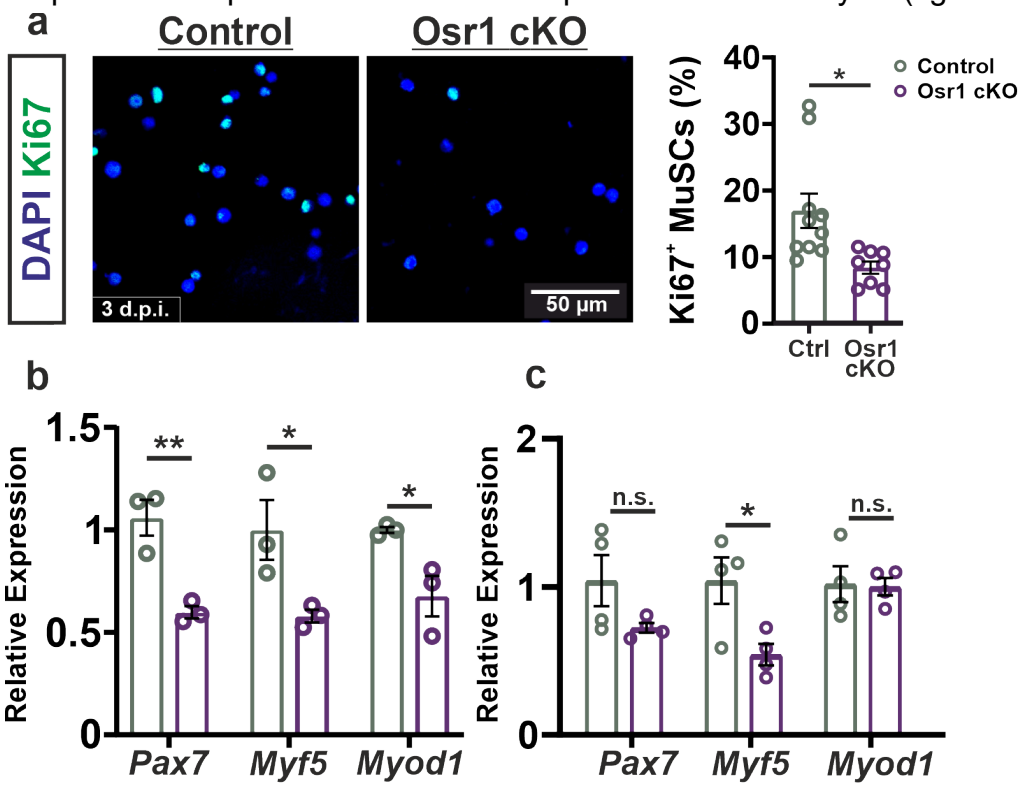

Figure 27: Osr1 cKO MuSCs defects in proliferation and in activation state at 3 dpi
(a) Immunostaining of Ki67 cytospun FACS isolated MuSCs at 3 dpi (left), quantification of Ki67$^+$ MuSCs (right) showed an almost two-fold reduction in proliferation rate of Osr1 cKO. (b) RT-qPCR on 3 dpi. Mutant MuSCs express lower levels of important regulating genes for MuSCs states. (c) RT-qPCR on 3 dpi total muscle samples showed significant lower expression of Myf5 in the mutants. Data are presented as mean ± SEM (n = 3 - 10); statistical analysis was done using two-tailed Student's t tests: n.s. not significant, * p<0.05, **p<0.01.

Quantification of the staining revealed an approximately 40% reduction in the proliferative MuSCs numbers of the Osr1 cKO at 3 dpi. In order to get a further insight into the activation state of MuSCs at this timepoint, RT qPCR for *Pax7*, *Myf5* and *Myod1* was performed on FACS sorted MuSCs (figure 27b). The expression level of all three genes was significantly downregulated in the mutant MuSCs (40% reduction in *Pax7* and *Myf5*, 30% reduction in *Myod1* expression). These results indicate a universal defect in the activation and differentiation of MuSCs. Lastly, RT qPCR for the same genes was performed on whole injured muscle tissue at 3 dpi (figure 27c). Although, *Pax7* expression tended to be lower in the Osr1 cKO MuSCs, *Pax7* and *Myod1* expression was not regulated in the mutants. Expression of *Myf5* though was found to be almost 50% lower in the mutant group. Muscle regeneration can be

functional in lower levels of Myf5 but in a much slower pace, allowing however dystrophic changes to appear (Zammit, 2017).

The population of MuSCs stops expanding approximately 5-6 dpi and their numbers decline gradually over 7-10 dpi. Therefore, I analyzed the proliferation rate of MuSCs at a later stage, at 7 dpi. Intriguingly, the proliferation defect was persistent over regeneration in the mutant, with the freshly isolated cytospun MuSCs to exhibit 50% reduction in Ki67 expression (figure 28a). Concomitantly, MuSC viability was impaired when measure via TUNEL staining (figure 28b). Mutant MuSCs manifested almost two times higher apoptosis in comparison with control MuSCs. In spite of the reduced proliferation and the increased apoptotic rate, the number of MuSCs population was not affected when measured via flow cytometry (figure 28c). MuSCs cell numbers were found to possess the same percentage in the muscle resident cell population in both the control and the Osr1 cKO animals at 7 dpi.

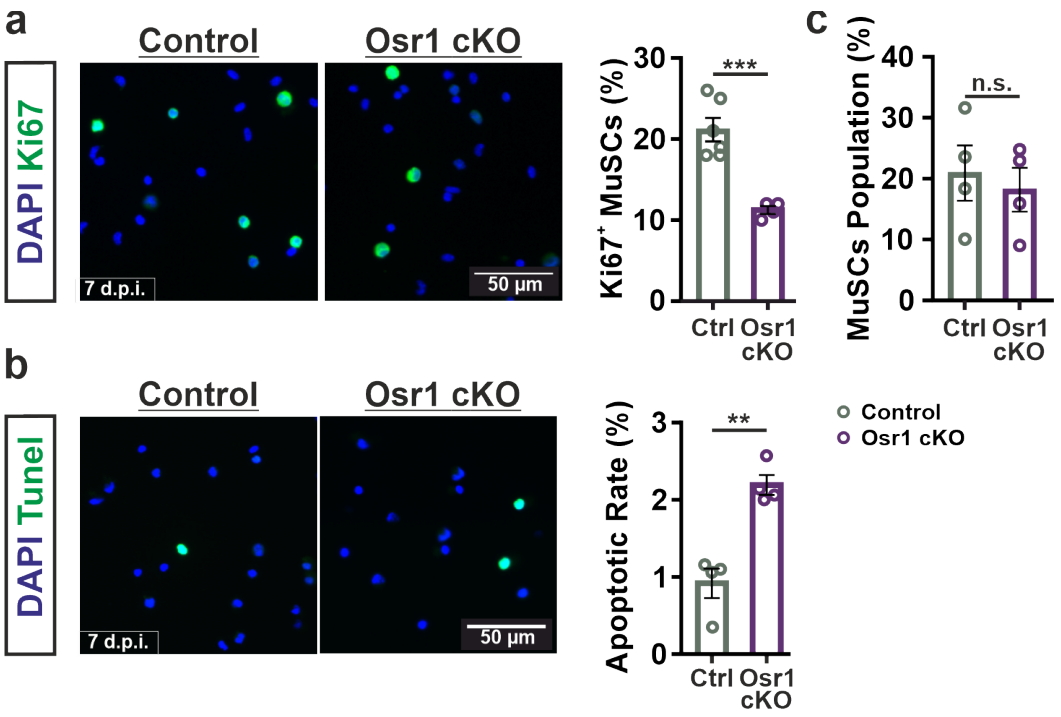

Figure 28: Alterations in proliferation and apoptosis rates of mutant MuSCs at 7 dpi
(a) Immunostaining of Ki67 on 7 dpi MuSCs revealed 50% less positive cells in the Osr1 cKO. (b) TUNEL staining on 7 dpi MuSCs showed higher positive cells in the Osr1 cKO. (c) Equal number of MuSCs in the two groups measured by FACS. Data are presented as mean ± SEM (n = 4 - 6); statistical analysis was done using two-tailed Student's t tests: n.s. not significant, **p<0.01, ***p<0.001.

Similarly, RT qPCR was also performed at 7 dpi MuSCs and revealed that on the one hand levels of *Pax7* and *Myf5* remained unaltered, on the other hand though expression of *Myod1* was still downregulated in the mutants (figure 29a). This result points to the existence of a continuous defect in the activation and differentiation of MuSCs on late regeneration. To further confirm the exact state of MuSCs that is defected in the Osr1 cKO, FACS isolated cells were immunostained for Pax7 and/or MyoD (figure 29b). Notably, that experiment showed a 30% increase in $Pax7^+/MyoD^-$ cells, equal $Pax7^+/MyoD^+$ transit amplifying cells and lastly 40% reduced $Pax7^-/MyoD^+$ committed cells in the Osr1 cKO animals. Taken together, these quantifications show that loss of *Osr1* prior to injury, might not affect MuSCs numbers at 7 dpi but results in inhibiting MuSCs activation and thus in higher number of quiescent cells ($Pax7^+$) and lower amount of transient amplifying cells ($Pax7^+/MyoD^+$).

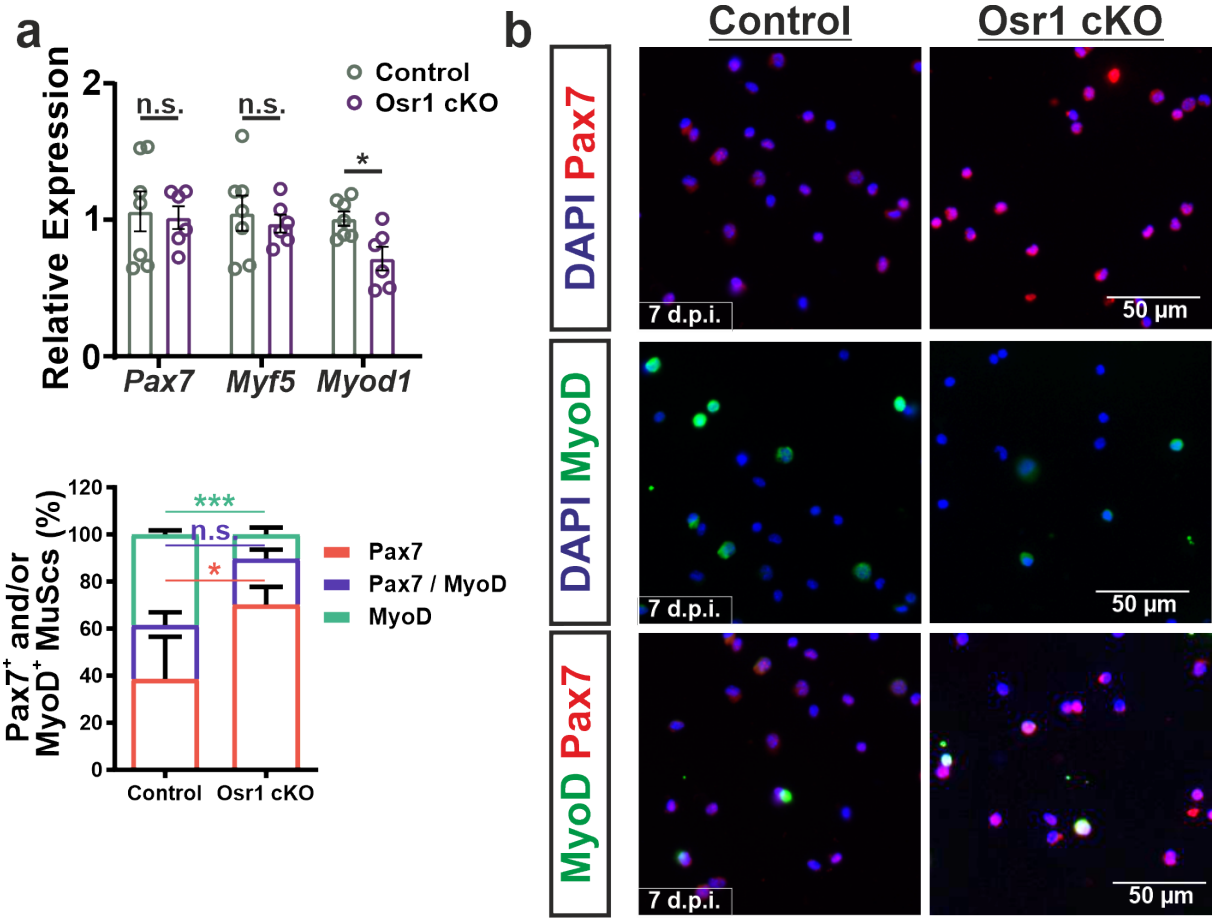

Figure 29: Upon *Osr1* deletion activation of MuSCs is defected at 7 dpi
(a) RT qPCR analysis on FACS isolated 7 dpi MuSCs revealed lower expression of *Myod1* in the mutants. (b) Immunostainings and quantification of Pax7 and/or MyoD on MuSCs. Higher number of $Pax7^+$ MuSCs were quantified in the Osr1 cKO while lower was the percentage of the $MyoD^+$ MuSCs, when compared to control MuSCs. Data are presented as mean ± SEM (n = 4 - 7); statistical analysis was done using two-tailed Student's t tests: n.s. not significant, *p<0.05, ***p<0.001.

Analysis of MuSCs at 3 dpi showed that apart from the defects in their activation states, proliferation was also defected and therefore, less MuSCs were present in the mutants. Although, cell numbers were unaltered at 7 dpi, both events of proliferation and of apoptosis were shown to be affected in the mutants. A question arose from this observation, how can MuSCs numbers be equal between controls and mutants at 7 dpi in spite of their lower proliferation rate? Figure 30a provides a graphical depiction of a plausible answer to this question. At the onset of regeneration MuSCs are rapidly expanding. Loss of Osr1 in FAPs though, inhibits their proliferative potential and mutant MuSCs fail to reach the expected levels at 3 dpi, as I described in the beginning of the section. The number of Osr1 cKO MuSCs remains always lower than the control (due to proliferation / apoptosis defects) on the first days after injury, when inflammation takes place. On early regeneration, when MuSCs give rise to myocytes, MuSCs numbers from both groups start declining and therefore, the mutant number of MuSCs coincides with the one from the control at day 7.

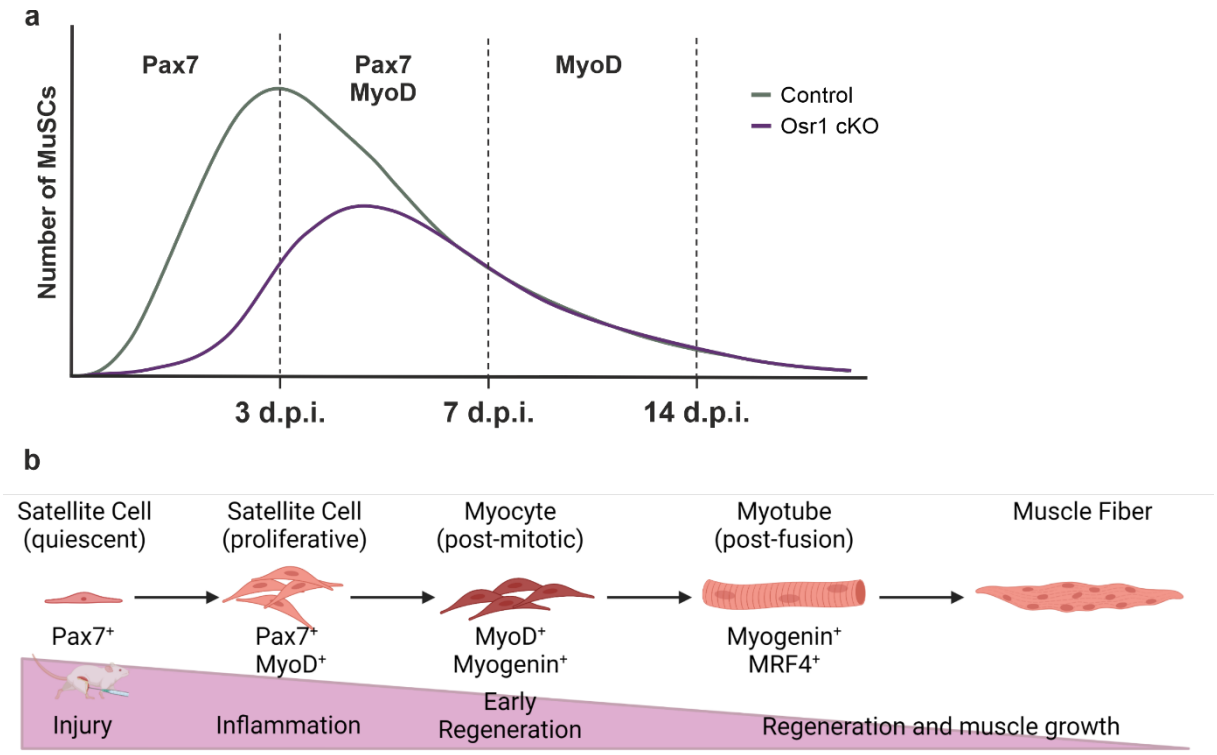

Figure 30: Initial fail of Osr1 cKO MuSCs to expand upon injury
(a) Schematic representation depicting mutant MuSCs failure to proliferate at 3 dpi while at 7 dpi their numbers decline, reaching this way the same level with the control MuSCs. (b) Mutant MuSCs don`t possess a regenerative potential and regeneration is delayed at 7 dpi with the majority of them being in the quiescent state. Image created with BioRender.com.

In figure 30b the different states of MuSCs are depicted. In short, when MuSCs ($Pax7^+$) respond to injury, are rapidly activated and generate proliferating $Pax7^+$ / $MyoD^+$ cells which some of them differentiate ($MyoD^+$) into myoblasts, ultimately fusing with existing myofibers or with each another to form new myotubes. MuSCs of the Osr1 cKO at 7 dpi were shown to be more $Pax7^+$ and less $MyoD^+$. Thus, regeneration is delayed in the Osr1 cKO, with more MuSCs being in the quiescent state at 7 dpi whereas the majority of MuSCs in the control promote myogenesis.

In sum, the results of this section conclude, that loss of *Osr1* expression by FAPs during regeneration can, in a non-cell autonomous manner, alter the function of MuSCs by affecting MuSC activation, proliferation and survival, leading to impaired muscle regeneration. Since FAPs population was first described, their contribution to efficient wound healing through the generation of a beneficial microenvironment for MuSCs had as well been meticulously reported (Joe et al., 2010). Considering that, as well as the specificity of *Osr1* expression in FAPs (previous section), I decided to proceed with investigating the outcome of *Osr1* deficiency in FAPs population concomitant to injury.

4.4 *Osr1* deficiency has an intrinsic defect on FAPs

In section 1.1, *Osr1* was shown to be expressed specifically in FAPs during muscle regeneration at various timepoints. Previous work performed in the lab supports also *Osr1* specificity in adult FAPs (Stumm et al., 2018). Osr1 cKO animals exhibited delayed regeneration, while the analysis of the mutant MuSCs in section 2.3 revealed a propensity for MuSCs to remain in a quiescent state upon muscle injury, whereas MuSCs in the control get activated to support myogenesis and thus, muscle regeneration. However, since *Osr1* is not expressed in MuSCs but in FAPs, generated the question why do mutant MuSCs exhibit these major defects. I thereby hypothesized that loss of *Osr1* must also influence FAPs function, disrupting advantageous interaction between FAPs and MuSCs in several levels. Therefore, in this section Osr1 cKO FAPs were analyzed both *in vivo* and *in vitro*, in order to elucidate which defects can be caused of the loss of *Osr1*.

4.4.1 Establishment of an *in vitro* model for *Osr1* recombination

To study the effect of *Osr1* deletion on FAPs, adherent connective tissue fibroblasts (aFbs) were isolated from skeletal muscle. These cells have been shown in the study of Contreras et al., 2019 to mimic both biochemically and phenotypically the identity of FACS sorted FAPs (Contreras et al., 2019b). Both cell populations express the same amount of *Tcf7l2* and *PDGFRa*, while the advantage of using these cells in *in vitro* assays is the low cost of their isolation (preplating vs FACS sorting) and the shorter time needed for similar isolation efficiency.

In order to analyze the result of *Osr1* deficiency in FAPs *in vitro*, I performed *in vitro* recombination with 4-OHT (4-Hydroxytamoxifen), the active metabolite of tamoxifen. Cell treatment with this compound allows, whenever cre-recombinase is expressed, a subsequent deletion of floxed genes. For this purpose, I used the CAGG Cre Osr1 flox line, extracted the FAPs and proceeded with 4-OHT treatment. This results in a generation of an Osr1 knock-out cell population with a stable modification in its genome, that allows expansion and further analysis of cells response to *Osr1* deletion.

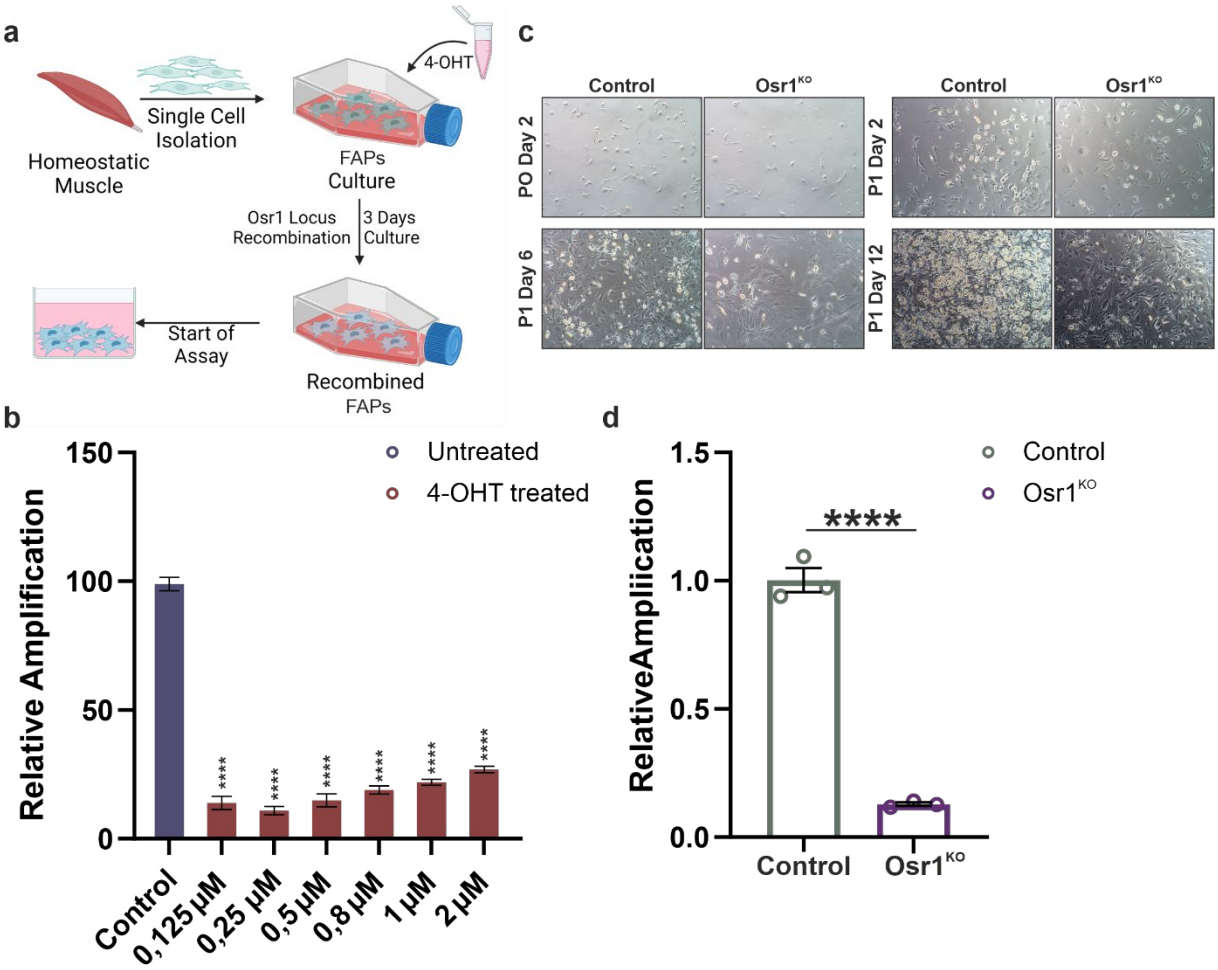

Figure 31: Establishment of an *in vitro Osr1* recombination system
(a) Schematic representation of the process followed for FAPs treatment with 4-OHT. (b) Osr1 exon 2 amplification on genomic level upon treatment of cells with different amounts of 4-OHT. Highest efficiency in deletion of Osr1 was observed after treatment with 0,25-0,5 µM 4-OHT. (c) Brightfield images of FAPs cells undergoing Osr1 recombination during establishment of the method. Differences in the cell numbers and adipocyte formation is visible already at day 6 of Passage 1. (d) RT-qPCR on genomic DNA isolated from the experiment shown in (c) revealed high efficiency of the system used. Data are presented as mean ± SEM (n = 3); statistical analysis was done using two-tailed Student's t tests: ****p<0.0001.

In short, to establish the generation of the Osr1 cKO *in vitro*, FAPs were isolated via pre-plating from a homeostatic muscle and treated directly upon isolation with 4-OHT in order to recombine immediately the locus of *Osr1*. From this point on, cultured *in vitro* recombined FAPs from the Osr1 cKO animals will be termed as Osr1^{KO}. Cells were expanded for 3-4 days approximately and then were used directly for cell differentiation or apoptosis assays (figure 31a). At this point, is worth referring that both control and Osr1^{KO} aFbs were treated with 4-OHT in order to eliminate the apoptotic factor of the tamoxifen from any experimental read-out. A titration step of 4-OHT concentration when applied on FAPs was essential since there are no studies available with 4-OHT treatment on FAPs cells *in vitro*. Figure 31b depicts the relative

amplification of the genomic locus for the exon 2 of *Osr1*, as measured via RT-qPCR in genomic DNA isolated from control and Osr1^{KO} FAPs treated with different amounts of 4-OHT. High efficiency of *Osr1* locus recombination was observed in all the samples, with the most efficient being after treatment with 0,25 µM of 4-OHT. Moreover, direct recombination of *Osr1* in passage 0 in FAPs resulted in lower number of cells in comparison with the control treated aFbs (figure 31c). This can be attributed to differences in the isolation efficiency protocol or in the muscle size of the animal. Intriguingly, in passage 1 of 4-OHT treated cells from the control animals were proliferating and expanding in a normal rate. On the other hand, the expansion rate of Osr1^{KO} aFbs was constantly lower. Note the difference in the amount of lipid formation on day 12 between the control and the Osr1 cKO treated FAPs. In order to validate the efficiency of the newly established *in vitro* system, the recombination was evaluated with a genomic RT-qPCR on the exon 2 of *Osr1* (figure 31d). I found an approximately 85% reduction in the amplification of the *Osr1* exon 2 locus in the *in vitro* recombined Osr1^{KO} FAPs when compared to the treated cells from the control animals. Altogether, these data show that the 4-OHT system can be successfully applied on freshly isolated FAPs with the intention of studying *Osr1* knock-out on these cells, providing high recombination efficiency.

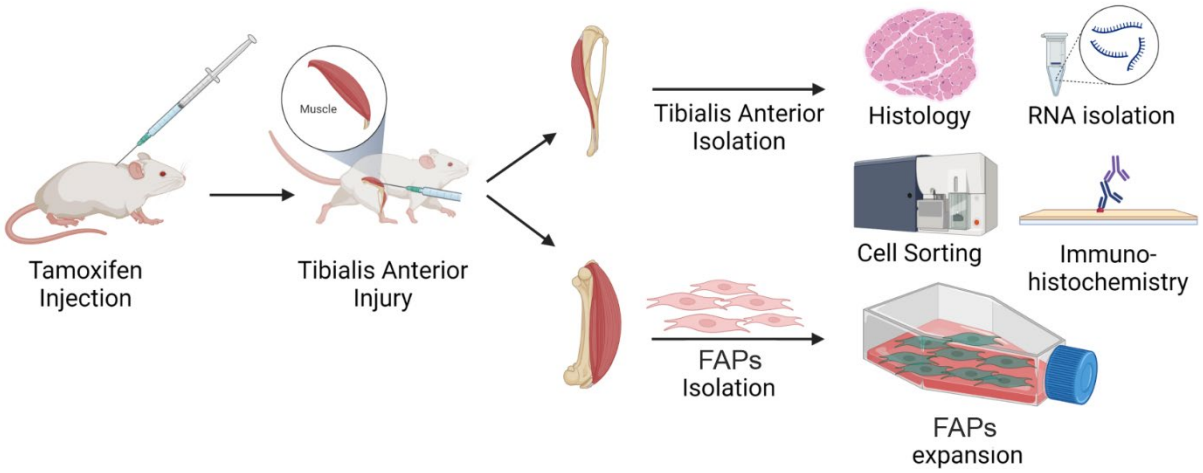

Figure 32: Schematic representation of FAPs isolation from non-injured hindlimbs
Injured T.A. was used for all the FAPs and histology experiments. Hindlimb uninjured muscles were used for FAPs isolation and used for *in vitro* assays. Cells were thereby considered to be in alerted state.

To minimize the number of animals needed for this project, I decided in some occasions to make use of the rest of the muscles from the injured CAGG Cre Osr1 flox animals. These animals are injected with tamoxifen prior to the T.A. injury and therefore *Osr1* locus recombination is taking place *in vivo* (figure 32). Isolating the injured T.A.

on several timepoints was used mainly for histology experiments, for isolating RNA either from whole muscle or individual populations, for FACS sorting and for immunofluorescence of cells or tissues. Therefore, in some occasions I proceeded with the isolation of FAPs from the rest of the muscles from the hindlimbs of the injured individuals. These FAPs are considered as alerted cells and did not need further treatment with 4-OHT *in vitro*.

4.4.2 *Osr1* deficiency *in vitro* affects FAPs viability

Upon system establishment, FAPs were isolated from healthy animals and treated with 4-OHT *in vitro*. The recombination efficiency was tested once again on day 6 of culture via RT-qPCR but this time on mRNA transcripts. Interestingly, an approximately 98% reduction in the mRNA expression of *Osr1* in the FAPs from the mutant animals was found. This further verifies the efficiency of the system also in the gene expression level (figure 33a). Similar to figure 31c, it was observed that mutant FAPs were not expanding in a similar rate as the control cells, although the seeding density of the recombined cells was the same. Therefore, the cell numbers were measured after 6 days of culture and showed a 50% reduction in viability of mutant FAPs (figure 33b). Finally, mutant cells exhibited a 2-fold increase in apoptosis as measured via TUNEL staining on day 4 of culture, explaining in part the lower cell numbers that were noticed before (figure 33c). Altogether, the appliance of the conditional recombination of the Osr1flox allele *in vitro* allowed me to prove that defects in FAPs cell numbers and apoptosis are cell autonomous and can be thus, attributed explicitly to loss of *Osr1* expression.

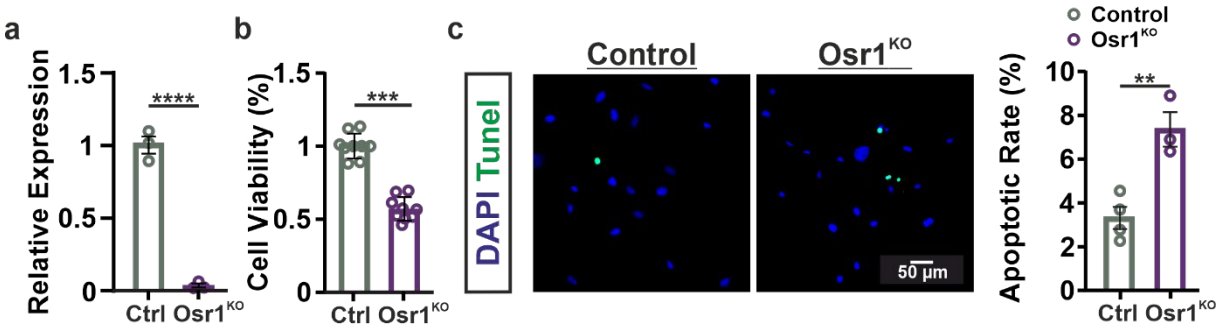

Figure 33: *In vitro* recombination of *Osr1* in FAPs inhibits cells expansion
(a) RT-qPCR of *Osr1* expression on day 6 of cultured FAPs. 98% downregulation of *Osr1* expression was measured in recombined FAPs. (b) Quantification of FAPs number on day 6 of culture. Lower cell numbers were measured in the well with Osr1^{KO} FAPs. (c) TUNEL staining on recombined FAPs showed two-fold induction in the apoptotic rate of Osr1^{KO} cells. Data are presented as mean ± SEM (n = 3-9); statistical analysis was done using two-tailed Student's t tests: **p<0.01, ***p<0.001, ****p<0.0001.

4.4.3 Conditional inactivation of *Osr1* has a similar effect on FAPs *in vivo*

To elucidate the exact defects in FAPs caused by loss of *Osr1* on the regeneration process, FAP behavior was analyzed at 3 and at 7 dpi. Similar to MuSCs cell numbers on the same timepoints (figures 26b and 28c), FAP number was also decreased approximately by 8% at 3 dpi in the Osr1 cKO but remained on similar levels at 7 dpi, as analyzed by flow cytometry (figure 34a). Despite that, at 7 dpi freshly isolated and stained for Ki67 Osr1 cKO FAPs showed a decreased proliferation (approx. 80%) in comparison to the control FAPs (figure 34b). Comparatively, TUNEL staining at the same timepoint revealed an almost 3-fold induction in the apoptosis of the Osr1 cKO FAPs (figure 34c). These *in vivo* results are in line with the *in vitro* data shown in the subsection before. Thus, expression of *Osr1* in FAPs is essential for the pool expansion not only in homeostatic conditions *in vitro* but also upon regenerative cues *in vivo*.

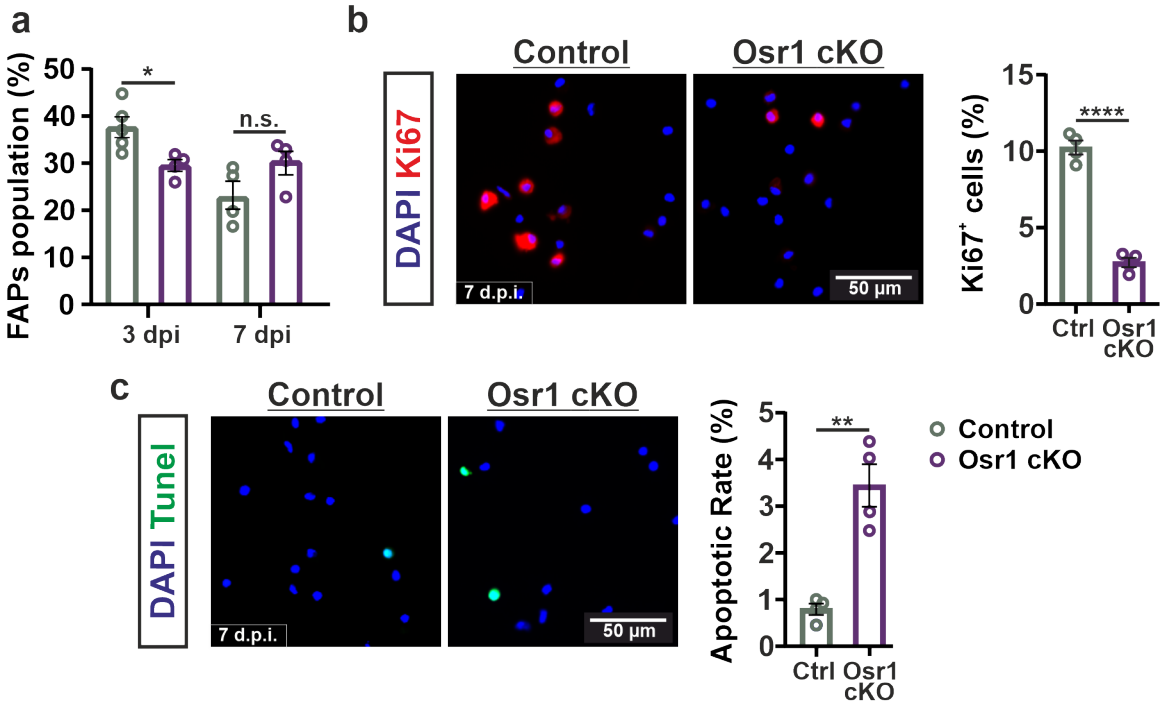

Figure 34: *In-vivo* defects of *Osr1* deletion in FAPs during regeneration
(a) FAPs numbers were decreased in the mutants at 3 dpi but remained on similar levels at 7 dpi Numbers are shown as percentage normalized to the total amount of muscle resident tissue cells, measured by FACs. (b) Freshly isolated cytospun FAPs stained for Ki67 showed decreased proliferation of Osr1 cKO FAPs at 7 dpi (c) TUNEL staining on FACs sorted FAPs revealed 3,5-fold induction of apoptosis in the mutant cells. Data are presented as mean ± SEM (n = 4-5); statistical analysis was done using two-tailed Student's t tests: n.s. not significant, *p<0.05, **p<0.01, ****p<0.0001.

4.4.4 Transcriptome analysis of GFP expressing FAPs at 3 and at 7 dpi

Having found that deletion of *Osr1* leads to defects in FAPs viability both *in vivo* and *in vitro*, transcriptome analysis of FAPs was performed. For this, FAPs that were FACS-isolated based on their expression of GFP (efficiently recombined cells with active *Osr1* promoter) were used, hence enriching for cells from the regenerative region. Since data for MuSCs/FAPs proliferation and apoptosis were acquired at 3 and at 7 dpi, GFP expressing FAPs were isolated also at these two timepoints.

The efficient deletion of floxed exon 2 and the following exon 3 was confirmed in the RNA-seq data at 3 dpi by uploading the data to the International Genome Browser and the reads for the individual exons can be seen in the figure 35a. As a threshold for the differentially expressed gene, the fold change of a gene`s expression in mutant versus in control GFP^+ FAPs was set to 1.2. Following statistical analysis, all the up- and down-regulated genes in the Osr1 cKO FAPs were depicted in a volcano plot as single dots, where the dots of significantly regulated genes are color coded with red for the upregulated ones and with blue for the downregulated (figure 35b). This analysis revealed in total 950 differentially expressed (DE) genes between control and Osr1 cKO FAPs, from which 261 were upregulated and 689 were downregulated in the mutant. Following RNA-sequencing, differentially expressed genes were analyzed, performing a gene ontology (GO) analysis. Gene ontology analysis for the genes upregulated in Osr1 cKO FAPs yielded terms related to the extracellular matrix (ECM) or cell-ECM attachment, such as “Collagen-containing ECM” under the cellular compartment GO group, “Extracellular structural constituent” under the molecular function GO group, and “Cell adhesion” under the biological process GO group (figure 35c). As for the downregulated genes, terms from the biological process like “innate immune response” and “regulation of immune system” were enriched (figure 35c).

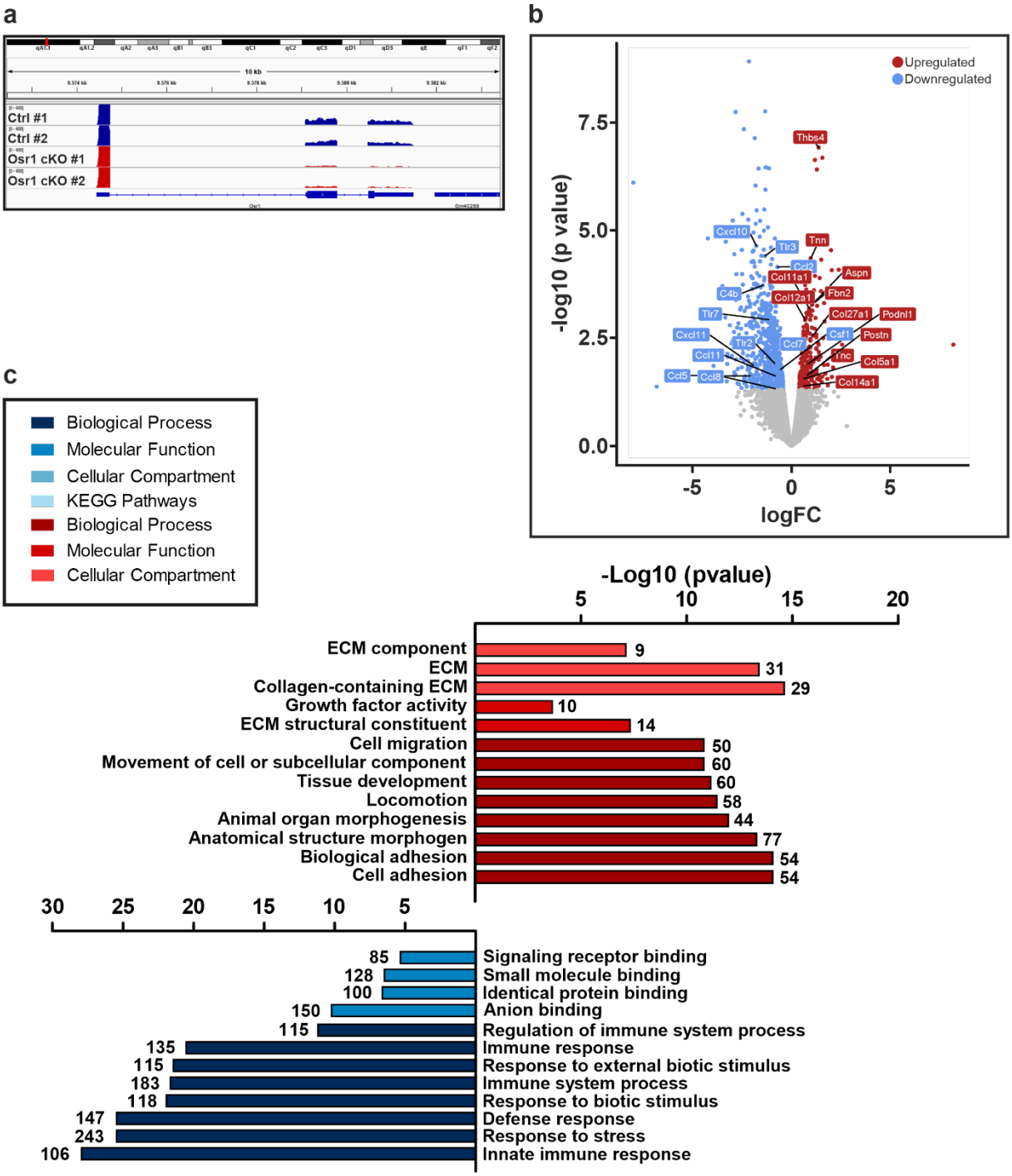

Figure 35: Transcriptome analysis of GFP⁺ FAPs at 3 dpi
(a) Mapped reads for the individual exons of the *Osr1* in the IGV database validates *Osr1* exon 2 and 3 deletion in the GFP⁺ cells from the Osr1 cKO tissue. (b) Volcano plot depicting 261 DE upregulated and 689 DE downregulated genes in the Osr1 cKO GFP FAPs with fold change higher than 1.2. (c) GO analysis for the upregulated DE genes yielded terms related to the ECM and for the downregulated DE genes related to the immune response. Significance of each term is plotted as the -$\log_{10}$ of the pvalue. The number next to each bar indicates the number of genes belonging to each term.

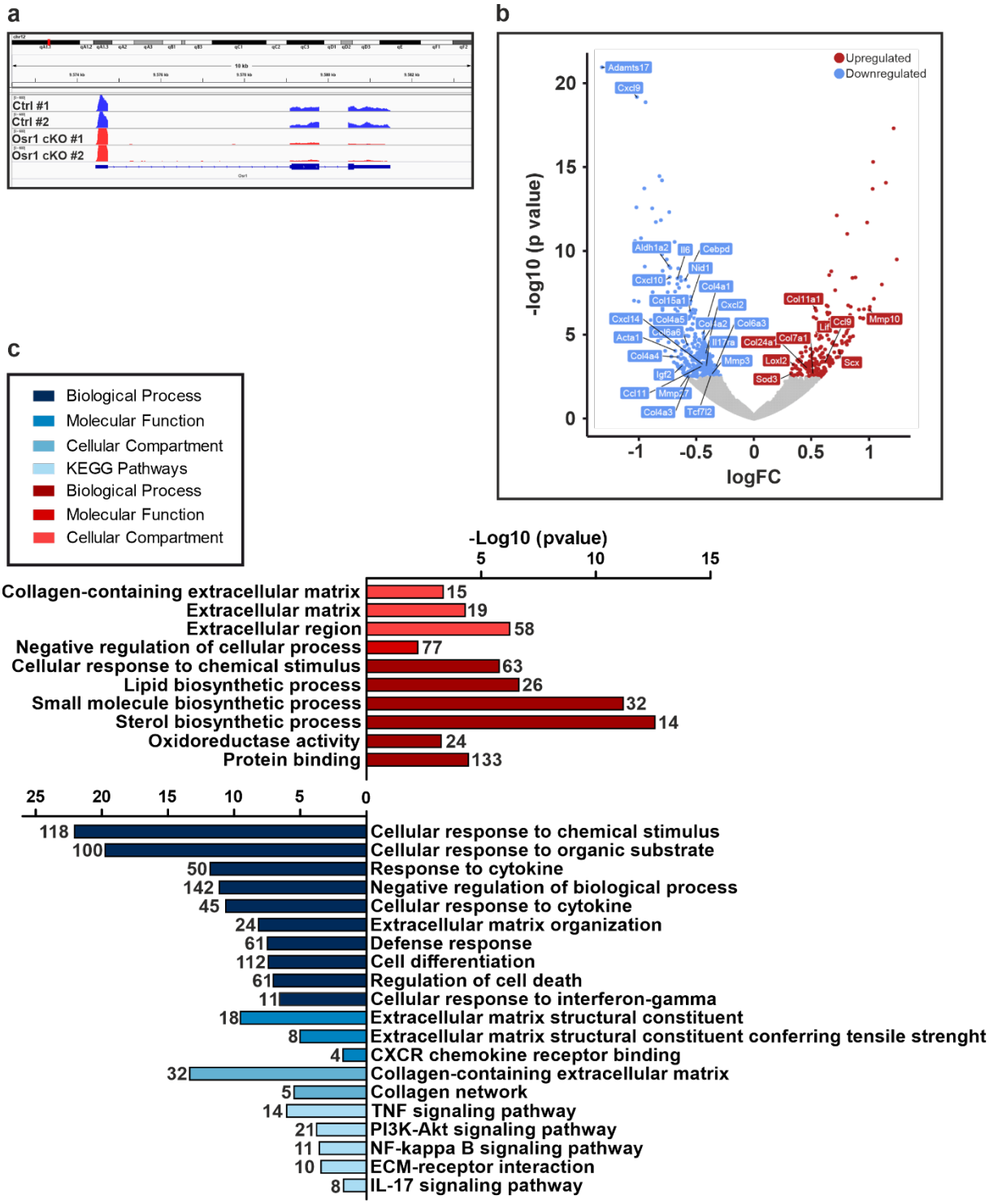

Figure 36: Transcriptome analysis of GFP⁺ FAPs at 7 dpi
(a) Recombination of *Osr1* exon 2 and 3 validation uploading the mapped reads to the IGV browser. Lower reads in the Osr1 cKO depicted with red. (b) Volcano plot depicting 206 DE upregulated and 338 DE downregulated genes in the Osr1 cKO GFP FAPs with fold change higher than 1.2. (c) GO analysis for the upregulated DE genes yielded terms related to the ECM and for the downregulated DE genes related to the immune response. Significance of each term is plotted as the -$\log_{10}$ of the p-value. The number next to each bar indicates the number of genes belonging to each term.

Interestingly, similar results were acquired upon analysis of the 7 dpi GFP$^+$ FAPs. The efficiency of the recombination at this timepoint is depicted in figure 36a. Reads for the exon 2 and exon 3 of *Osr1* locus were found to be significantly less in the mutant FAPs. In total, 544 differentially expressed genes were regulated in the Osr1 cKO cells at 7 dpi, 206 being upregulated and 338 downregulated. The distribution of the DE genes was once again designed using a volcano plot (figure 36b). In line with the results obtained at 3 dpi amongst genes upregulated in Osr1cKO FAPs, GO analysis yielded terms such as “extracellular matrix” and “collagen-containing extracellular matrix” from the GO group cellular compartment (figure 36c). In the downregulated terms, “response to cytokines” and “defense response” from the biological process group, were enriched in the Osr1 cKO FAPs (figure 36c).

Subsequently, overlaps in the GO terms analysis at 3 and a 7 dpi were observed both in the upregulated and in the downregulated terms, mainly affecting ECM-related and immune response-related gene expression. To further confirm these overlaps, a comparison study between the two datasets was performed (figure 37a). In total 96 genes were identified to be regulated at both timepoints in the Osr1 cKO FAPs. From these 96 genes, 32 of them were commonly upregulated and 45 were downregulated in the Osr1cKO FAPs. The rest 19 genes were not regulated in the same direction between the 3 and the 7 dpi datasets. Figure 37b depicts a heat map for the z-score of some common regulated gene reads that resulted from this analysis. These genes were mined from the GO terms analysis for the commonly regulated 96 genes, which showed an enrichment of e.g. “collagen-containing extracellular matrix” in upregulated genes and e.g. “defense response” in downregulated genes (figure 37c). Interestingly, note that TNFα signaling pathway was found to be downregulated at both timepoints. Thus, the consistency of the data was also verified through this comparison, indicating that loss of *Osr1* prior to injury is enough to alter FAPs gene expression related to key regenerative events.

To conclude, the data shown in this section demonstrated that *Osr1* expression in FAPs regulate several of the key functions ascribed to this cell population during the regeneration process (Wosczyna et al., 2019). The establishment of an *in vitro* recombination system and its high efficiency allowed me to show that upon genomic deletion of *Osr1*, FAPs tend to go under apoptosis and their expansion is affected. This tendency was also verified *in vivo* together with defected proliferation rate of Osr1 cKO FAPs. Furthermore, loss of *Osr1* leads to a lasting shift in FAPs transcriptional profile

altering the expression of genes encoding ECM components and remodeling factors, as well as of genes encoding components of immune related signaling. The activation of the immune response is time-wise the first process that was shown to be regulated in the Osr1 cKO animals. Therefore, in the next section a thorough comparison of several immune cell populations that participate in this event was performed.

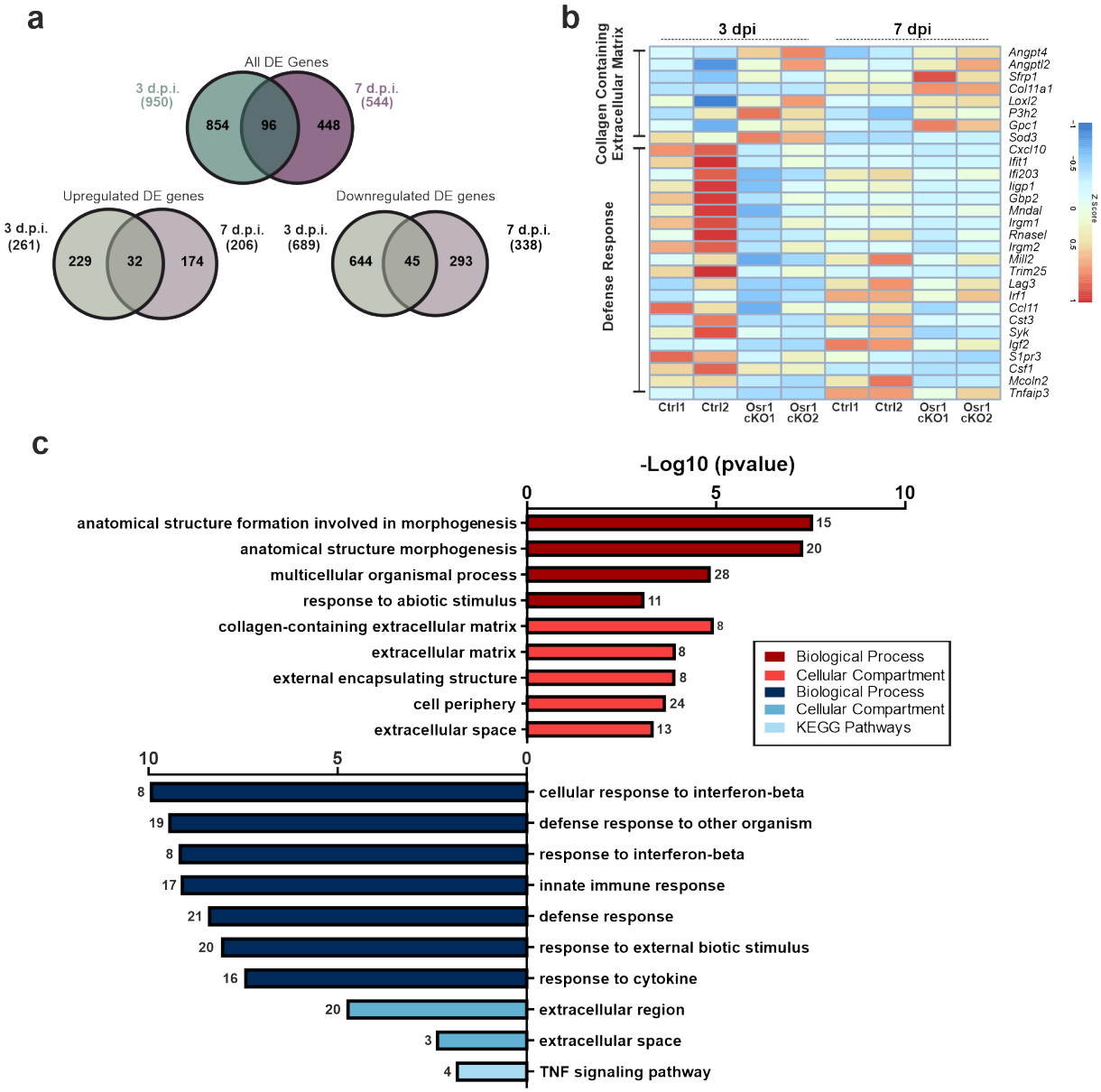

Figure 37: Comparison of transcriptome data from GFP⁺ FAPs at 3 and 7 dpi
(a) Venn diagrams showing 96 common regulated genes between the two datasets, 32 of which were in both cases upregulated and 45 were downregulated (b) Heat maps of common regulated genes. Upregulated common genes are related to ECM whereas downregulated common genes to immune response, indicating a stable effect of *Osr1* deficiency in function of FAPs during regeneration. Individual gene reads are transformed and depicted as z-score. (c) GO terms analysis of common regulated genes. Collagen containing extracellular matrix is upregulated in the mutant while terms related to the defense mechanism are downregulated. Significance of each term is plotted as the -log10 of the p-value. The number next to each bar indicates the number of genes belonging to each term.

4.5 Expression of *Osr1* orchestrates FAPs-immune cell interplay and allows early macrophage polarization

4.5.1 *Osr1* deficient FAPs exhibit altered cytokine secretion

The transcriptome analysis shown in the previous section, identified the immune response as a potential primary target of the defects in the Osr1 cKO animals. At both timepoints of regeneration, genes that are transcribed to cytokines and to paracrine factors were found to be downregulated in the GFP⁺ FAPs of the mutant animals (figure 38). The majority of these genes should under normal conditions get dynamically overexpressed upon injury in order to aid the regeneration process, by activating and stimulating the immune response. More specifically at 3 dpi members of the MCP

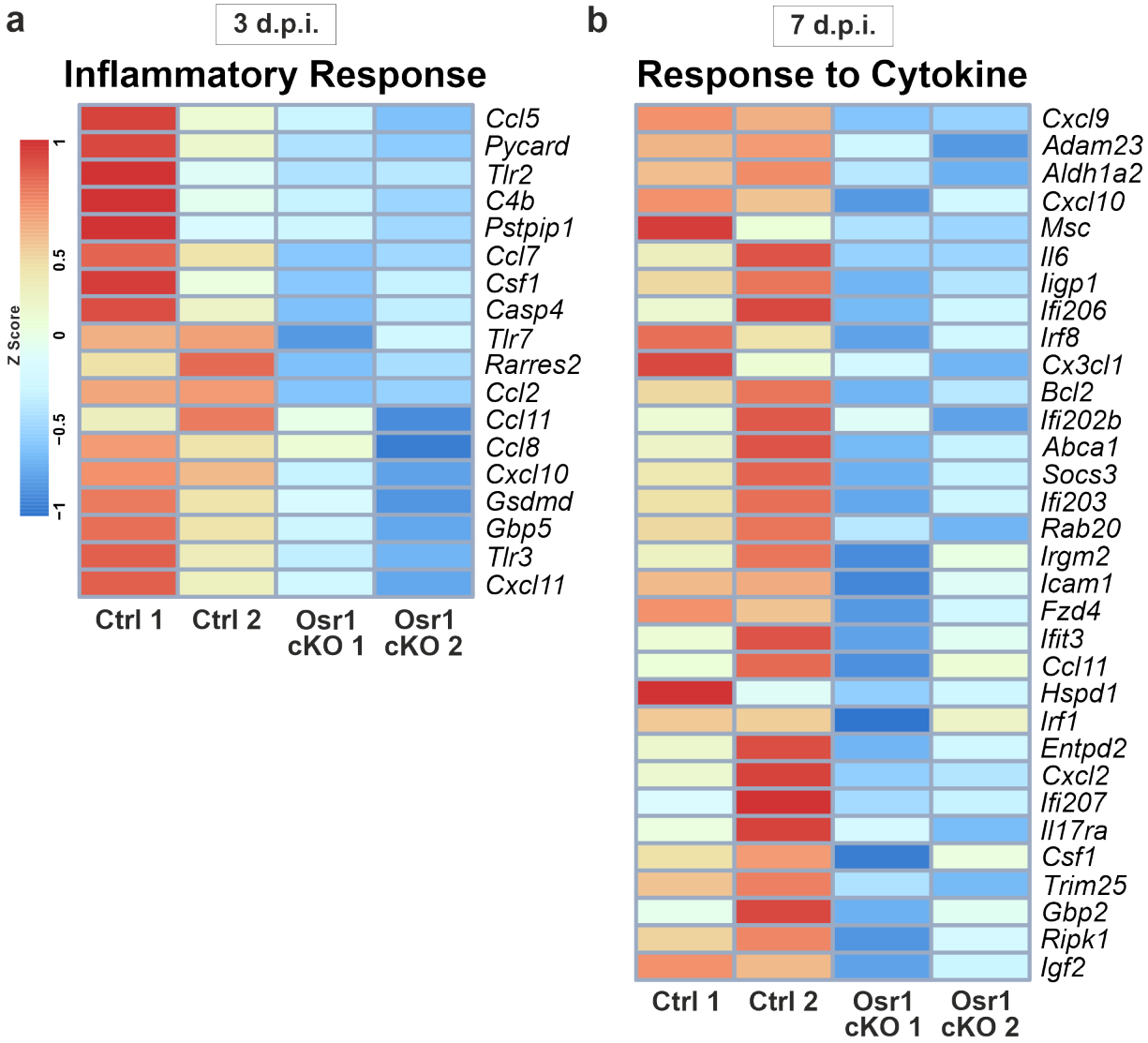

Figure 38: Genes of secreted cytokines are downregulated in GFP⁺ FAPs
Heat map of genes being downregulated, associated with (a) the inflammatory response at 3 dpi and (b) the defense response to cytokines at 7 dpi. Individual gene reads are transformed and depicted as z-score.

(monocyte chemotactic protein) chemokine family e.g. *Ccl2*, *Ccl8* and *Ccl11*, were downregulated significantly in the Osr1 cKO FAPs (figure 38a). These cytokines are mainly expressed by FAPs in muscle regeneration (Oprescu et al., 2020) and have the important role to shape the plasticity of the macrophages. The difference in the expression of genes belonging to the GO term “Inflammatory Response” is depicted as a heat map in figure 38a. In addition, gene expression of the GO term “Response to Cytokine”, mined from the data analysis of the 7 dpi GFP$^+$ FAPs, is shown in a heat map in figure 38b. In this heat map the depicted genes encode cytokines that are also involved in the inflammatory response. For instance, Ccl11, a chemoattractant of immune cells, Bcl2 the apoptotic associated protein and the myokine IL6.

In figure 36c was shown that 4 of the downregulated DE genes at 7 dpi belong to the TNFα signaling pathway, as these were mined in the KEGG database. TNFα is one of the major controlling factors of FAPs expansion related to the defense response already from the onset of regeneration, mainly produced by the infiltrating M1 pro-inflammatory macrophages (Lemos et al., 2015). Therefore, all the DE genes from both datasets were uploaded in the BioPlanet database of the NCBI in order to validate whether the TNFα pathway is included in the top 10 regulated pathways in the Osr1 cKO FAPs. Interestingly, the term “TNFα effects on cytokine activity, cell motility and apoptosis” was significantly regulated at 3 dpi (figure 39a) but also at 7 dpi (figure 39b). Of note, once again the terms immune system and extracellular matrix emerged also, in the results of this analysis. The majority of the genes belonging to the TNFα effects term, were found to be downregulated in the Osr1 cKO GFP$^+$ FAPs (e.g. *Ccl2*, *Ccl5*, *Ccl11*, *Cxcl10*, *Cxcl11*). The expression level of the TNFα term-related genes at both timepoints is depicted in the cytokine heatmaps (figure 39c).

In sum, extensive transcriptome data analysis from the GFP$^+$ FAPs at both timepoints revealed that *Osr1* deletion leads to altered cytokine profile secretion in FAPs. This might in turn affect i) the infiltration of immune cells in the site of the injury, ii) the macrophage polarization switch iii) as well as the response of FAPs to high levels of M1 macrophage-secreted TNFα.

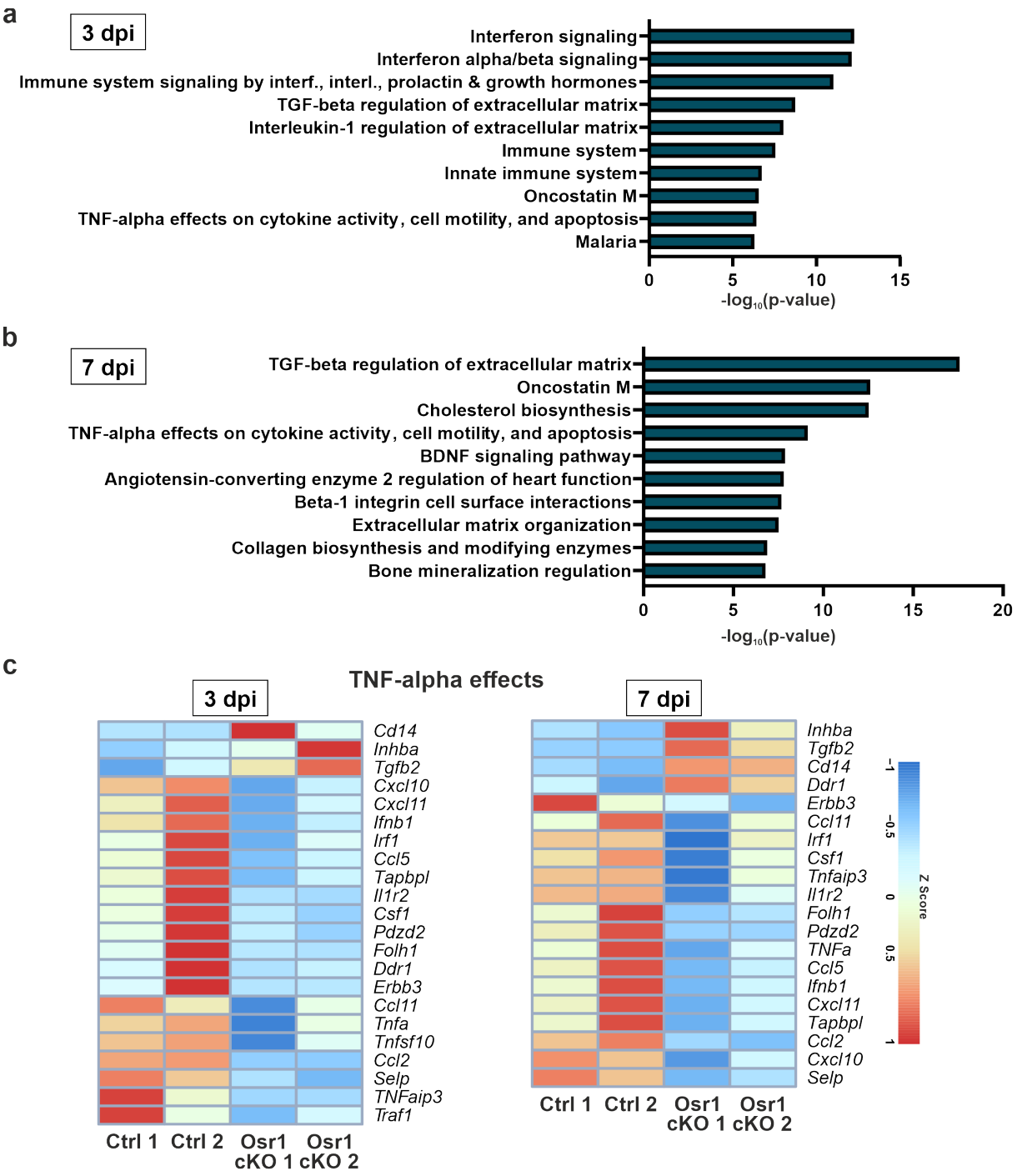

Figure 39: TNFα signaling appears to be downregulated in the mutants
Analysis of all DE genes using the Bioplanet 2019 NIH database (a) at 3 dpi and (b) at 7 dpi indicated that TNFα pathway is regulated in the Osr1 cKO FAPs. Heat maps of the genes belonging to the TNFα pathway mined from the transcriptome data. The majority of the genes belonging to this pathway are downregulated both (c) at 3 dpi and (d) at 7 dpi. Individual gene reads are transformed and depicted as z-score.

4.5.2 Advanced immune cells profiling at 3 dpi Osr1 cKO

Immune cells infiltration is amongst the primary events during muscle regeneration (Bentzinger et al., 2013a) and the exact regulation of immune cell differentiation and activity is essential for the regenerative process (Chazaud, 2020). Having established that cytokine secretion by Osr1 cKO FAPs is impaired, we analyzed how this distorted signaling profile affects the early inflammatory phase of regeneration. Thereby, in collaboration with Christian Bucher from the research group of Sven Geißler, we performed an unbiased survey of immune cell types via flow cytometry. This was performed in the regenerating muscle of control and mutant animals at 3 dpi Control and Osr1 cKO muscles from 3 dpi animals were processed and stained with antibodies for cell markers of the different populations. The antibodies used allowed for a detailed profile analysis of several immune cell populations with strong expression of the markers stained for and resulted in distinct population clustering (figure 40a). In the tSNE plots separate clusters for two major cell populations can be seen in both groups: the macrophages ($CD45^+$ Lin^-CD11c^- $CD11b^+$ $Ly6G^-$) and the neutrophils ($CD45^+$ Lin^- $CD11c^-$ $CD11b^+$ $Ly6G^+$). The number of the single isolated cells that were processed in the flow cytometry did not differ between the two groups (figure 40b). A first quantification and distribution of the identified populations in a pie chart did not show major differences between control and Osr1 cKO immune cell subpopulations (figure 40c). In the last years, the ratio of CD8/CD4 Tcells is used as a marker of pathological evolution of a disease or an injury. Recently it has been reported that high CD8/CD4 ratio has been associated with an impaired bone healing outcome (Garrido-Rodríguez et al., 2021, Schlundt et al., 2019). The percentages of $CD4^+$ and the $CD8^+$ T cells ($CD45^+$ $B220^+$) were found to be equal in the blood of the animals (CD8/CD4 ratio lower than 1 for both groups), indicating that there was no difference in the inflammatory status of the two groups (figure 41a). In order to show that the animals used are immunocompetent further analysis of the T cells was performed. Looking into T_{cm} (T central memory: $CD62L^+$ $CD44^+$), T_{em} (effective memory: $CD62L^-$ $CD44^+$) and $T_{naïve}$ subsets ($CD62L^+$ $CD44^-$), we verified that all the animals were still naïve in their immunological memory (figure 41b). Therefore, possible differences that could emerge in the immune populations of the injured animals can be attributed to the injure induced inflammation process and not to the recall abilities of T cells upon potential reinfection.

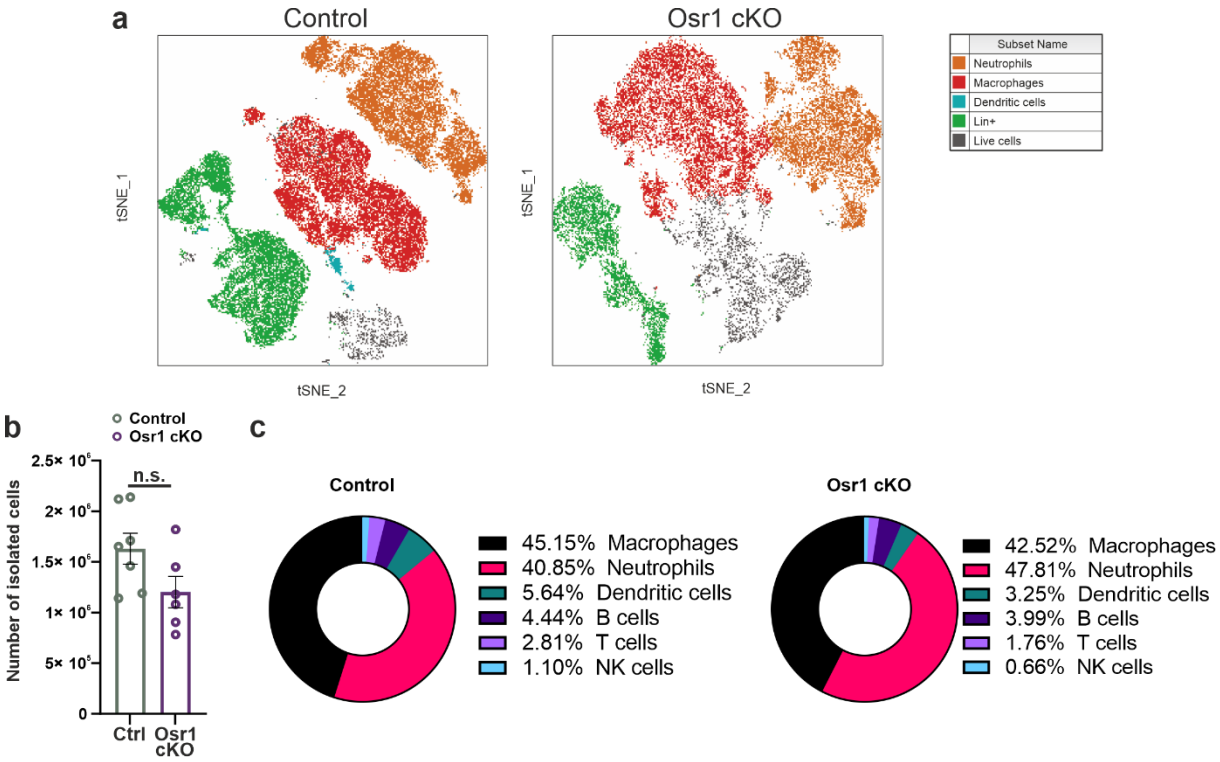

Figure 40: Flow cytometry analysis of immune cells population at 3 dpi
(a) Distinct tSNE cluster formation of neutrophils, macrophages and dendritic cells validating the efficiency of the marker used in the flow cytometry analysis. (b) Quantification of the total cells extracted from the injured muscles. Similar number of isolated cells from the two groups were processed in this approach. (c) Distribution of all the populations that were identified via flow cytometry in the control and the Osr1 cKO did not identify at first a major difference. Data are presented as mean ± SEM (n = 6-7); statistical analysis was done using Mann-Whitney test: n.s. not significant.

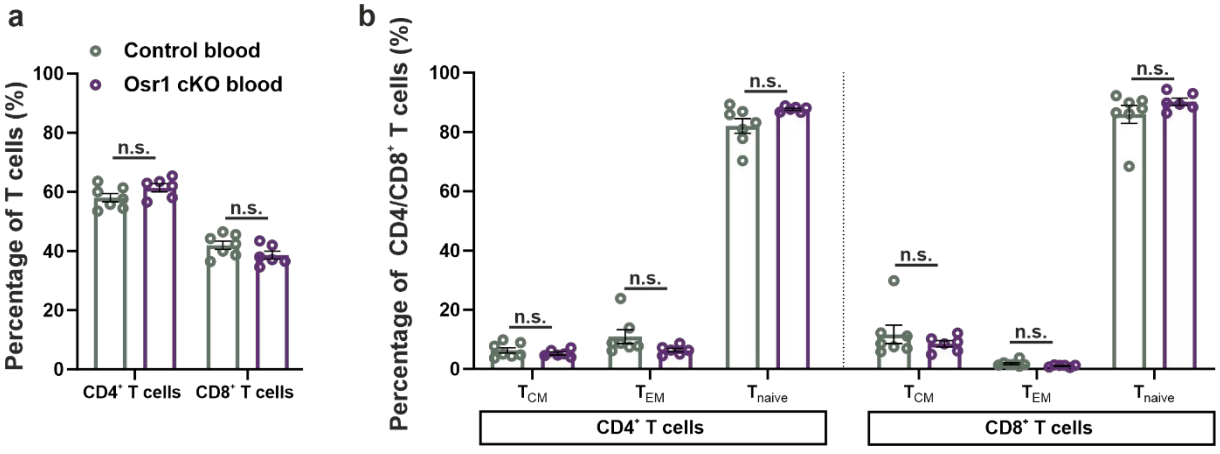

Figure 41: Immunocompetence of the analyzed animals
(a) Quantification of $CD4^+$ and $CD8^+$ T cells. Equal number of T cells found in muscle and blood of both groups indicating that the animals used were immunocompetent. (b) Elevated T naïve cells in both groups show that the animals never initiated an immune response before. Data are presented as mean ± SEM (n = 6-7); statistical analysis was done using Mann-Whitney test: n.s. not significant.

Remarkably, almost 85% of the total isolated cells from the injured muscle were found to be leukocytes ($CD45^+$), with their numbers to be on similar levels between the two groups (figure 42a). Most of these cells were found to origin from the myeloid origin (macrophages, neutrophils, dendritic cells). The distribution levels of myeloid cells to the separate populations were not different between the two groups (figure 42b). Similarly, equal numbers of lymphoid cells i.e. T cells ($CD45^+CD3^+$) and B cells ($CD45^+B220^+$) were quantified in the two groups (figure 42c).

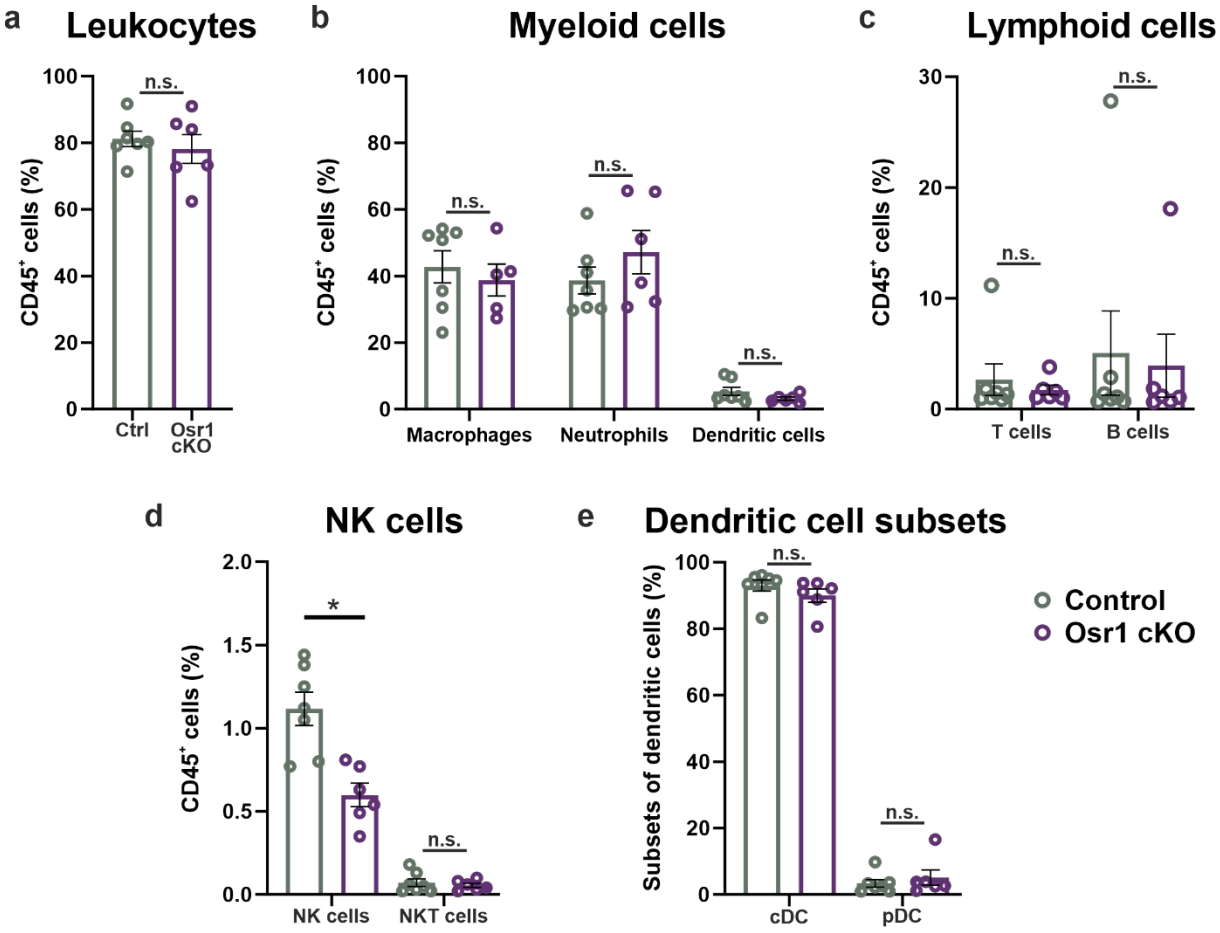

Figure 42: Analysis of leukocytes subpopulations revealed decrease in the NKs number in the injured Osr1 cKO
(a) Quantification of leukocytes. Almost 85% of all cells in the injured muscle were leukocytes. No difference was observed in the two groups. (b) Analysis of the cells belonging to the myeloid lineage. Cell numbers of the myeloid subpopulations were shown to be almost equally distributed. (c) Lymphoid cell population analysis showed no difference between the two groups. (d) Quantification of the NK population. Significantly lower number of NK cells in the mutant, while NKT numbers were almost identical. (e) Dendritic cells analysis did not reveal a difference between the two groups. Data are presented as mean ± SEM (n = 6-7); statistical analysis was done using Mann-Whitney test: n.s. not significant.

One of the first population numbers that was found to be significantly lower in the Osr1 cKO muscle was the natural killer cells (NK: $CD45^+$ $CD335^+$). Almost 50% less NK cells were identified in the mutant muscles (figure 42d). Although not much is known about the function of NK cells in muscle injury, these cells hold an important role in

regeneration of other tissues since they produce cytokines supportive of tissue repair, while inhibiting tissue fibrosis (Tosello-Trampont et al., 2017). Natural killer T cells (NKT: $CD45^+$ $CD335^+$ $CD3^+$) were separated from NK cells and their cell numbers were comparable between the two groups (figure 42d). Lastly, dendritic cells (DCs) were separated in cDCs (conventional DCs: $CD11c^{hi}$ $B220^-CD4^-CD8^-$) and in pDCs (plasmacytoid DCs: $CD11c^{low}B220^+$) and their populations were proportionate (figure 42e). Collectively, up to this point the only difference detected between the Osr1 cKO and the control immune cells composition, is the lower numbers of NK cells quantified in the injured mutants.

4.5.3 Osr1 expression in FAPs is essential for the phenotypical switch of macrophages

Neutrophils and macrophages are the most predominant inflammatory cell types to be found in acute muscle injury. Neutrophils appear on the site of the injury already two hours after the initial trauma and remain active until 2 dpi, while the population of macrophages reaches peak concentration at 4 dpi and stays significantly elevated for days (Tidball and Villalta, 2010, Chazaud, 2020). Therefore, the populations of macrophages and neutrophils were also sorted in this analysis both in the injured muscle as well as in the isolated blood from the hearts of the injured individuals. The analysis of the blood served as a negative control in order to exclude potential systemic defects of the *Osr1* recombination in the circulatory immune cells of the animals. This allowed us to be certain that any differences in the populations of neutrophils and macrophages in the muscle, would be ascribed to the *Osr1* deficiency in FAPs during muscle regeneration. In this sorting, cells of the adaptive immunity (B cells, T cells, NK cells) Lin^+ cells were stained for $CD335^+$ $CD3^+$ $CD19^+$ and were excluded from the analysis. As neutrophils, cells being $CD45^+Lin^-CD11c^-CD11b^+Ly6G^+$ were counted and macrophages were considered to be $CD45^+Lin^-CD11c^-CD11b^+Ly6G^-$. At first, no statistical important differences were found in the populations of neutrophils and macrophages, neither in muscle nor in blood samples (figure 43a).

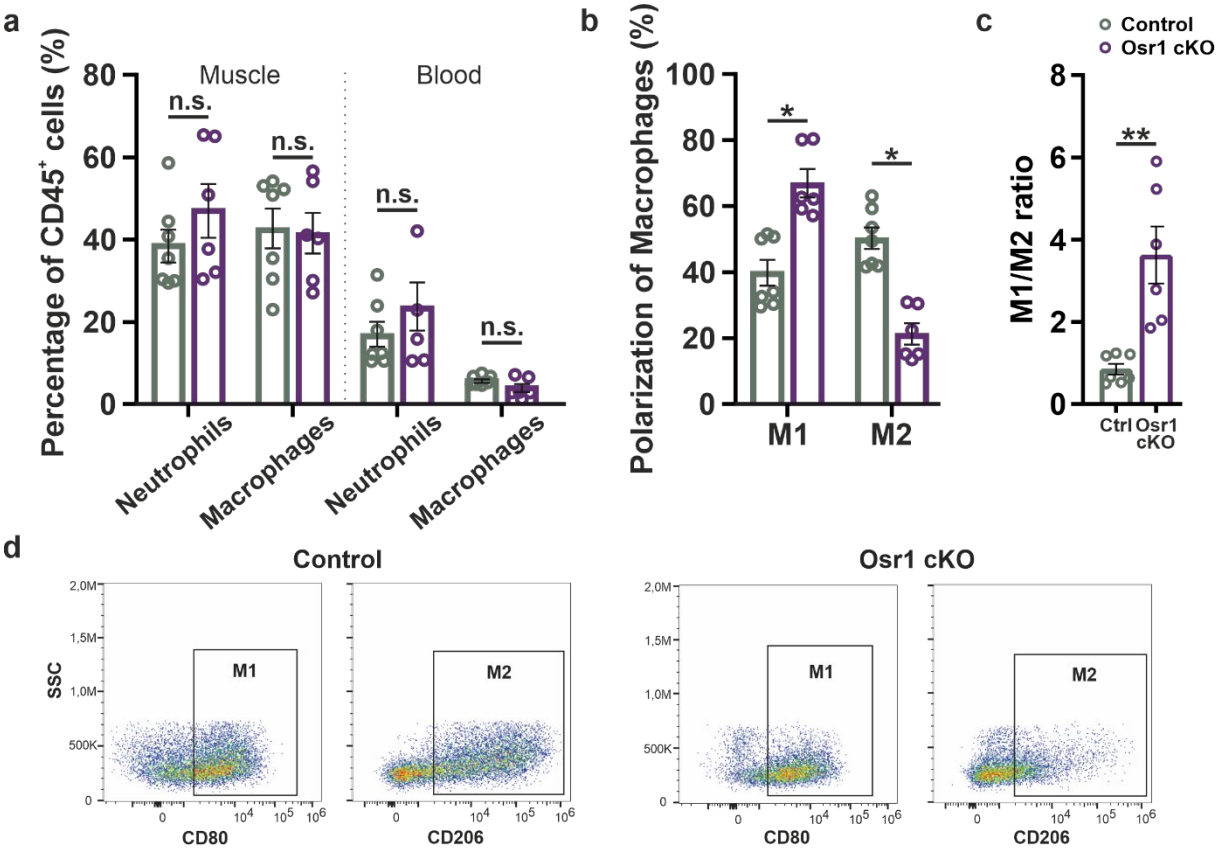

Figure 43: **Loss of *Osr1* has no effect on macrophage/neutrophil infiltration but affects macrophage polarization**
(a) Neutrophils and macrophages populations measured in muscle and in blood for potential systemic defects. No difference was found in the percentage of these cells between the two groups. (b) Significantly higher numbers of M1 MPs while lower numbers of M2 MPs were measured in the Osr1 cKO, revealing an inhibition in the macrophage switch upon deletion of *Osr1* in FAPs. (c) Depiction of the M1/M2 ratio as measured in b. Four times higher M1/M2 ratio in the Osr1 cKO in comparison with the control. Data are presented as mean ± SEM (n = 6-7); statistical analysis was done using Mann-Whitney test: n.s. not significant, *p<0.05.

Interestingly, further investigation in the polarization profile of the macrophages (MΦs) revealed significant differences between the distribution of MΦs in the pro-inflammatory M1 ($CD206^{-}$ $CD80^{+}$ $CD86^{+}$) and in the anti-inflammatory M2 ($CD206^{+}$ $CD80^{-}$ $CD86^{-}$) states (figure 43b). An increase of 30% in the numbers of M1 MΦs was measured in the Osr1 cKO samples whereas M2 MΦs decreased by 60% in the same group when compared to the control. Having found the differences in the MΦs subgroups, the ratio of M1 to M2 macrophages was calculated as a marker of the inflammatory status of the regenerative environment. Higher ratio value indicates more M1 MΦs present thus, a pro-inflammatory setting whereas lower ratio value designates an anti-inflammatory milieu. Notably, a 3-fold decrease of M1 to M2 switch was shown in the Osr1 cKO muscles. That ascribes a defected switch in the polarization state of the macrophages within the Osr1 cKO 3 dpi muscles and consequently, a more prominent pro-inflammatory environment (figure 43c).

Despite the elevated expression of *CD68* and *CD80* (M1 markers) which tended to be upregulated in the Osr1 cKO muscle, the differences found were not statistically significant (figure 44a). However, in agreement with an impaired / delayed M1/M2 switch, relative gene expression levels of *CD163*, *CD206* and *Arg-1* (M2 markers) were significantly lower in the mutant whole muscle lysate (figure 44b). Note that the markers used in the RT-qPCR are specific for the targeted immune cell subgroups and are not expressed by any other cell type in the muscle tissue.

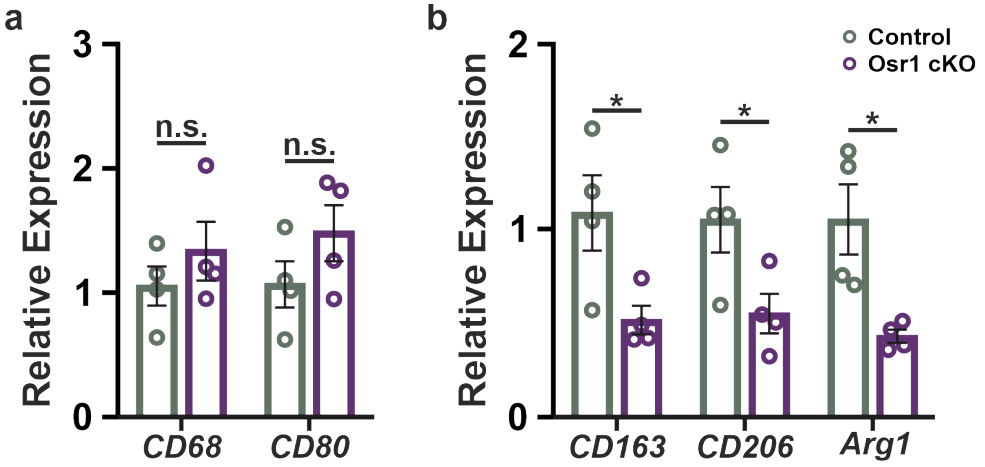

Figure 44: Higher expression of M2 marker genes in total lysate of 3 dpi muscles
(a) Expression level of CD68 and CD86 tended to be higher in the Osr1 cKO at 3 dpi as measured by RT-qPCR, validating the flow cytometry results. (b) Levels of *CD163*, *CD206* and *Arg1* expression, specific markers of M2 MΦs, are significantly lower in the Osr1 cKO injured muscle, in accordance with the lower numbers of M2 MΦs shown before. Data are presented as mean ± SEM (n = 4); statistical analysis was done using two-tailed Student's t tests: n.s. not significant, *p<0.05.

To further confirm the differences in the M1 and M2 MΦs subgroups, the co-immunostainings for CD80 (as a M1 marker) and for CD206 (as a M2 marker) shown in section 4.1.5. were quantified (figure 19a and figure 19b). Quantification of the positive cells at 3 dpi did not show any differences at this stage between the distribution of MΦs in M1 and M2 states in both control and Osr1 cKO tissue (figure 45a). Note though, that the magnitude of the mechanical injury generates autofluorescence signal at 3 dpi. This does not permit a reliable quantification of all positive cells. A decrease in the amount of $CD80^+$ cells was quantified in the Osr1 cKO at 5 dpi when compared to the control, whereas equal percentages of $CD206^+$ cells were present in both groups (figure 45b). This result was not in accordance with the strong anti-inflammatory profile of the control animals quantified via flow cytometry at 5 dpi. A possible explanation for that could be that in the Osr1 cKO proliferation and numbers of M1 and M2 MΦs is in general defected, with their populations declining faster than the ones in control animals, similar to the SCs behavior depicted in figure 30a.

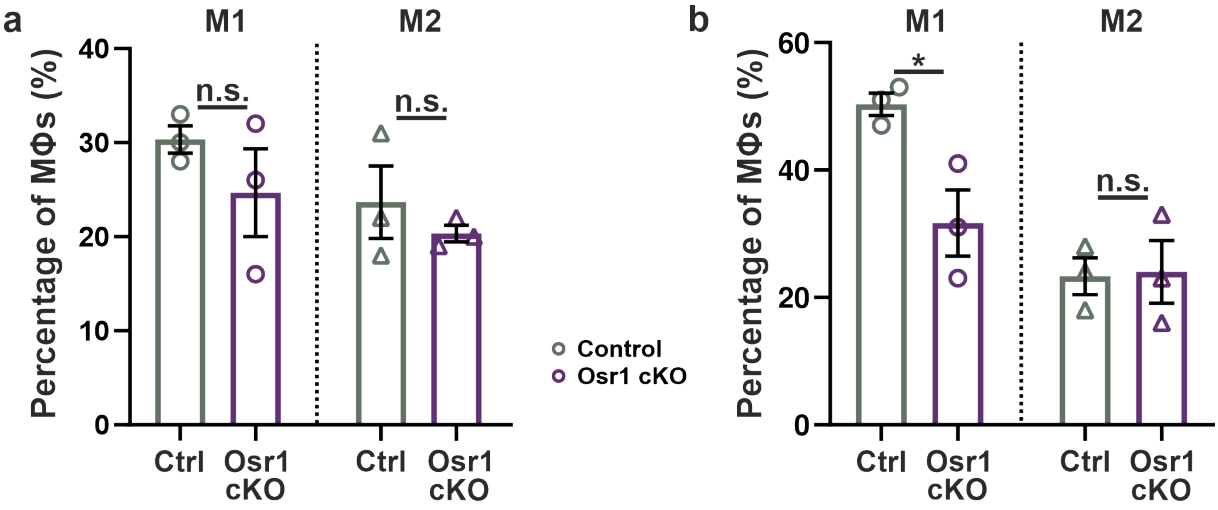

Figure 45: Lower numbers of CD80⁺ cells stained at 5 dpi Osr1 cKO tissue
(a) Quantification of the stained tissue at 3 dpi for CD80⁺ and CD206⁺ cells did not show a difference between the M1 and the M2 MΦs infiltration. Note, that CD80 is also expressed by B cells and dendritic cells. (b) At 5 dpi less M1 cells were counted in the mutant, while no difference was found in the M2 MΦ subpopulation. Data are presented as mean ± SEM (n = 3); statistical analysis was done using two-tailed Student's t tests: n.s. not significant, *p<0.05.

4.5.4 Co-culture of macrophages with FAPs from 3 dpi muscle

An *in vitro* approach was followed to validate the finding that loss of *Osr1* expression in FAPs upon injury can affect the polarization switch of macrophages. In short, control and Osr1 cKO mice were injured and at 3 dpi FAPs were isolated via pre-plating. At the same time BMM (bone marrow-derived macrophages) were isolated and stimulated with M-CSF (macrophage colony stimulated factor) up to differentiation in the macrophage/monocyte lineage. Indirect co-culture of monocytes (below) and 3 dpi expanded FAPs (in transwell inserts) was performed (figure 46a). As positive controls, monocytes were treated with IFNγ (M1 stimulation) and with IL4 (M2 stimulation). RT-qPCR for M1 and M2 markers was at the end performed on RNA isolated from the cultured macrophages.

The relative expression for the M1 markers *iNOS*, *IL6* and *IL1b*, was found to be elevated in the M1 positive control (IFNγ stimulated monocytes) while no difference was detected between the MΦs cultured with Osr1 cKO FAPs and with control FAPs (figure 46b). Similarly, expression of M2 markers *RetnLa*, *Arg1* and *Chi3l1* was induced in the M2 positive control samples (IL4 stimulated monocytes) but no significant change was noted in any other group (figure 46c). Remarkably, the expression of *Ccl2* and *Ccl3* was induced in the wells with the FAPs control transwell and was significantly higher than in the co-culture with Osr1 cKO FAPs (figure 46d). Note that Ccl2 and Ccl3 cytokine signaling is essential during muscle regeneration. It regulates the activation

state of inflammatory cells, inducing this way muscle repair (Tidball, 2017). Furthermore, the expression level of the M2 cytokines *IL4*, *IL10* and *TGFβ* was lower when MΦs were cultured together with the Osr1 cKO than with the control FAPs (figure 46e). Interestingly, IL10 is a myokine shown to regulate the switch from a M1 to M2 MΦs phenotype *in vivo*, being necessary for normal growth and regeneration (Deng et al., 2012). All together, these data prove that although FAPs alone might not have the ability to regulate MΦs polarization *in vitro*, Osr1$^+$ FAPs regulated MΦs cytokine secretome that induced their phenotypical switch from a pro- to an anti-inflammatory profile.

In summary, this section demonstrates that Osr1 cKO FAPs downregulate genes that encode for important cytokines, a defect that is persistent from 3 to 7 dpi. Paracrine signaling of FAPs is to a certain extent also important for the activation of the inflammatory response. However, *Osr1* expression in FAPs is not required for the on-time infiltration of monocytes and macrophages upon injury, but is required for their transition from a pro- to an anti- inflammatory phenotype *in vivo*. This also functionally involves FAPs in the timely M1-M2 switch required for efficient muscle regeneration. In addition, TNFα signaling was found to be downregulated in the Osr1 cKO despite its higher numbers of M1 macrophages, which are the main producers of TNFα. Finally, Osr1$^+$ FAPs alone are not potent to affect the MΦs phenotype *in vitro*. On the other hand, they can indirectly stimulate the M1-M2 switch by inducing MΦs cytokine secretion.

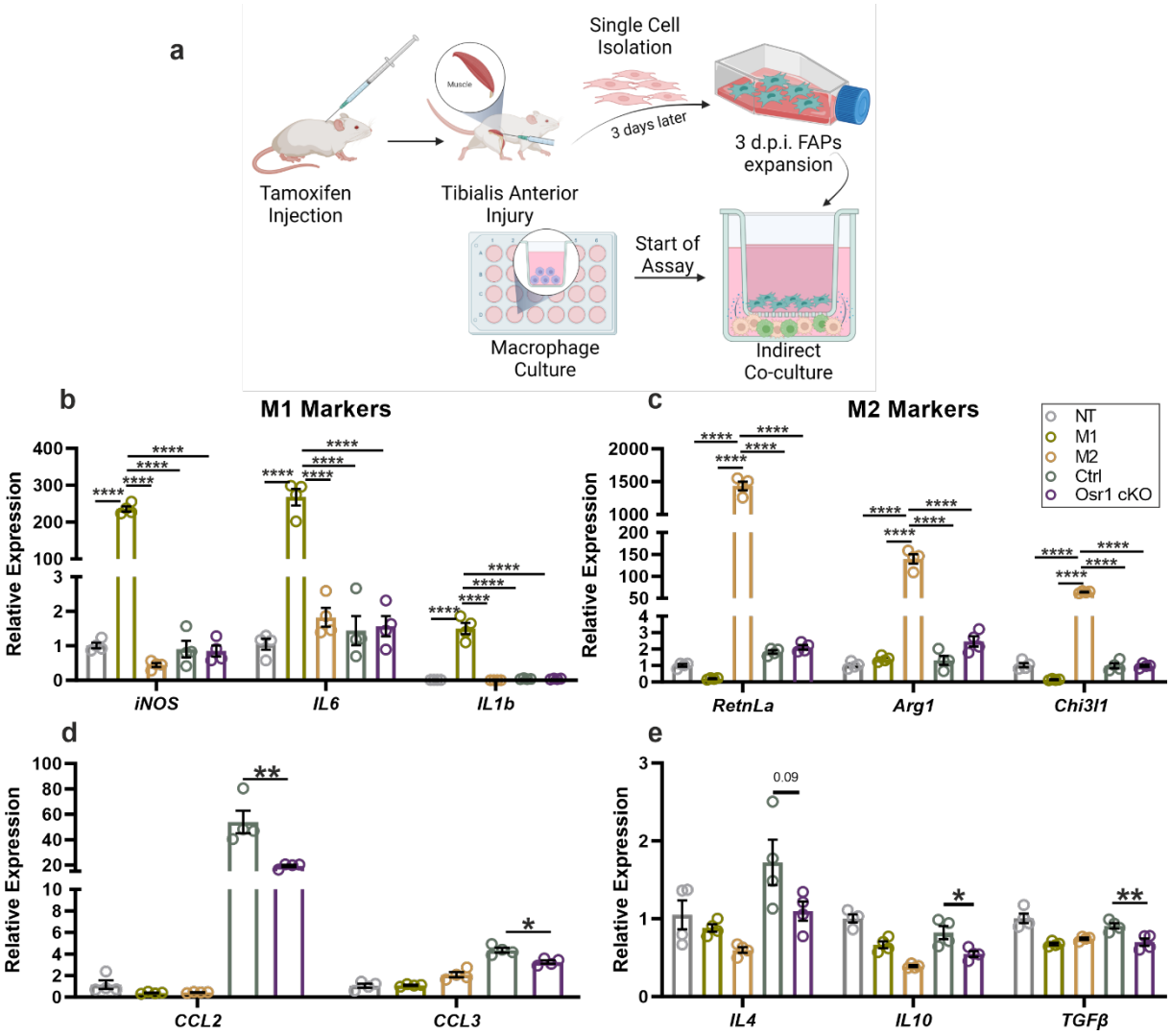

Figure 46: Indirect co-culture of MΦs and 3 dpi FAPs affects MΦs cytokine secretion
(a) Schematic representation of the assay. FAPs were isolated from 3 dpi muscles and expanded. Simultaneously, BMM were isolated from bone marrow and stimulated until differentiation to macrophages. Both populations were then co-culture for 3 days and RNA was isolated from the MΦs in order to check their activation status. (b) Induced expression level of M1 markers in the positive M1 control. No difference in their expression was found between the samples cultured together with the control and the Osr1 cKO FAPs. (c) The positive M2 control expressed high levels of typical M2 marker genes. Similar levels of M2 expression shown in the rest of the samples. (d) Increased expression of *Ccl2* and *Ccl3* genes in the MΦs cultured with 3 dpi control FAPs in comparison to the ones cultured with 3 dpi Osr1 cKO FAPs, indicating the importance of Osr1^{+} FAPs in activating the polarization potential of MΦs. (e) The relative expression of *IL4*, *IL10* and *TGFβ*, encoded by M2 MΦs, was downregulated in the MΦs cultured with Osr1 cKO FAPs. Data are presented as mean ± SEM (n = 4); statistical analysis was done using two-tailed Student's t tests: n.s. not significant, *p<0.05, **p<0.01, ****p<0.0001.

4.6 Osr1 deficient FAPs favor a fibrogenic shift producing an adverse ECM

4.6.1 Osr1 cKO and mdx derived FAPs share similar fibrogenic signature

One of FAPs main functions described both in development and in regeneration processes, is the formation of their microenvironment through ECM protein secretion (Joe et al., 2010, Vallecillo-Garcia et al., 2017). Following the peak of FAPs proliferation at 3 dpi, M1 MΦs restrain FAPs further expansion by secreting TNFα.

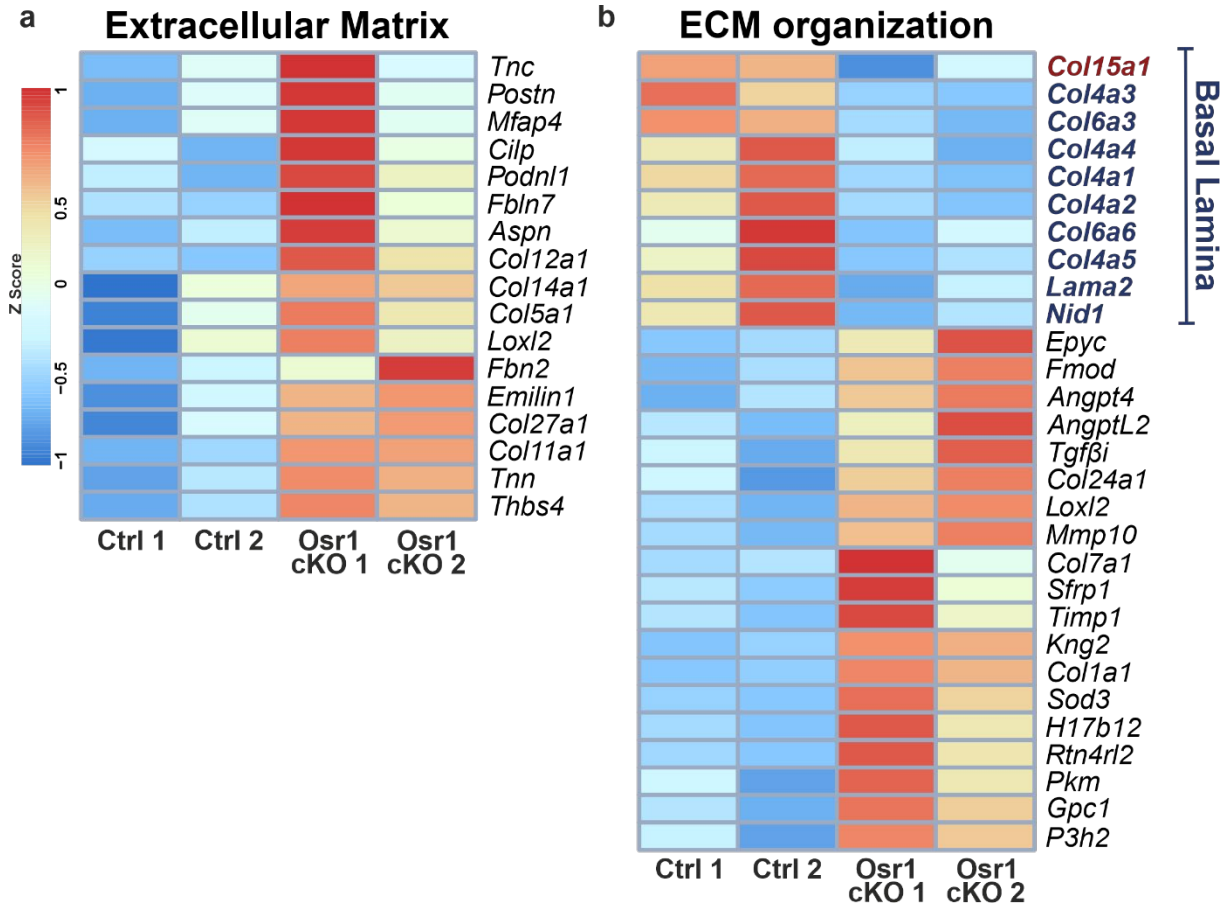

Figure 47: Extracellular matrix composition is altered in mutant FAPs
Heat map of genes expression transcripts related to (a) the extracellular matrix at 3 dpi and (b) the extracellular matrix organization at 7 dpi. All the genes shown at 3 dpi tended to be upregulated in the Osr1 cKO FAPs. Similarly, at 7 dpi most of ECM related genes were upregulated while genes encoding for proteins of the basal lamina were downregulated in the mutant FAPs. Individual gene reads are transformed and depicted as z-score.

Then the pro-regenerative phenotype of M2 MΦs becomes apparent, secreting TGFβ which leads to matrix production by FAPs. Transcriptome analysis of the GFP^{+} FAPs highlighted the regulation of several genes coding for ECM components (figure 35c

and 36c). GO analysis showed upregulation of ECM related terms at 3 and at 7 dpi in the mutant.

At 3 dpi ECM-coding genes appeared globally upregulated in Osr1 cKO FAPs. Figure 47a shows a heatmap of significantly DE genes belonging to this category. Amongst these were genes coding for major proteins of the fibrotic matrix like *Tnc*, *Postn*, *Col.5a1* and *Col.12a1*. However, at 7 dpi ECM GO terms were also found to be enriched in downregulated genes (figure 36c). Interestingly, the majority of the ECM genes downregulated in the Osr1 cKO FAPs at 7 dpi were those coding for muscle basal lamina proteins (e.g. *Col.4a1*, *Nid1*, *Lama2*), correlating with the defective myofiber formation described in section 2.1. (figure 47b). Other structural ECM components (for instance Col7a1, Col.11a1) as wells as ECM-modifying enzymes (e.g. the fibrotic markers Timp1 and Loxl2) were upregulated in 7 dpi Osr1 cKO FAPs.

To further characterize the shift in the ECM gene expression, I compared the transcriptome datasets of the Osr1 cKO to the DE genes of FAPs from wild type and mdx mice acquired from the study of Malecova et al.,2018 (figure 48). This revealed a common 173 DE genes; 89 DE genes were shared between mdx and 3 dpi Osr1cKO, 64 DE genes between mdx and 7 dpi Osr1cKO, and 20 DE genes between mdx and both time points (figure 48a). GO analysis of shared DE genes highlighted ECM-related terms as “collagen containing extracellular matrix” between mdx FAPs and 3 dpi as well as 7 dpi Osr1cKO FAPs (figure 48b and 48c). These similarities in the formation of the collagenous matrix together with the excessive fibrotic phenotype of the mdx mice, are in line with the observations made for the Osr1 cKO in the section 2.2. Finally, heatmap depiction showed an at least in part common direction of ECM gene deregulation between mdx FAPs and Osr1cKO FAPs (figure 48d and figure 48e). Note that at 3 dpi genes coding for major proteins of the ECM like *Tnc*, *Postn* and *Col.27a1* are commonly upregulated in the mdx and the Osr1 cKO. Intriguingly, at 7 dpi the expression of basal lamina components e.g. Lama2 and Col.4a4 are commonly inhibited along with the matrix metalloproteinase MMP27.

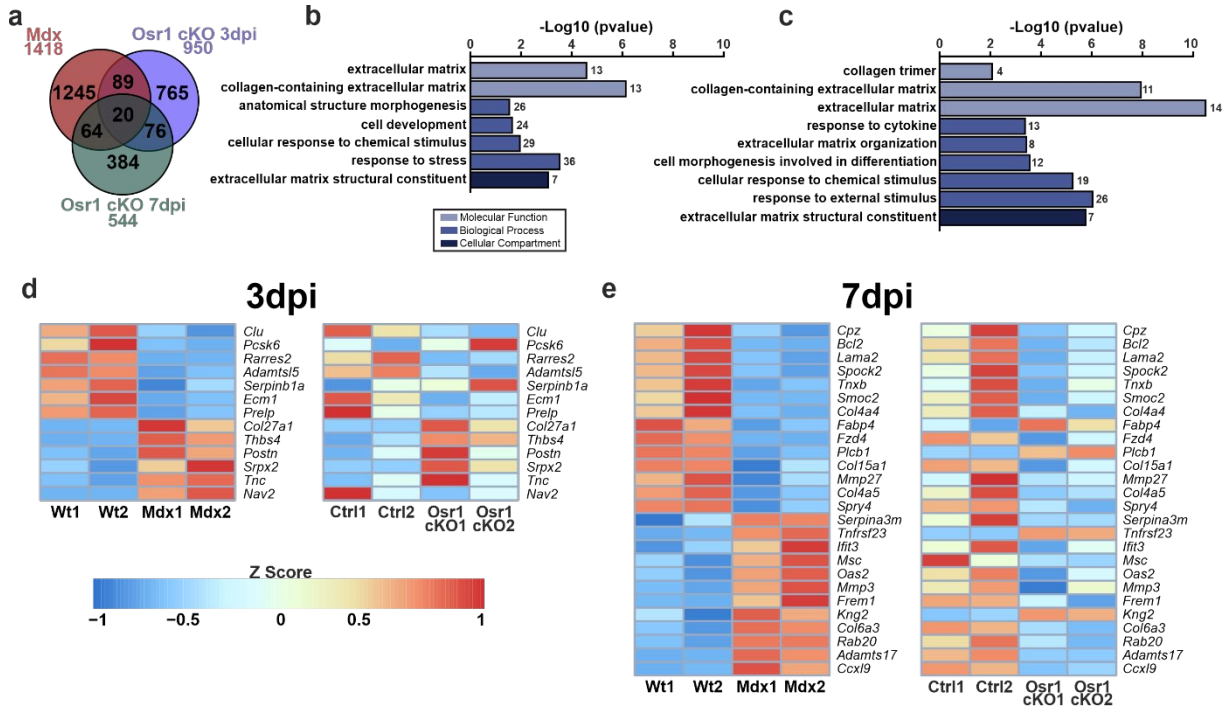

Figure 48: Osr1 cKO FAPs transcriptome reveal similarities to the mdx derive FAPs
(a) Venn diagram depicting common regulated genes between the uninjured mdx FAPs, the 3 dpi and the 7 dpi Osr1 cKO FAPs. (b) GO analysis using the common regulated genes of the mdx and the 3 dpi datasets yielded terms related to the collagenous extracellular matrix. (c) Extracellular matrix terms were also identified in the GO common DE gene analysis between mdx and 7 dpi FAPs. Significance of each term is plotted as the -$\log_{10}$ of the p-value. The number next to each bar indicates the number of genes belonging to each term. Heat maps of the transcript reads of genes belonging to the collagen containing ECM term from the comparison of mdx FAPs with (d) the 3 dpi and (e) the 7 dpi transcriptome data. Individual gene reads are transformed and depicted as z-score.

In the study of Giuliani et al., 2021 a Sca1 heterogeneous FAPs population was described which is prominent in pathological conditions or in ageing. Interestingly, it was shown that isolated FAPs from mdx mice consist mainly of Sca1^{high} cells. These FAPs are more prone to enter the adipogenic differentiation upon induction, while in the presence of fibrogenic stimuli Sca1^{high} FAPs secrete a non-beneficial ECM, high in Col.1a1 and Timp1 (Giuliani et al., 2021b). Based on these observations, I re-analyzed the flow cytometry data acquired at 3 and at 7 dpi, gating for Sca1^{low} and Sca1^{high} FAPs populations, following the same threshold of the aforementioned study (figure 49). Gating and quantification of the Sca1 subpopulations at 3 dpi FAPs, showed that almost the entire population of FAPs is Sca1^{high} (almost 90% in both groups). However, no significant difference was found between control and Osr1 cKO (figure 49a). Remarkably, at 7 dpi the Sca1 distribution changed, with the Osr1 cKO FAPs consisting of a higher percentage of Sca1^{high} FAPs and lower levels of Sca1^{low} FAPs when compared to the control (figure 49b). Therefore, this analysis revealed another

similarity of the Osr1 cKO with the mdx FAPs, being consistent with the observations described above.

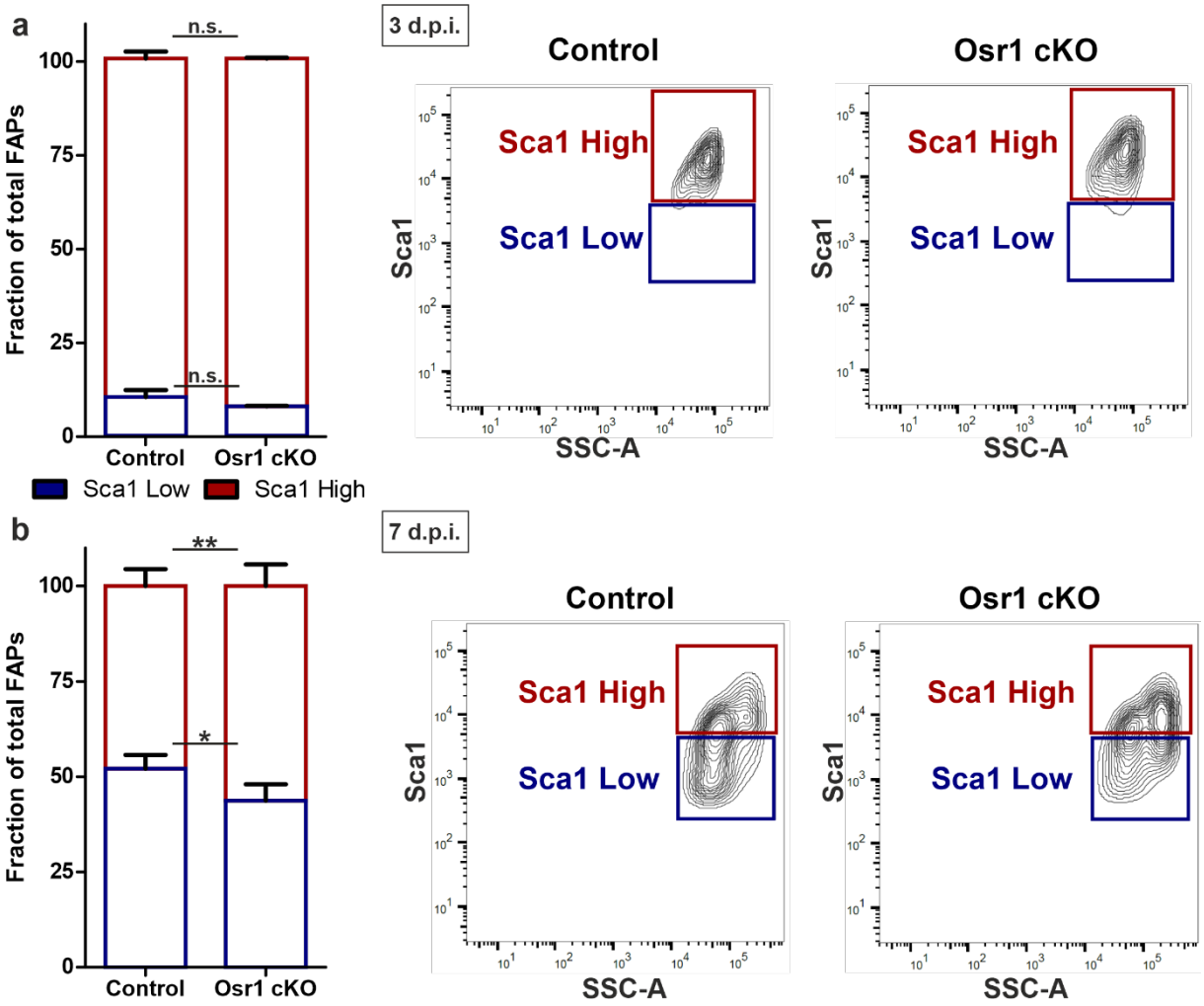

Figure 49: The subpopulation of Sca1^{high} is higher in the mutants at 7 dpi
(a) Quantification of Sca1^{low} and Sca1^{high} subpopulations of FAPs at 3 dpi did not reveal any differences between the two groups. (b) Osr1 cKO FAPs consist of less Sca1 low and more Sca1^{high} FAPs in comparison to the control. Data are presented as mean ± SEM (n = 5-6); statistical analysis was done using two-tailed Student's t tests: n.s. not significant, *p<0.05, **p<0.01.

4.6.2 Skewed differentiation potential of FAPs upon *Osr1* deletion *in vivo*

During embryonic development *Osr1*-deficient FAP-like developmental cells manifested a shift in ECM gene expression from a pro-myogenic to a more cartilage- and tendon-like ECM (Vallecillo-Garcia et al., 2017). Based on this observation, I asked how does *Osr1* deletion affect FAPs chondrogenic potential in regeneration. Thus, I systemically mined for the tendon and cartilage expressed genes referred in this study and checked their expression in the transcriptome data (figure 50). The expression of

the tenogenic markers *Tnmd*, *Mkx*, *Scx* and *Tnc* was induced in the Osr1 cKO at both timepoints. Interestingly, genes associated with cartilage and tendon, like *Col.24a1* and *Fmod*, followed the same tendency. Regarding the cartilage marker expression profile, only *Trps1* was commonly upregulated at both timepoints, but several other unique markers were upregulated either at 3 or at 7 dpi.

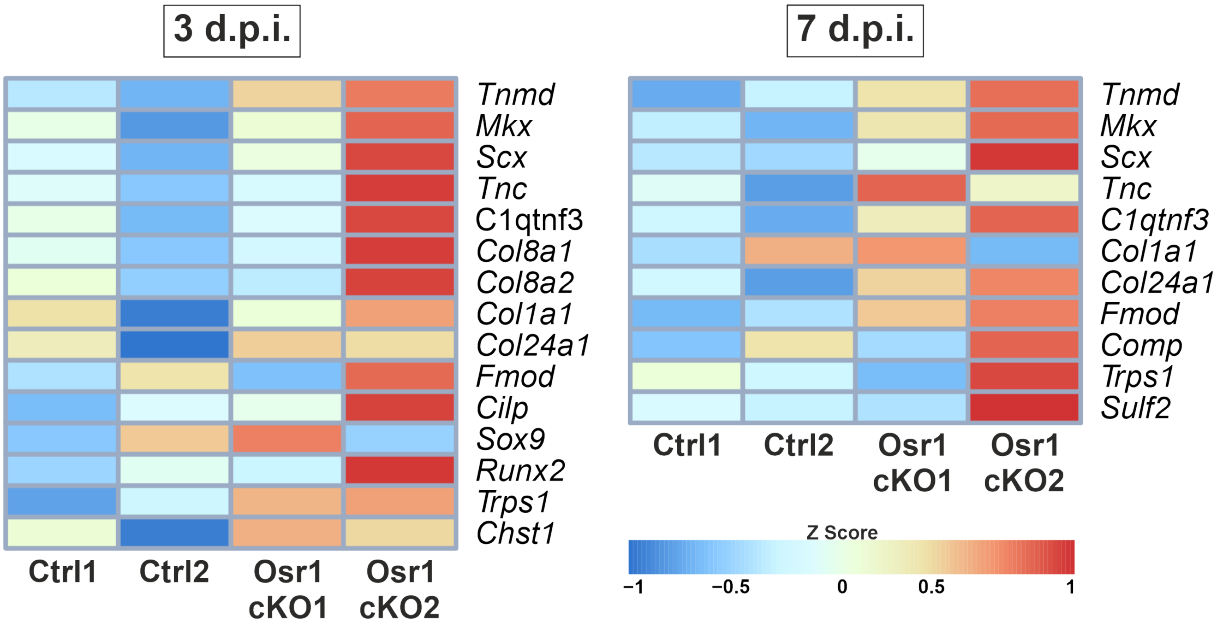

Figure 50: Chondro- and tenogenic genes are upregulated in the mutants
Heat maps of transcript reads mined from the transcriptome data are upregulated in the Osr1 cKO on both timepoints. Individual gene reads are transformed and depicted as z-score.

Apart from fibroblastic and adipogenic differentiation, FAPs are multipotent, capable also of chondrogenesis and osteogenesis. Several studies have described the wide potential of FAPs both *in vitro* and *in vivo* (Giordani et al., 2019, Wosczyna et al., 2012, Scott et al., 2019). Having found the enhanced tenogenic gene expression levels at 3 and at 7 dpi, the study of Oprescu et al., 2020 was used once again to decipher potential differences in the FAPs subpopulations at the two timepoints of the transcriptome data. Therefore, the significantly DE genes from our datasets were projected against the identity genes of the separate FAPs cluster and the similarities with each cluster were quantified for both timepoints (figure 51). Interestingly, one of the Osr1 cKO samples showed increased percentages of identical genes with the tenogenic FAP subpopulation whereas this subpopulation was completely absent from one of the control samples at 3 dpi (figure 51a). This difference became more apparent at 7 dpi where both of the Osr1 cKO analyzed samples exhibited a tendency towards tenogenic differentiation. Note that even though both mutants showed slightly higher percentage compared to one of the controls, this increased to a 2-fold difference when

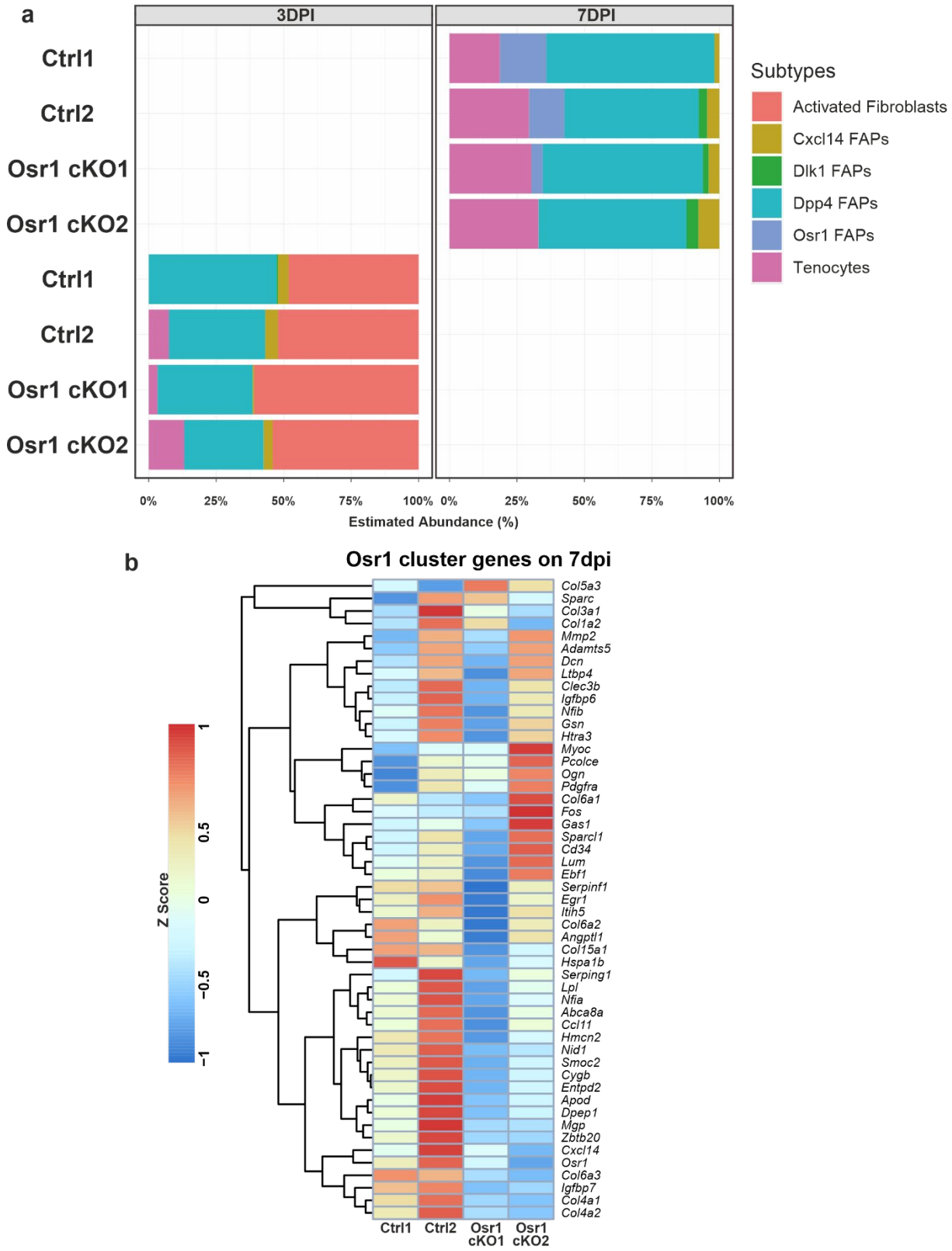

Figure 51: Osr1 cluster is absent in the Osr1 cKO at 7 dpi
(a) Projection of 3 and 7 dpi DE genes on FAPs subpopulations from the study of Oprescu et al., 2020 and quantification of their distribution in the separate clusters. (b) Heat map of transcript reads from the Osr1+ subpopulation at 7 dpi. Individual gene reads are transformed and depicted as z-score.

compared to the other control sample. A second finding that emerged from this analysis and is worth mentioning was the complete absence of the Osr1^{+} FAPs subpopulation at 7 dpi. In the Oprescu study Osr1 is a distinct marker of a whole FAPs subpopulation being very prominent at the end of the regeneration, at 21 dpi. Intriguingly, Osr1^{+} FAPs were described to be responsible for secreting cell signaling related genes such as *Ccl1*, *Bmp4* and *Bmp5*. Therefore, this underlines the importance of *Osr1* expression for the existence of the Osr1^{+} subpopulation since this could not be detected upon deletion of *Osr1*. Thus, figure 51b depicts a heat map of the expression levels of all the signature genes of the Osr1 cluster at 7 dpi. In total, 27 genes out of total 51 signature genes are shown to be downregulated upon deletion of Osr1, explaining therefore the defect in detecting the Osr1 subpopulation when analyzing the transcriptome data from the 7 dpi FAPs.

4.6.3 Osr1 regulates the pro-myogenic composition of ECM *in vitro*

In the previous subsections the altered differentiation potential of Osr1 cKO FAPs *in vivo* was described. In order to validate the Osr1 regulation of FAPs differentiation potential, I used the *in vitro* 4-OHT tamoxifen system described in section 2.4.1. and generated an Osr1^{KO} FAPs progeny. Note that the FAPs used here were isolated from healthy uninjured mice. In line with the observations made the previous subsections, the first observation was that Osr1^{KO} FAPs exhibit defected adipogenic potential (figure 52a). After knocking-out Osr1, cells were cultured for six days and spontaneously differentiated into adipocytes. Staining with Oil Red O revealed that Osr1^{KO} cells lose their adipogenic capacity which was later verified also with immunostaining for perilipin (*Plin*), staining the surface of the produced lipid droplets (figure 52b). Remarkably, the Osr1^{KO} FAPs exhibited a reduced endogenous adipogenic differentiation almost by 40% (figure 52c). Under normal culture conditions FAPs differentiate only into fibroblast or adipocytes. Thus, the lower number of adipocytes quantified in the Osr1^{KO} samples indicate that these cells differentiate more readily into fibroblasts. To validate that, cultured FAPs were stained for Col.VI and Fn1, two major components of the fibroblastic ECM (figure 52d). Secretion of Col.VI, as well as of Fn1, was indeed higher around the Osr1^{KO} cells, with the latter being prominent only in the Osr1^{KO} samples. This observation was validated through quantification of the Fn1/Col.VI staining around each cell, which showed a two-fold induction in Fn1 secretion (figure 52e) and a 30%

increase in the amount of Col.VI deposition in the Osr1^{KO} (figure 52f). Taken together, this experiment showed an intrinsic requirement for Osr1 expression in differentiating FAPs even in the absence of injury cues.

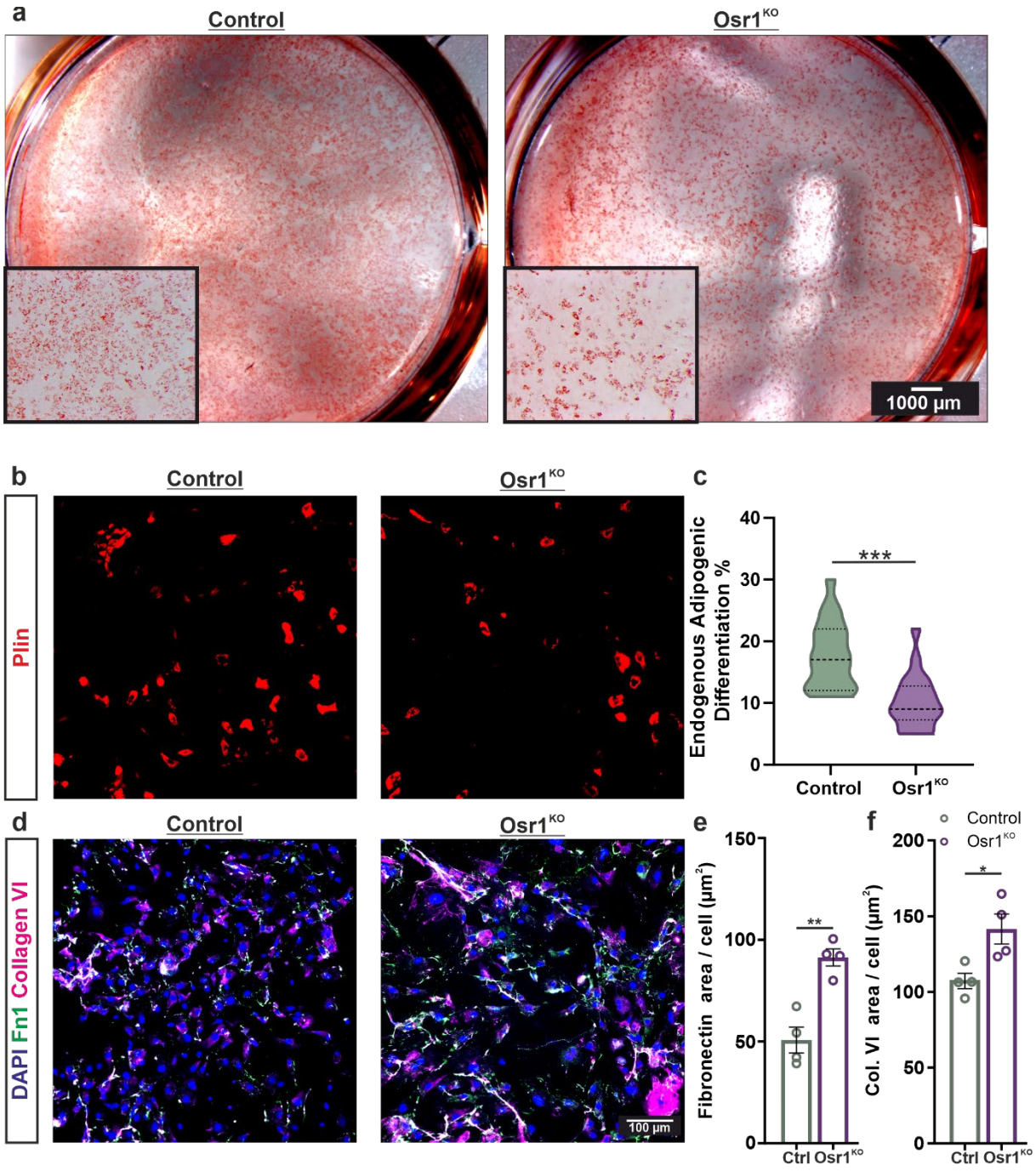

Figure 52: Induced fibrogenic differentiation of the Osr1^{KO} FAPs
(a) Oil Red O staining on cultured FAPs revealed smaller adipogenic potential of recombined *in vitro* FAPs. (b) Perilipin immunostaining performed on recombined FAPs. (c) Quantification of (b) showed less perilipin positive cells in the Osr1^{KO} FAPs. Single numerical data are plotted as a distribution, the thick dotted line represents the mean. (d) Co-immunostaining of Fn1 and Col.VI on recombined FAPs. Quantification of Fn1 in (e) and Col.VI staining in (f) revealed a larger positive area for these markers. Data are presented as mean ± SEM (n = 4); statistical analysis was done using two-tailed Student's t tests: n.s. not significant, *p<0.05, **p<0.01, ***p<0.001.

Results

Based on the altered ECM secretion described above but also as resulted from the transcriptome analysis *in vivo* and the mdx comparison, I therefore analyzed whether the ECM produced by Osr1 cKO FAPs influences myogenic differentiation. In this assay FAPs were isolated from the uninjured muscles of 7 dpi animals (figure 32) and cultured for 21 days. That allowed them to deposit a coherent ECM coating on the tissue culture well (figure 53a). The decellularization efficiency was then tested on the produced dECM using detergents and subsequent gentle washing step to remove cellular debris (figure 53b). Collagen VI staining showed that despite the fragility of the dECM, this approach did not destroy the structure of the deposited matrix while at the same time almost all of the attached cells were removed. Therefore, this protocol was further used in overconfluent culture of FAPs.

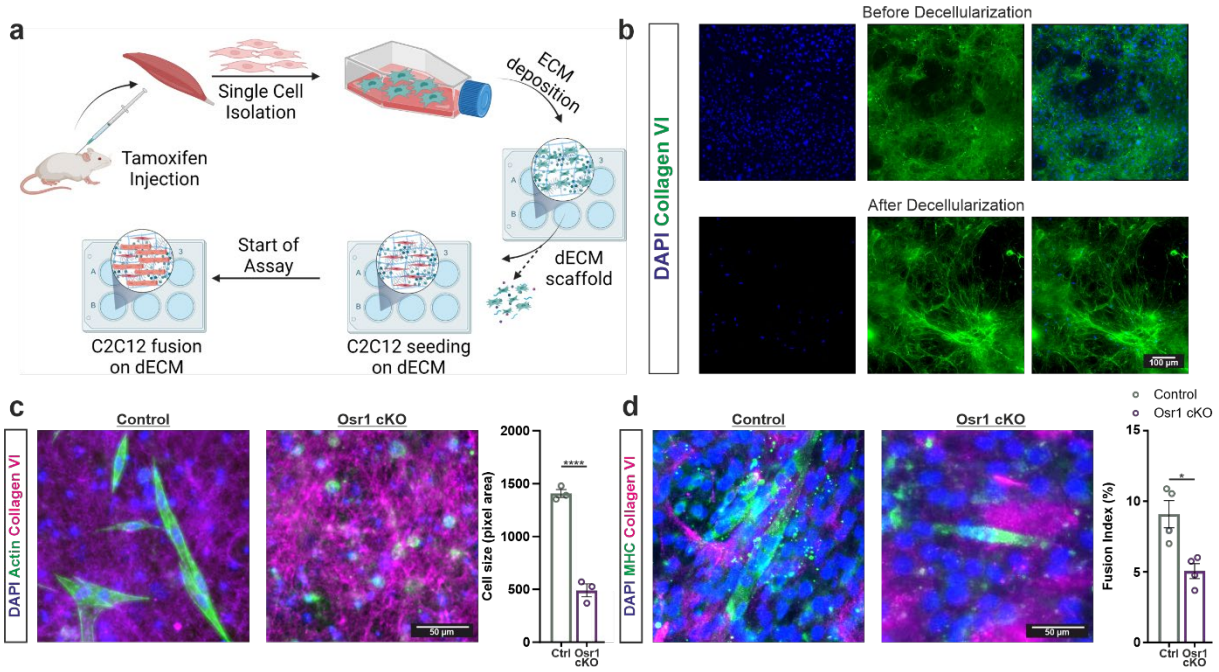

Figure 53: Osr1 cKO FAPs produce an anti-myogenic ECM
(a) Schematic representation of decellularization assay and culture of C2C12 on dECM (b) Efficiency of the dECM method showing intact Collagen VI network after the decellularization. (c) C2C12 differentiated for 2 days on dECM. Quantification of cells spread by actin staining showed a decrease in C2C12 size on the Osr1 cKO dECM. (d) 5 days of C2C12 differentiation on dECM and immunostaining with MHC. Two-fold decrease in the fusion index was quantified for the cells on the Osr1 cKO dECM. Data are presented as mean ± SEM (n = 3-4); statistical analysis was done using two-tailed Student's t tests: *p<0.05, ****p<0.0001.

Upon decellularization, C2C12 myoblasts were cultured for 2 days in differentiation conditions on the dECM. While C2C12 cells cultivated on control dECM showed the typical spindle-shaped morphology, cells on Osr1 cKO dECM remained circular and failed to spread (figure 53c). Quantification of the cell size, measuring the actin staining, revealed an approx. 3-fold decrease in the spreading of C2C12 on the Osr1

cKO scaffold. Following that, the myogenic differentiation of C2C12 was also measured after 5 days of myogenic culture by assessing the fusion index. C2C12 cells cultivated on control dECM formed large multinucleated myotubes, while cells cultured on Osr1cKO dECM showed strongly impaired formation (40% lower) of multinucleated myotubes (figure 53d).

This section provided data that deletion of *Osr1* prior to injury contributes in enhancing the fibrogenic potential FAPs, thus developing an ECM gene secretion expression profile similar to the one of mdx derived FAPs. Furthermore, FAPs differentiation into chondrocytes/tenocytes seems to be also ruled by *Osr1* expression. In sum, loss of *Osr1* promotes a pro-fibrogenic transcription shift followed by altered ECM deposition both *in vivo* and *in vitro*, regulating negatively the myogenic process.

4.7 Osr1 cKO FAPs affect myogenesis via TGFβ signaling

The analysis of the transcriptome data from 3 and 7 dpi GFP⁺ FAPs, highlighted the importance of *Osr1* expression during regeneration for two main procedures i) extracellular matrix formation and ii) cytokine secretion. Therefore, I decided to isolate these two major properties of FAPs and identify their potential effect on myogenesis. In the previous section, the defect of a severe fibrotic ECM production was described. How though could the second most affected term in Osr1 cKO FAPs regulate myoblast fusion is a question still unanswered. In this section, the paracrine signaling of Osr1 cKO FAPs and its impact on myogenesis will be on focus.

4.7.1 Paracrine signaling effect of mutant FAPs on myogenesis

The beneficial effect of FAPs on myoblast fusion has been reported already from the first time of their first description (Joe et al., 2010). In direct co-culture assays used in that study, one cannot disentangle the effect of the secreted ECM from the effect of the secreted factors. To answer the question if the molecules secreted by Osr1 cKO FAPs can inhibit myogenesis similarly to their produced ECM, indirect co-culture experiments were performed using the transwell approach (figure 54a).

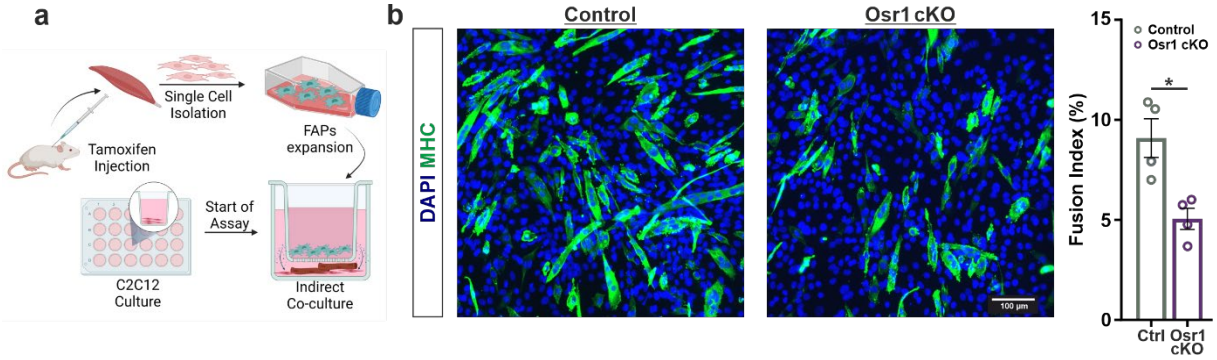

Figure 54: Osr1 cKO FAPs inhibit myogenesis when co-cultured with C2C12 cells
(a) Schematic representation of co-culture assay. FAPs are cultured in a transwell insert and placed above ready to differentiate C2C12 cells. (b) Immunostaining with MHC of 4 days differentiated C2C12 cells. Quantification of the fusion index indicated a 40% almost decrease in the C2C12 co-cultured with Osr1 cKO FAPs. Data are presented as mean ± SEM (n = 4); statistical analysis was done using two-tailed Student's t tests: *p<0.05.

FAPs were isolated from tamoxifen treated mice, expanded and seeded in transwell inserts. Inserts were then transferred on wells with C2C12 cells and the differentiation assay was initiated. Intriguingly, after 4 days of differentiation the fusion index of C2C12 cells co-cultured with Osr1 cKO FAPs was almost 40% lower compared to C2C12 cells cultured with control FAPs (figure 54b). It is worth referring at this point that the number of the C2C12 cells seeded on the plate was five times higher than the

FAPs number seeded in the transwell insert. The concentration of secreted factors is directly depended on the number of cells. Therefore, the inhibition of C2C12 fusion could be also more severe under the presence of a more potent environment.

In order to strengthen this hypothesis, CM was generated by Osr1 cKO and control FAPs (figure 55a). Serum free CM was collected once FAPs were over-confluent and used upon supplementation with 2% horse serum for the differentiation of C2C12 cells (figure 55b). While CM from control FAPs did not increase C2C12 myogenic differentiation as assessed by the fusion index, myogenesis was strongly repressed (approx. 80% reduction) when using CM from Osr1 cKO FAPs (figure 55b). Note that, C2C12 cells treated with Osr1 cKO CM failed to form long multinucleated myotubes. In contrast mononucleated cells positive for myosin heavy chain were mainly observed, suggesting a failure in myoblast fusion.

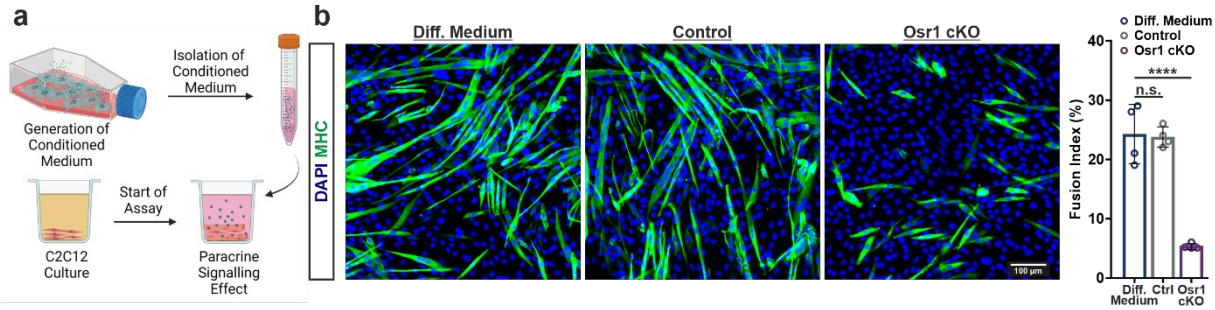

Figure 55: Paracrine signaling of Osr1KO FAPs blocks fusion of C2C12 cells
(a) Schematic representation of CM isolation of FAPs and its use as differentiation medium for C2C12 cells. (b) Immunostaining with MHC of 4 days differentiated C2C12 cells. Fusion index was quantified and showed similar levels of myogenesis for C2C12 cultured in normal differentiation medium and CM from control FAPs, whereas a 3-fold decrease was observed when cultured with $Osr1^{KO}$ CM Data are presented as mean ± SEM (n = 3); statistical analysis was done using two-tailed Student's t tests: n.s. not significant, ****p<0.0001.

4.7.2 Deletion of *Osr1* in FAPs upregulates *Tgfβ* expression levels

One of the first effects to be shown for TGFβ was the inhibition of the myogenic differentiation in vitro, by suppressing the expression of MyoD and myogenin (Massague et al., 1986, Olson et al., 1986). It has been recently shown that this procedure is also regulated via the control of actin cytoskeleton-related genes (Girardi et al., 2021). Mining for *Tgfβ* isoforms expression levels in the transcriptome data revealed an upregulation of *Tgfβ* transcripts at both timepoints (figure 56a). More specifically, *Tgfβ1* and *Tgfβ2* were upregulated in the Osr1 cKO on both timepoints, while expression of *Tgfβ3* was lower in the mutants at 7 dpi. Expression levels of *Tgfβ* isoforms were also quantified via RT-qPCR on in vitro recombined FAPs, isolated from

uninjured healthy mice (figure 56b). Interestingly, *Tgfβ1* was significantly upregulated in the Osr1 cKO FAPs and expression of *Tgfβ2* tended as well to be higher in the mutant cells. No differences were measured in the expression levels of *Tgfβ3*. Thus, this experiment proves that *Osr1* regulates intrinsically *Tgfβ1* expression *in vitro* also in homeostatic conditions. The pathway analysis of common regulated genes between the 3 and the 7 dpi transcriptome data, shown in figure 39, revealed that many DE genes cluster under the BioPlanet pathway "TGFβ regulation of extracellular matrix". An additional analysis in the BioPlanet pathways of the upregulated DE genes at 3 dpi showed an enrichment to the TGFβ term, ranking now first in the list (figure 56c).

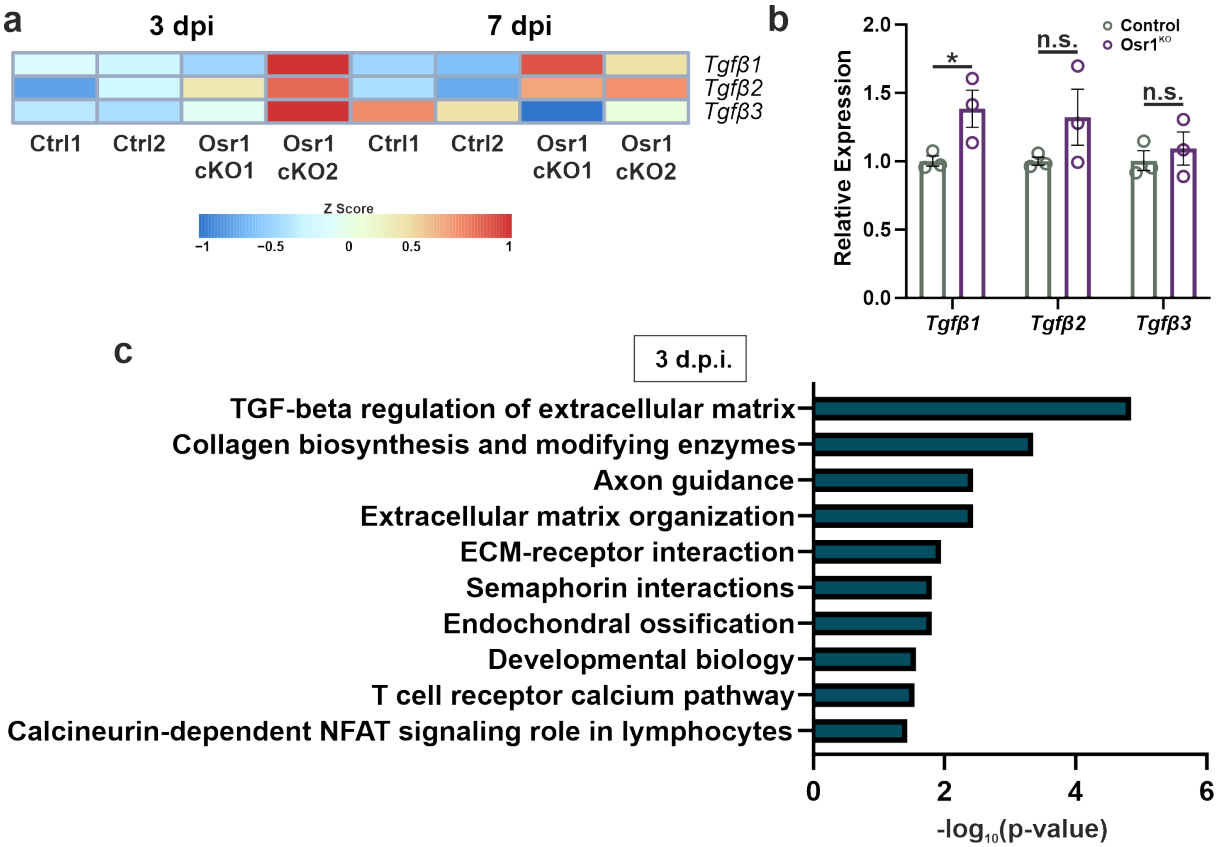

Figure 56: *Tgfβ* expression in upregulated in the Osr1 cKO
(a) Heat maps of the *Tgfβ* isoforms expression mined from the trascriptome data at 3 and at 7 dpi *Tgfβ1/2* are upregulated in the Osr1 cKO in both timepoints, *Tgfβ3* expression is higher only at 3 dpi. (b) Expression of *Tgfβ1* is upregulated significantly and *Tgfβ2/3* tend to go up in Osr1KO in vitro FAPs, as measured by RT-qPCR. (c) Analysis of the upregulated DE genes from the transcriptome data at 3 dpi using the Bioplanet 2019 database, highlighted the contribution of these genes in the TGFβ regulation of ECM in the Osr1 cKO. Data are presented as mean ± SEM (n = 3); statistical analysis was done using two-tailed Student's t tests: n.s. not significant, *p<0.0001.

Having found that TGFβ pathway is regulated in the Osr1 cKO injured FAPs and knowing the inhibiting role that TGFβ has on myogenesis, I was prompted to perform a rescue experiment to verify the presence of TGFβ in the Osr1 cKO CM. To show that, I used the small molecule SB431542 (SB), an inhibitor of the TGFβ Type 1 receptor kinase. First, the efficiency of the acquired SB was validated by treating C2C12 under differentiation. Treatment of myoblasts with SB is known to induce myogenic differentiation. Western blot performed on C2C12 protein lysates showed

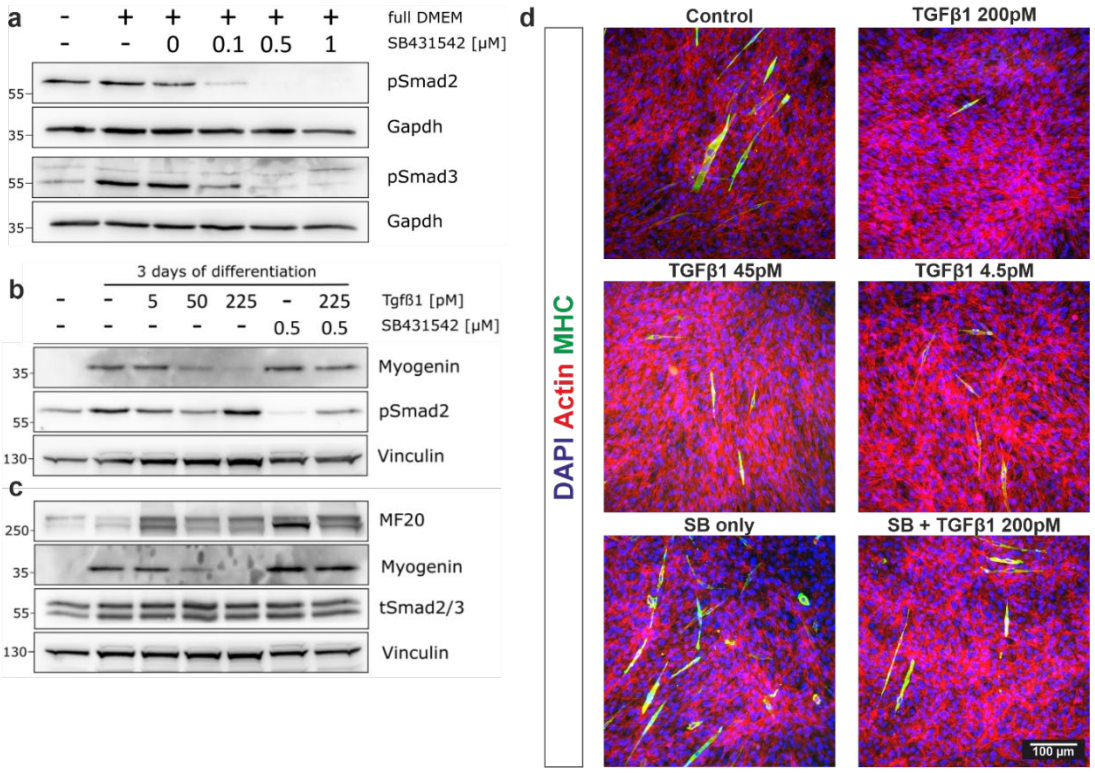

Figure 57: Induction of myogenesis after inhibiting the TGFβ receptor type 1 kinase using the SB431548

Western blots performed on protein lysate from C2C12 cells (a) upon treatment with different amount of SB431542 and differentiated for three days. Protein levels of pSmad2 and pSmad3 were found to be lower with higher concentration of SB431542. (b) Treatment of C2C12 cells with TGFβ1 resulted in lower protein levels of myogenin and normal detection of pSmad2. Simultaneous treatment with TGFβ1 and SB431542 resulted in higher levels of myogenin and lower levels of pSmad2. (c) Total protein levels of Smad2/3 used as negative control were found to be equal in all the samples. (d) Co-immunofluorescence staining of MHC and actin in C2C12 cells differentiated for two days and treated with TGFβ1 and/or with SB431542. Less MHC positive cells can be observed with higher concentration of TGFβ1 used. Upon C2C12 treatment with SB431542 without and with the highest amount of TGFβ1, more cells were stained with MHC.

that treatment of C2C12 cells with 0.5μM SB and higher, could reduce the protein levels of pSmad2 and pSmad3, indicating successful inhibition of the TGFβ pathway (figure 57a). The SB mediated induction of myoblast fusion has been reported in the past years (Krueger and Hoffmann, 2010, Watt et al., 2010). To verify the functionality of the SB in my assays, C2C12 were differentiated for 3 days and treated at the same time with different concentrations of TGFβ1 or with 0.5μM SB or both at the same time

(figure 57b, 57c, 57d). Protein levels of the late differentiation marker myogenin was shown to be decreased with higher concentrations of TGFβ1, validating the anti-myogenic effect of TGFβ (figure 57b, 57c). On the other hand, myogenin was overexpressed upon inhibition of the TGFβ pathway, even in the presence of external TGFβ1 in the medium, highlighting the potency of the SB small molecule. This tendency was also observed in the protein levels of MHC (detected with MF20), although with a subtler defect. Absence of pSmad2 detection in the SB treated sample validated the efficiency of the treatment and the total Smad2/3 protein levels were measured in all the samples as negative controls. Finally, the effects of these treatments can also be seen in figure 57d where immunofluorescence stainings for MHC and actin are shown. Decreasing the concentration of TGFβ1 in the medium, increased the amount of MHC^{+} cells, while a weak effect was observed when the highest concentration of TGFβ1 was added in pre-treated cells with SB (figure 57d).

Having established C2C12 treatment with SB and verified its potency against TGFβ pathway, the CM treatment experiment was performed again, this time in combination with SB treatment (figure 58a). Differentiation of C2C12 using CM from control FAPs, induced this time myoblastic fusion by 20%. Interestingly, a reduction of 20% was observed with the Osr1 cKO CM (figure 58b). As expected, pre-treatment of the cells with SB, induced myogenic differentiation by 30% in samples treated with normal differentiation medium and by 20% in samples with control CM. Remarkably, a 35% increase in the fusion potential was present in the sample treated with Osr1 cKO CM and SB. Note though, that the final fusion index still remained in lower levels than the respective effect of the SB alone or in combination with the control CM. The effect of the SB treatment in all the samples can be verified from the presence of hypertrophic multinucleated fibers, which has been reported before.

Taken together, results shown in this section demonstrate that *Osr1* regulates the paracrine signaling activity of FAPs both *in vivo* and *in vitro*. Osr1 cKO FAPs negatively regulate myogenic differentiation not only via alterations in the composition of the secreted ECM but also through upregulation of the TGFβ signaling pathway, explaining in part the strong fibrotic phenotype observed upon injury.

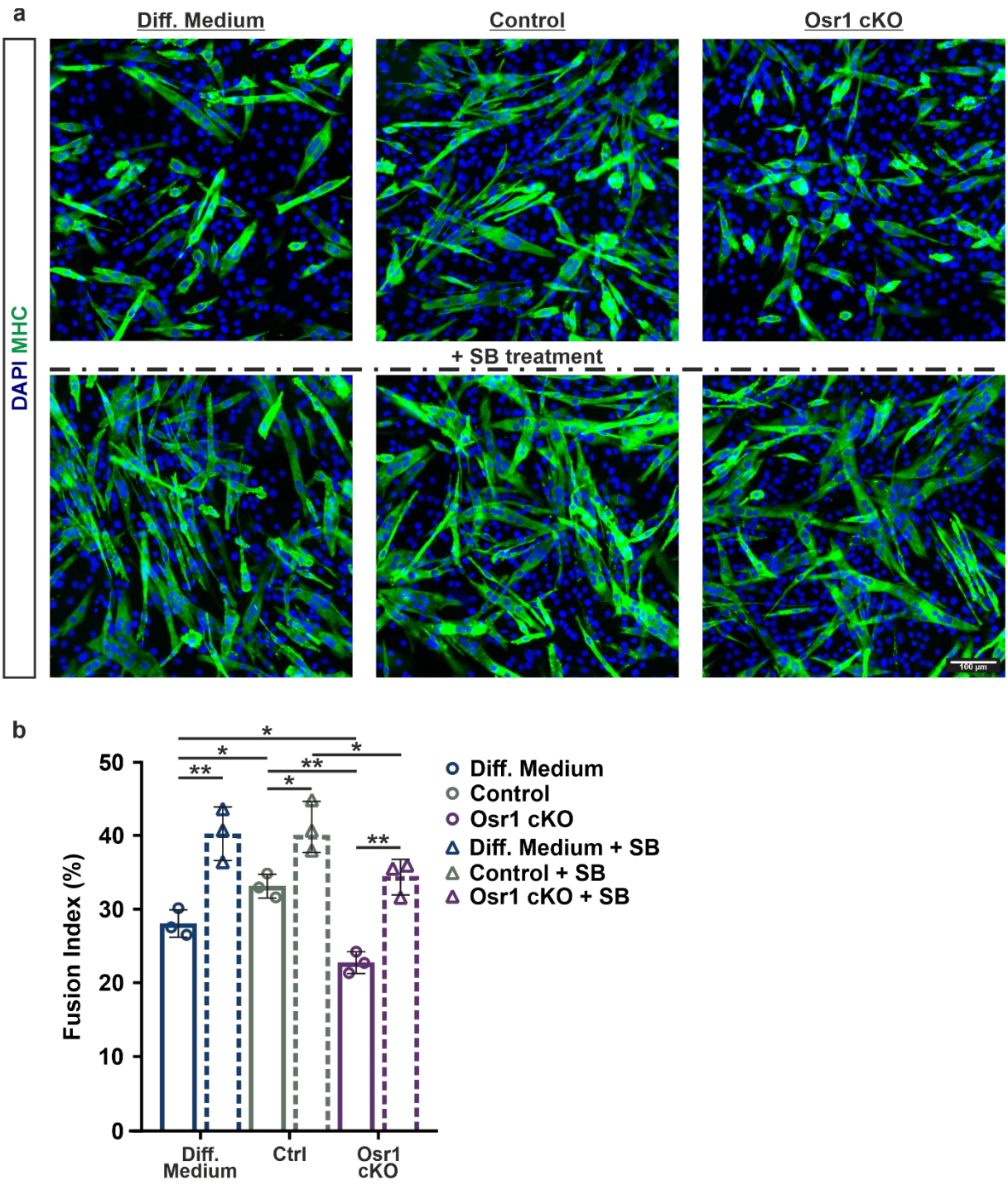

Figure 58: Pretreatment with SB431542 rescues the anti-myogenic effect of the Osr1 cKO CM

(a) Immunostaining with MHC of 3 days differentiated C2C12 cells, using CM from FAPs without and with SB431542 pretreatment. (b) Quantification of the fusion index showed higher values index in the cells treated with Control CM and lower when differentiated in $Osr1^{KO}$ CM. An induction of myogenesis was observed in all the groups when cells were treated with SB431542. Data are presented as mean ± SEM (n = 3); statistical analysis was done using two-tailed Student's t tests: *p<0.05, **p<0.01.

4.8 Summary of results

The aim of this study was to describe the role of *Osr1* expression by the fibro-adipogenic progenitors in murine muscle regeneration using an Osr1 cKO mouse model, primary mouse FAPs and C2C12 myoblasts. The key findings of this study are:

1. *Osr1* is expressed only by FAPs and is essential for efficient muscle regeneration. Generation of the Osr1 cKO mouse model and a longitudinal histological analysis revealed several defects in the regeneration process that lead to delayed muscle regeneration with smaller fiber size.
2. Excessive fibrotic tissue is formed during the regenerative process in the mutant injured muscle, which persists until the later timepoints. Mechanical measurements revealed altered tissue stiffness values in the Osr1 cKO. The injured region was significantly softer than the respective injured control, possibly contributing to the inhibition of the regenerative process.
3. The MuSCs pool is affected in the mutants, although MuSCs themselves do not express *Osr1*. This highlights the importance of *Osr1* expression by FAPs, since it can in a non-cell autonomous manner, affect MuSCs proliferation, apoptosis and differentiation.
4. Deficiency of *Osr1* has an intrinsic effect on FAPs. An *in vitro Osr1* recombination model validated the importance of *Osr1* in FAPs for their proliferation. This defect was also confirmed *in vivo*, where Osr1 cKO FAPs exhibited lower proliferation and higher apoptosis values. Transcriptome analysis of FAPs at 3 and at 7 dpi highlighted defects in gene regulation related to i) the immune response and ii) the extracellular matrix.
5. Further analysis of the transcriptome data revealed an altered secretome of Osr1cKO FAPs which might have an effect on the regulation of the inflammatory response. An advanced screening of the immune cell populations at 3 dpi showed no defects in the infiltration of macrophages in the Osr1 cKO muscle. However, the polarization of macrophages was shown to be affected. The ratio of M1:M2 macrophages was 1:1 in the mutant while this was significantly shifted in the control muscle. There the ratio was 1:3, indicating a progressive anti-inflammatory environment.
6. The mdx and the Osr1 cKO FAPs share common fibrogenic profile as shown with the comparison of transcriptome data. *In vitro* $Osr1^{KO}$ cells differentiate more readily into fibroblasts and their adipogenic potential is skewed. *In vitro*

decellularization assays verified the production of a non-beneficial Osr1^{KO} ECM with anti-myogenic properties.

7. The paracrine signaling of Osr1 cKO FAPs was also found to hold anti-myogenic properties. The differences in ECM formation and fibrogenic differentiation upon *Osr1* deletion are followed by an upregulation of *Tgfβ1* in FAPs. *In vitro* experiments on differentiating C2C12 show that cells fusion is lower when using CM from Osr1KO FAPs while this effect is rescued when the activation of the TGFβ pathway is blocked.

In conclusion, this study highlights the role not only of FAPs in muscle regeneration, but also of *Osr1* expressing FAPs. These cells orchestrate a plethora of effects that also influence the pro-regenerative function of MuSCs and macrophages.

5 Discussion

The primary function of our musculoskeletal system is locomotor activity, maintenance of posture and breathing. However, direct trauma (like intensive physical activity or lacerations) can lead to muscular injury or this can also be a result of an indirect cause such as a genetic mutation or a neurological dysfunction. If left untreated these injuries can result in loss of muscle mass, locomotive deficiency, even to lethality. The remarkable regenerative capacity of muscle includes activation of cellular responses and the coordinated interplay of various cell types. The extensive and numerous studies of the satellite cells, the muscle stem cells, have contributed to unraveling molecular pathways involved in skeletal muscle regeneration. However, the maladaptive accumulation of fibrofatty infiltrations is the hallmark of multiple pathologies where tissue degenerates due to non-resolved inflammation or chronic damage. The muscle resident FAPs are stromal cells with a multidifferentional potential. They actively build and shape the extracellular matrix and hold an immunomodulatory function due to their crosstalk with other muscle resident and non-resident cells. Remarkably, a great portion of differentiated cells that contribute to ectopic tissue formation in muscle are of FAPs origin. While FAPs regulate several processes in muscle homeostasis and regeneration, their exact role is still unclear. Nevertheless, in the last five years, their functions and their plasticity potentials are being constantly unraveled.

The expression of the transcription factor *Osr1* was characterized in FAP-like cells during muscle development. Moreover, regenerative FAPs are instructed by their developmental program since they re-express *Osr1* during muscle regeneration upon proliferation. However, lethality of *Osr1* deficiency at early fetal stages impeded further *in vivo* investigations of the role of Osr1^{+} FAPs in skeletal muscle regeneration.

5.1 Osr1^{+} FAPs are essential for efficient muscle regeneration

5.1.1 *Osr1* specificity in FAPs and generation of a knock-out line

In order to perform functional gene studies, mouse models are an essential tool because of their high similarity to the human anatomy, physiology and genetics. In contrast to the *in vitro* studies, they allow for better understanding of the cellular interactions in a tissue context while at the same time the cell of interest is not isolated from its cellular environment.

The limiting factor of the lethality of *Osr1* deficiency in mouse fetal stages does not allow breeding *Osr1* knock-out mice and investigate the function of *Osr1* in adult injured mice. Therefore, a new mouse model was generated that enabled a conditional *Osr1* knock-out prior to injury. For this purpose, the Osr1$^{flox/+}$ line was generated from the Osr1$^{LacZ/+}$ reporter line, which was introduced in the study of Stumm and colleagues (Stumm et al., 2018). The Osr1$^{flox/+}$ is a transgene line that carries the loxP sequences (flox) flanking the *Osr1* exon 2 while at the same time, a GFP sequence can be used upon inversion as a reporter of the *Osr1* promoter activation. In order for all these to take place, the expression of Cre recombinase is necessary, whose gene in our mouse model was under the control of the CAGG promoter and therefore is expressed in all the cell types of the mouse (CAGG$^{CreERt2/+}$ line provided by Dr. Heiner Schrewe) (Hayashi and McMahon, 2002).

The mediated Cre excision of exon 2 in CAGG $^{CreERt2/+}$ Osr1$^{flox/+}$ line was first validated by genomic quantitative RT-qPCR at several timepoints. Genomic DNA was isolated from part of the quadriceps muscle tissue and primers specific for the exon 2 of *Osr1* were used. At all timepoints the recombination efficiency of the knock-out animals was shown to be around 50-60%. Interestingly, isolation of mRNA from 3 dpi whole injured T.A. muscle and performance of RT-qPCR showed an 85% reduction in the transcripts of the *Osr1* gene, verifying the high recombination efficiency of the mouse model. However, it must be noted that for the heterozygous Osr1$^{flox/+}$ animals used as control, the *eGFP* gene inserted between exon 2 and exon 3 of *Osr1* might reduce the transcript level of *Osr1*, due to a splicing efficiency impairment (hypomorphic allele). The proper inversion of the GFP cassette and the subsequent expression of GFP upon injury was measured through the detection of green fluorescent cells by fluorescence cell sorting.

Discussion

Summarizing, in this thesis the conditional Osr1 knock-out CAGG $^{CreERt2/+}$ Osr1$^{flox/flox}$ was used that enabled the study of *Osr1* deletion in regenerative muscle. This reporter mouse model was used for a longitudinal histological study of muscle regeneration efficiency but also to identify FAPs with active *Osr1* promoter in order to proceed with transcriptome and FACS analyses.

In the CAGG $^{CreERt2/+}$ Osr1$^{flox/flox}$ recombination of *Osr1* locus takes place in every tissue and cells since the expression of Cre recombinase is controlled by the CAGG promoter. This might raise questions regarding the suitability of this line in studying specifically the deletion of *Osr1* in FAPs upon muscle injury since possible phenotypes could be attributed to loss of *Osr1* expressions in other cell types of the muscle or even of another tissue. To tackle that problem, first the expression of *Osr1* was checked in the Tabula Muris compendium where single cell transcriptome data from adult mice are included (Schaum et al., 2018). In this database, one can verify that *Osr1* in muscle is mainly expressed by the mesenchymal stromal cells, which also include FAPs. Transcript reads of the *Osr1* gene were found to be enriched only in the cluster of muscle resident cells in published transcriptome data (Scott et al., 2019). With a further investigation inside this cluster, it was confirmed that *Osr1* is only expressed in the Sca1^{+} cells. Taking advantage of the GFP reporter cassette in the CAGG $^{CreERt2/+}$ Osr1$^{flox/flox}$ mouse model, the Sca1^{+} population was shown to be positive for GFP. The approx. 0,25% of the endothelial and immune cells expressing GFP can be attributed to the gating strategy used and therefore was considered non-important. Finally, mining for *Osr1* expression in the single cell data published by Oprescu and colleagues at different timepoints of regeneration, proved that *Osr1* is mainly expressed (both in homeostasis and in regeneration) to a very high extent by the PDGFRa^{+} population (Oprescu et al., 2020). From this analysis, it can also be appreciated that PDGFRa is a better marker than Sca1 for FAPs since the latter is also expressed by immune cells and therefore *Osr1* and *Sca1* expression co-localized only in the FAPs population. Altogether, these data eliminate the possibility of a systemic defect of *Osr1* deletion or of attributing any potential muscle phenotype to the expression of *Osr1* by another cell type in the regenerative milieu. However, one should note that most studies perform shallow depth of RNA sequencing. Although this might be sufficient to identify cell type, cells that express low levels of a transcription factor can be discounted (Zhang et al., 2020).

A potential future approach to the studies of *Osr1* function in regeneration would be the generation of a conditional *Osr1* knock-out only in FAPs. This could be achieved by crossing the PDGFRa^{Cre} line, used in FAPs depletion studies, with the Osr1^{flox} line (Uezumi et al., 2021, Wosczyna et al., 2019). The regenerative capacity and the phenotype observations that would be made on this line should be similar to the ones using the CAGG^{Cre} Osr1^{flox}, based on everything that was referred before about *Osr1* specificity.

5.1.2 Impact of *Osr1* deletion in fiber maturation and resolution of necrotic tissue

In embryonic development muscle resident TCF7L2 expressing stromal cells are essential to proper muscle development (Kardon et al., 2003, Mathew et al., 2011). These cells were shown to overlap with mesenchymal stromal cells expressing *Osr1*, which can be considered the progenitors of adult FAPs (Vallecillo-Garcia et al., 2017). Many studies focused on the contribution of the TCF7L2 cells also to muscle regeneration. Genetic lineage ablation of around 40% of TCF7L2^{+} cells resulted in premature differentiation and exhaustion of the MuSCs pool, which had a defect in the size of the regenerating fibers (Murphy et al., 2011). Interestingly, in humans TCF7L2^{+} cells provide also support to myogenesis and play an important role in muscle regeneration (Mackey et al., 2017). Depletion of FAPa^{+} (fibroblast activation protein alpha) muscle resident stromal cells caused an atrophic phenotype in adult mice, with decreased muscle mass and rapid weight loss. This phenotype was accompanied by reduced expression of *follistatin* and *Lama2* as well as by altered hematopoiesis (Roberts et al., 2013a).

In the last years, FAPs necessity to efficient muscle regeneration has been demonstrated. Depletion of the PDGFRa^{+} cells and their lineage resulted in smaller myofibers and reduced CSA distribution during regeneration while FAPs ablated mice exhibited also 30-40% less mass. The Tsuchida group recently confirmed these results while in addition was shown that the expression of the muscle specific E3 ubiquitin ligase MAFbx was increased. Altogether, these three groups up to today have demonstrated that muscle resident PDGFRa^{+} FAPs are vital for the regenerative capacity of the muscle and their loss leads to inhibited myogenesis (Roberts et al., 2013a, Wosczyna et al., 2019, Uezumi et al., 2021). Interestingly, although loss of *Osr1* does not result in FAPs depletion in the injured line used in this study, the distribution

of muscle fiber size, especially the ones from 5 and 10 dpi, followed the same trend seen in the DTA-mediated ablation of PDGFRa^{+} FAPs (Uezumi et al., 2021, Wosczyna et al., 2019). The Osr1 cKO animals showed a marked delay in muscle regeneration with eMHC being persistent throughout the regeneration phase in the mutant injured tissue. The fiber size of fibers in the regenerative region was constantly smaller in the mutant apart from 3 dpi, when no differences were observed. At this timepoint the initial phase of inflammation is taking place, mainly fibers are being resolved and very few new fibers are formed. Therefore, this result was expected and indicates that the mutant and control animals begin their regenerative process from the same start point and there is not an initial advantage of the control injured muscle.

Multinucleated muscle fibers result from the fusion of mononucleated myoblasts and every incorporated myoblast nucleus is actively positioned in the center of the immature myotube (Folker and Baylies, 2013). Upon injury, fusion promoted to support myogenesis and therefore myotubes mature faster into myofibers. For many years scientist in the myology field used the quantification of the centrally located nuclei in a fiber as a read-out for fusion capacity and thus a regeneration speed index. Several automated tools have been developed for this quantification (Kastenschmidt et al., 2019). In this study, centrally located nuclei at 3 and at 5 dpi were stained positive for CD80, a marker for M1 macrophages. Therefore, quantification of the CNF ratio is not a reliable approach for estimating regeneration efficiency at early timepoints. Nevertheless, calculating the CNF distribution at 5 (only for eMHC^{+} fibers) revealed an initial delay of myofiber maturation for the Osr1 cKO. This finding is in line with the smaller myofiber size and the persistence of eMHC^{+} fibers. Interestingly, the CNF distribution at 17 dpi showed an opposite trend with the mutant being richer in trinucleated fibers whereas the control had more binucleated fibers. At this timepoint though, since the number of eMHC^{+} fibers is low, every CNF fiber was included in the measurement and thus one cannot be certain that central nuclei belong to fused myoblasts. This impairment of fiber maturation can possibly be also induced by the accumulation of randomly distributed necrotic fiber which was observed in the mutants at 10 dpi. This phenomenon is the histopathological hallmark of several myopathies such as the immune-mediated necrotizing myopathy, leading to myofiber degeneration (Vattemi et al., 2014). Despite all these alterations in the regenerative area (smaller myofiber size, defected myofiber maturation, accumulation of necrotic fibers), a defect in the mass of the injured or uninjured contralateral muscle was not observed.

However, the increased accumulation of fibrotic tissue in the Osr1 cKO or the small size of the lesion created from the injury model might be the reason for this absence of difference.

5.2 Osr1 cKO FAPs: drivers of muscle fibrosis

5.2.1 Elevated levels of fibrosis upon *Osr1* deletion

Tissue fibrosis is the hallmark of many degenerative diseases that involve asynchronous/ constant tissue regeneration and inflammatory response, it can affect every organ and is accounted for half of deaths in the industrialized world (Henderson et al., 2020). Progressive fibrosis is connected with excessive ECM deposition that eventually leads to connective tissue hyperplasia (Lieber and Ward, 2013, Serrano et al., 2011). Connective tissue`s principal components are the ECM and the residing stromal cells that continuously build and shape their microenvironment. Pathological fibrosis of muscle under chronic damage though, is different than the normal phase of scar tissue formation following a single round of injury (Smith and Barton, 2018). In these cases, inflammatory activated fibroblasts secrete a large amount of ECM proteins, replacing myofibers with wound scar which will eventually lead to failure of muscle function and even death (Fadic et al., 2006, Pakshir and Hinz, 2018). Given the importance of muscle tissue fibrosis, the origin of malfunctioning fibroblast and their contribution in myopathies has been studies extensively the last ten years. The *in vivo* fibrogenic potential of FAPs has been characterized since their first description, when PDGFRa^{GFP} tracing cells were transplanted into irradiated skeletal toxin injured muscle. The PDGFRa^{GFP} FAPS were shown to not contribute in myofiber formation but accumulated in areas with high ECM deposition (Hamilton et al., 2003, Uezumi et al., 2011). A plethora of studies has demonstrated that PDGFRa^{+} FAPs reside in areas of increased non-functional ECM in cases of Duchenne muscular dystrophies patients and dystrophic mdx mouse models (Uezumi et al., 2014, Lemos et al., 2015, Kopinke et al., 2017, Contreras et al., 2019a, Mázala et al., 2020). Remarkably, deletion of *Osr1* prior to injury resulted in excessive deposition of persisting thick collagenous ECM which formed a scar tissue and was at later timepoints encircling the regenerating fibers of the mutants. Additionally, injured mutants exhibited smaller myofibers which is always observed in situations where fibrosis occurs. This elevated fibrotic tissue

formation was verified through two different methods, with immunostainings for Collagen VI but also with the histological staining of Picrus Sirius Red staining (PSR). At this point is worth mentioning that polarized light imaging of the PSR can provide valuable information about the composition of the matrix, since it can separate between Collagen I and III. Decreased Collagen I vs. III ratio has been shown to lead to lower stiffness and thus, lower regeneration abilities (Miller et al., 2001). Therefore, this could be a potential future approach to define the structural composition of the accumulating matrix in the mutants.

This study underlined the importance of *Osr1* expression in FAPs for orchestrating proper scar tissue formation. Deletion of *Osr1* dysregulated the regenerative FAPs in the milieu and this can be compared to the function of pathologically dysregulated FAPs. They are the source of fibrosis in several congenital muscular dystrophies including human DMD, mouse mdx lines, facioscapulohumeral dystrophy (FSHD), limb-girdle muscular dystrophy and ALS neuromuscular disease (Theret et al., 2021, Molina et al., 2021). Of note, PDGFRa^{+} derived myofibroblasts are not the only source of fibropathological disorders and scarring. It cannot be excluded that other tissue perivascular cells (e.g. pericytes) or immune cells (M1 macrophages) may also participate in the injury-induced matrix remodeling (Henderson et al., 2020, Henderson et al., 2013, Pakshir et al., 2020, Lemos and Duffield, 2018). In sum, numerous studies show that muscle scarring originates from PDGFRa^{+} FAPs and in the case of the Osr1 cKO mouse model, this possibly originates from Osr1 cKO FAPs.

5.2.2 Mechanical properties of the injured region and regeneration

Precise quantification of muscle fibrosis can be difficult due to the fact that a deterministic quantitative model of collagen arrangement is not available for muscle ECM. Till now methods used to quantify fibrosis in muscle are: i) calculate histologically the area fraction of an ECM staining together accompanied by observations of large increase in muscle fiber variation, ii) using a biochemical assay to verify the collagen content and iii) performing a functional assay to determine the stiffness of the muscle. A combination of two from the aforementioned methods is usually preferred although it is not possible to quantitatively interchange results between the assays (Guimarães et al., 2020).

The ECM in muscle plays an important role in transmitting forces produced by muscle forces to the tendon. To perform this function, the ECM should remain intact during muscle strain while proper function of the ECM is dependent on the mechanical properties of the tissue. It has been demonstrated that whole muscle stiffness is changing by the stiffness of both muscle fibers and ECM in pathological context and in aging (Wood et al., 2014, Lieber and Ward, 2013, Lacraz et al., 2015, Stearns-Reider et al., 2017, Brashear et al., 2021).

In order to evaluate the extensive fibrotic tissue in the mutants, the mechanical properties of the injured muscle were measured via nanoindentation. Several tissue stiffness techniques have been developed the last years measuring either passive stiffness or local forces of the tissue (e.g. atomic force microscopy, shear wave elastography, strain elastography etc.) (Lee et al., 2021). Therefore, a direct comparison of the exact stiffness values of the tissue should be avoided if these values were not acquired through the same method. Nanoindentation was first established on wild type uninjured and injured muscle sections, where a transient increase in muscle stiffness of the regenerative area was observed. This is in agreement with the observations of increased passive muscle stiffness upon injury and underlines the importance of tissue stiffening for proper regeneration. Remarkably, the stiffness values of the injured mutant were always lower than the respective values of the injured control. Increased fibrotic tissue formation and decreased stiffness were thus, the two main characteristics of the Osr1 cKO injured interstitial tissue. Examining the percentages of collagenous matrix measured at 3/5/10 dpi (same timepoints with stiffness measurements), one can notice that while deposition of collagen gradually increases in the mutants it decreases in the control from 5 to 10 dpi. This fact together with the decreased stiffness indicate that the composition of the ECM secreted in the mutant must be altered. It is worth referring at this point, that although many diseases are linked with increased stiffness, only contractive muscle function has been directly linked to it (Brashear et al., 2021). Higher stiffness is shown no to be defined by the amount of collagen deposition but rather by the collagen post translational modifications like collagen cross-linking or the alignment of collagen fibers (Swift et al., 2013, Smith and Barton, 2014, Brashear et al., 2021, Georges et al., 2007, Jones et al., 2018, Taufalele et al., 2019).

In total, the Osr1 cKO injured muscles exhibited increased fibrosis but decreased stiffness of the injured region which indicates modification in the structure, the

composition or the collagen architecture of the muscle. Moreover, defects in FAPs function have also been connected recently with decreases in muscle force, while in collagen VI mutants excessive fibrosis with lower stiffness and poor myogenesis have also been reported (similar to the Osr1 cKO model) (Wosczyna et al., 2019, Uezumi et al., 2021, Urciuolo et al., 2013). Thus, it is proposed that *Osr1* expression in FAPs is essential for the production of a pro-regenerative ECM supporting MuSCs myogenic differentiation via appropriate biomechanical signaling.

5.3 Non-cell autonomous defects of *Osr1* deficiency on MuSCs population

The dynamic multicellular response to muscle injury is characterized by discrete steps and is followed by the concomitant proliferation of two quiescent muscle resident cells, the FAPs and the MuSCs. These two populations reside close to each another but are separated via the basal lamina and they expand rapidly from days 2 to 5 upon injury (Bentzinger et al., 2013a). The interaction between stromal cells and MuSCs in skeletal muscle regeneration was first described forty years ago where the numbers of these two populations was shown to increase simultaneously with a similar trend upon muscle injury (Church, 1970). However, it was only recently when researchers demonstrated that FAPs regulate MuSCs function and vice versa (Joe et al., 2010, Murphy et al., 2011, Uezumi et al., 2010, Uezumi et al., 2021, Fiore et al., 2016).

Since deletion of *Osr1* prior to injury lead to inhibition of regeneration with smaller size of regenerating fibers and taking into consideration the supportive role of Osr1^{+} FAPs in embryonic muscle development (Vallecillo-Garcia et al., 2017), the population of MuSCs in the mutant was examined. During the early phase of regeneration (at 3 dpi) decreased MuSCs numbers were observed in the injured mutant muscle caused by decreased proliferation rate. At this timepoint, a higher reduction of MuSCs was counted on muscle sections immunostainings with Pax7 antibody than it was counted with the a7-integrin antibody via FACS. The differences in the results between the two methods can be attributed i) either to the different antibody used for MuSCs detection ii) or to the fact that our injury model is not consistent and thus, the entire muscle isolated cells used for the FACS contained cells from injured and uninjured areas (dilution of the effect). At 7 dpi no difference was detected in the number of MuSCs however MuSCs from the Osr1 cKO exhibited lower proliferation and higher apoptotic

rate. This is partially contradictory to the numbers of MuSCs calculated by FACs but a possible explanation can be that MuSCs from the mutant fail initially to expand and therefore do not reach the same peak numbers with the control derived MuSCs. Therefore, they possibly exhibit defects in their expansion rate from the onset of regeneration and when at 7 dpi numbers of control MuSCs decrease (due to the normal apoptotic clearance) they overlap with the numbers of the always lower Osr1 cKO MuSCs. In addition, the data from this study suggest impaired activation of MuSCs with lower numbers of MyoD^{+} cells and decreased *Myod1* mRNA expression at 7 dpi. This altogether will result in a decreased pool of differentiating myoblasts able to fuse and form new myofibers. Similar impairments in myogenic cell pool expansion and the consequent reduction in the size of newly formed fibers have been reported in multiple studies where the initial expansion and function of FAPs was defected or when the total FAPs population was defected (Wosczyna et al., 2019, Uezumi et al., 2021, Petrilli et al., 2020, Joe et al., 2010).

Expansion of the MuSCs pool is a prerequisite for regeneration, but still results in failed regeneration if differentiation is prevented, as in the case of DMD muscular dystrophy (Kottlors and Kirschner, 2010). Expression levels of *Pax7*, *Myf5* and *Myod1* were downregulated in the Osr1 cKO MuSCs at 3 dpi. Loss of *Myod1* and *Myf5* in regenerating muscle has been demonstrated that is the cause of poor regenerative abilities, leading to impaired differentiation (Yamamoto et al., 2018). Similarly, loss of *Pax7* expression reduced MuSCs proliferation and therefore skewed the regenerative potential (von Maltzahn et al., 2013, Zammit et al., 2006). In addition, lower expression levels of *Myod1* were measured for the Osr1 cKO MuSCs at 7 dpi, while immunostainings showed an increase in the Pax7^{+}/MyoD^{-} and a decrease in the Pax7^{-}/MyoD^{+} population. These effects can be interpreted as a consequence of impaired MuSCs activation in the mutant injured muscle. Of note, decreased MuSCs cell viability, overlapped the effect of *Osr1* ablation during development, while decreased activation and differentiation was not observed in this model, arguing for partially conserved, but also context-specific roles for *Osr1* in development and in regeneration (Vallecillo-Garcia et al., 2017).

Taking into consideration the stiffness defects discussed above in the injured mutant muscle, it is worth mentioning at this point that the biophysical and biomechanical ECM properties impact also the fate of MuSCs. Increased stiffness of the microenvironment has proven *in vitro* to be beneficial for MuSCs proliferation and differentiation and is

therefore in accordance to the stiffness/ MuSCs defects of the injured Osr1 cKO (Silver et al., 2021, Trensz et al., 2015). Conclusively, these data suggest that Osr1^{+} FAPs are critical to support MuSCs expansion and activation via remodeling and producing a transient ECM but also through other mechanisms, which will be further discussed in next sections.

5.4 *Osr1* is required for FAP pool expansion

In this project, the generation of the CAGG^{Cre} Osr1^{flox} line allowed for *in vivo* investigation of the role of *Osr1* in muscle regeneration. In order to further characterize the expression of *Osr1* in FAPs and to address its potential function in cell autonomous defects in these cells, an *in vitro* Osr1 cKO model was established. Taking advantage of the fact that CreERT2 is efficiently activated by the 4-OHT (the tamoxifen metabolite trans-4-OH-Tamoxifen), *in vitro* recombination of the *Osr1* locus was performed on FAPs with a recombination efficiency of approx. 98%, higher than the respective *in vivo* efficacy. Interestingly, generation of the Osr1^{KO} FAPs line demonstrated that *Osr1* must regulate FAPs proliferation and apoptosis, suggesting that these events are independent of FAPs crosstalk with other cells in the regenerative milieu.

Since their first description in 2010, FAPs were shown to rapidly expand in the first four days of injury, expressing proliferation markers and increasing the ratio of FAPs/MuSCs during this period (Petrilli et al., 2020, Joe et al., 2010). A strong increase in cellular apoptosis has been observed only later at ten days post injury, when also FAPs numbers gradually return to basal levels (Kopinke et al., 2017, Lemos et al., 2015). Remarkably FAPs numbers in the Osr1 cKO animals were measured to be lower at 3 dpi. While no difference in FAPs numbers was observed at 7 dpi, Osr1 cKO isolated FAPs at 7 dpi exhibited decreased proliferation and increased apoptotic rates. However, it is hard to explain how FAPs numbers between the mutant and the control animals were equal since their population exhibited 50% less proliferation rates and three-fold induction in apoptosis. This might be in part explained by the two different techniques used to acquire these data or FAPs Osr1 cKO population expansion might follow the same trendline with the MuSCs, explained before. How lack of *Osr1* affects FAPs viability requires further investigation. Nevertheless, the *in vivo* results of *Osr1* deletion in the FAP pool are in agreement with the *in vitro* behavior of the Osr1^{KO} FAPs, indicating an initial failure of FAP pool expansion, which is based on the cell-

autonomous function of *Osr1*. The importance of FAPs pool expansion has been underlined in FAPs depletion studies, where although tamoxifen injection in PDGFRa $Cre^{ER\text{-}DTX}$ mice did not induce myofiber necrosis in homeostatic muscle, it prolonged though necrosis and it impacted the regenerative capacity of the muscle upon acute muscle injury (Uezumi et al., 2021, Wosczyna et al., 2019). Thus, at least a major part of the Osr1 cKO phenotype can also be explained by the initially decreased FAP pool which may be insufficient to properly support regeneration. Interestingly, similar defects to the Osr1 cKO were described in a study where cardiotoxin injury in dystrophic mice resulted also in poor myogenic differentiation due to the initial failed expansion of the FAPs pool (Petrilli et al., 2020).

Fibrotic scar tissue formation is often associated with fatty infiltration after a single round of injury (Biltz et al., 2020, Xu et al., 2021) but also in many myopathies, including DMD (Uezumi et al., 2014, Kopinke et al., 2017), limb-girdle muscular dystrophy (Hogarth et al., 2019) or after rotator cuff tears (Lee et al., 2020, Kang et al., 2018). In most of these cases, the increase in numbers of $PDGFRa^{+}$ FAPs is the reason at some extent for the pathological exacerbated fibrotic/fat deposition. In contrast to these reports, in this study excessive fibrosis was one of the main defects of the mutants, although the population of the Osr1 cKO failed to expand. Nevertheless, deregulated fibrotic deposition could also be assigned to defects in the differentiation program of FAPs, which will be further discussed later.

5.5 Control of macrophage polarization by FAPs

5.5.1 Impacts of *Osr1* deletion on FAPs secretome

Muscle-resident and non-resident immune cells play an important role in tissue homeostasis, regeneration and inflammatory diseases (Chazaud, 2020, Theret et al., 2022). In particular, macrophages are important for MuSCs stimulation and their depletion has a great impact on muscle regeneration upon injury (Lemos et al., 2015, Juban et al., 2018). However, not much is known about the interplay of FAPs and macrophages at a resting state while their crosstalk in tissue regeneration has recently gained a lot of attention. Genetic lineage depletion of $PDGFRa^{+}$ cell did not lead to a defect in the immune population neither in short time (9-14 days) nor in a longer period

(9 months) in the absence of muscle injury (Wosczyna et al., 2019). Although many cells are participating in the attraction of macrophages in the trauma region, regenerative FAPs establish an environment rich in inflammatory cues 24 hours post injury by secreting a mixture of chemokines and cytokines, facilitating thus the infiltration of pro-inflammatory macrophages (Scott et al., 2019, Mashinchian et al., 2018).

During limb embryonic development transcriptome analysis of Osr1 KO cells indicated a downregulation in the gene expression of several signaling factors (e.g. *Cxcl12*) (Vallecillo-Garcia et al., 2017). A few years later, in adult injured muscle the single cell RNA-seq study of Oprescu and colleagues referred to *Osr1* as a marker of a FAPs population, which is mainly responsible for secreting signaling molecules in regeneration (Oprescu et al., 2020). In this project, transcriptome analysis of GFP^+ FAPs verified the importance of *Osr1* in regulating gene expression related to the inflammatory response. Osr1cKO FAPs showed downregulation of a variety of cytokine genes, several of which have been involved in macrophage polarization. Members of the MCP (monocyte chemotactic protein) chemokine family, which in muscle are expressed mainly by FAPs and less by myogenic and immune cells, were downregulated in Osr1 cKO FAPs (De Micheli et al., 2020a). Expression of *Ccl2*, an inflammatory cytokine, was significantly reduced in the Osr1 cKO FAPs. Through its receptor CCR2, CCL2 regulates macrophage phenotypical switch by inducing M2 polarization (Roca et al., 2009) and inhibiting proinflammatory cytokine production (Sierra-Filardi et al., 2014). In addition, *Ccl8* and *Ccl11* were significantly downregulated in Osr1 cKO FAPs. In cancer metastasis the proteins CCL8 (Farmaki et al., 2020) and CCL11 (eotaxin) (Tripathi et al., 2014) act as M2 macrophage recruiters and have a pro-angiogenic role. Furthermore, Osr1 cKO FAPs showed a downregulation of *Il6*, which might also contribute to failed MuSC activation and expansion. The myokines IL6 (Joe et al., 2010) and IL10 (Lemos et al., 2012) are secreted by FAPs and have been reported by several studies to have an anti-inflammatory role and to promote regeneration. The beneficial role IL6 for myogenic differentiation has been also shown *in vitro* (Joe et al., 2010). On the other hand, in amyotrophic lateral sclerosis (ALS) the increased IL6 production by FAPs resulted in muscle atrophy and fibrotic tissue formation (Madaro et al., 2018, Contreras et al., 2016). Of note is worth mention at this point that FAPs are in addition the main producers of IL33, which promotes the proliferation of muscle regulatory T cells

(Kuswanto et al., 2016). Both *Il10* and *Il33* were not though significantly regulated in the transcriptome data. Thus, several FAP expressed cytokines may contribute to the macrophage M1-M2 polarization, however this remains to be tested *in vitro* using co-culture assays or FAPs CM with monocytes/ macrophages.

5.5.2 Bidirectionality of FAPs-macrophage crosstalk

The intricate primary response of FAPs in the initiation and the development of granulation tissue indicate that FAPs are essential key players and modulators of the initial immune response (Theret et al., 2021). Depletion of the FAPs population prior to muscle injury has been reported to result in $CD45^+$ cells infiltration defects, leading to defects in myogenesis and enhanced fibrotic tissue formation (Wosczyna et al., 2019). Remarkably, although deletion of *Osr1* lead to lower FAPs numbers at 3 dpi in the mutant, no defect was detected in the amount of the infiltrated $CD45^+$ cells. Taking into consideration the role of cytokines that were found to be regulated in the Osr1 cKO, a thorough analysis was further performed on the identity of the $CD45^+$ cells with the focus on the macrophage polarization phenotype.

Proinflammatory M1 macrophages produce TNFα which has an early pro-apoptotic effect on FAPs in order to regulate their expansion following injury resolution (Lemos et al., 2015, Juban et al., 2018). The critical role of the initial monocyte infiltration has been validated in a Ccr2 KO mouse model, where it resulted in inhibited FAPs clearance, increased fibro-fatty deposition and thus, to impaired muscle healing (Lu et al., 2011a, Lemos et al., 2015, Lu et al., 2011b). Interestingly, in contrast to that finding, in aged mice opportune *Ccr2* inhibition upon injury induces myogenic differentiation and aids recovery due to the absence of an inflammatory environment (Blanc et al., 2020). On the other hand, anti-inflammatory macrophages secrete TGFβ supporting FAPs survival and enhancing their myofibroblast differentiation and ECM secretion (Stepien et al., 2020). This delicate balance of short exposure to TNFα and low levels of TGFβ restrains FAPs from acquiring an anti-regenerative role seen in several myopathies (Lemos et al., 2015, Muñoz-Cánoves and Serrano, 2015). This project provides first evidence that FAPs and macrophages interact in a bidirectional manner. Deletion of *Osr1* in FAPs might not have affected the infiltration of neutrophils and macrophages in the injured region, but it impaired their phenotypical M1-M2 switch, leading to an accumulation of pro-inflammatory M1 macrophages. The differences in

M1 and M2 distribution in the mutant could not be validated with immunostainings on tissue sections at 3 dpi. This might be explained by different techniques used. First, FACS sorting is a highly sensitive method scanning populations for more than one marker and second, the whole muscle single cell population was processed before FACS sorting whereas for tissue staining one plain section from the injured region was immunostained.

In muscle regeneration, macrophages are not the only immune cells that FAPs interact with. Infiltration of NK cells have also been demonstrated to be crucial for regenerative myogenesis through the secretion of IFNγ (Cheng et al., 2008, Panduro et al., 2018). Moreover, it was recently shown that NK cells do not target fibrotic cells but they restrain the aberrant expansion of neutrophils (Larouche et al., 2022). In myocarditis, NK cells hold an anti-inflammatory role by preventing a sustained inflammatory state (Ong et al., 2015). The increased TGFβ signaling in degenerative muscle inhibits thus the cytotoxicity of the NK cells (Ghiringhelli et al., 2005). Remarkably, the infiltration of NK cells was also shown to be defected in the injured mutant, an additional defect that potentially together with an TGFβ rich environment contributes in the impairment of the regenerative process. In order to elucidate whether there is a potential persistence of the neutrophils in the Osr1 cKO muscle or what is the long-term effect in the NK population pool, the FACS analysis should be performed also on later timepoints of regeneration.

The transition from an M1 to an M2 inflammatory response coincides with a transition from the early proliferative stage to the later differentiative stage of myogenesis (Tidball and Villalta, 2010). The defects in the polarization switch in the injured mutant might lead to higher levels of pro-inflammatory cytokines that promote myoblast proliferation and inhibit differentiation. Conversely, M2 macrophages contribution in stimulating myogenic differentiation and fusion (Arnold et al., 2007), may be prevented in the Osr1 cKO, explaining in part the smaller regenerating fibers of the mutant. Increased M1 polarization in the Osr1 cKO model could explain exacerbated FAP apoptosis which was discussed before. However, Osr1KO homeostatic FAPs exhibited increased apoptosis *in vitro* which indicates that this event is independent of FAPs-macrophages crosstalk. Nevertheless, at this point it is impossible to disentangle the contribution of deregulated macrophage polarization from other factors to the myogenesis defects in the Osr1 cKO mouse model. The fact though that myoblasts proliferation is defected in the mutants (in contrast to studies of increased M1 activation) and that myogenic

differentiation was linked to FAPs function *in vitro* (discussed further later), argues for a dominant role of defective direct FAPs-MuSCs crosstalk during the onset of regeneration.

In order to be able to distinguish between an impairment or a delay in the M1-M2 switch, a second timepoint (possibly at 7 dpi) should in the future be involved in the analysis. This experiment would add valuable information in the current knowledge of muscle regeneration, since an imbalance of M2 macrophages has been shown to trigger an M1 macrophage inflammatory response, leading to a constant cycle of degeneration and poor regeneration (Vidal et al., 2008a). These asynchronous waves of inflammation in dystrophies lead to an increased secretion of the latent form of TGFβ (LTBP4) which once cleaved enriches the environment in TGFβ concentrations. In these cases, the accumulated macrophages do not act anymore to repair myofiber damage but to induce fibrosis (Juban et al., 2018, Nitahara-Kasahara et al., 2014).

Pathway analysis using all the DE genes from the transcriptome data at 3 and at 7 dpi revealed that the TNFa pathway was deregulated in Osr1 cKO FAPs. Most of the genes belonging to this term were found to be downregulated in the mutants. Considering the fact that there were more M1 macrophages in the Osr1 cKO, this would mean that the regenerative milieu is richer in TNFa, since this is the main molecule secreted by M1 macrophages to limit FAPs expansion. However, increased FAPs apoptosis was preserved after *in vitro* recombination, thus increased apoptosis of FAPs must be independent of M1 macrophage presence and TNFa. This suggests that *Osr1* deficient FAPs may either have a defect in their response to TNFa signaling or that they enter senescence in order to protect themselves from apoptosis. Hypothetically, this might in turn explain their persistence during later phases of regeneration, which in the end causes increased ECM deposition. Nevertheless, this merits further experimental testing, possibly in an *in vitro* system where the response of either fresh isolated injured or *in vitro* recombined $Osr1^{KO}$ FAPs would be monitored upon TNFa treatment.

Data from this project suggest that one of the main roles of $Osr1^{+}$ FAPs expansion upon injury is the secretion of cytokines to stimulate the inflammatory response (Oprescu et al., 2020). Remarkably, the $Osr1^{+}$ FAPs cluster vanished in the Osr1 cKO dataset at 7 dpi. That indicates the absence not only of signaling factors but also of genes encoding for proteins of basal lamina (e.g. Col4, Col6, Col15, Nid1) from the

regenerative environment of the Osr1 cKO injured muscle. The signaling potential of FAPs was also validated *in vitro* in co-culture experiments with macrophages. Upon co-culture with *Osr1* deficient FAPs and absence of exogenous polarization stimuli, transcript levels of *Ccl2* and *Ccl3* in the macrophages were reduced. These cytokines are essential for the initiation of the inflammatory response and for macrophage polarization (Xiao et al., 2016). Nevertheless, this assay would need to be repeated by a simultaneous polarization stimulation of the macrophage culture in order to validate whether *Osr1* expression has the potential to either push the phenotypical change towards one side or the other. In sum, these experiments suggest that FAPs are in principal immunomodulatory cells that are responsible of secreting a large number of factors. In their majority these molecules do not affect macrophage polarization but act to stimulate their inflammatory status and are essential to efficient regeneration.

5.6 *Osr1* controls the FAP-mediated pro-myogenic niche

5.6.1 Dystrophic identity of Osr1 cKO FAPs

In muscle regeneration FAPs are responsible for shaping the microenvironment, producing a transient ECM (Scott et al., 2019) and supporting MuSCs differentiation and self-renewal (Mozzetta et al., 2013, Heredia et al., 2013), although MuSCs still contribute to shaping their own niche in the injured region (Bröhl et al., 2012, Urciuolo et al., 2013, Bentzinger et al., 2013b). The last years single cell transcriptome analyses have unraveled ECM components that are secreted specifically by FAPs e.g. Sfrp4 and Fbn1 (De Micheli et al., 2020b), Col.4/6/15 (Scott et al., 2019), Col.1a1 and Col.6a3 (Farup et al., 2020). In total, FAPs set orchestrated guidelines set for the composition of the basal membrane and the ECM, which are crucial for efficient muscle regeneration.

Osr1$^+$ developmental FAP-like cells were shown to shape a pro-myogenic niche and transcriptome analysis showed regulation of many ECM related genes in the Osr1 mutants (Vallecillo-Garcia et al., 2017). Similar to their developmental progenitors, transcriptome analysis of the adult Osr1 cKO FAPs revealed an upregulation of genes that encode major proteins of the ECM (e.g. *Col5a1, Col11a1, Col12a1, Tnc, Postn*). A comparative analysis between the upregulated DE genes at 3 and 7 dpi highlighted

a persistence of this defect since GO terms related to the ECM were commonly significantly upregulated. Remarkably, at 7 dpi genes related to ECM proteins of the basal lamina were downregulated in the mutant FAPs. In muscular dystrophies the inadequacy in MuSCs proliferation has been partially attributed to alterations in the constitution of the basal lamina (Ross et al., 2012). Amongst the downregulated basal lamina genes were: i) *Col15a1*, whose deficiency has been linked to skeletal myopathies (Eklund et al., 2001), and ii) *Lama2*, whose absence is defective in one of the most severe neuromuscular diseases, the LAMA2 related congenital muscular dystrophy (Barraza-Flores et al., 2020) and Duchenne muscular dystrophy (Sarkozy et al., 2020). Moreover, *Col6* genes were also found to be downregulated in the mutants. It has been shown that Col.6 secreted by FAPs in muscle regeneration is specifically essential for regulating MuSCs quiescence (Urciuolo et al., 2013).

In addition, Osr1 cKO FAPs were found to regulate genes in common with FAPs from uninjured mdx mice. Interestingly, GO analysis for these genes highlighted the upregulation of the term „collagen containing extracellular matrix" with the majority of common genes being upregulated. Intriguingly, several of the ECM-related genes upregulated at 7 dpi mutants have been reported to be components of a pro-inflammatory fibrotic environment. For instance, fibromodulin (*Fmod*) is expressed by cardiac fibroblasts in heart failure (Andenæs et al., 2018, Pourhanifeh et al., 2019), while angiopoietin-like 4 (*Angptl4*) is upregulated in the bone marrow under inflammatory conditions (Schumacher et al., 2015). Furthermore, overexpression of angiopoietin-like 2 (*Angptl2*) has been linked to chronic inflammation and to acceleration of muscular dystrophy (Kadomatsu et al., 2014, Zhao et al., 2018). Finally, secreted frizzled-related protein 1 (*Sfrp1*) has been shown in a muscular dystrophy model to inhibit myogenic differentiation both *in vivo* and *in vitro* (Descamps et al., 2008, Sohn et al., 2015).

Conclusively, these data represented the primary evidence for a skewed differentiation potential of Osr1 cKO FAPs that leads to reshaping an unbeneficial ECM, having the hallmarks of a dystrophic environment.

5.6.2 ECM remodeling in the Osr1 cKO inhibits myogenesis

In pathological and in chronic conditions, FAPs are over-activated, expand uncontrollably and remain in high numbers differentiating towards several MSC lineages based on the type and the severity of the damage. In normal conditions, a significant number of activated fibroblasts and myofibroblasts derive from the PDGFRa^{+} FAPs upon injury or can also be generated *in vitro* via the FAPs stimulation with profibrotic cytokines (e.g. TGFβ) (Contreras et al., 2019a, Contreras et al., 2019b, Theret et al., 2021). Therefore, the combination of defects in ECM composition together with the impact on the regenerative potential of the mutants, lead to further investigations of the Osr1 cKO FAPs differentiation potential.

Function of FAPs was impaired on several levels in the Osr1 cKO animals. *In vitro* differentiation assays showed a strongly reduced adipogenic differentiational potential of Osr1^{KO} FAPs, while the fibrogenic differentiation was strongly favored. Although, in the both developmental and adult Osr1^{KO} FAPs transcriptome data *Col.6* genes were downregulated, *in vitro* experiments showed a higher area of Col.6 secretion around the differentiated mutant cells. This can be explained by the fact that since Osr1KO FAPs mainly differentiate into fibroblasts, more cells will express *Col.6* and thus a bigger area will be stained for its protein. Reduction of FAPs adipogenesis through the TGFβ pathway has also been described *in vitro* upon treatment of FAPs with CM from M1 polarized macrophages. On the other hand CM from M2 macrophages enhanced FAPs adipogenic potential (Moratal et al., 2018). The higher percentage of M1 macrophages accumulating in the mutant regenerative niche together with the *in vitro* defected adipogenic potential of Osr1KO FAPs, might as well account for the increased fibrosis observed in the Osr1 cKO model. Alterations in the differentiation program of FAPs will subsequently also lead to differences in the composition of the secreted ECM. The structure of the secreted ECM from Osr1 KO FAP-like embryonic cells had already been shown in the past to inhibit myogenic cell proliferation in an *in vitro* dECM deposition system. In this project, dECM matrices were produced following a different decellularization protocol (detergent based) in order to further preserve the key ECM proteins and mechanical proteins and in order to remove the majority of cellular debris (Xing et al., 2015). Interestingly, as a result of the defects in the differentiation potential of Osr1 cKO FAPs, the generated Osr1 cKO dECM scaffold inhibited initial cell spreading and myogenic fusion of C2C12 cultured cells.

Muscle`s regenerative potential declines by aging. Increased fibrosis, impaired myogenic fusion and low-grade chronic inflammation lead to insufficient healing outcome (Brack and Rando, 2008, Etienne et al., 2020, Rahman et al., 2020). In the last years, studies have demonstrated that aged FAPs exhibit a primed fibrogenic fate as well as reduced proliferative capacity and adipogenic potential (Mueller et al., 2016, Lukjanenko et al., 2019). Similar to the Osr1 cKO FAPs, it has been also reported that the secretion of the ECM is deregulated in aged FAPs. Constant ECM deposition during aging interferes with MuSCs essential functions, impairing thus muscle regeneration (Lukjanenko et al., 2019). Therefore, the results of this study show that loss of *Osr1* expression in FAPs has the potential to alter FAPs core functions in a similar way that aging does.

The latest single cell studies have pointed towards a stratification of FAPs into subpopulations, which coexist during regeneration or are timely controlled cellular states (De Micheli et al., 2020b, Scott et al., 2019, Oprescu et al., 2020, Giordani et al., 2019). FAPs have been reported to be closely related to tendon progenitors assisting the regeneration of the myotendinous junction (Scott et al., 2019) but also to contribute to heterotopic lesions formation by giving rise to osteogenic cells in a BMP2 rich environment (Eisner et al., 2020). Remarkably, analysis of the transcriptome data revealed that *Osr1* deficiency leads to a skewed FAP phenotype with a shift to a more tendon/cartilage like profile, in line with the observations made in the *Osr1* deficient FAP-like cells in muscle development (Vallecillo-Garcia et al., 2017). Interestingly, amongst these genes is *Col11a1*, which is mainly expressed by tenocytes during muscle regeneration, as well as *Col24a1*, a protein that regulates osteoblastic differentiation and is part of the mineralized bone ECM (Matsuo et al., 2008, Wang et al., 2012). Lastly, deconvolution analysis of the FAPs transcriptome also confirmed an increased tendency of the Osr1 cKO FAPs to regulate genes related to the tenogenic clusters identified by single cell profiling (Oprescu et al., 2020). In summary, these data suggest that Osr1: i) acts as a gatekeeper of FAPs trans-differentiation by regulating gene expression related to several FAPs subtypes and ii) prevents FAPs from retaining detrimental fibroblastic states, such as the tenogenic one, which secrete a deleterious for myogenesis matrix.

5.7 Crosstalk of Osr1 cKO FAPs and myoblasts

In muscle regeneration the formation of new muscle tissue is carefully assisted by the shaping of the regenerative ECM. Accordingly, FAPs reside always close to myofibers and upon injury are one of the most important mediators for inducing MuSCs activation and proliferation (Joe et al., 2010, Uezumi et al., 2010). Therefore, the crosstalk of FAPs and MuSCs has been in the center of muscle regenerative therapies in the last years. *In vivo*, reduction or depletion in the FAPs population has always been accompanied by a similar effect on MuSCs pool (Petrilli et al., 2020, Uezumi et al., 2021, Wosczyna et al., 2019). *In vitro*, direct co-culture experiments of these two populations have demonstrated that FAPs induce MuSCs exit of quiescence and differentiation, indicating that ECM and paracrine signaling of FAPs are beneficial for myogenesis (Joe et al., 2010, Uezumi et al., 2021).

This project highlighted the FAPs-derived ECM as one of the components of the milieu that participates in efficient myogenesis. In order to disentangle the effect of FAPs paracrine signaling from the effect of the deposited ECM on MuSCs function, indirect transwell co-culture experiments have showed that secreted factors from TCF7L2^{+} cells induce myogenic fusion as well as slow myosin heavy chain expression (Mathew et al., 2011). In a similar experimental setup, Osr1^{+} FAP like cells in muscle development have been demonstrated to stronger support MuSCs differentiation in comparison to when these were cultured with Osr1 KO cells (Vallecillo-Garcia et al., 2017). Therefore, in this project a same experimental approach was followed to further characterize Osr1^{+} FAPs-myoblasts interaction. Remarkably, isolated FAPs in alert state from injured Osr1 cKO individuals secrete signaling molecules that inhibit myogenic fusion in contrast to control FAPs. This effect was validated in two different set ups: i) in an indirect co-culture transwell assay ii) generation of FAPs CM and its appliance on cultured myoblasts. The inhibitory effect of the Osr1 cKO FAPs secretome was shown to be concentration-dependent, since the CM (higher concentration in signaling factors than co-culture in transwell with FAPs) reduced myogenic fusion two times stronger than the FAPs in the transwell assay. At this point is worth mentioning that CM from myoblastic cells has also been demonstrated to promote FAPs proliferation (Vumbaca et al., 2021) while CM from mature myotubes favored the fibrogenic over the adipogenic FAPs differentiation (Moratal et al., 2019).

Fibrosis is a frequent feature of muscular dystrophies and is associated, amongst other signaling mechanisms, with increased TGFβ signaling (Hogarth et al., 2021, Smith and Barton, 2018, Accorsi et al., 2020, Ismaeel et al., 2019). Intriguingly, intramuscular TGFβ injection concomitant to injury resulted in accumulation of a fibrotic ECM comparable to the one reported in the Osr1 cKO model (Pessina et al., 2014). In regenerating muscle, TGFβ is secreted mainly by the proinflammatory macrophages but also by FAPs, inducing their fibrogenic differentiation and ECM secretion (Theret et al., 2021). In line with their *in vitro* favored fibrogenic differentiation and *in vivo* fate switch to a teno/chondrogenic fate, several upregulated ECM genes are direct targets of TGFβ signaling and usually are found to be upregulated in muscular dystrophies (e.g. *Scx, Tgfβi, Col.7a1, Timp1*) (Mendias et al., 2012, Vindevoghel et al., 1998, Bensalah et al., 2022). In addition, gene pathway analysis revealed that the TGFβ pathway is regulated at both 3 and 7 dpi in Osr1 cKO FAPs (upregulation of *Tgfβ1* and *Tgfβ2*) and more specifically it was the first term to emerge when only the 3 dpi upregulated DE genes were used. Interestingly, *Tgfβ1* expression was increased in Osr1KO FAPs *in vitro* even in the absence of injury. Thus, all the aforementioned events indicate an increased TGFβ signaling in the microenvironment of the Osr1 cKO muscle promoting fibrosis.

One of the first roles assigned to TGFβ was its anti-myogenic effect on differentiating myoblasts (Florini and Magri, 1989) and since then many studies have focused on that function . Exacerbated TGFβ signaling has been observed in muscular dystrophies and in regenerating muscle (Girardi et al., 2021, Krueger and Hoffmann, 2010, Watt et al., 2010, Theret et al., 2022). However, it was only until recently that the mechanism of this inhibitory action was described. Girardi and colleagues demonstrated that TGFβ reduces cell spreading by controlling actin related genes, limiting thus myoblast fusion and myofiber size (Girardi et al., 2021). Remarkably, the myogenesis-inhibiting effect of Osr1 cKO FAPs could be counteracted once the TGFβ signaling was blocked. Hindering the function of the TGFβ receptor type I resulted in a two-times higher increase in the myogenic fusion when Osr1 cKO CM was used in comparison to the control. This finding strengthens the suggestion that CM from Osr1 cKO contains higher concentrations of TGFβ molecules. Nevertheless, additional experiments are needed to validate whether FAPs secrete protease enzymes that release the latent form of TGFβ bound in the collagenous matrix or if active TGFβ itself is produced by Osr1 cKO FAPs. Moreover, pSmad3 immunofluorescence stainings on myoblasts

treated with Osr1 cKO CM could serve as an additional proof of the TGFβ pathway activation.

In sum, Osr1 cKO secrete signaling factors that act as inhibitors for myogenic fusion, such as TGFβ. Increased TGFβ signaling in the mutant microenvironment may not only impair myogenesis during regeneration but also enhance the fibrogenic differentiation of FAPs in an autocrine manner, contributing thus to persistent fibrosis.

6 Summary

Osr1$^+$ FAPs orchestrate efficient muscle regeneration

1. Upon skeletal muscle injury Osr1$^+$ FAPs start to proliferate in the injured area fostering regeneration through i) producing signaling molecules and ii) reshaping the ECM.

2. Osr1$^+$ FAPs at 3 dpi secrete cytokines involved in the M1-M2 macrophage polarization. At this point the presence of M1 and M2 macrophage in the regenerative milieu is balanced.

3. Osr1$^+$ FAPs induce myogenic fusion through their paracrine signaling.

4. Osr1$^+$ FAPs shape a regenerative ECM which also fosters myogenic fusion.

5. Efficient regeneration is thus achieved; mature large muscle fibers have replaced the injured area and fibrotic tissue is slowly resolved.

6. Deletion of *Osr1* prior to injury dysregulate genes in FAPs related to ECM and inflammatory response.

7. Osr1 cKO fail to initially proliferate and expand, while MuSCs exhibit a similar defect.

8. Downregulation of chemokines in the Osr1 cKO FAPs result in a higher distribution of macrophages in the M1 than in the M2 state, tilting the balance towards a strong pro-inflammatory status.

9. Paracrine signaling of Osr1 cKO FAPs inhibits myogenic fusion, amongst others also via the upregulation of the TGFβ pathway.

10. Excessive fibrosis and differentiation defects in *Osr1* deficient FAPs assist the production of an unbeneficial ECM which hinders myogenesis.

11. Therefore, the Osr1 cKO regenerative potential is defected, exhibiting hallmarks of myopathies and dystrophy such as smaller regenerating fibers and excessive fibrosis.

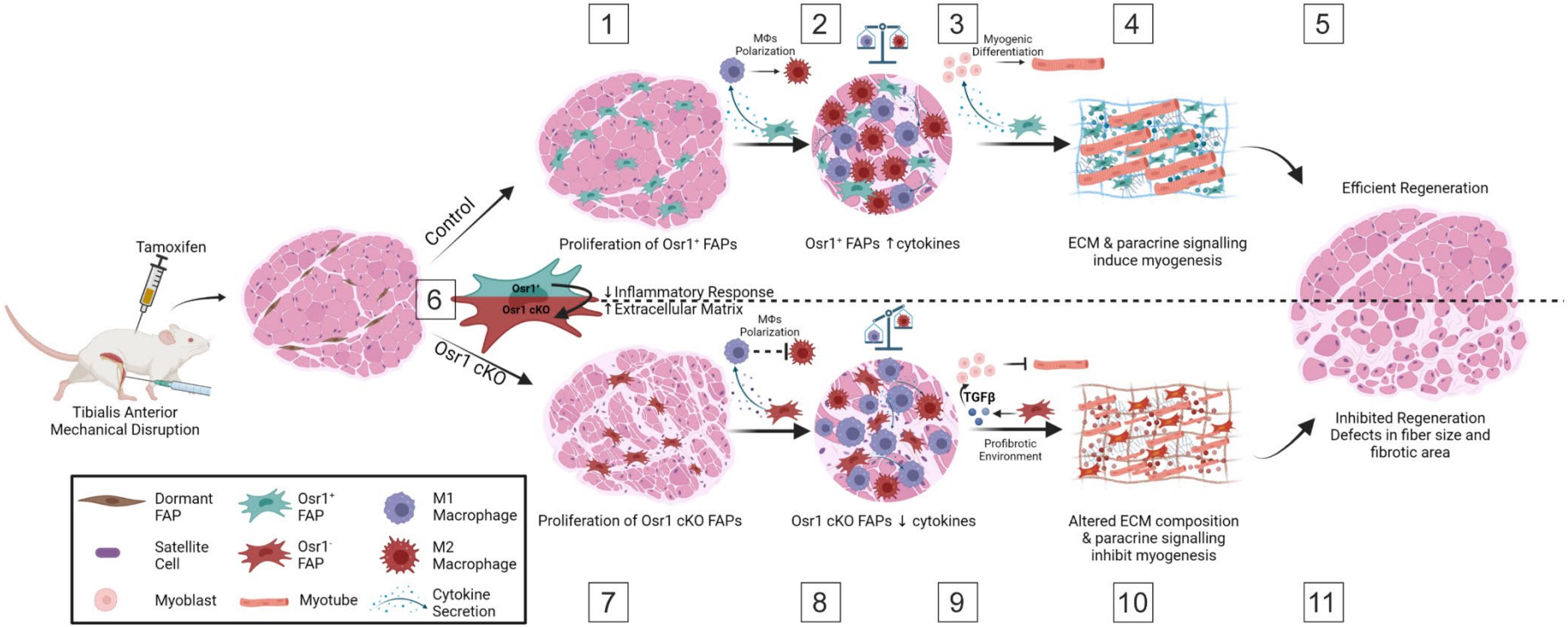

Image created with BioRender.com.

7 Future Perspectives

In continuation of the two studies that highlighted the recapitulation of a FAP developmental program by expressing *Osr1* upon injury, this project elucidated the functions of Osr1$^+$ FAPs in muscle regeneration. Analysis of the regenerative potential in several timepoints and investigating the defects in several populations of the milieu offered new insights in the FAP-macrophage-MuSCs network. These data would contribute in further understanding the complexity of FAPs interactions in the injured muscle as well as the control of FAPs differentiation potential by *Osr1* expression.

Single cell RNA seq analysis at different timepoints of regeneration would decipher how loss of *Osr1* interferes with the cellular dynamics in skeletal muscle regeneration. Defects in the distribution of every cell population as well as possible interactions between them would be a valuable lesson from this approach. Moreover, investigation of the *Osr1* transcriptional regulator complex would also be of extreme interest. What is downstream/ upstream of *Osr1*, can we model the 3D architecture of the *Osr1* locus, which are the involved enhancer communities? These are all questions that if answered would shed light on how Osr1 regulates FAPs functions and differentiation.

The regenerative potential of muscle declines with age and in several myopathies. A combination of several events leads to reduced muscle mass, increased atrophy, tissue frailty but also to induced fibrogenic differentiation of FAPs. In aged muscles (also in aged mdx muscles), FAPs exhibit also defects in their proliferation and reduced adipogenic potential. How is though *Osr1* regulated in these conditions? The potential repressed expression of *Osr1* in FAPs or the failure of injured FAPs to reactivate *Osr1* under these conditions needs to be further studied. The impaired regenerative potential of Osr1 cKO muscles suggest that secreted molecules by Osr1$^+$ FAPs might serve as plausible therapeutics in order to boost the endogenous regenerative capacity of muscles.

Despite the central role of myogenesis and therefore of MuSCs in regenerative studies, identifying FAPs physiology would lead to significant medical advances. Permanent scar formation in all the tissues affect the functionality and in chronic cases might even lead to organ failure. FAPs heterogeneity and their function needs to be better described in cases of chronic damage, in cachexia, in regeneration, in aging induced sarcopenia. Moreover, the role of FAPs in neuromuscular diseases as well as the

interaction between FAPs-nerve cells and how it affects tissue integrity needs also to be further investigated. Conclusively, cell-based therapies and pharmacological treatments targeting FAPs or FAPs subpopulations could serve as key therapeutic approach to slow or to prevent fibrofatty infiltration and muscle degeneration.

8 References

ACCORSI, A., CRAMER, M. L. & GIRGENRATH, M. 2020. Fibrogenesis in LAMA2-Related Muscular Dystrophy Is a Central Tenet of Disease Etiology. *Frontiers in Molecular Neuroscience,* 13.

ANDENÆS, K., LUNDE, I. G., MOHAMMADZADEH, N., DAHL, C. P., ARONSEN, J. M., STRAND, M. E., PALMERO, S., SJAASTAD, I., CHRISTENSEN, G., ENGEBRETSEN, K. V. T. & TØNNESSEN, T. 2018. The extracellular matrix proteoglycan fibromodulin is upregulated in clinical and experimental heart failure and affects cardiac remodeling. *PLOS ONE,* 13**,** e0201422.

ARNOLD, L., HENRY, A., PORON, F., BABA-AMER, Y., VAN ROOIJEN, N., PLONQUET, A., GHERARDI, R. K. & CHAZAUD, B. 2007. Inflammatory monocytes recruited after skeletal muscle injury switch into antiinflammatory macrophages to support myogenesis. *J Exp Med,* 204**,** 1057-69.

BARRAZA-FLORES, P., BATES, C. R., OLIVEIRA-SANTOS, A. & BURKIN, D. J. 2020. Laminin and Integrin in LAMA2-Related Congenital Muscular Dystrophy: From Disease to Therapeutics. *Frontiers in molecular neuroscience,* 13**,** 1-1.

BENSALAH, M., MURAINE, L., BOULINGUIEZ, A., GIORDANI, L., ALBERT, V., YTHIER, V., DHIAB, J., OLIVER, A., HANIQUE, V., GIDARO, T., PERIÉ, S., LACAU ST-GUILY, J., CORNEAU, A., BUTLER-BROWNE, G., BIGOT, A., MOULY, V., NEGRONI, E. & TROLLET, C. 2022. A negative feedback loop between fibroadipogenic progenitors and muscle fibres involving endothelin promotes human muscle fibrosis. *Journal of Cachexia, Sarcopenia and Muscle,* n/a.

BENTZINGER, C. F., WANG, Y. X., DUMONT, N. A. & RUDNICKI, M. A. 2013a. Cellular dynamics in the muscle satellite cell niche. *EMBO reports,* 14**,** 1062-1072.

BENTZINGER, C. F., WANG, Y. X., VON MALTZAHN, J., SOLEIMANI, V. D., YIN, H. & RUDNICKI, M. A. 2013b. Fibronectin regulates Wnt7a signaling and satellite cell expansion. *Cell stem cell,* 12**,** 75-87.

BERNASCONI, P., DI BLASI, C., MORA, M., MORANDI, L., GALBIATI, S., CONFALONIERI, P., CORNELIO, F. & MANTEGAZZA, R. 1999. Transforming growth factor-β1 and fibrosis in congenital muscular dystrophies. *Neuromuscular Disorders,* 9**,** 28-33.

BILTZ, N. K., COLLINS, K. H., SHEN, K. C., SCHWARTZ, K., HARRIS, C. A. & MEYER, G. A. 2020. Infiltration of intramuscular adipose tissue impairs skeletal muscle contraction. *The Journal of Physiology,* 598**,** 2669-2683.

BIRESSI, S. & RANDO, T. A. 2010. Heterogeneity in the muscle satellite cell population. *Seminars in Cell & Developmental Biology,* 21**,** 845-854.

BLANC, R. S., KALLENBACH, J. G., BACHMAN, J. F., MITCHELL, A., PARIS, N. D. & CHAKKALAKAL, J. V. 2020. Inhibition of inflammatory CCR2 signaling promotes aged muscle regeneration and strength recovery after injury. *Nature Communications,* 11.

BOONEN, K. J., ROSARIA-CHAK, K. Y., BAAIJENS, F. P., VAN DER SCHAFT, D. W. & POST, M. J. 2009. Essential environmental cues from the satellite cell niche: optimizing proliferation and differentiation. *Am J Physiol Cell Physiol,* 296**,** C1338-45.

References

BRACK, A. S., CONBOY, I. M., CONBOY, M. J., SHEN, J. & RANDO, T. A. 2008. A temporal switch from notch to Wnt signaling in muscle stem cells is necessary for normal adult myogenesis. *Cell stem cell,* 2**,** 50-59.

BRACK, A. S., CONBOY, M. J., ROY, S., LEE, M., KUO, C. J., KELLER, C. & RANDO, T. A. 2007. Increased Wnt signaling during aging alters muscle stem cell fate and increases fibrosis. *Science,* 317**,** 807-10.

BRACK, A. S. & RANDO, T. A. 2008. Age-dependent changes in skeletal muscleregeneration. *Skeletal Muscle Repair and Regeneration.* Springer.

BRASHEAR, S. E., WOHLGEMUTH, R. P., GONZALEZ, G. & SMITH, L. R. 2021. Passive stiffness of fibrotic skeletal muscle in mdx mice relates to collagen architecture. *The Journal of Physiology,* 599**,** 943-962.

BRÖHL, D., VASYUTINA, E., MACIEJ, GRIGER, J., RASSEK, C., RAHN, H.-P., PURFÜRST, B., WENDE, H. & BIRCHMEIER, C. 2012. Colonization of the Satellite Cell Niche by Skeletal Muscle Progenitor Cells Depends on Notch Signals. *Developmental Cell,* 23**,** 469-481.

BUCHER, C. H., SCHLUNDT, C., WULSTEN, D., SASS, F. A., WENDLER, S., ELLINGHAUS, A., THIELE, T., SEEMANN, R., WILLIE, B. M., VOLK, H.-D., DUDA, G. N. & SCHMIDT-BLEEK, K. 2019. Experience in the Adaptive Immunity Impacts Bone Homeostasis, Remodeling, and Healing. *Frontiers in Immunology,* 10.

BUTTERFIELD, T. A., BEST, T. M. & MERRICK, M. A. 2006. The dual roles of neutrophils and macrophages in inflammation: a critical balance between tissue damage and repair. *Journal of athletic training,* 41**,** 457.

CALVO, B., RAMÍREZ, A., ALONSO, A., GRASA, J., SOTERAS, F., OSTA, R. & MUÑOZ, M. 2010. Passive nonlinear elastic behaviour of skeletal muscle: experimental results and model formulation. *Journal of biomechanics,* 43**,** 318-325.

CAMPS, J., BREULS, N., SIFRIM, A., GIARRATANA, N., CORVELYN, M., DANTI, L., GROSEMANS, H., VANUYTVEN, S., THIRY, I., BELICCHI, M., MEREGALLI, M., PLATKO, K., MACDONALD, M. E., AUSTIN, R. C., GIJSBERS, R., COSSU, G., TORRENTE, Y., VOET, T. & SAMPAOLESI, M. 2020. Interstitial Cell Remodeling Promotes Aberrant Adipogenesis in Dystrophic Muscles. *Cell Reports,* 31**,** 107597.

CARRIÓN, J. A., TORRES, F., CRESPO, G., MIQUEL, R., GARCÍA-VALDECASAS, J.-C., NAVASA, M. & FORNS, X. 2010. Liver stiffness identifies two different patterns of fibrosis progression in patients with hepatitis C virus recurrence after liver transplantation. *Hepatology,* 51**,** 23-34.

CAYROL, C. & GIRARD, J.-P. 2014. IL-33: an alarmin cytokine with crucial roles in innate immunity, inflammation and allergy. *Current Opinion in Immunology,* 31**,** 31-37.

CHAKKALAKAL, J. V., JONES, K. M., BASSON, M. A. & BRACK, A. S. 2012a. The aged niche disrupts muscle stem cell quiescence. *Nature,* 490**,** 355-360.

CHAKKALAKAL, J. V., JONES, K. M., BASSON, M. A. & BRACK, A. S. 2012b. The aged niche disrupts muscle stem cell quiescence. *Nature,* 490**,** 355-60.

CHAPMAN, M. A., MEZA, R. & LIEBER, R. L. 2016. Skeletal muscle fibroblasts in health and disease. *Differentiation,* 92**,** 108-115.

CHAPMAN, M. A., MUKUND, K., SUBRAMANIAM, S., BRENNER, D. & LIEBER, R. L. 2017. Three distinct cell populations express extracellular matrix proteins and increase in number during skeletal muscle fibrosis. *American Journal of Physiology-Cell Physiology,* 312**,** C131-C143.

CHAPMAN, M. A., PICHIKA, R. & LIEBER, R. L. 2015. Collagen crosslinking does not dictate stiffness in a transgenic mouse model of skeletal muscle fibrosis. *Journal of Biomechanics,* 48**,** 375-378.

CHAZAUD, B. 2020. Inflammation and Skeletal Muscle Regeneration: Leave It to the Macrophages! *Trends in Immunology,* 41**,** 481-492.

CHENG, M., NGUYEN, M.-H., FANTUZZI, G. & KOH, T. J. 2008. Endogenous interferon-γ is required for efficient skeletal muscle regeneration. *American Journal of Physiology-Cell Physiology,* 294**,** C1183-C1191.

CHURCH, J. 1970. Cell populations in skeletal muscle after regeneration.

CONSTANTIN, B. 2014. Dystrophin complex functions as a scaffold for signalling proteins. *Biochimica et Biophysica Acta (BBA) - Biomembranes,* 1838**,** 635-642.

CONTRERAS, O., CRUZ-SOCA, M., THERET, M., SOLIMAN, H., TUNG, L. W., GROPPA, E., ROSSI, F. M. & BRANDAN, E. 2019a. The cross-talk between TGF-β and PDGFRα signaling pathways regulates stromal fibro/adipogenic progenitors' fate. *Journal of Cell Science,* 132**,** jcs232157.

CONTRERAS, O., REBOLLEDO, D. L., OYARZÚN, J. E., OLGUÍN, H. C. & BRANDAN, E. 2016. Connective tissue cells expressing fibro/adipogenic progenitor markers increase under chronic damage: relevance in fibroblast-myofibroblast differentiation and skeletal muscle fibrosis. *Cell and Tissue Research,* 364**,** 647-660.

CONTRERAS, O., ROSSI, F. M. & BRANDAN, E. 2019b. Adherent muscle connective tissue fibroblasts are phenotypically and biochemically equivalent to stromal fibro/adipogenic progenitors. *Matrix Biology Plus,* 2.

CORNELISON, D., FILLA, M. S., STANLEY, H. M., RAPRAEGER, A. C. & OLWIN, B. B. 2001. Syndecan-3 and syndecan-4 specifically mark skeletal muscle satellite cells and are implicated in satellite cell maintenance and muscle regeneration. *Developmental biology,* 239**,** 79-94.

COSGROVE, B. D., GILBERT, P. M., PORPIGLIA, E., MOURKIOTI, F., LEE, S. P., CORBEL, S. Y., LLEWELLYN, M. E., DELP, S. L. & BLAU, H. M. 2014. Rejuvenation of the muscle stem cell population restores strength to injured aged muscles. *Nature Medicine,* 20**,** 255-264.

COSGROVE, B. D., SACCO, A., GILBERT, P. M. & BLAU, H. M. 2009. A home away from home: challenges and opportunities in engineering in vitro muscle satellite cell niches. *Differentiation,* 78**,** 185-194.

COULTER, D. E., SWAYKUS, E., BERAN-KOEHN, M., GOLDBERG, D., WIESCHAUS, E. & SCHEDL, P. 1990. Molecular analysis of odd-skipped, a zinc finger encoding segmentation gene with a novel pair-rule expression pattern. *The EMBO journal,* 9**,** 3795-3804.

COULTER, D. E. & WIESCHAUS, E. 1988. Gene activities and segmental patterning in Drosophila: analysis of odd-skipped and pair-rule double mutants. *Genes & Development,* 2**,** 1812-1823.

CSAPO, R., GUMPENBERGER, M. & WESSNER, B. 2020. Skeletal Muscle Extracellular Matrix – What Do We Know About Its Composition, Regulation, and Physiological Roles? A Narrative Review. *Frontiers in Physiology,* 11.

DADGAR, S., WANG, Z., JOHNSTON, H., KESARI, A., NAGARAJU, K., CHEN, Y.-W., HILL, D. A., PARTRIDGE, T. A., GIRI, M. & FREISHTAT, R. J. 2014. Asynchronous remodeling is a driver of failed regeneration in Duchenne muscular dystrophy. *Journal of Cell Biology,* 207**,** 139-158.

DE MICHELI, A. J., LAURILLIARD, E. J., HEINKE, C. L., RAVICHANDRAN, H., FRACZEK, P., SOUEID-BAUMGARTEN, S., DE VLAMINCK, I., ELEMENTO, O. & COSGROVE, B. D. 2020a. Single-Cell Analysis of the Muscle Stem Cell

Hierarchy Identifies Heterotypic Communication Signals Involved in Skeletal Muscle Regeneration. *Cell Reports,* 30**,** 3583-3595.e5.

DE MICHELI, A. J., SPECTOR, J. A., ELEMENTO, O. & COSGROVE, B. D. 2020b. A reference single-cell transcriptomic atlas of human skeletal muscle tissue reveals bifurcated muscle stem cell populations. *Skeletal Muscle,* 10**,** 19.

DEBEER, P., DE RAVEL, T., DEVRIENDT, K., FRYNS, J. P., HUYSMANS, C. & VAN DE VEN, W. 2002. Human homologues of Osr1 and Osr2 are not involved in a syndrome with distal limb deficiencies, oral abnormalities, and renal defects. *American journal of medical genetics,* 111**,** 455-456.

DELLAVALLE, A., MAROLI, G., COVARELLO, D., AZZONI, E., INNOCENZI, A., PERANI, L., ANTONINI, S., SAMBASIVAN, R., BRUNELLI, S. & TAJBAKHSH, S. 2011. Pericytes resident in postnatal skeletal muscle differentiate into muscle fibres and generate satellite cells. *Nature communications,* 2**,** 1-11.

DELLAVALLE, A., SAMPAOLESI, M., TONLORENZI, R., TAGLIAFICO, E., SACCHETTI, B., PERANI, L., INNOCENZI, A., GALVEZ, B. G., MESSINA, G. & MOROSETTI, R. 2007. Pericytes of human skeletal muscle are myogenic precursors distinct from satellite cells. *Nature cell biology,* 9**,** 255-267.

DENG, B., WEHLING-HENRICKS, M., VILLALTA, S. A., WANG, Y. & TIDBALL, J. G. 2012. IL-10 Triggers Changes in Macrophage Phenotype That Promote Muscle Growth and Regeneration. *The Journal of Immunology,* 189**,** 3669-3680.

DESCAMPS, S., ARZOUK, H., BACOU, F., BERNARDI, H., FEDON, Y., GAY, S., REYNE, Y., ROSSANO, B. & LEVIN, J. 2008. Inhibition of myoblast differentiation by Sfrp1 and Sfrp2. *Cell and Tissue Research,* 332**,** 299-306.

DEY, D., BAGAROVA, J., HATSELL, S. J., ARMSTRONG, K. A., HUANG, L., ERMANN, J., VONNER, A. J., SHEN, Y., MOHEDAS, A. H., LEE, A., EEKHOFF, E. M. W., SCHIE, A. V., DEMAY, M. B., KELLER, C., WAGERS, A. J., ECONOMIDES, A. N. & YU, P. B. 2016. Two tissue-resident progenitor lineages drive distinct phenotypes of heterotopic ossification. *Science Translational Medicine,* 8**,** 366ra163-366ra163.

DIMARIO, J. X. & STOCKDALE, F. E. 1995. Differences in the developmental fate of cultured and noncultured myoblasts when transplanted into embryonic limbs. *Exp Cell Res,* 216**,** 431-42.

DORAN, A. C., YURDAGUL, A. & TABAS, I. 2020. Efferocytosis in health and disease. *Nature Reviews Immunology,* 20**,** 254-267.

EISNER, C., CUMMINGS, M., JOHNSTON, G., TUNG, L. W., GROPPA, E., CHANG, C. & ROSSI, F. M. 2020. Murine Tissue-Resident PDGFRα+ Fibro-Adipogenic Progenitors Spontaneously Acquire Osteogenic Phenotype in an Altered Inflammatory Environment. *Journal of Bone and Mineral Research,* 35**,** 1525-1534.

EKLUND, L., PIUHOLA, J., KOMULAINEN, J., SORMUNEN, R., ONGVARRASOPONE, C., FASSLER, R., MUONA, A., ILVES, M., RUSKOAHO, H., TAKALA, T. E. S. & PIHLAJANIEMI, T. 2001. Lack of type XV collagen causes a skeletal myopathy and cardiovascular defects in mice. *Proceedings of the National Academy of Sciences,* 98**,** 1194-1199.

ELBAZ, M., YANAY, N., AGA-MIZRACHI, S., BRUNSCHWIG, Z., KASSIS, I., ETTINGER, K., BARAK, V. & NEVO, Y. 2012. Losartan, a therapeutic candidate in congenital muscular dystrophy: Studies in the dy2J/dy2J Mouse. *Annals of Neurology,* 71**,** 699-708.

ETIENNE, J., LIU, C., SKINNER, C. M., CONBOY, M. J. & CONBOY, I. M. 2020. Skeletal muscle as an experimental model of choice to study tissue aging and rejuvenation. *Skeletal Muscle,* 10**,** 4.

FADIC, R., MEZZANO, V., ALVAREZ, K., CABRERA, D., HOLMGREN, J. & BRANDAN, E. 2006. Increase in decorin and biglycan in Duchenne Muscular Dystrophy: role of fibroblasts as cell source of these proteoglycans in the disease. *Journal of Cellular and Molecular Medicine,* 10**,** 758-769.

FARMAKI, E., KAZA, V., CHATZISTAMOU, I. & KIARIS, H. 2020. CCL8 Promotes Postpartum Breast Cancer by Recruiting M2 Macrophages. *iScience,* 23**,** 101217.

FARUP, J., JUST, J., DE PAOLI, F., LIN, L., JENSEN, J. B., BILLESKOV, T., SANCHEZ ROMAN, I., CÖMERT, C., MØLLER, A. B., MADARO, L., GROPPA, E., FRED, R. G., KAMPMANN, U., PEDERSEN, S. B., BROSS, P., STEVNSNER, T., ELDRUP, N., PERS, T. H., ROSSI, F. M. V., PURI, P. L. & JESSEN, N. 2020. Human skeletal muscle CD90+ fibro-adipogenic progenitors are associated with muscle degeneration in type 2 diabetic patients. Cold Spring Harbor Laboratory.

FIORE, D., JUDSON, R. N., LOW, M., LEE, S., ZHANG, E., HOPKINS, C., XU, P., LENZI, A., ROSSI, F. M. V. & LEMOS, D. R. 2016. Pharmacological blockage of fibro/adipogenic progenitor expansion and suppression of regenerative fibrogenesis is associated with impaired skeletal muscle regeneration. *Stem Cell Research,* 17**,** 161-169.

FLORINI, J. R. & MAGRI, K. A. 1989. Effects of growth factors on myogenic differentiation. *American Journal of Physiology-Cell Physiology,* 256**,** C701-C711.

FOLKER, E. & BAYLIES, M. 2013. Nuclear positioning in muscle development and disease. *Frontiers in Physiology,* 4.

FRONTERA, W. R. & OCHALA, J. 2015. Skeletal Muscle: A Brief Review of Structure and Function. *Calcified Tissue International,* 96**,** 183-195.

FRY, C. S., KIRBY, T. J., KOSMAC, K., MCCARTHY, J. J. & PETERSON, C. A. 2017. Myogenic Progenitor Cells Control Extracellular Matrix Production by Fibroblasts during Skeletal Muscle Hypertrophy. *Cell Stem Cell,* 20**,** 56-69.

FRY, C. S., LEE, J. D., MULA, J., KIRBY, T. J., JACKSON, J. R., LIU, F., YANG, L., MENDIAS, C. L., DUPONT-VERSTEEGDEN, E. E., MCCARTHY, J. J. & PETERSON, C. A. 2015. Inducible depletion of satellite cells in adult, sedentary mice impairs muscle regenerative capacity without affecting sarcopenia. *Nature Medicine,* 21**,** 76-80.

GARRIDO-RODRÍGUEZ, V., HERRERO-FERNÁNDEZ, I., CASTRO, M. J., CASTILLO, A., ROSADO-SÁNCHEZ, I., GALVÁ, M. I., RAMOS, R., OLIVAS-MARTÍNEZ, I., BULNES-RAMOS, Á., CAÑIZARES, J., LEAL, M. & PACHECO, Y. M. 2021. Immunological features beyond CD4/CD8 ratio values in older individuals. *Aging,* 13**,** 13443-13459.

GATTAZZO, F., URCIUOLO, A. & BONALDO, P. 2014. Extracellular matrix: a dynamic microenvironment for stem cell niche. *Biochim Biophys Acta,* 1840**,** 2506-19.

GEORGES, P. C., HUI, J.-J., GOMBOS, Z., MCCORMICK, M. E., WANG, A. Y., UEMURA, M., MICK, R., JANMEY, P. A., FURTH, E. E. & WELLS, R. G. 2007. Increased stiffness of the rat liver precedes matrix deposition: implications for fibrosis. *American Journal of Physiology-Gastrointestinal and Liver Physiology,* 293**,** G1147-G1154.

GHIRINGHELLI, F., MÉNARD, C., TERME, M., FLAMENT, C., TAIEB, J., CHAPUT, N., PUIG, P. E., NOVAULT, S., ESCUDIER, B. & VIVIER, E. 2005. CD4+ CD25+ regulatory T cells inhibit natural killer cell functions in a transforming growth factor–β–dependent manner. *The Journal of experimental medicine,* 202**,** 1075-1085.

References

GILBERT, P. M., HAVENSTRITE, K. L., MAGNUSSON, K. E., SACCO, A., LEONARDI, N. A., KRAFT, P., NGUYEN, N. K., THRUN, S., LUTOLF, M. P. & BLAU, H. M. 2010. Substrate elasticity regulates skeletal muscle stem cell self-renewal in culture. *Science,* 329**,** 1078-81.

GILDA, J. E., KO, J.-H., ELFASSY, A.-Y., TROPP, N., PARNIS, A., AYALON, B., JHE, W. & COHEN, S. 2021. A semiautomated measurement of muscle fiber size using the Imaris software. *American Journal of Physiology-Cell Physiology,* 321**,** C615-C631.

GILLIES, A. R. & LIEBER, R. L. 2011. Structure and function of the skeletal muscle extracellular matrix. *Muscle & Nerve,* 44**,** 318-331.

GIORDANI, L., HE, G. J., NEGRONI, E., SAKAI, H., LAW, J. Y. C., SIU, M. M., WAN, R., CORNEAU, A., TAJBAKHSH, S., CHEUNG, T. H. & LE GRAND, F. 2019. High-Dimensional Single-Cell Cartography Reveals Novel Skeletal Muscle-Resident Cell Populations. *Molecular Cell,* 74**,** 609-621.e6.

GIRARDI, F., TALEB, A., EBRAHIMI, M., DATYE, A., GAMAGE, D. G., PECCATE, C., GIORDANI, L., MILLAY, D. P., GILBERT, P. M., CADOT, B. & LE GRAND, F. 2021. TGFbeta signaling curbs cell fusion and muscle regeneration. *Nat Commun,* 12**,** 750.

GIULIANI, G., ROSINA, M. & REGGIO, A. 2021a. Signaling pathways regulating the fate of fibro/adipogenic progenitors (FAPs) in skeletal muscle regeneration and disease. *The FEBS Journal*.

GIULIANI, G., VUMBACA, S., FUOCO, C., GARGIOLI, C., GIORDA, E., MASSACCI, G., PALMA, A., REGGIO, A., RICCIO, F., ROSINA, M., VINCI, M., CASTAGNOLI, L. & CESARENI, G. 2021b. SCA-1 micro-heterogeneity in the fate decision of dystrophic fibro/adipogenic progenitors. *Cell Death & Disease,* 12.

GLASS, G. E., CHAN, J. K., FREIDIN, A., FELDMANN, M., HORWOOD, N. J. & NANCHAHAL, J. 2011. TNF-a promotes fracture repair by augmenting the recruitment and differentiation of muscle-derived stromal cells. *Proceedings of the National Academy of Sciences,* 108**,** 1585-1590.

GOLDSTEIN, R. E., COOK, O., DINUR, T., PISANTÉ, A., KARANDIKAR, U. C., BIDWAI, A. & PAROUSH, Z. E. 2005. An eh1-like motif in odd-skipped mediates recruitment of Groucho and repression in vivo. *Molecular and cellular biology,* 25**,** 10711-10720.

GOSSELIN, L. E., WILLIAMS, J. E., DEERING, M., BRAZEAU, D., KOURY, S. & MARTINEZ, D. A. 2004. Localization and early time course of TGF-β1 mRNA expression in dystrophic muscle. *Muscle & Nerve: Official Journal of the American Association of Electrodiagnostic Medicine,* 30**,** 645-653.

GREFTE, S., VULLINGHS, S., KUIJPERS-JAGTMAN, A., TORENSMA, R. & VON DEN HOFF, J. 2012. Matrigel, but not collagen I, maintains the differentiation capacity of muscle derived cells in vitro. *Biomedical materials,* 7**,** 055004.

GROS, J., MANCEAU, M., THOMÉ, V. & MARCELLE, C. 2005. A common somitic origin for embryonic muscle progenitors and satellite cells. *Nature,* 435**,** 954-958.

GUIMARÃES, C. F., GASPERINI, L., MARQUES, A. P. & REIS, R. L. 2020. The stiffness of living tissues and its implications for tissue engineering. *Nature Reviews Materials,* 5**,** 351-370.

HAMILTON, T. G., KLINGHOFFER, R. A., CORRIN, P. D. & SORIANO, P. 2003. Evolutionary Divergence of Platelet-Derived Growth Factor Alpha Receptor Signaling Mechanisms. *Molecular and Cellular Biology,* 23**,** 4013-4025.

HASSON, P., DELAURIER, A., BENNETT, M., GRIGORIEVA, E., NAICHE, L. A., PAPAIOANNOU, V. E., MOHUN, T. J. & LOGAN, M. P. O. 2010. Tbx4 and Tbx5 Acting in Connective Tissue Are Required for Limb Muscle and Tendon Patterning. *Developmental Cell,* 18**,** 148-156.

HAYASHI, S. & MCMAHON, A. P. 2002. Efficient Recombination in Diverse Tissues by a Tamoxifen-Inducible Form of Cre: A Tool for Temporally Regulated Gene Activation/Inactivation in the Mouse. *Developmental Biology,* 244**,** 305-318.

HELMBACHER, F. & STRICKER, S. 2020. Tissue cross talks governing limb muscle development and regeneration. *Seminars in Cell & Developmental Biology,* 104**,** 14-30.

HENDERSON, N. C., ARNOLD, T. D., KATAMURA, Y., GIACOMINI, M. M., RODRIGUEZ, J. D., MCCARTY, J. H., PELLICORO, A., RASCHPERGER, E., BETSHOLTZ, C., RUMINSKI, P. G., GRIGGS, D. W., PRINSEN, M. J., MAHER, J. J., IREDALE, J. P., LACY-HULBERT, A., ADAMS, R. H. & SHEPPARD, D. 2013. Targeting of αv integrin identifies a core molecular pathway that regulates fibrosis in several organs. *Nature Medicine,* 19**,** 1617-1624.

HENDERSON, N. C., RIEDER, F. & WYNN, T. A. 2020. Fibrosis: from mechanisms to medicines. *Nature,* 587**,** 555-566.

HEREDIA, J. E., MUKUNDAN, L., CHEN, F. M., MUELLER, A. A., DEO, R. C., LOCKSLEY, R. M., RANDO, T. A. & CHAWLA, A. 2013. Type 2 innate signals stimulate fibro/adipogenic progenitors to facilitate muscle regeneration. *Cell,* 153**,** 376-88.

HOGARTH, M. W., DEFOUR, A., LAZARSKI, C., GALLARDO, E., DIAZ MANERA, J., PARTRIDGE, T. A., NAGARAJU, K. & JAISWAL, J. K. 2019. Fibroadipogenic progenitors are responsible for muscle loss in limb girdle muscular dystrophy 2B. *Nature Communications,* 10.

HOGARTH, M. W., UAPINYOYING, P., MÁZALA, D. A. G. & JAISWAL, J. K. 2021. Pathogenic role and therapeutic potential of fibro-adipogenic progenitors in muscle disease. *Trends in Molecular Medicine*.

IERONIMAKIS, N., HAYS, A., PRASAD, A., JANEBODIN, K., DUFFIELD, J. S. & REYES, M. 2016. PDGFRα signalling promotes fibrogenic responses in collagen-producing cells in Duchenne muscular dystrophy. *The Journal of Pathology,* 240**,** 410-424.

ISHITOBI, M., HAGINOYA, K., ZHAO, Y., OHNUMA, A., MINATO, J., YANAGISAWA, T., TANABU, M., KIKUCHI, M. & IINUMA, K. 2000. Elevated plasma levels of transforming growth factor β1 in patients with muscular dystrophy. *Neuroreport,* 11**,** 4033-4035.

ISMAEEL, A., KIM, J.-S., KIRK, J. S., SMITH, R. S., BOHANNON, W. T. & KOUTAKIS, P. 2019. Role of transforming growth factor-β in skeletal muscle fibrosis: a review. *International journal of molecular sciences,* 20**,** 2446.

JAMES, R. G., KAMEI, C. N., WANG, Q., JIANG, R. & SCHULTHEISS, T. M. 2006. Odd-skipped related 1 is required for development of the metanephric kidney and regulates formation and differentiation of kidney precursor cells.

JAMES, R. G. & SCHULTHEISS, T. M. 2005. Bmp signaling promotes intermediate mesoderm gene expression in a dose-dependent, cell-autonomous and translation-dependent manner. *Developmental biology,* 288**,** 113-125.

JOE, A. W., YI, L., NATARAJAN, A., LE GRAND, F., SO, L., WANG, J., RUDNICKI, M. A. & ROSSI, F. M. 2010. Muscle injury activates resident fibro/adipogenic progenitors that facilitate myogenesis. *Nat Cell Biol,* 12**,** 153-63.

JONES, M. G., ANDRIOTIS, O. G., ROBERTS, J. J. W., LUNN, K., TEAR, V. J., CAO, L., ASK, K., SMART, D. E., BONFANTI, A., JOHNSON, P., ALZETANI, A.,

CONFORTI, F., DOHERTY, R., LAI, C. Y., JOHNSON, B., BOURDAKOS, K. N., FLETCHER, S. V., MARSHALL, B. G., JOGAI, S., BRERETON, C. J., CHEE, S. J., OTTENSMEIER, C. H., SIME, P., GAULDIE, J., KOLB, M., MAHAJAN, S., FABRE, A., BHASKAR, A., JAROLIMEK, W., RICHELDI, L., O'REILLY, K. M. A., MONK, P. D., THURNER, P. J. & DAVIES, D. E. 2018. Nanoscale dysregulation of collagen structure-function disrupts mechano-homeostasis and mediates pulmonary fibrosis. *eLife,* 7**,** e36354.

JUBAN, G. & CHAZAUD, B. 2017. Metabolic regulation of macrophages during tissue repair: insights from skeletal muscle regeneration. *FEBS Letters,* 591**,** 3007-3021.

JUBAN, G., SACLIER, M., YACOUB-YOUSSEF, H., KERNOU, A., ARNOLD, L., BOISSON, C., BEN LARBI, S., MAGNAN, M., CUVELLIER, S., THERET, M., PETROF, B. J., DESGUERRE, I., GONDIN, J., MOUNIER, R. & CHAZAUD, B. 2018. AMPK Activation Regulates LTBP4-Dependent TGF-beta1 Secretion by Pro-inflammatory Macrophages and Controls Fibrosis in Duchenne Muscular Dystrophy. *Cell Rep,* 25**,** 2163-2176 e6.

JUDSON, R. N., ZHANG, R.-H. & ROSSI, F. M. A. 2013. Tissue-resident mesenchymal stem/progenitor cells in skeletal muscle: collaborators or saboteurs? *FEBS Journal,* 280**,** 4100-4108.

KADOMATSU, T., ENDO, M., MIYATA, K. & OIKE, Y. 2014. Diverse roles of ANGPTL2 in physiology and pathophysiology. *Trends in Endocrinology & Metabolism,* 25**,** 245-254.

KAIKITA, K., HAYASAKI, T., OKUMA, T., KUZIEL, W. A., OGAWA, H. & TAKEYA, M. 2004. Targeted deletion of CC chemokine receptor 2 attenuates left ventricular remodeling after experimental myocardial infarction. *The American journal of pathology,* 165**,** 439-447.

KANG, X., YANG, M. Y., SHI, Y. X., XIE, M. M., ZHU, M., ZHENG, X. L., ZHANG, C. K., GE, Z. L., BIAN, X. T., LV, J. T., WANG, Y. J., ZHOU, B. H. & TANG, K. L. 2018. Interleukin-15 facilitates muscle regeneration through modulation of fibro/adipogenic progenitors. *Cell Commun Signal,* 16**,** 42.

KARDON, G., CAMPBELL, J. K. & TABIN, C. J. 2002. Local Extrinsic Signals Determine Muscle and Endothelial Cell Fate and Patterning in the Vertebrate Limb. *Developmental Cell,* 3**,** 533-545.

KARDON, G., HARFE, B. D. & TABIN, C. J. 2003. A Tcf4-Positive Mesodermal Population Provides a Prepattern for Vertebrate Limb Muscle Patterning. *Developmental Cell,* 5**,** 937-944.

KASTENSCHMIDT, J. M., ELLEFSEN, K. L., MANNAA, A. H., GIEBEL, J. J., YAHIA, R., AYER, R. E., PHAM, P., RIOS, R., VETRONE, S. A., MOZAFFAR, T. & VILLALTA, S. A. 2019. QuantiMus: A Machine Learning-Based Approach for High Precision Analysis of Skeletal Muscle Morphology. *Frontiers in Physiology,* 10.

KATOH, M. 2002. Molecular cloning and characterization of OSR1 on human chromosome 2p24. *International journal of molecular medicine,* 10**,** 221-225.

KIRIAEV, L., KUEH, S., MORLEY, J. W., NORTH, K. N., HOUWELING, P. J. & HEAD, S. I. 2021. Lifespan analysis of dystrophic mdx fast-twitch muscle morphology and its impact on contractile function. Cold Spring Harbor Laboratory.

KLINGLER, W., JURKAT-ROTT, K., LEHMANN-HORN, F. & SCHLEIP, R. 2012. The role of fibrosis in Duchenne muscular dystrophy. *Acta Myol,* 31**,** 184-95.

KÖLBEL, H., HATHAZI, D., JENNINGS, M., HORVATH, R., ROOS, A. & SCHARA, U. 2019. Identification of Candidate Protein Markers in Skeletal Muscle of Laminin-211-Deficient CMD Type 1A-Patients. *Frontiers in Neurology,* 10.

KOPINKE, D., ROBERSON, E. C. & REITER, J. F. 2017. Ciliary Hedgehog Signaling Restricts Injury-Induced Adipogenesis. *Cell,* 170**,** 340-351.e12.

KOTTLORS, M. & KIRSCHNER, J. 2010. Elevated satellite cell number in Duchenne muscular dystrophy. *Cell and Tissue Research,* 340**,** 541-548.

KRUEGER, C. & HOFFMANN, F. M. 2010. Identification of Retinoic Acid in a High Content Screen for Agents that Overcome the Anti-Myogenic Effect of TGF-Beta-1. *PLoS ONE,* 5**,** e15511.

KUANG, S., KURODA, K., LE GRAND, F. & RUDNICKI, M. A. 2007. Asymmetric Self-Renewal and Commitment of Satellite Stem Cells in Muscle. *Cell,* 129**,** 999-1010.

KULESHOV, M. V., JONES, M. R., ROUILLARD, A. D., FERNANDEZ, N. F., DUAN, Q., WANG, Z., KOPLEV, S., JENKINS, S. L., JAGODNIK, K. M. & LACHMANN, A. 2016. Enrichr: a comprehensive gene set enrichment analysis web server 2016 update. *Nucleic acids research,* 44**,** W90-W97.

KUSWANTO, W., BURZYN, D., PANDURO, M., WANG, K. K., JANG, Y. C., WAGERS, A. J., BENOIST, C. & MATHIS, D. 2016. Poor Repair of Skeletal Muscle in Aging Mice Reflects a Defect in Local, Interleukin-33-Dependent Accumulation of Regulatory T Cells. *Immunity,* 44**,** 355-367.

LACRAZ, G., ROULEAU, A.-J., COUTURE, V., SÖLLRALD, T., DROUIN, G., VEILLETTE, N., GRANDBOIS, M. & GRENIER, G. 2015. Increased Stiffness in Aged Skeletal Muscle Impairs Muscle Progenitor Cell Proliferative Activity. *PLOS ONE,* 10**,** e0136217.

LAN, Y., KINGSLEY, P. D., CHO, E.-S. & JIANG, R. 2001. Osr2, a new mouse gene related to Drosophila odd-skipped, exhibits dynamic expression patterns during craniofacial, limb, and kidney development. *Mechanisms of development,* 107**,** 175-179.

LAROUCHE, J. A., FRACZEK, P. M., KURPIERS, S. J., YANG, B. A., DAVIS, C., CASTOR-MACIAS, J. A., SABIN, K., ANDERSON, S., HARRER, J., HALL, M., BROOKS, S. V., JANG, Y. C., WILLETT, N., SHEA, L. D. & AGUILAR, C. A. 2022. Neutrophil and natural killer cell imbalances prevent muscle stem cell–mediated regeneration following murine volumetric muscle loss. *Proceedings of the National Academy of Sciences,* 119**,** e2111445119.

LATROCHE, C., WEISS-GAYET, M., MULLER, L., GITIAUX, C., LEBLANC, P., LIOT, S., BEN-LARBI, S., ABOU-KHALIL, R., VERGER, N. & BARDOT, P. 2017. Coupling between myogenesis and angiogenesis during skeletal muscle regeneration is stimulated by restorative macrophages. *Stem cell reports,* 9**,** 2018-2033.

LE GRAND, F. & RUDNICKI, M. A. 2007. Skeletal muscle satellite cells and adult myogenesis. *Current Opinion in Cell Biology,* 19**,** 628-633.

LEBLANC, E., TRENSZ, F., HAROUN, S., DROUIN, G., BERGERON, É., PENTON, C. M., MONTANARO, F., ROUX, S., FAUCHEUX, N. & GRENIER, G. 2011. BMP-9-induced muscle heterotopic ossification requires changes to the skeletal muscle microenvironment. *Journal of Bone and Mineral Research,* 26**,** 1166-1177.

LEE, C., AGHA, O., LIU, M., DAVIES, M., BERTOY, L., KIM, H. T., LIU, X. & FEELEY, B. T. 2020. Rotator Cuff Fibro-Adipogenic Progenitors Demonstrate Highest Concentration, Proliferative Capacity, and Adipogenic Potential Across Muscle Groups. *Journal of Orthopaedic Research,* 38**,** 1113-1121.

LEE, Y., KIM, M. & LEE, H. 2021. The Measurement of Stiffness for Major Muscles with Shear Wave Elastography and Myoton: A Quantitative Analysis Study. *Diagnostics,* 11**,** 524.

References

LEES-SHEPARD, J. B., YAMAMOTO, M., BISWAS, A. A., STOESSEL, S. J., NICHOLAS, S.-A. E., COGSWELL, C. A., DEVARAKONDA, P. M., SCHNEIDER, M. J., CUMMINS, S. M., LEGENDRE, N. P., YAMAMOTO, S., KAARTINEN, V., HUNTER, J. W. & GOLDHAMER, D. J. 2018. Activin-dependent signaling in fibro/adipogenic progenitors causes fibrodysplasia ossificans progressiva. *Nature Communications,* 9.

LEMOS, D. R., BABAEIJANDAGHI, F., LOW, M., CHANG, C. K., LEE, S. T., FIORE, D., ZHANG, R. H., NATARAJAN, A., NEDOSPASOV, S. A. & ROSSI, F. M. 2015. Nilotinib reduces muscle fibrosis in chronic muscle injury by promoting TNF-mediated apoptosis of fibro/adipogenic progenitors. *Nat Med,* 21**,** 786-94.

LEMOS, D. R. & DUFFIELD, J. S. 2018. Tissue-resident mesenchymal stromal cells: Implications for tissue-specific antifibrotic therapies. *Science Translational Medicine,* 10**,** eaan5174.

LEMOS, D. R., PAYLOR, B., CHANG, C., SAMPAIO, A., UNDERHILL, T. M. & ROSSI, F. M. V. 2012. Functionally Convergent White Adipogenic Progenitors of Different Lineages Participate in a Diffused System Supporting Tissue Regeneration. *STEM CELLS,* 30**,** 1152-1162.

LEPPER, C., PARTRIDGE, T. A. & FAN, C.-M. 2011. An absolute requirement for Pax7-positive satellite cells in acute injury-induced skeletal muscle regeneration. *Development,* 138**,** 3639-3646.

LI, Y., LI, F., LIN, B., KONG, X., TANG, Y. & YIN, Y. 2014. Myokine IL-15 regulates the crosstalk of co-cultured porcine skeletal muscle satellite cells and preadipocytes. *Molecular Biology Reports,* 41**,** 7543-7553.

LIANG, W.-C., TIAN, X., YUO, C.-Y., CHEN, W.-Z., KAN, T.-M., SU, Y.-N., NISHINO, I., WONG, L.-J. C. & JONG, Y.-J. 2017. Comprehensive target capture/next-generation sequencing as a second-tier diagnostic approach for congenital muscular dystrophy in Taiwan. *PLOS ONE,* 12**,** e0170517.

LIEBER, R. L. & FRIDÉN, J. 2019. Muscle contracture and passive mechanics in cerebral palsy. *Journal of Applied Physiology,* 126**,** 1492-1501.

LIEBER, R. L. & WARD, S. R. 2013. Cellular Mechanisms of Tissue Fibrosis. 4. Structural and functional consequences of skeletal muscle fibrosis. *American Journal of Physiology-Cell Physiology,* 305**,** C241-C252.

LIU, X., LIU, Y., ZHAO, L., ZENG, Z., XIAO, W. & CHEN, P. 2017. Macrophage depletion impairs skeletal muscle regeneration: The roles of regulatory factors for muscle regeneration. *Cell Biology International,* 41**,** 228-238.

LU, H., HUANG, D., RANSOHOFF, R. M. & ZHOU, L. 2011a. Acute skeletal muscle injury: CCL2 expression by both monocytes and injured muscle is required for repair. *The FASEB Journal,* 25**,** 3344-3355.

LU, H., HUANG, D., SAEDERUP, N., CHARO, I. F., RANSOHOFF, R. M. & ZHOU, L. 2011b. Macrophages recruited via CCR2 produce insulin-like growth factor-1 to repair acute skeletal muscle injury. *The FASEB Journal,* 25**,** 358-369.

LUKJANENKO, L., KARAZ, S., STUELSATZ, P., GURRIARAN-RODRIGUEZ, U., MICHAUD, J., DAMMONE, G., SIZZANO, F., MASHINCHIAN, O., ANCEL, S., MIGLIAVACCA, E., LIOT, S., JACOT, G., METAIRON, S., RAYMOND, F., DESCOMBES, P., PALINI, A., CHAZAUD, B., RUDNICKI, M. A., BENTZINGER, C. F. & FEIGE, J. N. 2019. Aging Disrupts Muscle Stem Cell Function by Impairing Matricellular WISP1 Secretion from Fibro-Adipogenic Progenitors. *Cell Stem Cell*.

MACKEY, A. L., MAGNAN, M., CHAZAUD, B. & KJAER, M. 2017. Human skeletal muscle fibroblasts stimulate in vitro myogenesis and in vivo muscle regeneration. *The Journal of physiology,* 595**,** 5115-5127.

MADARO, L., PASSAFARO, M., SALA, D., ETXANIZ, U., LUGARINI, F., PROIETTI, D., ALFONSI, M. V., NICOLETTI, C., GATTO, S., DE BARDI, M., ROJAS-GARCIA, R., GIORDANI, L., MARINELLI, S., PAGLIARINI, V., SETTE, C., SACCO, A. & PURI, P. L. 2018. Denervation-activated STAT3-IL-6 signalling in fibro-adipogenic progenitors promotes myofibres atrophy and fibrosis. *Nat Cell Biol,* 20**,** 917-927.

MALECOVA, B., GATTO, S., ETXANIZ, U., PASSAFARO, M., CORTEZ, A., NICOLETTI, C., GIORDANI, L., TORCINARO, A., DE BARDI, M., BICCIATO, S., DE SANTA, F., MADARO, L. & PURI, P. L. 2018. Dynamics of cellular states of fibro-adipogenic progenitors during myogenesis and muscular dystrophy. *Nat Commun,* 9**,** 3670.

MARINKOVIC, M., FUOCO, C., SACCO, F., CERQUONE PERPETUINI, A., GIULIANI, G., MICARELLI, E., PAVLIDOU, T., PETRILLI, L. L., REGGIO, A., RICCIO, F., SPADA, F., VUMBACA, S., ZUCCOTTI, A., CASTAGNOLI, L., MANN, M., GARGIOLI, C. & CESARENI, G. 2019. Fibro-adipogenic progenitors of dystrophic mice are insensitive to NOTCH regulation of adipogenesis. *Life Science Alliance,* 2**,** e201900437.

MASHINCHIAN, O., PISCONTI, A., LE MOAL, E. & BENTZINGER, C. F. 2018. Chapter Two - The Muscle Stem Cell Niche in Health and Disease. *In:* SASSOON, D. (ed.) *Current Topics in Developmental Biology.* Academic Press.

MASSAGUE, J., CHEIFETZ, S., ENDO, T. & NADAL-GINARD, B. 1986. Type beta transforming growth factor is an inhibitor of myogenic differentiation. *Proceedings of the National Academy of Sciences,* 83**,** 8206-8210.

MATHEW, S. J., HANSEN, J. M., MERRELL, A. J., MURPHY, M. M., LAWSON, J. A., HUTCHESON, D. A., HANSEN, M. S., ANGUS-HILL, M. & KARDON, G. 2011. Connective tissue fibroblasts and Tcf4 regulate myogenesis. *Development,* 138**,** 371-384.

MATSUO, N., TANAKA, S., YOSHIOKA, H., KOCH, M., GORDON, M. K. & RAMIREZ, F. 2008. Collagen XXIV (Col24a1) Gene Expression is a Specific Marker of Osteoblast Differentiation and Bone Formation. *Connective Tissue Research,* 49**,** 68-75.

MAURO, A. 1961. Satellite cell of skeletal muscle fibers. *The Journal of Cell Biology,* 9**,** 493-495.

MÁZALA, D. A. G., NOVAK, J. S., HOGARTH, M. W., NEARING, M., ADUSUMALLI, P., TULLY, C. B., HABIB, N. F., GORDISH-DRESSMAN, H., CHEN, Y.-W., JAISWAL, J. K. & PARTRIDGE, T. A. 2020. TGF-β–driven muscle degeneration and failed regeneration underlie disease onset in a DMD mouse model. *JCI Insight,* 5.

MENDIAS, C. L., GUMUCIO, J. P., DAVIS, M. E., BROMLEY, C. W., DAVIS, C. S. & BROOKS, S. V. 2012. Transforming growth factor-beta induces skeletal muscle atrophy and fibrosis through the induction of atrogin-1 and scleraxis. *Muscle & nerve,* 45**,** 55-59.

MEYER, G., MCCULLOCH, A. & LIEBER, R. 2011. A nonlinear model of passive muscle viscosity.

MILLER, T. A., LESNIEWSKI, L. A., MULLER-DELP, J. M., MAJORS, A. K., SCALISE, D. & DELP, M. D. 2001. Hindlimb unloading induces a collagen isoform shift in the soleus muscle of the rat. *American Journal of Physiology-Regulatory, Integrative and Comparative Physiology,* 281**,** R1710-R1717.

MITCHELL, K. J., PANNÉREC, A., CADOT, B., PARLAKIAN, A., BESSON, V., GOMES, E. R., MARAZZI, G. & SASSOON, D. A. 2010. Identification and

characterization of a non-satellite cell muscle resident progenitor during postnatal development. *Nature Cell Biology,* 12**,** 257-266.

MOLINA, T., FABRE, P. & DUMONT, N. A. 2021. Fibro-adipogenic progenitors in skeletal muscle homeostasis, regeneration and diseases. *Open Biology,* 11.

MORATAL, C., ARRIGHI, N., DECHESNE, C. A. & DANI, C. 2019. Control of Muscle Fibro-Adipogenic Progenitors by Myogenic Lineage is Altered in Aging and Duchenne Muscular Dystrophy. *Cellular physiology and biochemistry : international journal of experimental cellular physiology, biochemistry, and pharmacology,* 53**,** 1029-1045.

MORATAL, C., RAFFORT, J., ARRIGHI, N., REKIMA, S., SCHAUB, S., DECHESNE, C. A., CHINETTI, G. & DANI, C. 2018. IL-1beta- and IL-4-polarized macrophages have opposite effects on adipogenesis of intramuscular fibro-adipogenic progenitors in humans. *Sci Rep,* 8**,** 17005.

MOURIKIS, P., SAMBASIVAN, R., CASTEL, D., ROCHETEAU, P., BIZZARRO, V. & TAJBAKHSH, S. 2012. A Critical Requirement for Notch Signaling in Maintenance of the Quiescent Skeletal Muscle Stem Cell State. *Stem Cells,* 30**,** 243-252.

MOURIKIS, P. & TAJBAKHSH, S. 2014. Distinct contextual roles for Notch signalling in skeletal muscle stem cells. *BMC Developmental Biology,* 14**,** 2.

MOZZETTA, C., CONSALVI, S., SACCONE, V., TIERNEY, M., DIAMANTINI, A., MITCHELL, K. J., MARAZZI, G., BORSELLINO, G., BATTISTINI, L., SASSOON, D., SACCO, A. & PURI, P. L. 2013. Fibroadipogenic progenitors mediate the ability of HDAC inhibitors to promote regeneration in dystrophic muscles of young, but not old Mdx mice. *EMBO Molecular Medicine,* 5**,** 626-639.

MUELLER, A. A., VAN VELTHOVEN, C. T., FUKUMOTO, K. D., CHEUNG, T. H. & RANDO, T. A. 2016. Intronic polyadenylation of PDGFRα in resident stem cells attenuates muscle fibrosis. *Nature,* 540**,** 276-279.

MUGFORD, J. W., SIPILÄ, P., MCMAHON, J. A. & MCMAHON, A. P. 2008. Osr1 expression demarcates a multi-potent population of intermediate mesoderm that undergoes progressive restriction to an Osr1-dependent nephron progenitor compartment within the mammalian kidney. *Developmental biology,* 324**,** 88-98.

MUÑOZ-CÁNOVES, P. & SERRANO, A. L. 2015. Macrophages decide between regeneration and fibrosis in muscle. *Trends in Endocrinology & Metabolism,* 26**,** 449-450.

MURPHY, M. M., LAWSON, J. A., MATHEW, S. J., HUTCHESON, D. A. & KARDON, G. 2011. Satellite cells, connective tissue fibroblasts and their interactions are crucial for muscle regeneration. *Development,* 138**,** 3625-3637.

NARITA, S. & YORIFUJI, H. 1999. Centrally nucleated fibers (CNFs) compensate the fragility of myofibers in mdx mouse. *NeuroReport,* 10.

NGUYEN, J. H., CHUNG, J. D., LYNCH, G. S. & RYALL, J. G. 2019. The Microenvironment Is a Critical Regulator of Muscle Stem Cell Activation and Proliferation. *Frontiers in Cell and Developmental Biology,* 7.

NITAHARA-KASAHARA, Y., HAYASHITA-KINOH, H., CHIYO, T., NISHIYAMA, A., OKADA, H., TAKEDA, S. I. & OKADA, T. 2014. Dystrophic mdx mice develop severe cardiac and respiratory dysfunction following genetic ablation of the anti-inflammatory cytokine IL-10. *Human Molecular Genetics,* 23**,** 3990-4000.

NOGUCHI, S., OGAWA, M., MALICDAN, M. C., NONAKA, I. & NISHINO, I. 2017. Muscle Weakness and Fibrosis Due to Cell Autonomous and Non-cell

Autonomous Events in Collagen VI Deficient Congenital Muscular Dystrophy. *EBioMedicine,* 15**,** 193-202.

NOVAK, M. L. & KOH, T. J. 2013. Macrophage phenotypes during tissue repair. *Journal of Leukocyte Biology,* 93**,** 875-881.

NÜSSLEIN-VOLHARD, C. & WIESCHAUS, E. 1980. Mutations affecting segment number and polarity in Drosophila. *Nature,* 287**,** 795-801.

OISHI, T., UEZUMI, A., KANAJI, A., YAMAMOTO, N., YAMAGUCHI, A., YAMADA, H. & TSUCHIDA, K. 2013. Osteogenic Differentiation Capacity of Human Skeletal Muscle-Derived Progenitor Cells. *PLOS ONE,* 8**,** e56641.

OLSON, E. N., STERNBERG, E., HU, J. S., SPIZZ, G. & WILCOX, C. 1986. Regulation of myogenic differentiation by type beta transforming growth factor. *The Journal of Cell Biology,* 103**,** 1799-1805.

ONG, S., LIGONS, D. L., BARIN, J. G., WU, L., TALOR, M. V., DINY, N., FONTES, J. A., GEBREMARIAM, E., KASS, D. A. & ROSE, N. R. 2015. Natural killer cells limit cardiac inflammation and fibrosis by halting eosinophil infiltration. *The American journal of pathology,* 185**,** 847-861.

OPRESCU, S. N., YUE, F., QIU, J., BRITO, L. F. & KUANG, S. 2020. Temporal Dynamics and Heterogeneity of Cell Populations during Skeletal Muscle Regeneration. *iScience,* 23**,** 100993.

PAKSHIR, P. & HINZ, B. 2018. The big five in fibrosis: Macrophages, myofibroblasts, matrix, mechanics, and miscommunication. *Matrix Biology,* 68-69**,** 81-93.

PAKSHIR, P., NOSKOVICOVA, N., LODYGA, M., SON, D. O., SCHUSTER, R., GOODWIN, A., KARVONEN, H. & HINZ, B. 2020. The myofibroblast at a glance. *Journal of Cell Science,* 133.

PANDURO, M., BENOIST, C. & MATHIS, D. 2018. Treg cells limit IFNγ production to control macrophage accrual and phenotype during skeletal muscle regeneration. *Proceedings of the National Academy of Sciences,* 115**,** E2585-E2593.

PANNÉREC, A., MARAZZI, G. & SASSOON, D. 2012. Stem cells in the hood: the skeletal muscle niche. *Trends in Molecular Medicine,* 18**,** 599-606.

PESSINA, P., CABRERA, D., MORALES, M. G., RIQUELME, C. A., GUTIÉRREZ, J., SERRANO, A. L., BRANDAN, E. & MUÑOZ-CÁNOVES, P. 2014. Novel and optimized strategies for inducing fibrosis in vivo: focus on Duchenne Muscular Dystrophy. *Skeletal Muscle,* 4**,** 7.

PESSINA, P., KHARRAZ, Y., JARDÍ, M., FUKADA, S.-I., SERRANO, A. L., PERDIGUERO, E. & MUÑOZ-CÁNOVES, P. 2015. Fibrogenic cell plasticity blunts tissue regeneration and aggravates muscular dystrophy. *Stem cell reports,* 4**,** 1046-1060.

PETRILLI, L. L., SPADA, F., PALMA, A., REGGIO, A., ROSINA, M., GARGIOLI, C., CASTAGNOLI, L., FUOCO, C. & CESARENI, G. 2020. High-Dimensional Single-Cell Quantitative Profiling of Skeletal Muscle Cell Population Dynamics during Regeneration. *Cells,* 9**,** 1723.

PINGEL, J., BARTELS, E. & NIELSEN, J. 2017. New perspectives on the development of muscle contractures following central motor lesions. *The Journal of physiology,* 595**,** 1027-1038.

POURHANIFEH, M. H., MOHAMMADI, R., NORUZI, S., HOSSEINI, S. A., FANOUDI, S., MOHAMADI, Y., HASHEMZEHI, M., ASEMI, Z., MIRZAEI, H. R., SALARINIA, R. & MIRZAEI, H. 2019. The role of fibromodulin in cancer pathogenesis: implications for diagnosis and therapy. *Cancer Cell International,* 19.

References

QAZI, T. H., DUDA, G. N., ORT, M. J., PERKA, C., GEISSLER, S. & WINKLER, T. 2019. Cell therapy to improve regeneration of skeletal muscle injuries. *Journal of Cachexia, Sarcopenia and Muscle,* 10**,** 501-516.

QIN, J. Y., ZHANG, L., CLIFT, K. L., HULUR, I., XIANG, A. P., REN, B.-Z. & LAHN, B. T. 2010. Systematic Comparison of Constitutive Promoters and the Doxycycline-Inducible Promoter. *PLoS ONE,* 5**,** e10611.

QUINN, L., STRAITBODEY, L., ANDERSON, B., ARGILES, J. & HAVEL, P. 2005. Interleukin-15 stimulates adiponectin secretion by 3T3-L1 adipocytes: Evidence for a skeletal muscle-to-fat signaling pathway. *Cell Biology International,* 29**,** 449-457.

RAHMAN, F. A., ANGUS, S. A., STOKES, K., KARPOWICZ, P. & KRAUSE, M. P. 2020. Impaired ECM Remodeling and Macrophage Activity Define Necrosis and Regeneration Following Damage in Aged Skeletal Muscle. *International Journal of Molecular Sciences,* 21**,** 4575.

REGGIO, A., ROSINA, M., PALMA, A., CERQUONE PERPETUINI, A., PETRILLI, L. L., GARGIOLI, C., FUOCO, C., MICARELLI, E., GIULIANI, G., CERRETANI, M., BRESCIANI, A., SACCO, F., CASTAGNOLI, L. & CESARENI, G. 2020. Adipogenesis of skeletal muscle fibro/adipogenic progenitors is affected by the WNT5a/GSK3/β-catenin axis. *Cell Death & Differentiation,* 27**,** 2921-2941.

REIMAND, J., ISSERLIN, R., VOISIN, V., KUCERA, M., TANNUS-LOPES, C., ROSTAMIANFAR, A., WADI, L., MEYER, M., WONG, J. & XU, C. 2019. Pathway enrichment analysis and visualization of omics data using g: Profiler, GSEA, Cytoscape and EnrichmentMap. *Nature protocols,* 14**,** 482-517.

RELAIX, F. & ZAMMIT, P. S. 2012. Satellite cells are essential for skeletal muscle regeneration: the cell on the edge returns centre stage. *Development,* 139**,** 2845-2856.

RIGGIN, C. N., SARVER, J. J., FREEDMAN, B. R., THOMAS, S. J. & SOSLOWSKY, L. J. 2014. Analysis of Collagen Organization in Mouse Achilles Tendon Using High-Frequency Ultrasound Imaging. *Journal of Biomechanical Engineering,* 136.

ROBERTS, E. W., DEONARINE, A., JONES, J. O., DENTON, A. E., FEIG, C., LYONS, S. K., ESPELI, M., KRAMAN, M., MCKENNA, B. & WELLS, R. J. 2013a. Depletion of stromal cells expressing fibroblast activation protein-α from skeletal muscle and bone marrow results in cachexia and anemia. *Journal of Experimental Medicine,* 210**,** 1137-1151.

ROBERTS, E. W., DEONARINE, A., JONES, J. O., DENTON, A. E., FEIG, C., LYONS, S. K., ESPELI, M., KRAMAN, M., MCKENNA, B., WELLS, R. J. B., ZHAO, Q., CABALLERO, O. L., LARDER, R., COLL, A. P., O'RAHILLY, S., BRINDLE, K. M., TEICHMANN, S. A., TUVESON, D. A. & FEARON, D. T. 2013b. Depletion of stromal cells expressing fibroblast activation protein-α from skeletal muscle and bone marrow results in cachexia and anemia. *Journal of Experimental Medicine,* 210**,** 1137-1151.

ROCA, H., VARSOS, Z. S., SUD, S., CRAIG, M. J., YING, C. & PIENTA, K. J. 2009. CCL2 and Interleukin-6 Promote Survival of Human CD11b+ Peripheral Blood Mononuclear Cells and Induce M2-type Macrophage Polarization. *Journal of Biological Chemistry,* 284**,** 34342-34354.

RODGERS, J. T., KING, K. Y., BRETT, J. O., CROMIE, M. J., CHARVILLE, G. W., MAGUIRE, K. K., BRUNSON, C., MASTEY, N., LIU, L., TSAI, C.-R., GOODELL, M. A. & RANDO, T. A. 2014. mTORC1 controls the adaptive transition of quiescent stem cells from G0 to GAlert. *Nature,* 510**,** 393-396.

RODRIGUES, M., ECHIGOYA, Y., MARUYAMA, R., LIM, K. R. Q., FUKADA, S.-I. & YOKOTA, T. 2016. Impaired regenerative capacity and lower revertant fibre expansion in dystrophin-deficient mdx muscles on DBA/2 background. *Scientific Reports,* 6**,** 38371.

RODRÍGUEZ, C. I., BUCHHOLZ, F., GALLOWAY, J., SEQUERRA, R., KASPER, J., AYALA, R., STEWART, A. F. & DYMECKI, S. M. 2000. High-efficiency deleter mice show that FLPe is an alternative to Cre-loxP. *Nature genetics,* 25**,** 139-140.

ROSS, J., BENN, A., JONUSCHIES, J., BOLDRIN, L., MUNTONI, F., HEWITT, J. E., BROWN, S. C. & MORGAN, J. E. 2012. Defects in Glycosylation Impair Satellite Stem Cell Function and Niche Composition in the Muscles of the Dystrophic LargemydMouse. *STEM CELLS,* 30**,** 2330-2341.

SACCO, A., DOYONNAS, R., KRAFT, P., VITOROVIC, S. & BLAU, H. M. 2008. Self-renewal and expansion of single transplanted muscle stem cells. *Nature,* 456**,** 502-6.

SACLIER, M., CUVELLIER, S., MAGNAN, M., MOUNIER, R. & CHAZAUD, B. 2013a. Monocyte/macrophage interactions with myogenic precursor cells during skeletal muscle regeneration. *FEBS Journal,* 280**,** 4118-4130.

SACLIER, M., YACOUB-YOUSSEF, H., MACKEY, A. L., ARNOLD, L., ARDJOUNE, H., MAGNAN, M., SAILHAN, F., CHELLY, J., PAVLATH, G. K., MOUNIER, R., KJAER, M. & CHAZAUD, B. 2013b. Differentially Activated Macrophages Orchestrate Myogenic Precursor Cell Fate During Human Skeletal Muscle Regeneration. *Stem Cells,* 31**,** 384-396.

SAMBASIVAN, R., YAO, R., KISSENPFENNIG, A., VAN WITTENBERGHE, L., PALDI, A., GAYRAUD-MOREL, B., GUENOU, H., MALISSEN, B., TAJBAKHSH, S. & GALY, A. 2011. Pax7-expressing satellite cells are indispensable for adult skeletal muscle regeneration. *Development,* 138**,** 3647-3656.

SANES, J. R. 2003. The Basement Membrane/Basal Lamina of Skeletal Muscle. *Journal of Biological Chemistry,* 278**,** 12601-12604.

SANTINI, M. P., MALIDE, D., HOFFMAN, G., PANDEY, G., D'ESCAMARD, V., NOMURA-KITABAYASHI, A., ROVIRA, I., KATAOKA, H., OCHANDO, J., HARVEY, R. P., FINKEL, T. & KOVACIC, J. C. 2020. Tissue-Resident PDGFRα+ Progenitor Cells Contribute to Fibrosis versus Healing in a Context- and Spatiotemporally Dependent Manner. *Cell Reports,* 30**,** 555-570.e7.

SARKOZY, A., FOLEY, A. R., ZAMBON, A. A., BÖNNEMANN, C. G. & MUNTONI, F. 2020. LAMA2-related dystrophies: clinical phenotypes, disease biomarkers, and clinical trial readiness. *Frontiers in Molecular Neuroscience,* 13**,** 123.

SASS, F., FUCHS, M., PUMBERGER, M., GEISSLER, S., DUDA, G., PERKA, C. & SCHMIDT-BLEEK, K. 2018. Immunology Guides Skeletal Muscle Regeneration. *International Journal of Molecular Sciences,* 19**,** 835.

SAULIER-LE DRÉAN, B., NASIADKA, A., DONG, J. & KRAUSE, H. M. 1998. Dynamic changes in the functions of Odd-skipped during early Drosophila embryogenesis. *Development,* 125**,** 4851-4861.

SCHAUM, N., KARKANIAS, J., NEFF, N. F., MAY, A. P., QUAKE, S. R., WYSS-CORAY, T., DARMANIS, S., BATSON, J., BOTVINNIK, O., CHEN, M. B., CHEN, S., GREEN, F., JONES, R. C., MAYNARD, A., PENLAND, L., PISCO, A. O., SIT, R. V., STANLEY, G. M., WEBBER, J. T., ZANINI, F., BAGHEL, A. S., BAKERMAN, I., BANSAL, I., BERDNIK, D., BILEN, B., BROWNFIELD, D., CAIN, C., CHEN, M. B., CHEN, S., CHO, M., CIROLIA, G., CONLEY, S. D., DARMANIS, S., DEMERS, A., DEMIR, K., DE MORREE, A., DIVITA, T., DU

BOIS, H., DULGEROFF, L. B. T., EBADI, H., ESPINOZA, F. H., FISH, M., GAN, Q., GEORGE, B. M., GILLICH, A., GREEN, F., GENETIANO, G., GU, X., GULATI, G. S., HANG, Y., HOSSEINZADEH, S., HUANG, A., IRAM, T., ISOBE, T., IVES, F., JONES, R. C., KAO, K. S., KARNAM, G., KERSHNER, A. M., KISS, B. M., KONG, W., KUMAR, M. E., LAM, J. Y., LEE, D. P., LEE, S. E., LI, G., LI, Q., LIU, L., LO, A., LU, W.-J., MANJUNATH, A., MAY, A. P., MAY, K. L., MAY, O. L., MAYNARD, A., MCKAY, M., METZGER, R. J., MIGNARDI, M., MIN, D., NABHAN, A. N., NEFF, N. F., NG, K. M., NOH, J., PATKAR, R., PENG, W. C., PENLAND, L., PUCCINELLI, R., RULIFSON, E. J., SCHAUM, N., SIKANDAR, S. S., SINHA, R., SIT, R. V., SZADE, K., TAN, W., TATO, C., TELLEZ, K., TRAVAGLINI, K. J., TROPINI, C., WALDBURGER, L., VAN WEELE, L. J., et al. 2018. Single-cell transcriptomics of 20 mouse organs creates a Tabula Muris. *Nature,* 562**,** 367-372.

SCHIAFFINO, S. & MAMMUCARI, C. 2011. Regulation of skeletal muscle growth by the IGF1-Akt/PKB pathway: insights from genetic models. *Skeletal Muscle,* 1**,** 4.

SCHIAFFINO, S., PEREIRA, M. G., CICILIOT, S. & ROVERE-QUERINI, P. 2017. Regulatory T cells and skeletal muscle regeneration. *The FEBS journal,* 284**,** 517-524.

SCHIAFFINO, S., ROSSI, A. C., SMERDU, V., LEINWAND, L. A. & REGGIANI, C. 2015. Developmental myosins: expression patterns and functional significance. *Skeletal Muscle,* 5.

SCHLUNDT, C., REINKE, S., GEISSLER, S., BUCHER, C. H., GIANNINI, C., MÄRDIAN, S., DAHNE, M., KLEBER, C., SAMANS, B., BARON, U., DUDA, G. N., VOLK, H.-D. & SCHMIDT-BLEEK, K. 2019. Individual Effector/Regulator T Cell Ratios Impact Bone Regeneration. *Frontiers in Immunology,* 10.

SCHUMACHER, A., DENECKE, B., BRAUNSCHWEIG, T., STAHLSCHMIDT, J., ZIEGLER, S., BRANDENBURG, L.-O., STOPE, M. B., MARTINCUKS, A., VOGT, M., GÖRTZ, D., CAMPOREALE, A., POLI, V., MÜLLER-NEWEN, G., BRÜMMENDORF, T. H. & ZIEGLER, P. 2015. Angptl4 is upregulated under inflammatory conditions in the bone marrow of mice, expands myeloid progenitors, and accelerates reconstitution of platelets after myelosuppressive therapy. *Journal of Hematology & Oncology,* 8.

SCIMÈ, A., DESROSIERS, J., TRENSZ, F., PALIDWOR, G. A., CARON, A. Z., ANDRADE-NAVARRO, M. A. & GRENIER, G. 2010. Transcriptional profiling of skeletal muscle reveals factors that are necessary to maintain satellite cell integrity during ageing. *Mech Ageing Dev,* 131**,** 9-20.

SCOTT, R. W., AROSTEGUI, M., SCHWEITZER, R., ROSSI, F. M. V. & UNDERHILL, T. M. 2019. Hic1 Defines Quiescent Mesenchymal Progenitor Subpopulations with Distinct Functions and Fates in Skeletal Muscle Regeneration. *Cell Stem Cell,* 25**,** 797-813 e9.

SEALE, P., SABOURIN, L. A., GIRGIS-GABARDO, A., MANSOURI, A., GRUSS, P. & RUDNICKI, M. A. 2000. Pax7 Is Required for the Specification of Myogenic Satellite Cells. *Cell,* 102**,** 777-786.

SEFTON, E. M. & KARDON, G. 2019a. Chapter Five - Connecting muscle development, birth defects, and evolution: An essential role for muscle connective tissue. *In:* WELLIK, D. M. (ed.) *Current Topics in Developmental Biology.* Academic Press.

SEFTON, E. M. & KARDON, G. 2019b. Connecting muscle development, birth defects, and evolution: An essential role for muscle connective tissue. *Current topics in developmental biology,* 132**,** 137-176.

SERRANO, A. L., MANN, C. J., VIDAL, B., ARDITE, E., PERDIGUERO, E. & MUÑOZ-CÁNOVES, P. 2011. Chapter seven - Cellular and Molecular Mechanisms Regulating Fibrosis in Skeletal Muscle Repair and Disease. *In:* PAVLATH, G. K. (ed.) *Current Topics in Developmental Biology.* Academic Press.

SERRANO, A. L. & MUÑOZ-CÁNOVES, P. 2017. Fibrosis development in early-onset muscular dystrophies: Mechanisms and translational implications. *Seminars in Cell & Developmental Biology,* 64**,** 181-190.

SHEA, K. L., XIANG, W., LAPORTA, V. S., LICHT, J. D., KELLER, C., BASSON, M. A. & BRACK, A. S. 2010. Sprouty1 Regulates Reversible Quiescence of a Self-Renewing Adult Muscle Stem Cell Pool during Regeneration. *Cell Stem Cell,* 6**,** 117-129.

SHEFER, G., VAN DE MARK, D. P., RICHARDSON, J. B. & YABLONKA-REUVENI, Z. 2006. Satellite-cell pool size does matter: defining the myogenic potency of aging skeletal muscle. *Dev Biol,* 294**,** 50-66.

SHORE, E. M., XU, M., FELDMAN, G. J., FENSTERMACHER, D. A., CHO, T.-J., CHOI, I. H., CONNOR, J. M., DELAI, P., GLASER, D. L., LEMERRER, M., MORHART, R., ROGERS, J. G., SMITH, R., TRIFFITT, J. T., URTIZBEREA, J. A., ZASLOFF, M., BROWN, M. A. & KAPLAN, F. S. 2006. A recurrent mutation in the BMP type I receptor ACVR1 causes inherited and sporadic fibrodysplasia ossificans progressiva. *Nature Genetics,* 38**,** 525-527.

SIERRA-FILARDI, E., NIETO, C., DOMÍNGUEZ-SOTO, Á., BARROSO, R., SÁNCHEZ-MATEOS, P., PUIG-KROGER, A., LÓPEZ-BRAVO, M., JOVEN, J., ARDAVÍN, C., RODRÍGUEZ-FERNÁNDEZ, J. L., SÁNCHEZ-TORRES, C., MELLADO, M. & CORBÍ, Á. L. 2014. CCL2 Shapes Macrophage Polarization by GM-CSF and M-CSF: Identification of CCL2/CCR2-Dependent Gene Expression Profile. *The Journal of Immunology,* 192**,** 3858-3867.

SILVER, J. S., GÜNAY, K. A., CUTLER, A. A., VOGLER, T. O., BROWN, T. E., PAWLIKOWSKI, B. T., BEDNARSKI, O. J., BANNISTER, K. L., ROGOWSKI, C. J., MCKAY, A. G., DELRIO, F. W., OLWIN, B. B. & ANSETH, K. S. 2021. Injury-mediated stiffening persistently activates muscle stem cells through YAP and TAZ mechanotransduction. *Science Advances,* 7**,** eabe4501.

SKALSKY, A. J. & MCDONALD, C. M. 2012. Prevention and management of limb contractures in neuromuscular diseases. *Physical Medicine and Rehabilitation Clinics,* 23**,** 675-687.

SMITH, L. R. & BARTON, E. R. 2014. Collagen content does not alter the passive mechanical properties of fibrotic skeletal muscle in mdx mice. *American Journal of Physiology-Cell Physiology,* 306**,** C889-C898.

SMITH, L. R. & BARTON, E. R. 2018. Regulation of fibrosis in muscular dystrophy. *Matrix Biology,* 68-69**,** 602-615.

SMITH, L. R., HAMMERS, D. W., SWEENEY, H. L. & BARTON, E. R. 2016. Increased collagen cross-linking is a signature of dystrophin-deficient muscle. *Muscle & Nerve,* 54**,** 71-78.

SMITH, L. R., PICHIKA, R., MEZA, R. C., GILLIES, A. R., BALIKI, M. N., CHAMBERS, H. G. & LIEBER, R. L. 2021. Contribution of extracellular matrix components to the stiffness of skeletal muscle contractures in patients with cerebral palsy. *Connective Tissue Research,* 62**,** 287-298.

SO, P. L. & DANIELIAN, P. S. 1999. Cloning and expression analysis of a mouse gene related to Drosophila odd-skipped. *Mechanisms of development,* 84**,** 157-160.

SOHN, J., LU, A., TANG, Y., WANG, B. & HUARD, J. 2015. Activation of non-myogenic mesenchymal stem cells during the disease progression in dystrophic dystrophin/utrophin knockout mice. *Human Molecular Genetics*.

References

SONG, E., OUYANG, N., HÖRBELT, M., ANTUS, B., WANG, M. & EXTON, M. S. 2000. Influence of alternatively and classically activated macrophages on fibrogenic activities of human fibroblasts. *Cellular immunology,* 204**,** 19-28.

SONG, Y., YAO, S., LIU, Y., LONG, L., YANG, H., LI, Q., LIANG, J., LI, X., LU, Y. & ZHU, H. 2017. Expression levels of TGF-β1 and CTGF are associated with the severity of Duchenne muscular dystrophy. *Experimental and therapeutic medicine,* 13**,** 1209-1214.

STANLEY, A., TICHY, E. D., KOCAN, J., ROBERTS, D. W., SHORE, E. M. & MOURKIOTI, F. 2022. Dynamics of skeletal muscle-resident stem cells during myogenesis in fibrodysplasia ossificans progressiva. *npj Regenerative Medicine,* 7**,** 5.

STEARNS-REIDER, K. M., D'AMORE, A., BEEZHOLD, K., ROTHRAUFF, B., CAVALLI, L., WAGNER, W. R., VORP, D. A., TSAMIS, A., SHINDE, S., ZHANG, C., BARCHOWSKY, A., RANDO, T. A., TUAN, R. S. & AMBROSIO, F. 2017. Aging of the skeletal muscle extracellular matrix drives a stem cell fibrogenic conversion. *Aging Cell,* 16**,** 518-528.

STEPIEN, D. M., HWANG, C., MARINI, S., PAGANI, C. A., SORKIN, M., VISSER, N. D., HUBER, A. K., EDWARDS, N. J., LODER, S. J., VASQUEZ, K., AGUILAR, C. A., KUMAR, R., MASCHARAK, S., LONGAKER, M. T., LI, J. & LEVI, B. 2020. Tuning Macrophage Phenotype to Mitigate Skeletal Muscle Fibrosis. *The Journal of Immunology,* 204**,** 2203-2215.

STRICKER, S., BRIESKE, N., HAUPT, J. & MUNDLOS, S. 2006. Comparative expression pattern of Odd-skipped related genes Osr1 and Osr2 in chick embryonic development. *Gene expression patterns,* 6**,** 826-834.

STRICKER, S., MATHIA, S., HAUPT, J., SEEMANN, P., MEIER, J. & MUNDLOS, S. 2012. Odd-skipped related genes regulate differentiation of embryonic limb mesenchyme and bone marrow mesenchymal stromal cells. *Stem cells and development,* 21**,** 623-633.

STUMM, J., VALLECILLO-GARCIA, P., VOM HOFE-SCHNEIDER, S., OLLITRAULT, D., SCHREWE, H., ECONOMIDES, A. N., MARAZZI, G., SASSOON, D. A. & STRICKER, S. 2018. Odd skipped-related 1 (Osr1) identifies muscle-interstitial fibro-adipogenic progenitors (FAPs) activated by acute injury. *Stem Cell Res,* 32**,** 8-16.

SUGIMOTO, M. A., VAGO, J. P., PERRETTI, M. & TEIXEIRA, M. M. 2019. Mediators of the Resolution of the Inflammatory Response. *Trends in Immunology,* 40**,** 212-227.

SWIFT, J., IVANOVSKA, I. L., BUXBOIM, A., HARADA, T., DINGAL, P. C. D. P., PINTER, J., PAJEROWSKI, J. D., SPINLER, K. R., SHIN, J.-W., TEWARI, M., REHFELDT, F., SPEICHER, D. W. & DISCHER, D. E. 2013. Nuclear Lamin-A Scales with Tissue Stiffness and Enhances Matrix-Directed Differentiation. *Science,* 341**,** 1240104.

SWINEHART, I. T., SCHLIENTZ, A. J., QUINTANILLA, C. A., MORTLOCK, D. P. & WELLIK, D. M. 2013. Hox11 genes are required for regional patterning and integration of muscle, tendon and bone. *Development,* 140**,** 4574-4582.

TANIGUCHI, M., KURAHASHI, H., NOGUCHI, S., SESE, J., OKINAGA, T., TSUKAHARA, T., GUICHENEY, P., OZONO, K., NISHINO, I., MORISHITA, S. & TODA, T. 2006. Expression profiling of muscles from Fukuyama-type congenital muscular dystrophy and laminin-α2 deficient congenital muscular dystrophy; is congenital muscular dystrophy a primary fibrotic disease? *Biochemical and Biophysical Research Communications,* 342**,** 489-502.

TAUFALELE, P. V., VANDERBURGH, J. A., MUÑOZ, A., ZANOTELLI, M. R. & REINHART-KING, C. A. 2019. Fiber alignment drives changes in architectural and mechanical features in collagen matrices. *PLOS ONE,* 14**,** e0216537.

TENA, J. J., NETO, A., DE LA CALLE-MUSTIENES, E., BRAS-PEREIRA, C., CASARES, F. & GÓMEZ-SKARMETA, J. L. 2007. Odd-skipped genes encode repressors that control kidney development. *Developmental biology,* 301**,** 518-531.

THERET, M., ROSSI, F. M. V. & CONTRERAS, O. 2021. Evolving Roles of Muscle-Resident Fibro-Adipogenic Progenitors in Health, Regeneration, Neuromuscular Disorders, and Aging. *Front Physiol,* 12**,** 673404.

THERET, M., SACLIER, M., MESSINA, G. & ROSSI, F. M. V. 2022. Macrophages in Skeletal Muscle Dystrophies, An Entangled Partner. *Journal of Neuromuscular Diseases,* 9**,** 1-23.

TIDBALL, J. G. 2011. Mechanisms of Muscle Injury, Repair, and Regeneration. *Comprehensive Physiology.*

TIDBALL, J. G. 2017. Regulation of muscle growth and regeneration by the immune system. *Nature Reviews Immunology,* 17**,** 165-178.

TIDBALL, J. G. & VILLALTA, S. A. 2010. Regulatory interactions between muscle and the immune system during muscle regeneration. *American Journal of Physiology-Regulatory, Integrative and Comparative Physiology,* 298**,** R1173-R1187.

TIERNEY, M. T., AYDOGDU, T., SALA, D., MALECOVA, B., GATTO, S., PURI, P. L., LATELLA, L. & SACCO, A. 2014. STAT3 signaling controls satellite cell expansion and skeletal muscle repair. *Nature Medicine,* 20**,** 1182-1186.

TONKIN, J., TEMMERMAN, L., SAMPSON, R. D., GALLEGO-COLON, E., BARBERI, L., BILBAO, D., SCHNEIDER, M. D., MUSARÒ, A. & ROSENTHAL, N. 2015. Monocyte/Macrophage-derived IGF-1 Orchestrates Murine Skeletal Muscle Regeneration and Modulates Autocrine Polarization. *Molecular Therapy,* 23**,** 1189-1200.

TOSELLO-TRAMPONT, A., SURETTE, F. A., EWALD, S. E. & HAHN, Y. S. 2017. Immunoregulatory Role of NK Cells in Tissue Inflammation and Regeneration. *Frontiers in Immunology,* 8.

TRENSZ, F., LUCIEN, F., COUTURE, V., SÖLLRALD, T., DROUIN, G., ROULEAU, A.-J., GRANDBOIS, M., LACRAZ, G. & GRENIER, G. 2015. Increased microenvironment stiffness in damaged myofibers promotes myogenic progenitor cell proliferation. *Skeletal Muscle,* 5**,** 5.

TRENSZ, F., LUCIEN, F., COUTURE, V., SÖLLRALD, T., DROUIN, G., ROULEAU, A.-J., GRANDBOIS, M., LACRAZ, G. & GRENIER, G. 2016. Increased microenvironment stiffness in damaged myofibers promotes myogenic progenitor cell proliferation. *Skeletal Muscle,* 5.

TRIPATHI, C., TEWARI, B. N., KANCHAN, R. K., BAGHEL, K. S., NAUTIYAL, N., SHRIVASTAVA, R., KAUR, H., BHATT, M. L. B. & BHADAURIA, S. 2014. Macrophages are recruited to hypoxic tumor areas and acquire a Pro-Angiogenic M2-Polarized phenotype via hypoxic cancer cell derived cytokines Oncostatin M and Eotaxin. *Oncotarget,* 5**,** 5350-5368.

UEZUMI, A., FUKADA, S.-I., YAMAMOTO, N., TAKEDA, S. I. & TSUCHIDA, K. 2010. Mesenchymal progenitors distinct from satellite cells contribute to ectopic fat cell formation in skeletal muscle. *Nature Cell Biology,* 12**,** 143-152.

UEZUMI, A., IKEMOTO-UEZUMI, M. & TSUCHIDA, K. 2014. Roles of nonmyogenic mesenchymal progenitors in pathogenesis and regeneration of skeletal muscle. *Front Physiol,* 5**,** 68.

References

UEZUMI, A., IKEMOTO-UEZUMI, M., ZHOU, H., KUROSAWA, T., YOSHIMOTO, Y., NAKATANI, M., HITACHI, K., YAMAGUCHI, H., WAKATSUKI, S., ARAKI, T., MORITA, M., YAMADA, H., TOYODA, M., KANAZAWA, N., NAKAZAWA, T., HINO, J., FUKADA, S.-I. & TSUCHIDA, K. 2021. Mesenchymal Bmp3b expression maintains skeletal muscle integrity and decreases in age-related sarcopenia. *Journal of Clinical Investigation,* 131.

UEZUMI, A., ITO, T., MORIKAWA, D., SHIMIZU, N., YONEDA, T., SEGAWA, M., YAMAGUCHI, M., OGAWA, R., MATEV, M. M., MIYAGOE-SUZUKI, Y., TAKEDA, S., TSUJIKAWA, K., TSUCHIDA, K., YAMAMOTO, H. & FUKADA, S. 2011. Fibrosis and adipogenesis originate from a common mesenchymal progenitor in skeletal muscle. *J Cell Sci,* 124**,** 3654-64.

UPADHYAY, J., XIE, L., HUANG, L., DAS, N., STEWART, R. C., LYON, M. C., PALMER, K., RAJAMANI, S., GRAUL, C., LOBO, M., WELLMAN, T. J., SOARES, E. J., SILVA, M. D., HESTERMAN, J., WANG, L., WEN, X., QIAN, X., NANNURU, K., IDONE, V., MURPHY, A. J., ECONOMIDES, A. N. & HATSELL, S. J. 2017. The Expansion of Heterotopic Bone in Fibrodysplasia Ossificans Progressiva Is Activin A-Dependent. *Journal of Bone and Mineral Research,* 32**,** 2489-2499.

URCIUOLO, A., QUARTA, M., MORBIDONI, V., GATTAZZO, F., MOLON, S., GRUMATI, P., MONTEMURRO, F., TEDESCO, F. S., BLAAUW, B., COSSU, G., VOZZI, G., RANDO, T. A. & BONALDO, P. 2013. Collagen VI regulates satellite cell self-renewal and muscle regeneration. *Nat Commun,* 4**,** 1964.

VALLECILLO-GARCIA, P., ORGEUR, M., VOM HOFE-SCHNEIDER, S., STUMM, J., KAPPERT, V., IBRAHIM, D. M., BORNO, S. T., HAYASHI, S., RELAIX, F., HILDEBRANDT, K., SENGLE, G., KOCH, M., TIMMERMANN, B., MARAZZI, G., SASSOON, D. A., DUPREZ, D. & STRICKER, S. 2017. Odd skipped-related 1 identifies a population of embryonic fibro-adipogenic progenitors regulating myogenesis during limb development. *Nat Commun,* 8**,** 1218.

VARGA, T., MOUNIER, R., PATSALOS, A., GOGOLÁK, P., PELOQUIN, M., HORVATH, A., PAP, A., DANIEL, B., NAGY, G., PINTYE, E., POLISKA, S., CUVELLIER, S., SABRINA, BRIAN, SPITE, M., CHESTER, CHAZAUD, B. & NAGY, L. 2016. Macrophage PPARγ, a Lipid Activated Transcription Factor Controls the Growth Factor GDF3 and Skeletal Muscle Regeneration. *Immunity,* 45**,** 1038-1051.

VATTEMI, G., MIRABELLA, M., GUGLIELMI, V., LUCCHINI, M., TOMELLERI, G., GHIRARDELLO, A. & DORIA, A. 2014. Muscle biopsy features of idiopathic inflammatory myopathies and differential diagnosis. *Autoimmunity Highlights,* 5**,** 77-85.

VERMA, M., ASAKURA, Y., MURAKONDA, B. S. R., PENGO, T., LATROCHE, C., CHAZAUD, B., MCLOON, L. K. & ASAKURA, A. 2018a. Muscle Satellite Cell Cross-Talk with a Vascular Niche Maintains Quiescence via VEGF and Notch Signaling. *Cell Stem Cell,* 23**,** 530-543.e9.

VERMA, M., ASAKURA, Y., MURAKONDA, B. S. R., PENGO, T., LATROCHE, C., CHAZAUD, B., MCLOON, L. K. & ASAKURA, A. 2018b. Muscle satellite cell cross-talk with a vascular niche maintains quiescence via VEGF and notch signaling. *Cell stem cell,* 23**,** 530-543. e9.

VIDAL, B., SERRANO, A. L., TJWA, M., SUELVES, M., ARDITE, E., DE MORI, R., BAEZA-RAJA, B., DE LAGRÁN, M. M., LAFUSTE, P. & RUIZ-BONILLA, V. 2008a. Fibrinogen drives dystrophic muscle fibrosis via a TGFβ/alternative macrophage activation pathway. *Genes & development,* 22**,** 1747-1752.

VIDAL, B., SERRANO, A. L., TJWA, M., SUELVES, M., ARDITE, E., DE MORI, R., BAEZA-RAJA, B., MARTÍNEZ DE LAGRÁN, M., LAFUSTE, P., RUIZ-BONILLA, V., JARDÍ, M., GHERARDI, R., CHRISTOV, C., DIERSSEN, M., CARMELIET, P., DEGEN, J. L., DEWERCHIN, M. & MUÑOZ-CÁNOVES, P. 2008b. Fibrinogen drives dystrophic muscle fibrosis via a TGFβ/alternative macrophage activation pathway. *Genes & Development,* 22**,** 1747-1752.

VINDEVOGHEL, L., KON, A., LECHLEIDER, R. J., UITTO, J., ROBERTS, A. B. & MAUVIEL, A. 1998. Smad-dependent transcriptional activation of human type VII collagen gene (COL7A1) promoter by transforming growth factor-β. *Journal of Biological Chemistry,* 273**,** 13053-13057.

VON MALTZAHN, J., JONES, A. E., PARKS, R. J. & RUDNICKI, M. A. 2013. Pax7 is critical for the normal function of satellite cells in adult skeletal muscle. *Proc Natl Acad Sci U S A,* 110**,** 16474-9.

VUMBACA, S., GIULIANI, G., FIORENTINI, V., TORTOLICI, F., CERQUONE PERPETUINI, A., RICCIO, F., SENNATO, S., GARGIOLI, C., FUOCO, C., CASTAGNOLI, L. & CESARENI, G. 2021. Characterization of the Skeletal Muscle Secretome Reveals a Role for Extracellular Vesicles and IL1α/IL1β in Restricting Fibro/Adipogenic Progenitor Adipogenesis. *Biomolecules,* 11**,** 1171.

WANG, W., OLSON, D., LIANG, G., FRANCESCHI, R. T., LI, C., WANG, B., WANG, S. S. & YANG, S. 2012. Collagen XXIV (Col24α1) Promotes Osteoblastic Differentiation and Mineralization through TGF-β/Smads Signaling Pathway. *International Journal of Biological Sciences,* 8**,** 1310-1322.

WATT, K. I., JASPERS, R. T., ATHERTON, P., SMITH, K., RENNIE, M. J., RATKEVICIUS, A. & WACKERHAGE, H. 2010. SB431542 treatment promotes the hypertrophy of skeletal muscle fibers but decreases specific force. *Muscle & Nerve,* 41**,** 624-629.

WILSCHUT, K. J., HAAGSMAN, H. P. & ROELEN, B. A. 2010. Extracellular matrix components direct porcine muscle stem cell behavior. *Experimental cell research,* 316**,** 341-352.

WOOD, L. K., KAYUPOV, E., GUMUCIO, J. P., MENDIAS, C. L., CLAFLIN, D. R. & BROOKS, S. V. 2014. Intrinsic stiffness of extracellular matrix increases with age in skeletal muscles of mice. *J Appl Physiol (1985),* 117**,** 363-9.

WOSCZYNA, M. N., BISWAS, A. A., COGSWELL, C. A. & GOLDHAMER, D. J. 2012. Multipotent progenitors resident in the skeletal muscle interstitium exhibit robust BMP-dependent osteogenic activity and mediate heterotopic ossification. *Journal of Bone and Mineral Research,* 27**,** 1004-1017.

WOSCZYNA, M. N., KONISHI, C. T., PEREZ CARBAJAL, E. E., WANG, T. T., WALSH, R. A., GAN, Q., WAGNER, M. W. & RANDO, T. A. 2019. Mesenchymal Stromal Cells Are Required for Regeneration and Homeostatic Maintenance of Skeletal Muscle. *Cell Rep,* 27**,** 2029-2035 e5.

WOSCZYNA, M. N. & RANDO, T. A. 2018. A Muscle Stem Cell Support Group: Coordinated Cellular Responses in Muscle Regeneration. *Dev Cell,* 46**,** 135-143.

XIAO, W., LIU, Y. & CHEN, P. 2016. Macrophage Depletion Impairs Skeletal Muscle Regeneration: the Roles of Pro-fibrotic Factors, Inflammation, and Oxidative Stress. *Inflammation,* 39**,** 2016-2028.

XING, Q., YATES, K., TAHTINEN, M., SHEARIER, E., QIAN, Z. & ZHAO, F. 2015. Decellularization of fibroblast cell sheets for natural extracellular matrix scaffold preparation. *Tissue Engineering Part C: Methods,* 21**,** 77-87.

References

XU, J., LIU, H., PARK, J.-S., LAN, Y. & JIANG, R. 2014. Osr1 acts downstream of and interacts synergistically with Six2 to maintain nephron progenitor cells during kidney organogenesis. *Development,* 141**,** 1442-1452.

XU, Z., YOU, W., CHEN, W., ZHOU, Y., NONG, Q., VALENCAK, T. G., WANG, Y. & SHAN, T. 2021. Single-cell RNA sequencing and lipidomics reveal cell and lipid dynamics of fat infiltration in skeletal muscle. *Journal of Cachexia, Sarcopenia and Muscle,* 12**,** 109-129.

YAMAKAWA, H., KUSUMOTO, D., HASHIMOTO, H. & YUASA, S. 2020. Stem Cell Aging in Skeletal Muscle Regeneration and Disease. *International Journal of Molecular Sciences,* 21**,** 1830.

YAMAMOTO, M., LEGENDRE, N. P., BISWAS, A. A., LAWTON, A., YAMAMOTO, S., TAJBAKHSH, S., KARDON, G. & GOLDHAMER, D. J. 2018. Loss of MyoD and Myf5 in Skeletal Muscle Stem Cells Results in Altered Myogenic Programming and Failed Regeneration. *Stem Cell Reports,* 10**,** 956-969.

YANG, S. & PLOTNIKOV, S. V. 2021. Mechanosensitive Regulation of Fibrosis. *Cells,* 10**,** 994.

YANG, W. & HU, P. 2018. Skeletal muscle regeneration is modulated by inflammation. *Journal of Orthopaedic Translation,* 13**,** 25-32.

YIN, H., PRICE, F. & RUDNICKI, M. A. 2013. Satellite cells and the muscle stem cell niche. *Physiol Rev,* 93**,** 23-67.

YOSHIMOTO, Y., IKEMOTO-UEZUMI, M., HITACHI, K., FUKADA, S.-I. & UEZUMI, A. 2020. Methods for Accurate Assessment of Myofiber Maturity During Skeletal Muscle Regeneration. *Frontiers in Cell and Developmental Biology,* 8.

ZAMMIT, P. S. 2017. Function of the myogenic regulatory factors Myf5, MyoD, Myogenin and MRF4 in skeletal muscle, satellite cells and regenerative myogenesis. *Seminars in Cell & Developmental Biology,* 72**,** 19-32.

ZAMMIT, P. S., RELAIX, F., NAGATA, Y., RUIZ, A. P., COLLINS, C. A., PARTRIDGE, T. A. & BEAUCHAMP, J. R. 2006. Pax7 and myogenic progression in skeletal muscle satellite cells. 119**,** 1824-1832.

ZHANG, M. J., NTRANOS, V. & TSE, D. 2020. Determining sequencing depth in a single-cell RNA-seq experiment. *Nature Communications,* 11**,** 774.

ZHAO, J., TIAN, Z., KADOMATSU, T., XIE, P., MIYATA, K., SUGIZAKI, T., ENDO, M., ZHU, S., FAN, H., HORIGUCHI, H., MORINAGA, J., TERADA, K., YOSHIZAWA, T., YAMAGATA, K. & OIKE, Y. 2018. Age-dependent increase in angiopoietin-like protein 2 accelerates skeletal muscle loss in mice. *Journal of Biological Chemistry,* 293**,** 1596-1609.

ZHAO, L., SON, J. S., WANG, B., TIAN, Q., CHEN, Y., LIU, X., DE AVILA, J. M., ZHU, M.-J. & DU, M. 2020. Retinoic acid signalling in fibro/adipogenic progenitors robustly enhances muscle regeneration. *EBioMedicine,* 60**,** 103020.

ZHOU, L., LIU, J., OLSON, P., ZHANG, K., WYNNE, J. & XIE, L. 2015. Tbx5 and Osr1 interact to regulate posterior second heart field cell cycle progression for cardiac septation. *Journal of molecular and cellular cardiology,* 85**,** 1-12.

9 Appendix

9.1 List of DE genes in the transcriptome analysis

Table 21: Top 50 DE genes being regulated GFP$^+$ FAPs of the Osr1 cKO injured muscles at 3 and 7 dpi.

3 dpi			7 dpi		
Gene Name	Log_2FC	p-adj. value	Gene Name	Log_2FC	p-adj. value
Pcdhgb8	3,91	1E-19	Zim1	1,04	2,00E-29
Ucp2	-3,05	2E-19	Slpi	-0,82	1,10E-27
Tmem35	-2,14	6E-06	Eln	-0,80	6,46E-23
Bst1	-2,81	5E-05	Adamts17	1,15	3,90E-18
AK195902_gene	-1,32	5E-05	Cxcl9	1,03	1,93E-16
Irg1	-2,40	1E-04	Peg3	-0,95	3,12E-16
Plac8	-1,85	1E-04	Saa3	-1,02	9,91E-15
Thbs4	1,38	2E-04	Cyp51	-0,88	8,91E-13
Kif26b	1,57	3E-04	Fbln7	-0,74	5,28E-12
Myo7a	1,19	3E-04	Fgl2	0,72	8,51E-12
Hmga2	-1,65	4E-04	Dhcr24	-0,81	1,09E-11
AK199756_gene	-1,30	4E-04	Il1rl1	-0,85	2,20E-11
Rarres2	-1,13	4E-04	Nrep	0,98	2,20E-11
Slc7a2	1,29	4E-04	Cacna1a	0,81	2,57E-10
BC044745_gene	-7,98	7E-04	Pde12	-0,98	2,61E-10
Pycard	-1,81	8E-04	Cst3	-1,03	4,12E-10
Slco2a1	-1,31	9E-04	Emb	-0,69	6,36E-10
Hmga1	-1,75	3E-03	Gcc1	-0,80	1,10E-09
Ly6c1	-1,37	3E-03	Penk	-0,76	1,38E-09
Hdc	-2,47	3E-03	Msmo1	1,24	1,45E-09
Cngb3	-2,96	4E-03	Chl1	-0,74	6,39E-09
Aldh1b1	-2,17	4E-03	Dlk1	-0,95	1,08E-08
Slfn2	-1,58	4E-03	Abcg1	-0,73	1,55E-08
Dock10	-1,80	4E-03	Itpkc	-0,66	1,67E-08
Gdf15	-1,18	5E-03	Itgbl1	-0,79	8,81E-08
Enpp4	-1,39	5E-03	H19	0,67	1,71E-07
Sh2d6	-1,91	6E-03	Gzme	0,65	1,71E-07
Xdh	-1,60	7E-03	Aldh1a2	-0,73	4,06E-07
Pyhin1	-4,22	7E-03	Gm24270	-0,64	4,06E-07
Slco3a1	-0,83	7E-03	Spry1	0,88	4,81E-07
Hmgcs2	-3,31	8E-03	Iigp1	0,86	4,93E-07
Cxcl10	-1,77	1E-02	Cish	-0,66	6,54E-07
Cfb	-1,03	1E-02	Insig1	-0,60	6,71E-07
A630012P03Rik	-2,50	1E-02	Ldlr	-0,63	1,11E-06
Oas1c	-1,91	1E-02	Cxcl10	-0,74	1,41E-06

Slc15a3	-1,39	1E-02	Peg10	-0,66	1,41E-06
BC023483_gene	2,00	1E-02	Fdft1	1,11	1,48E-06
Irf5	-1,96	1E-02	Sqle	-0,57	1,51E-06
Sult1a1	-2,88	1E-02	IL6	-0,65	1,54E-06
Ifi203	-1,52	1E-02	Cebpd	0,71	1,80E-06
Tlr3	-1,34	1E-02	Lama2	-0,68	2,08E-06
Tnn	0,97	1E-02	Ace	-0,75	2,72E-06
Ccdc21	-0,97	1E-02	Sema5a	-0,88	3,05E-06
Pcdhgb5	1,51	2E-02	Gm6093	1,11	3,27E-06
Dhrs9	-1,92	2E-02	Adamts4	-0,57	3,96E-06
Casp4	-1,58	2E-02	Selenop	-0,65	4,84E-06
Hap1	-2,01	2E-02	Hmgcs1	0,71	6,36E-06
Rasa4	-1,89	2E-02	Dnajb1	-0,68	7,54E-06
Gch1	-1,03	2E-02	Hsph1	-0,75	7,95E-06
Serpina3f	-1,85	2E-02	Gramd1b	-0,88	7,95E-06

9.2 List of tables

9.3 List of figures

Appendix

9.4 Abbreviations

°C	Degree Celsius
µm	Micrometer
Acta2	Actin alpha 2
aFbs	Adherent connective tissue fibroblasts
Alpl	Alkaline phosphatase
Arg1	Arginase 1
bidest	Bidistillated
BMP-(X)	Bone morphogenic protein-X
bp	base pair
BSA	Bovine serum albumin
CM	Conditioned medium
Ccl-(X)	C-C motif chemokine ligand X
cDCs	Conventional DCs
cDNA	Complementary DNA
Chil3l1	Chitinase-3-like protein 1
cKO	Conditional knock-out
Col.X	Collagen X
CSA	Cross sectional area
Ctrl	Control
CXCL12	C-X-C motif chemokine ligand 12
D(X)	Day X
dpi	Days post injury
DAPI	4´,6´-Diamidino-2-phenylindole dihydrochloride
DCs	Dendritic cells
DE	Deregulated
dECM	Decellularized extracellular matrix
Dhh	Dessert hedgehog signaling
DMD	Duchenne muscular dystrophy
DMEM	Dulbecco’s modified Eagle’s medium
DMSO	Dimethyl sulfoxide
DNA	Deoxyribonucleic acid
dNTP	Deoxyribonucleotide triphosphate
DTX	Diptheria toxin

E	Embryonic stage
e.g.	For example
ECM	Extracellular matrix
EDTA	ethylenediaminetetraacetic acid
eMHC	Embryonic myosin heavy chain
FACS	Fluorescence-activated cell sorting
FAPs	Fibro-adipogenic progenitors
Fbln7	Fibulin 7
FBS	Fetal bovine serum
fl	Floxed
Fn1	Fibronectin
FOP	Fibrodysplasia ossificans progressiva
g	gram
GFP	Green fluorescent protein
GM	Growth medium
GO	Gene ontology
Gsk3	Glycogen synthase kinase 3
h	Hour
H&E	Hematoxylin and eosin staining
Hic1	HIC ZBTB transcriptional repressor 1
HO	Heterotopic ossification
Hox-(X)	Homeobox X
i.e.	That is
IFNγ	Interferon γ
IGF-1	Insulin like growth factor 1
IL-(X)	Interleukin-X
IMCT	Interstitial muscle connective tissue
iNOS	Nitric oxide synthase
kDa	Kilo Dalton
KO	Knock out
kPa	Kilopascal
L	Liter
Lam	Laminin
LGMDB2B	Limb girdle muscular dystrophy type 2

lin	Lineage
Loxl2	Lysyl oxidase like 2
LTBP4	Latent transforming growth factor binding protein 4
Ly6a/ Sca1	Stem cell antigen 1
M1	Pro-inflammatory macrophages
M2	Anti-inflammatory macrophages
M-CSF	Macrophage colony stimulated factor
Min	Minutes
mm	Millimeter
mM	Millimolar
MMP-(X)	Metalloproteinase X
MRF4	Muscle regulatory factor 4
MRFs	Muscle regulatory functions
mRNA	Messenger RNA
MSCs	Mesenchymal stem cells
MuSCs	Muscle stem cells
Myf5	Myogenic factor 5
MyHC	Myosin heavy chain
Myod1	Myogenic differentiation 1
MΦs	Macrophages
NK	Natural killers
ORO	Oil Red O
Osr1	Odd skipped related 1
P(X)	Passage X
PBS	Phosphate buffered saline
PBX	Phosphate buffered saline with Triton-X
PCR	Polymerase chain reaction
pDCs	Plasmacytoid DCs
PDGFRα	Platelet derived growth factor alpha
Peg3/ PW1	Paternally expressed 3
PICs	$PW1^{+}$ / $Pax7^{-}$ interstitial cells
Plin	Perilipin
Pol II	RNA Polymerase II
PSR	Picrus Sirius Red

rcf	Relative centrifugal force
RetnLa/ Fizz-1	Resistin like alpha
RKT	Receptor tyrosine kinase
RNA seq	RNA sequencing
RT-qPCR	Real time quantitative polymerase chain reaction
SDS	Sodium dodecyl sulfate
SDS-PAGE	Sodium dodecyl sulfate-polyacrylamide gel electrophoresis
SEM	Standard error of mean
SMAD	Sons of mothers against decapentaplegic
Spry1	Sprouty RTK signaling antagonist 1
T cm	T central memory cells
T em	T effective memory cells
T.A.	Tibialis anterior
TAM	Tamoxifen
Tbx4/5	T/box transcription factor 4/5
Tcf7l2/ Tcf4	Transcription factor 7 Like 2
TGFβ	Tissue growth factor beta
Thbs4	Thrombospondin 4
Tie2	TEK receptor tyrosinase kinase
TimpX	Tissue inhibitor of metalloproteinase X
Tnc	Tenascin C
TNFα	Tumor necrosis factor alpha
Treg	Regulatory T cells
TRM	Tissue resident macrophages
Vcam1	Vascular cell adhesion molecule 1
VEGF	Vascular endothelial growth factor
Wisp1	WNT1-inducible-signaling pathway protein
Wnt1	Wnt family member 1
WT	Wild type
αSMA	Alpha smooth muscle actin 1